Synthesis and characterization of nanoparticles and their bio-catalytic applications

THESIS

SUBMITTED TO

BABASAHEB BHIMRAO AMBEDKAR UNIVERSITY
(A CENTRAL UNIVERSITY)
LUCKNOW

BABASAHEB
BHIMRAO
AMBEDKAR
UNIVERSITY

प्रज्ञा शील करुणा
ESTABLISHED 1996

FOR THE DEGREE OF

Doctor of Philosophy

IN

APPLIED CHEMISTRY

Submitted by

Gulam Abbas

Enrollment No. 1377/16

Under the Supervision of

Prof. Gajanan Pandey

DEPARTMENT OF APPLIED CHEMISTRY
SCHOOL FOR PHYSICAL SCIENCES
BABASAHEB BHIMRAO AMBEDKAR UNIVERSITY
VIDYA VIHAR, RAE BARELI ROAD, LUCKNOW-226 025

2021

Dedicated to

Parents, Brothers, and Sisters…….

Love and anger both are synonyms, their extreme motivation causes them to acknowledge their feelings

Dedicated to supervisor

The kind of supervision received has provided a supersonicated way to achieve morality in humanity and challenge to sharpened research to focus & locus an ambition to bowing career opportunity

Research is a romance in the field of Scire, (Latin Science) to show the responsibility of rays to sparkled to Globalisation

CERTIFICATE

This is to certify that the thesis titled **"Synthesis and characterization of nanoparticles and their bio-catalytic applications"** submitted by **Mr. Gulam Abbas** is an original research work and has not been previously submitted in part or full for the award of any other degree or diploma to this or any other University.

The thesis submitted to Babasaheb Bhimrao Ambedkar University Lucknow satisfies all the requirements as stipulated in the *Doctor of Philosophy (Ph.D.) regulations -1999 as amended in 2008/2010/2013* and it is fit for submission and evaluation for the award of the degree of Doctor of Philosophy of the University.

Supervisor

Date: 26.07.2021

26.7.21

Head of the Department

Professor & Head
Department of Chemistry
School of Physical & Decision Sciences
Babasaheb Bhimrao Ambedkar University
(A Central University)
Lucknow-226025, Uttar Pradesh (INDIA)

DECLARATION

I, **Gulam Abbas** declare that the thesis entitled, **"Synthesis and characterization of nanoparticles and their bio-catalytic applications"** submitted by me for the degree of Doctor of Philosophy is the record of work carried out by me under the guidance of **Prof. Gajanan Pandey, Department of Applied Chemistry, School for Physical Sciences, Babasaheb Bhimrao Ambedkar University, (A Central University), Lucknow, U.P. India** and has not formed the basis for the award of any degree, diploma, associate ship, fellowship, titles in this or any other University or other institute of higher learning.

I declare that material obtained from other sources has been duly acknowledged in this thesis. And in last, I declare that the thesis is essentially free from all kinds of plagiarism.

G. Abbas
26/07/2021

Date: 26/07/2021

Place: Lucknow

Gulam Abbas
Department of Applied Chemistry
School for Physical Sciences
Babasaheb Bhimrao Ambedkar University
Lucknow-226025, India

ACKNOWLEDGEMENT

I wish to express my greatest gratitude and sincere thanks with a profound sense of expression to my honourable and esteemed supervisor **Prof. Gajanan Pandey, (Head of Department)** for their regular support in my Ph.D. research study, for patience, motivation, and immense sea of knowledge. His guidance helped in writing the thesis and to understand the ability of research aptitudes. His explanations, discussions, and motivations have gradually become the basis of my best publications.

I have also conveyed thanks **Prof. Kaman Singh, Prof. Devesh Kumar, Prof. B. C. Yadav, Prof. Abbas Ali Mehdi, Dr. Anjani Kumar Tiwari, Dr. Satyedra Kumar, Dr. Jawahar Lal Jat, Dr. Shailesh Kumar, Dr. Jyoti Pandey, Dr. Preeti Gupta, Dr. Suman Kushwaha** for their encouragement and insightful comments questioning session to improve my knowledge skill and learning ability to prove my existence and widen my research from various perspectives. And, warm thanks go to the Departmental lab staff for providing a friendly and motivating environment during the research work.

I wish to my reverence and great thanks to **Dr. Gaurav Hitkari, Dr. Sandhya Singh, Dr. Azad Kumar, Dr. Ajay Kumar, Dr. Deepak Kumar, Dr. Akhilesh Shukla, Dr. Manoj Shriniwas, Dr. Anupriya Adhikari, and Dr. Roopal Yadav** for their immense value, insightful comments, and suggestions to improve the quality of research work. I thank my fellow labmates Mr. Kijay Bahadur Singh, Miss Neelam Gautam, Mr. Anil Vyas, Miss Snigdha, Mr. Baldev Singh, Mr. Manoj Dhameja, Mr. Hariom Kumar, Mr. Dinesh Kumar, Miss Saumya Verma, Mr. Puneet Kumar, Mr. Ajay Yadav, Miss Priya Singh, Mr. Prashant Mishra, Mr. Ashok Kumar, Mr. Sumit Kumar, Miss Deepika Singh, Mr. Kuldeep Singh, Mr. Diptarka Roy, Mr. Narinder

Kumar, Mr. Indresh Shukla and Mr. Deen Dayal Upadhyay for their regular discussion and motivational inspiration to desire the best undertaking of works. I wish to convey a lot of thanks to the staff of department Mr. Sarvesh Gupta, Mr. Pankaj and from the very large depth of heart to Mr. Anuj Kumar Saini for their best command, helping nature and providing endless brilliancy to survive in struggling future. So, in end and not a final assumption, I wish to thanks to authors of all research papers, reviewers, articles, and book chapters to whom this work has been cited.

Research is an inspiration that comes to mind to those who can face the misfortunes of the global era to neutralize it.

G. Abbas
26/07/2021

Gulam Abbas
(Research scholar)

PREFACE

Since recent decades nanotechnology and its interdisciplinary fields are encouraging to synthesized nanoparticles, nanorods, graphene, nanocomposites to treat a number of infectious diseases (carcinomas, bacterial and viral infectiions), chemotherapeutic agents, antivirology responses and removal of contaminants to treat waste water from industries and other sources and how these nano's get enter the cell cycle to inhibit their functioning.

Nanoparticles/Nanocomposites/Nanostructures have shown an enormous awareness since decades as therapeutic mediators for many pathogenic disease like carcinomas, antimicrobial, antibacterial diseases. One of the major limitations however is their untargeted, nonspecific toxicity. Therefore the application of nanoparticles in biomedical fields it is essential that various process induced by these particles in human tissues and genetic material (DNA, RNA) to further improve their sensitizing properties. Hence for any material being developed for the therapeutic purpose, the determination of toxicity in human cells is highly important. Furthermore, by using metallic nanoparticles with a thermal method is an important alternative for the carcinomas therapy. Since optical properties of nanoparticles in infrared range have provided a pathway for the advancement of new techniques, carcinomas therapy using nanoparticles along with photo-thermal treatment has become more effective, so we are interested in exploring the cytotoxicity of metallic nanoparticles.

The complete research analysis has been divided in to seven chapters. First chapter consists a number of views described the method of synthesis of nanomaterials, nanostructure materials and their significance in their biocatalytic

reactions. The structure and properties dependent biocatalytic properties viz. anticarcinomas studies of nanostructure materials have been systematically reviewed. The leading objectives and brief framework of the present examination carried out in this thesis are described in brief.

Second chapter reveals detailed instrumentation techniques used in analysis and identification of prepared nanostructure/nancomposites/nanoparticles. These methods include the absorbance and band-gap analysis using the UV-visible spectroscopy, Dynamic light scattering (DLS)@zeta potentials, Fourier Transform Infrared Resonance (FTIR) spectroscopy, X-ray diffraction analysis (XRD), Surface Enhanced Raman spectroscopy (SERS), Brunauer-Emmett-Taylor analysis (BET), Scanning Electron Microscope (SEM) with Energy Dispersive Spectrum (EDS) analysis, Field Emissive Scanning Electron Microscopy (FESEM) and Transmission Electron Microscopy (TEM).

Third chapter represents the synthesis of different shapes and sized palladium nanoparticles (Pd NPs) by reducing potassium tetrachloropalladinate(II) by L-ascorbic acid (LAA) in aqueous solution phase in the presence of an amphiphilic nonionic surfactant poly ethylene glycol (PEG) via sonochemical method. Synthesized material has been characterized by XRD, SEM, TEM, EDX, FTIR, SERS, particle's distribution and zeta potential studies. Truncated octahedron/fivefold twinned pentagonal rods are formed at room temperature (25 °C) while hexagonal/trigonal plates are formed at 65 °C. XRD results show evolution of anisotropically grown, phase pure and well crystalline face centered cubic (fcc) Pd NPs at both temperatures. FTIR and SERS studies revealed adsorption of ascorbic acid (AA) and poly ethylene glycol (PEG) at NP's surface. Particle size distribution graph indicates formation of mesoporous particles having wide size distribution while the zeta potential particle's

surface is negatively charged and stable. The truncated octahedron/fivefold twinned pentagonal rods shaped Pd NPs, formed at room temperature while thermally stable and kinetically controlled hexagonal/trigonal plate-like Pd NPs have been evolved at higher temperature 65 °C. The obtained Pd NPs has a high surface area and narrow pore size distribution. To predict protein reactivity of Pd cluster, docking has been done with DNA and lung cancer effective proteins. The cytotoxicity of the Pd NPs has been screened on human lung cancer cells A-549 at 37 °C. The biological adaptability exhibited by Pd NPs has opened a pathway in biochemical applications.

The fourth chapter describes the synthesis of α-Fe_2O_3 NPs using polyethylene glycol (PEG) as a surfactant and L-ascorbic acid (LAA) as a stabilizer. The product has been characterized by UV-visible absorption spectroscopy, FTIR, Dynamic Light Scattering, particle size distribution analysis, X-ray diffraction analysis, TEM, FESEM, EDX and BET, which show formation of variable size and shape, mesoporous, PEG-coated α-Fe_2O_3 NPs (LAA@IONP-PEG) with β-FeOOH as an impurity. The present work emphasizes upon an anti-cancer study of LAA@IONP-PEG against renal carcinoma HEK-293 human embryonic kidney cell lines. The study suggests that LAA@IONP-PEG is a promising material against renal carcinoma HEK-293 human embryonic kidney cell lines. The docking study has confirmed anti-proliferative action of NPs through binding affinity with renal carcinoma molecular targets. The synthesized NPs show the synergistic effect with Axitinib as an anti-cancer drug effective against renal carcinoma cell lines. ROS and 1,1-diphenyl-2-picrylhydrazine (DPPH) free radical scavenging assay have shown the antioxidant capability of synthesized NPs. The efficient biocatalytic activity of LAA@IONP-PEG prescribes its use as one of the best suited drugs for the future perspectives against

fatal renal carcinoma and thus it is reckoned that synthesized NPs will have persistent utilization in different field of medical applications.

In the fifth chapter sonochemical synthesis of Cu_2O nanostructures (LAA@Cu_2O-PEG nanopolyhedra) by reduction of Cu(II) complex $K_3[CuCl_5]$ by L-ascorbic acid (LAA), stabilized by polyethylene glycol (PEG) and their cytotoxicity against HEK-293 Human embryonic kidney cell lines has been discussed. The products have been characterizes by UV-visible spectroscopy, FTIR, XRD, SEM (EDX), FESEM, TEM, particles size distribution and BET surface area analyses exhibited formation of well crystalline, mesoporous LAA@Cu_2O-PEG polyhedral nanostructures capped with PEG molecules. The molecular and computational analysis revealed the role of capturing protein in capping analysis and stabilization of Cu_2O nanopolyhedra. The synthesized LAA@Cu_2O-PEG nanopolyhedra were found to have a stable zeta potential in a range of -18±0.29mV. The IC_{50} of the prepared LAA@Cu_2O-PEG nanopolyhedra against renal carcinomas HEK-293 human embryonic kidney cell lines are in the range of 15-60 µM, inducing morphological changes in proteins.

In the sixth chapter controlled sizes and distribution nickel nanoparticles with enormous surface properties have been prepared by a novel method and cytotoxicity has been examined against cancer cell lines MCF-7 for the assessment of mortality and developmental changes. Nickel nanoparticles exposure was compared with respect to established antitumor drug. Cytotoxicity has significantly been increased when one or two layers of L-ascorbic acid and/or polyethylene glycol were deposited. Cytotoxicity and in silico studies suggested that the configuration of nanoparticles may affect cytotoxicity more and defects from Ni NPs exposure occur by biological MTT assay analysis.

In the seventh chapter Ag-Au nanocomposite has been prepared by reduction of silver and gold complexes ($K_3[AgCl_4]$),($K_3[AuCl_6]$) using L-Ascorbic acid (LAA) and polyethylene glycol (PEG) as reducing and capping agents respectively via sonochemical approach. The Ag-Au nanocomposite has been characterized by UV-visible absorption spectroscopy, FTIR, Dynamic Light Scattering (DLS), particle size distribution analysis, X-ray diffraction analysis, TEM, FESEM, EDX and BET. The data obtained exhibited formation of variable shape (like needles, rods, spirillum structures), mesoporous, LAA-PEG-coated Ag-Au nanocomposite (LAA-PEG@Ag-Au). Cytotoxicity of synthesized LAA-PEG@Ag-Au nanocomposite was analyzed against bronchial carcinomas A-549 lung cancer cell lines by MTT and SRB assays. Nanocomposites also induces the reactive oxygen species, (ROS) and suppression of reduced Glutathione, (GSH) resulting in damage to various cell components, DNA breaks, lipid membrane peroxidation and protein carbonylation which causes cytotoxicity by oxidative stress induced apoptosis and damage to cellular components The study suggests that LAA-PEG@Ag-Au nanocomposite is a promising material against bronchial carcinomas A-549 lung cancer cell lines. The docking study has confirmed anti-proliferative action of NPs through binding affinity with bronchial carcinoma molecular targets. The synthesized nanocomposite has shown the synergistic effect with cis-platin as an anti-cancer drug effective against bronchial carcinoma cell lines. ROS and 1,1-diphenyl-2-picrylhydrazine (DPPH) free radical scavenging assay have shown the good antioxidant capability of synthesized LAA-PEG@Ag-Au nanocomposite. The sulphorhodamine B (SRB) assay is used for the cell density determination, based on the measurement of cellular protein content. The study demonstrated that the lung cancer stem like cells obtained from A-549, which were cultured in serum free conditioned medium, had strong proliferation and self-

renewal abilities and expressed higher level of stem cell markers (CD24, CD44, CD90, CD133, CD147, CD166, CD326 etc.) as compared with A-549 adherent cells. The efficient biocatalytic activity of LAA-PEG@Ag-Au nanocomposite emphasizes its use as one of the best suited drugs for the future perspectives against fatal bronchial carcinoma and thus it is reckoned that synthesized LAA-PEG@Ag-Au nanocomposite will have broad utilization in different field of medical applications.

And in the last eighth chapter summary, conclusion and scope of further research work has been given.

CONTENTS

Chapter 1

General Introduction and Objectives of Current Work

"The chapter introduces a number of views described the method of synthesis of nanomaterials, nanostructure materials and their significance in biocatalytic reactions. The structure and properties dependent biocatalytic properties viz. anticarcinomas studies of nanostructure materials have been systematically reviewed. The leading objectives and brief framework of the present examination carried out in this thesis are described in brief."

1.1. Introduction

1.1.1. Nanotechnology

The credit for the discovery of the nanoparticles goes to Dr. Richard Feynman, (an American Physicist), by his famous talk, " That there is a plenty of rooms at the bottom" proposed in year 1959.[1] The term nanotechnology was initially coined by the Japanese scientist Professor Norio Taniguchi in an International conference held in Tokyo Science University, Tokyo in 1974 based on the subject on Production Enginering.[2] Professor Eric Drexler formulated the term nanotechnology in his famous book, "Engines of Creations" in 1986,[3] and popularization of knowledge of nanotechnology in his book, "Nanosystem : molecular machinery, manufacturing and computations".[4] Nanotechnology and its interdisciplinary fields are newly emerging advanced perspective area to import welfares in various fields of investigations and application in world of science and technology. Nanotechnology is commonly described an easily understandable, controllable and renovation of material on an atomic and molecular scale or in consequence of particles lesser in size estimated to lesser than 100 nm to produce materials built from them, essentially with novel behavior and properties.[5-6] The significance meaning of prefixed nano's is one billionth. The scaling of nanometer is equivalent to a billionth of meter scale or 10^{-9} part of a meter,[7] which indicates that these structures are extremely small (an inch is equal to 25,400,000 nanometers, a single sheet of newspapers consisting of 100,000 nm thickness or ten thousand times lesser comparable to width of human hair). As for an evaluation analysis the DNA's diameter, lymphocytes and viruses are 2.5, 20-30 and high on 7000 nm respectively.[8]

The present era witnessed that nanotechnology is an interdisciplinary field across the long established boundaries between information technology, engineering, chemistry, physics, biology and mathematics. These also give a great commitment to establish a future correspondence to develop breakthrough in modification for the direction of technological process in the massive range of utilities. It also summarizes a comprehensive study of research and improvement in the determination of accessing its perspective for technological innovations.

1.1.2. Nanostructures

The nanostructure of any shape and size are intermediate structure at microscopic and molecular level which possess one or more dimensions in a range of 100 nm or less.[5, 9] These nanosized structures contain enhanced behavior like improved hardness, ductility in ordinary inelastic materials, high tensile strength, erosion and corrosion resistance, wear-resistance and advanced chemical properties.[10] They are more popular in favor to its conventional and commercially accessible supplements, and possess a lot of commercial, scientific relevance in areas like drug delivery, analytical chemistry, bio-encapsulation, electronics, and magnetic, optical and mechanical devices. The modern area of technology has describing a number of nanostructures like one dimensional structure consisting nanotubes, nanorods, nanoribbons, nanowires to fascinate the terrific attention due to their fascinating properties and high aspect ratio.[11-15] This phase comprises the two dimensional electron confinement and delocalization along the axis of nanorod/tube/wire. One dimensional structure of several metals, metal oxide, semiconductor and its composites prepared by different routes are known and their applications have been projected for many sensors, solar cells and capacitors etc.

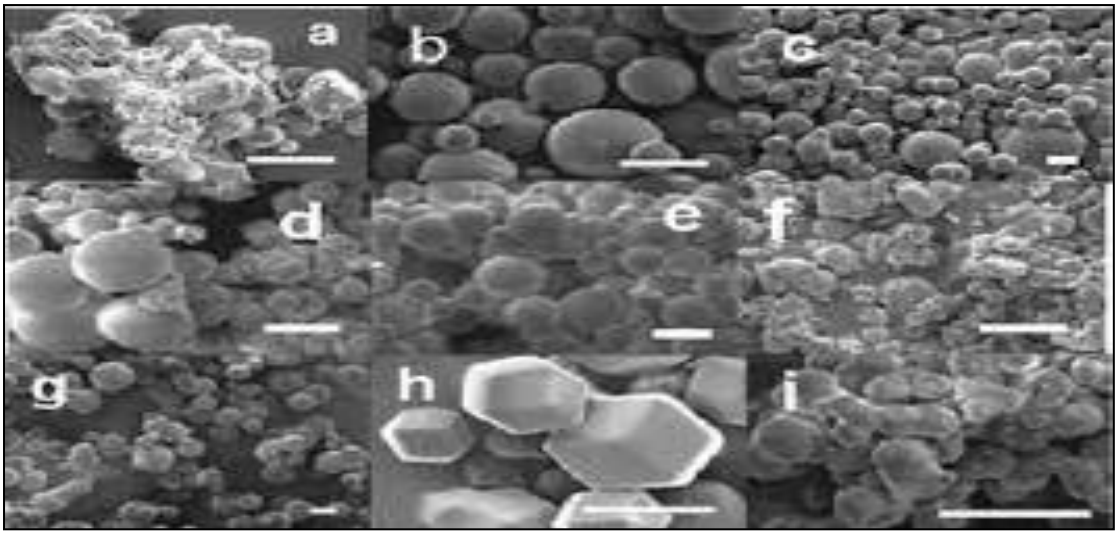

Figure.1.1. Different shapes of nanparticles.[11]

In year 2010, Noble prize was awarded to "Graphene", a single layered arrangement of carbon containing the state of hybridization sp^2 with honeycomb like resemblances. Due to its exciting physical and chemical behavior, it is used as a supporting substance with potential application in various devices.[16] So on behalf of aforementioned research, it is proved that graphene is a 2-D structure with its two dimensional nature performs significant role in identifying their exceptional set of behavior are recently shown preparation and accessing several inorganic equivalents of graphene i.e. various inorganic 2-D substance have enriched considerable attention.[16-17] These inorganic 2-D substances generally possess mono-layered graphene with a number of atoms and molecules. These are connected through weak Van der Waal forces and separated via exfoliation. The thickness of these mono-layered substances is reasonably less than 100 nm, the length and width may outstrip to nanometric dimensions. Noticeably, it has been attained on varying the number of monolayer; there is dramatic alteration in chemical properties. Among the numerous inorganic 2-D structures, the transition metal oxides and sulfides are well known for their comprehensive range of optical and electronic properties, which has increased

remarkable attention since past decades and considered as biggest competitors of graphene.

1.1.3. Types of Nanostructures

1.1.3.1. Nanoparticles

Generally, the nanoparticles are considered to be a most fundamental unit of technology and define particles in a size range of 100 nm and principally zero dimension in morphology. A numerous of nanoparticles are lesser in size and contain 21-15000 atoms, in range of Newtonian and Quantum scales.[18] These consist of single crystal, amorphous particles and polycrystalline substances with all probable morphological properties like cubic, spherical and platelets with a representative size of petty nanometers. Recently this field has attended an enormous attraction due to ability to synthesized, engineering nanotechnology and their utilization for the human welfares. So due to their more interest in science, this has been a more advantageous and evolutionary statement in the field of nanotechnology and its interdisciplinary sciences.[19]

1.1.3.2. Nanotubes

These can be described as one form of nanostructure material with one dimensional tube like hollow structure in nanometer scale to work as an electrical insulators or conductors. Credit for the discovery of nanotubes goes to L.V. Radushkevich et al. for their well-defined images of 50 nm diameter of carbon nanotubes in Soviet Journal of Physical Chemistry in 1952.[20] A single layer of nanotube contain one tube of graphite collectively known to be single walled nanotube (SWNT),[21] a numerous of several parallel and side by side tubes for their

multiwalled nanotubes (MWNT). Morphological properties of nanotubes control conductance, density and lattice structure.

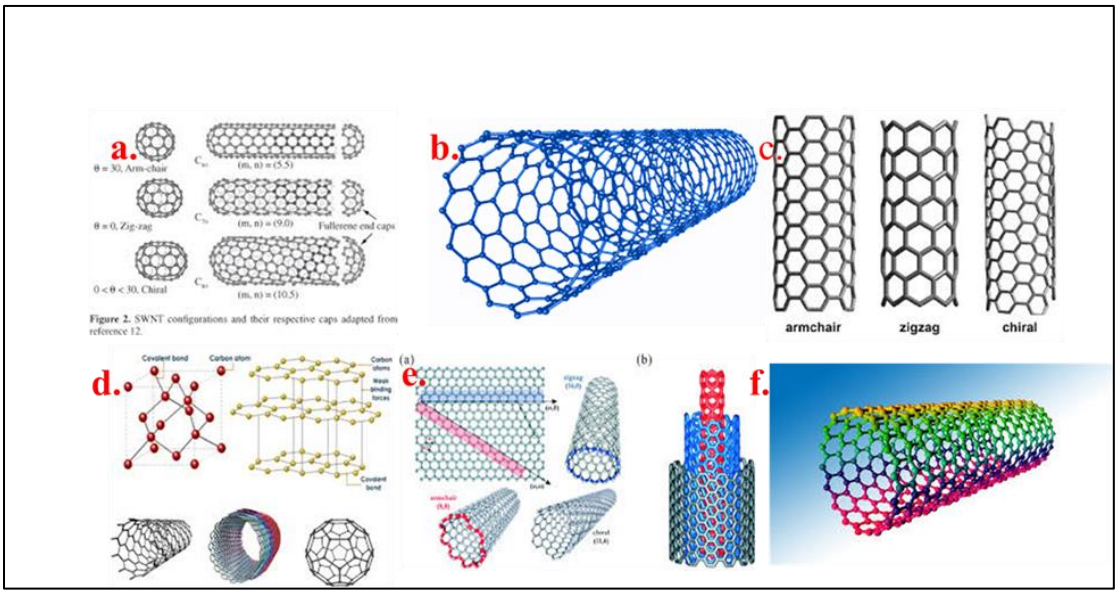

Fig.1.2. Types of nanotubes.[21,22]

Three kinds of nanotubes viz. armchair, zigzag and chiral, can be classified on the basis of enclosed carbon sheet arrangement in tube pattern with a well-defined geometry.[22] Kontos et al. proposed the nanotubular arrangement of titanium oxide (TiO_2) synthesized via electrochemical method using polyethylene glycol as solvents as an electrolytes. These nanotubular titanium oxides (TiO_2) are tested for the removal of organic contaminants like benzene and toluene under irradiation of ultraviolet light at room temperature and pressure. The photocatalytic behavior varies on altering the length of nanotube (NT) arrays.[23]

1.1.3.3. Nanowires

Nanowires are the special kind of nanostructures with one dimensional (1-D) orientation having cross sectional diameter in nanometer (10^{-9}) range. The nanostructures contain ratio of length to width greater than $1k^{th}$. These can also be

understood in terms of their thickness, which possess a strained thickness of 1-10 nm. At these stages the quantum mechanical effects are dominant and this stage is commonly known as the term "Quantum wires". Nanomaterials reforming towards the nanowires to afford more promising electron transport with minimum recombination loss than that from nanoparticles based solar cells. The main research work on the structural nanowires stated with very simple and three dimensional (3-D) classified nanostructure to improve higher photoactive efficiency.

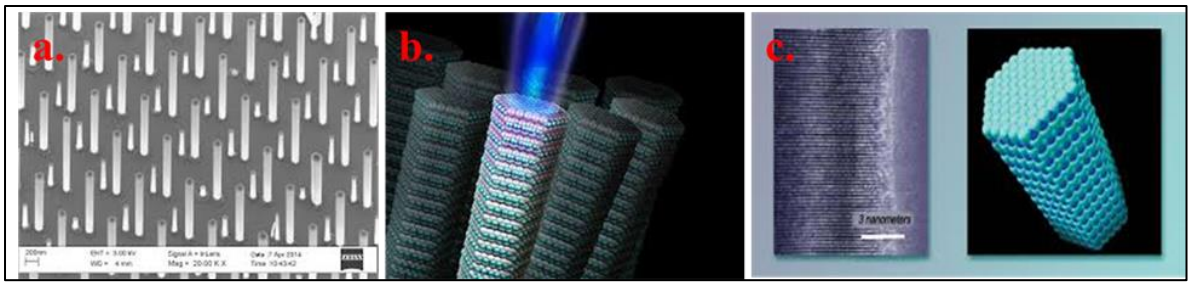

Fig. 1.3. a-c Structure of different nanowires.

1.1.3.4. Nanoribbons

These can be usually illustrated as two dimensional (2-D) layered structures with width approximated to 1-50 nm. Graphene were commonly received as nanoribbons. Pascal Ruffieux et al. mentioned that graphene based nanoribbons performed well electronic properties than continued graphene. Quantum confinement in terms of armchair nanoribbons and carbon nanotubes generate the considerable electronic band gap that are related to their structural boundary conditions.[24-25] The nanostructures containing zig-zag edges are estimated to host spin polarized electronic edge stage and serve as key points for the graphene based spintronics devices.[26] The electronic nanoribbons are mostly governed by structure of edges (armchair or

zigzag). Two dimensional structures of nanoribbons have an immense thermal and electrical conductivity.

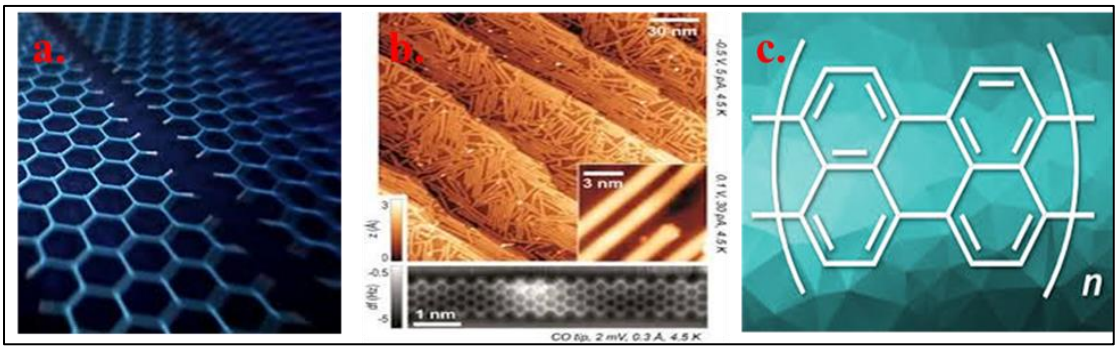

Fig.1.4.Different types on nanoribbons.

1.1.3.5. Nanorods

These materials are a one dimensional (1-D) nanostructure with their standard appearance ratio of length and width with in a range of 3-5 nm and their dimensions ranges from 1-100 nm. These may be fabricated through pure metals and semiconducting materials. These nanorod structured materials are initially interacting from their exclusive electrical and optical properties and optoelectronics with entirely depend on their morphological shape and size. The nanorods of silver and gold metals composites are being applied to be treated against cytotoxicity against cell lines passaging analysis, photovoltaic devices, and heterogeneous catalysis and chemical sensors because of its exceptional semiconducting and optical behavior. The optical behavior of these substance are a result of electronic interaction of electron of conduction band of metal and an electric field component of electromagnetic radiation but few cases Zinc oxide (ZnO),[27-33] has shown a forceful absorption in visible range of spectrum and in turn to unusual bright color which is not detected in bulk material.

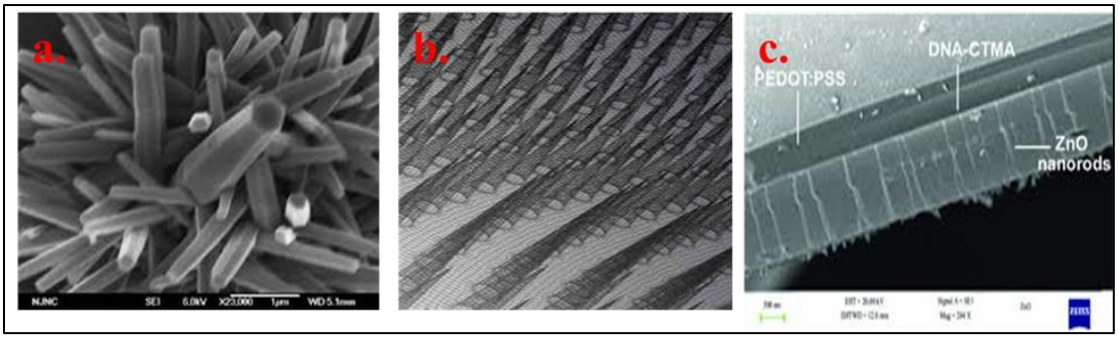

Fig.1.5. Differnt types of nanorods.

1.1.3.6. Nanocomposites

The multiphase materials which are achieved by the engineered consolidation of two or more dissimilar substances having one phase as reinforcing phase and occur in a kind of fiber sheet or particles. These can be implemented as supplementary materials as matrix phase. The most fundamental work of the matrix is to transmit stress between reinforced phases of matrix and defend them from machine driven and environmental destruction. Although an existence of particles in nanostructure composites increases its mechanical strength and stiffness. So an interdependent arrangement of more than two micro-components has dissimilar physical properties and chemical arrangement. The main intention of fabrication of composite material is to boost the property of substance without cooperating on the weakness of each other. Composite materials have symbiotically replaced the traditional materials in several advances such as light weight and high strength usage. An important justification behind the collection of composite material and their relevance is principally because of its extraordinary tensile strength at high temperature and more strength to weight ratio, high toughness and high resistance. The reinforcing materials of nanocomposites are robust with lesser in density and matrix is typically ductile and tough material. If the nanocomposite materials are systemically planned and

synthesized, they enhance the strength of materials with toughness of matrix to attain a combination of required properties, those even not gained in any material. The influence of composite initially depends on the quantity, arrangement and type of particle reinforcement in resin.

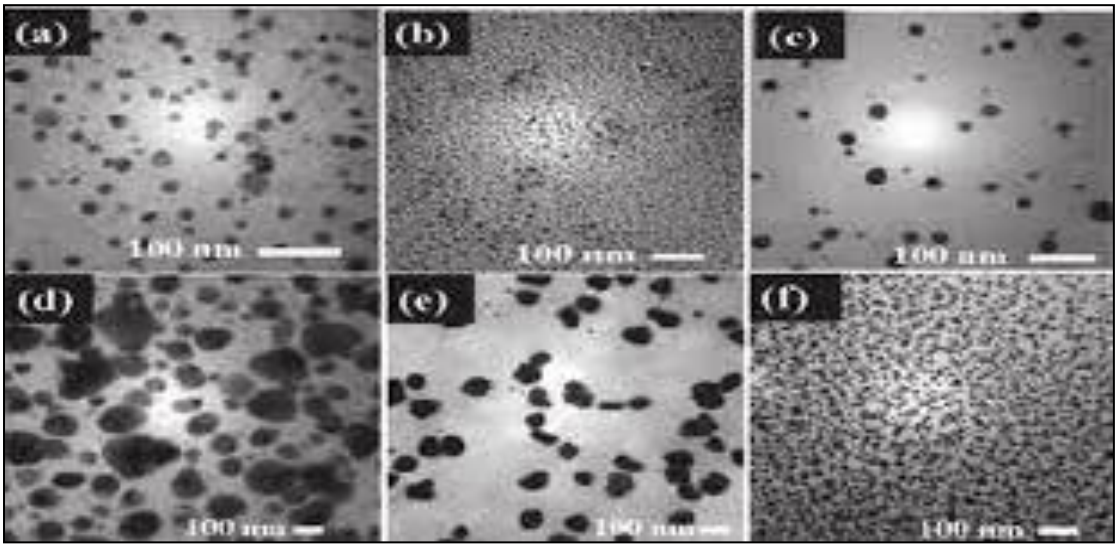

Fig.1.6. TEM images of Ag-Au nanocomposites.

Nanostructures also exhibit outstanding consequences for numerous applications such as antibacterial activity, bio-sensational behavior, gas sensation, paints, photo-catalysis, solar cell etc. Most commonly, palladium, iron, copper, silver, silver and gold composites, and cerium and ruthenium based nanocomposites are performing a number of photoactive performances including photocatalysis in visible light, cytotoxicity analysis etc. The metal oxide of zinc is also owe to appearance of intermediate states to absorb light to inhibit recombination of exciton during photoreduction.[34-37]

1.1.4. Properties of nanostructures

Nanostructure materials behave as a linkage among the bulk materials having the atomic and molecular structures. The bulk semiconductors are not able to change

with simple variation in shape and size i.e. in a bulk semiconducting materials, the properties are size independent and depend only on the chemical composition of materials. Due to their inimitable shape and size dependent wealth like photonics, optics, electronics and photo-catalytic performances, nanostructure materials have got more interest. The novel properties are fundamentally dependent on the shape and size of nanostructured materials or thin films as a result of contraction in dimension of materials or diminution in the length of nanoparticles below to ferromagnetic exchange length, Fermi level of electron etc.[38-39] The properties of nanostructure can be described as follows:

1.1.4.1. High Surface to Volume ratio

As the outer surface of nanomaterials have more significant characteristics and have shown vital properties against nanostructure materials. The existence of atoms on the outcome of nanostructure is more important chemically and thermodynamically related to their bulk atoms, as less neighboring coordinate system and more active bonds. The imperfections present on the nanoparticles produce or generate sub electronic states in the ground states in band gap, which shows trapping behavior for an electron or hole (exciton). For the nanoparticles the relation between the surface area and radius are inversely proportional to one another. So the relation between surface properties and size of nanostructures are interconnected,[40-43] the surface to volume ratio increases with the decrease in size value, the surface effects become more apparent and thereby easier to explore. Apart from this the gap between the energy levels of nanostructures are also concerned by these effects.[41-43] The system which has only few hundred atoms, an enormous number of atoms will be positioned on outward. Smaller the nanomaterials, greater the energy of surface contributed to the total energy of the surface, which makes considerable differences in

the properties of materials. Imperfections, size and residual stress etc. are also known to impact the ownership of nanoparticle materials.

1.1.4.2. Quantum confinement

Quantum confinement alters the optical performance of nanostructure materials. The optical, electronic and magnetic behavior of nanomaterials depends mainly on the size.[44] The electronic energy level are not in continuous as in bulk materials, and are changed to discrete and quantized energy level owing to the electronic confinement wave function to the spatial arrangement of particles. This phenomenon is known as quantum confinement and nanocrystals are said to quantum dots. So the electronic transition between the bands becomes discrete. The increase of band gap energy of semiconducting substances are a result of reduction in size or quantum confinement influences as compared to bulk materials.[45] The materials associated with larger nanoparticles, the excitation of electron throughout the band gap hinges the energy difference between the valence and the conduction band. When the size is confined near to the Bohr radius, quantum confinement effect initiates to impact the excitation energy throughout the band gap.[46-48] Based on the orientation of the environment, the quantum confinement have been subdivided in to three major categories as quantum wire, quantum well and quantum dots or nanocrystals.

Structure	**Quantum confinement**	**Number of free dimensions**
Bulk	0	3
Quantum well	1	2
Quantum wire	2	1
Quantum dot/ nanocrystal	3	0

1.1.4.3. Brownian motion

Brownian motion is originated by the irregular and continuous motion of miniature particles in liquid or gas. The particles of molecules are suspended entirely in the liquid or a gas due to inherently random nature of motion and collision with the bigger suspended particles, making them movable. At microstate level we can hardly see the movement of particles or why they move, but in case of Nano's origin, they move widely batted about by smaller particles.

1.1.5. Applications of nanostructures

1.1.5.1. Drug Delivery

A number of kind of nanostructures that can be used in drug delivery system, although these inorganic nanostructure can be utilized for their significant consideration since recent decades for consequence of their exceptional properties like high loading ability, chemical and physical robustness, less toxicity, straightforward and cheap manufacture in laboratory. Dendrimers like hyper-branched are class of nanostructures, having fabrication for wide applications to treat and the diagnosis of carcinomas. In these the drug molecules can be lined to side branches, and can be applied as specific coating agents to safeguards or distribute drugs to required sites or work as time release machine for biologically active agents in body. They also work as healing agents in the remedy of cancer, known as Boron Neutron Capture Therapy (BNCT). This medical procedure contains an injection of isotope of boron (^{10}B) along with non-radioactive pharmaceuticals. It is selectively migrated to the cancerous cells. When an injection of boron (^{10}B) is administered to patient, it is thermally treated with neutron and it be reacted with boron to release a number of alpha particles, in cancerous cells which destroy the tumor cells.[49] Dendrimers are also helpful in gene therapy by working as vectors, who are transporters, which transport genes through

the cell membranes to the nucleus.[50] Apart from these medical applications, they are also applied to expand industrial processes.

1.1.5.2. Space applications

A number of carbon nanotube (CNT) has been acquired for the utilization in space,[51] which significantly decreases the mass of space structures. These are excellent structures for the usage in space elevator cables, in respect to their unique properties like light weight and more strengthen nature. Carbon nanotubes (CNT) are also applicable for the further advancement of solar cells. These weightless nano-devices are used for the reflection of sunlight for the mobility of spacecraft and save huge amount of commercial fuel in the form of energy. So the use of nanostructures in the form of nanorobots is being used for making space suit for the aeronauts to protect themselves from space rubbles. Due to lightweight and stretching nature of nano-materials, these can be used as a coating agent to anti-corrosion and applicable in aerospace constituents like landing gear and constructive apparatus like drill bits and bulldozer blades.

1.1.5.3. Electronics

The carbon-nanotubes like nanostructures (CNT) are being utilized for the manufacture of hybrid with many types of polymer to fabricate composite samples and applicable as an electromagnetic protector in cell phones and static electricity resistance in cars. The applicability of carbon-nanotubes is being well known for the applications in the flat displays. In Light Emissive Diode (LED) recently zinc oxide (ZnO) and gallliun nitrides (GaN) nanoparticles are used.[52] In latest modern time, zinc oxide (ZnO) nanowires are being used for the display pattern on the flexible pattern.[52] LASER devices are composed of array of quantum dots and nanowires.[53] Carbon nanotubes (CNT) and nanostructures of cobalt, manganese and vanadium are being

useful in lithium-ion batteries for their improved importance.[53] Coated and dopants semiconducting materials are applicable for making some electrical goods to protect its properties. Silver nanostructures with polymer resin are used for the manufacture of major parts of refrigerator in order to restrict the growth and enhanced variety of bacteria and quashed odors. Besides applying coating with silver nanoparticles with coating agents other methods like silver wash method is applicable to expand the cleaning of cloths.

1.1.5.4. Displays

The manufacturing of displays with small consumption of energy could be consumed by consuming carbon nanotubes (CNT) which are used as a good conductor of electricity as consequence of their petite diameter of several nanometers. These can also be applied for the field emitters with an enormous high efficiency in field emission displays (FED).

1.1.5.5. Catalysis

The assistance of catalysis particularly from nanostructure materials have owed large surface to volume ratio. There is an extensive range of structures of nanomaterials from the fuel cells and catalytic conversion of photo-catalytic devices or the removal of contaminants of organic dyestuffs from the waste water. Inorganic metal semiconductor nanostructures have huge surface area so that there is an enhanced catalytic activity in short time interval owe to more catalytic reaction at an outer face. Nanocatalyst are simply isolated and reproduced with greater retention of catalyst activities than their bulk counterparts. The catalyst can effort as two different roles in degradation process, they can be the site of catalysis or they act as support for the catalytic pathway.[54]

1.1.6. Methods of synthesis of nanostructures

A number of methods have been applied for the synthesis of nanostructures, but two elementary processes are required with various rates of quality, cost and speed:

Top down method: Involve the breaking down of bulky fragments of materials to produce the preferred nanostructures as physical method.[54]

Bottom up method: Involve the collection of single atoms along with molecules into an essential nanostructures as chemical method.[55]

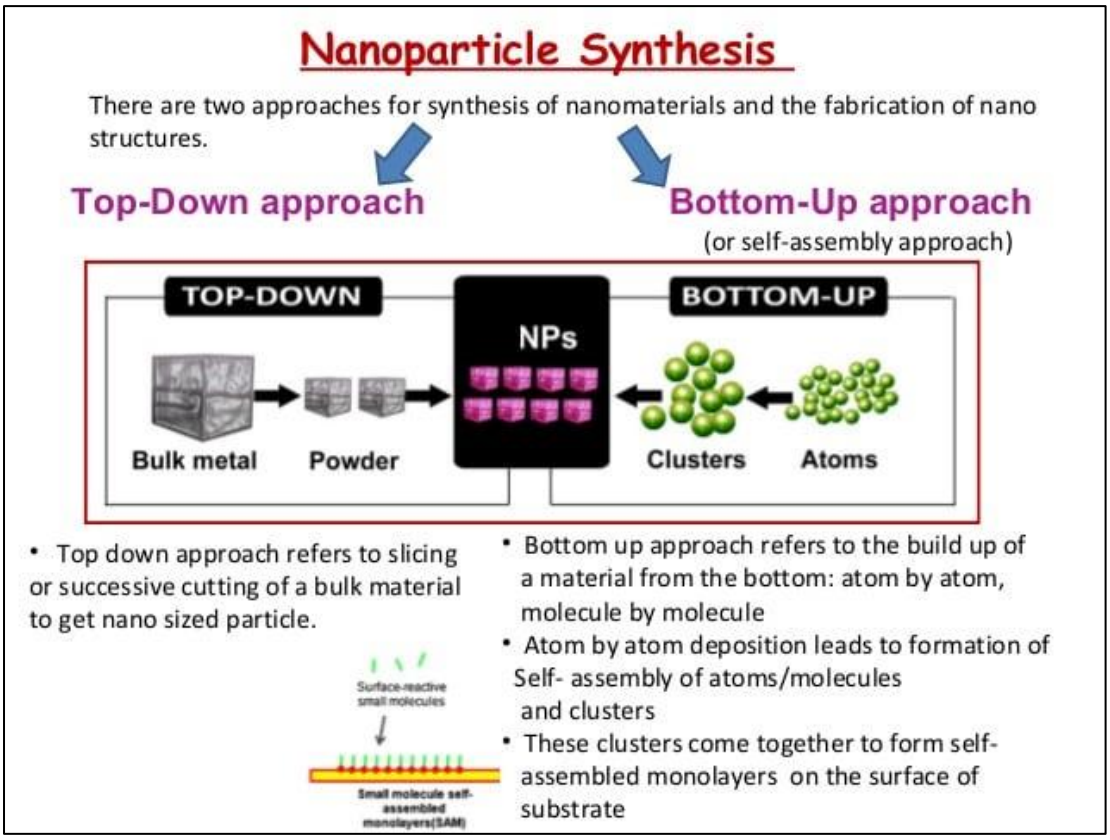

Fig.1.7. Synthesis of nanoparticles by top down and bottom up methods.

Many disciplines including subjects like physics, chemistry, biology and engineering are pursuing a wide assortment of methodologies for producing

nanomaterials. A number of techniques for the fabrication of nanoparticles are generally classified as either physical or chemical methods.[55]

1.1.7. Chemical method

1.1.7.1. Chemical vapor deposition

This is a chemical technique pragmatic for the fabrication of high purity and high functioning nanostructure solid samples. This is defined as any chemical process in which formerly precursor materials are vaporized and finally condensed for the solidification to produce solid phase materials. The methods are ordinarily applied to fabricate the coated materials to modify the corrosion resistance, electrical, mechanical, thermal, optical, and wear hindered properties of numerous substrates. These can also further applicable to design free-standing bodies, fiber, films and to infiltrate template to form the nanocomposite samples. Since recent time they have been commonly explored for the synthesis of several nanostructures. This method is typically occurring in a vacuum chamber. In this process if no chemical reactions are taking place, and then it is known as physical vapor deposition (PVD) otherwise it is termed as chemical vapor deposition (CVD).

1.1.7.2. Sol-gel method

This is a very imitable and versatile wet method for the production of various advanced nanostructure materials with cost effective, low cost at minimal temperature and informal control of shape and morphology.[56-60] The characteristic sol gel method, consisting hydrolysis of precursor materials e.g. inorganic salts, metal alkoxides and organic polymers, poly-condensation to produce suspended sol and then sol transformation occurred to gel phase by freezing process. Then, drying of this wet gel

along with treatment produces crystalline nanostructured materials. A vastly porous and low density material termed as aerogel is produced.

1.1.7.3. Hydrothermal synthesis

This includes a common and versatile method, accompanied in stainless steel containing container at an appropriate high temperature known as an autoclave. The autoclave discipline temperature or pressure along with Teflon liners with reaction medium solution, (aqueous). This process consisting, the reaction temperature to be enhanced boiling point of water (solvent) and extending pressure to vapor saturation. The core pressure be fashioned, during the reaction is hinged upon the quantity of solvent containing the autoclave. There are a number of groups of researchers, who had also used this technique for the fabrication of TiO_2, ZnO nanostructure,[61-65] etc.

1.1.7.4. Chemical co-precipitation

This is a very widely adopted method for the synthesis of desired nanomaterials like metal oxide nanoparticles, from its inorganic salts or precursors salt solution by the addition of salts in an inert atmosphere (in an existence of nitrogen or argon gases) at common temperature or at desirable temperature in huge scale with reasonable charge. The elemental composition like shape and size of the particles are mainly hinge for the precursor used (sulfates, chlorides, and nitrates). Nanostructure materials can be produced by two general ways viz. addition of basic solution in a very slow manner and in fast manner into precursor salt solution of metal.[66-69]

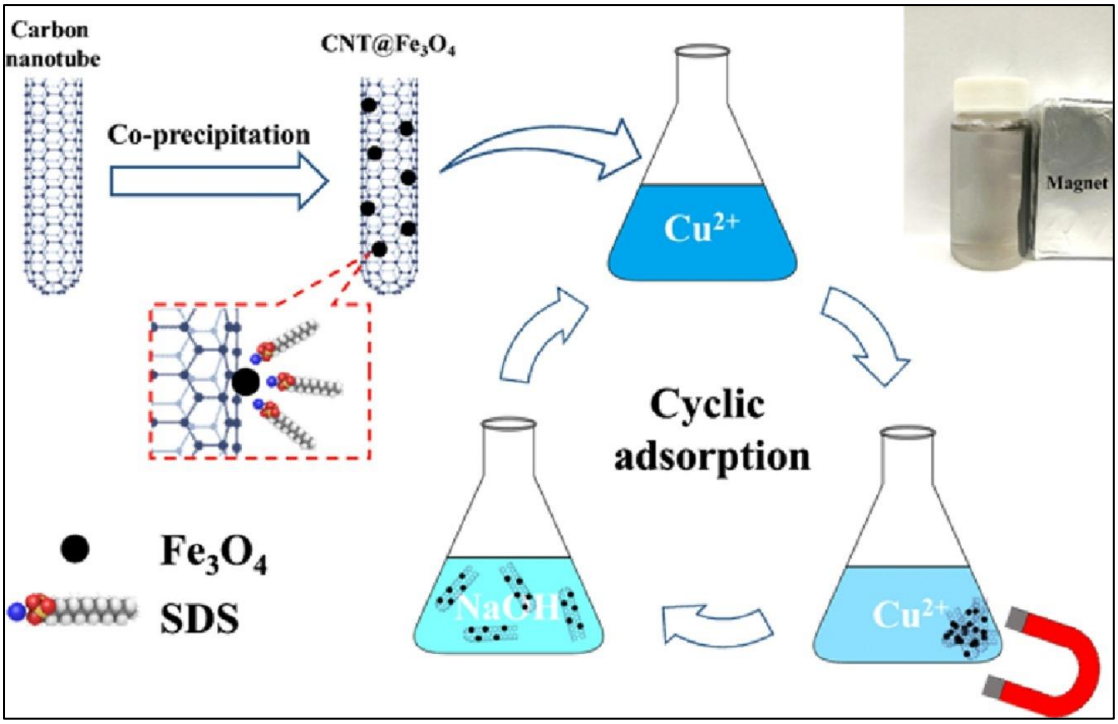

Fig.1.8. Co-precipitation method of preparation of nanoparticles.

1.1.7.5. Micelle and inverse micelle method

This includes the general accumulation of surfactants with well-mannered circulation of colloidal liquid at above the surfactant concentration known as critical micelle concentration (CMC). It is the concentration of surfactants, free solution in equilibrium with surfactants in an aggregated form. Micelle contains two parts, head and tail. Head part is hydrophilic in nature and is oriented towards the surrounding aqueous solvents and tail, hydrophobic lying towards the interior of micelle center. The concentration of existing lipid in solution has determined the self-organization of surfactants and lipid molecules. Lipid created layer on the outward of liquid and are dispersed in a solution below the CMC. CMC is ascertained by the chemical composition along with the ratio of head area to the tail length significantly. Reverse micelle are established in non-aqueous solvents owing to the arrangement of hydrophilic head group and hydrophobic tail group as inverse to each other. So, head

moves to inner side toward the center of micelle while hydrophobic tail is moved outward towards the non-aqueous media. Micelles have shaped like globular and roughly spherical and cylinder, ellipsoidal, bilayers are also possible. The shape of micelle is molecular arrangement of its surfactants molecules and solution circumstances like surface, concentration, pH, temperature and ionic strength.

1.1.7.6. Sonochemical technique

These methods employ high energy sound waves for construction of an ample range of nanoparticles containing huge surface area of transition metal oxides, sulfides, alloys, carbides and colloids. In the synthetic sonochemical process, transient high energy ultrasound waves with standard frequency is obtained into a reaction of meticulously selected metal complex precursors. Owing to vapor pressure, assured threshold during the sonolysis in solvent have wave discontinuity in solvent extraction and miniaturization origin cavities for construction, growth and collapsing of bubbles in liquid.[70-71]

1.1.7.7. Solvothermal process

The technique is virtually analogous to hydrothermal process excluding the non-aqueous solvents used in this method. In this technique, the enhanced temperature related to hydrothermal method, which is a cause to use dissimilar types of organic solvents possessing high boiling points. The solvothermal technique generally has much control than hydrothermal method for the fabrication of desired shape and size with homogenous distribution of crystalline nanostructures. This technique has been adopted as versatile tool for the fabrication of versatile of electric variety of nanostructure with required size and shape distribution.[72-74]

1.1.8. Physical methods

1.1.8.1. Physical vapor deposition

This method illustrates methods describing the vacuum deposition technique operated on the prepared nanomaterials and its coated substances. This method involves the vaporization of the precursor and then condensation to get nanostructures. The principal method for this technique involves thermal deposition, ion plating, ion implantation, sputtering, laser vaporization and laser surface alloying.

1.1.8.2. Laser ablation synthesis

The technique deals with the fabrication of nanostructure materials by applying high energy laser beam. This technique comprising the high energy laser beam concentrated on the reaction mixture. The laser beam conveys the short beam of high energy, adequate to evaporate the small portion of metal objective compressed in nanostructure material in reaction solvent. This technique is applied to produce the nanostructure samples of gold, silver, platinum, etc. However, this may be expanded to the fabrication of other nanostructure materials like metal alloys. The advantage of short pulse beam in this process is to consent the ablation process to accept a number of mediums containing more volatile to vastly reactive monomers. This process can be applied to a wide range of sample and reaction solvent assurance.

1.1.8.3. Mechanical Milling process

This method is applied to the fabrication of nanostructure materials for its simplicity and flexibility in an industrial scale. This process consist the bulk material to strongly pulverize in milling process to fabricate nanoparticles which also exist in various dimensions.

1.1.8.4. Arc discharge method

This is also a physical method for the synthesis of nanostructure materials. In this process, nanomaterials are produced through arc asserted dissection of bulk materials. In this process, two electrodes are held closer to each other and high voltage applied between them to produce electrical disruption for ion discharge. Enhancement of arc discharges to produce the thermal discharge and increases the temperature of plasma to some thousand degrees Celsius which potentially vaporizes the surface of electrode in the reaction medium. They produce the metal compact in the reaction medium to fabricate the nanostructure substances. The compacting reaction medium, applied voltage and electric current are the foremost factors that are responsible for the production of nanostructure materials. An enormously huge temperature created in between the nearer electrode to assist the aggregation of atoms to produce new particle that is dissimilar to electrode materials. The carbon nanotubes (CNT) are most frequently for this process.

1.1.9. Nucleation and growth of nanoparticles in solution phase

1.1.9.1. Classical nucleation

It is considered as a process which atomic nuclei work as a process for the crystal growth. Mullin has proposed that primary nucleation is an earlier instance of nucleation in which the absence of any other crystalline matter.[75] This can be applied to understand the nucleation of several chemical synthesis.[76-77] However the production of various types of solids do not constantly obeyed the classical method of crystallization in solution. Further, Habraken et al. has proposed that ion combination complex come together for biomimetic nucleation of calcium phosphate in classical and non-classical means. When uniform nuclei are formed in parent phase then homogenous nucleation arises and in case of heterogeneous nucleation,

inhomogeneity's structure like container surface, impurity, grain boundary and dislocation etc. In case of a liquid phase heterogeneous smoothly stable nucleating surface is also present. The nuclei obtained by the homogenous process can be thermodynamically stabilized by the total free energy of the particles describe as summation of surface free energy and bulk free energy.[75,78] If we consider the radius of spherical nanoparticle be r, surface energy, γ and bulk free energy as ΔG_v, have providing a total energy as given by the equation. The own free energy of the crystal ΔG_v depends on the atmospheric temperature (T), Boltzmann's constant (k_B), super saturation of solution (S) and molar volume (V). Then ΔG_v is described as in given equation:

$$\Delta G = 4\pi r^2 \gamma + \frac{4}{3}\pi r^3 \Delta G_v$$

$$\Delta G_v = \frac{\{-k_B T \, ln(S)\}}{v}$$

The surface energy is always a positive value due to this; the crystal free energy is always a negative quantity. It is possible to obtain the maximum free energy, which passes through a nucleus forming stable nucleus by differentiating ΔG w.r.t. r, and give it to zero i.e. dG/dr = 0, which provides a critical free energy. The pathway of critical free energy can be described as:

$$\Delta G_{crit} = \frac{4}{3}\pi \gamma {r_{crit}}^2 = \Delta G_{crit}^{homo}$$

$$r_{crit} = -\frac{2\gamma}{\Delta G v} = \frac{2\gamma v}{k_B T \, ln(S)}$$

The critical radius is related to their size, so that particle can stay alive in solution in lack of re-dissolution. The same process is to be applied on particle free energy, where critical free energy is mandatory to achieve stable in solution.

The kinetics of nucleation of N nanoparticles at time (t) can be defined with the help of Arrhenius rate equation:

$$k = A\, e^{-Ea/RT}$$

Where A is pre-exponential factor.

$$\frac{dN}{dT} = Aexp\left(\frac{-\Delta G_{crit}}{k_B T}\right)$$

$$\frac{dN}{dt} = Aexp\left(\frac{16\pi\gamma^3 v^2}{3{k_B}^3 T^3 (lnS)^2}\right)$$

Where S is super saturated solution, T is an absolute temperature, and ΔG_v is the surface free energy. Kwon and Hyeon,[78] studied by plotting these parameter. The super saturation shows the maximum effect on the rate of nucleation, when it changes its value from 2-4, the nucleation rate enhanced about 1070 times and deviation in the surface free energy produced by various surfactants.

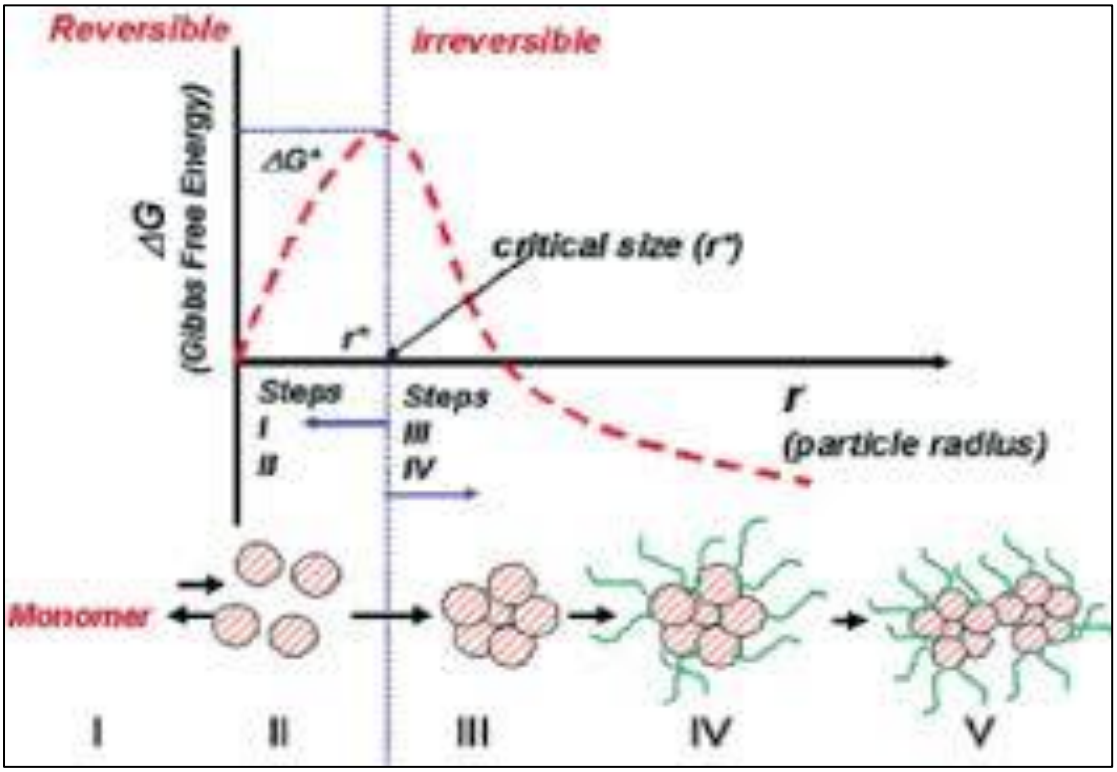

Fig.1.9. Free energy diagram of nucleation elucidating, presence of critical nucleus.

1.1.9.2. Classical growth

The growth of nanostructure materials mainly depend on the surface reaction and diffusion monomer on the surface.[79] The growth of nanostructures by diffusion on the surface is illustrated by the Fick's first law as:

$$J = 4\pi x^2 D \left(\frac{dC}{dx}\right)$$

Where x is the particle radius, D is the diffusion coefficient, C is the concentration at distance x respectively, and J is total flux of the monomer passes through a spherical plane with radius (x).

Fick's first law can be used for the case of growth of nanoparticles in solution. The distance from particle surface to the bulk of monomer is δ, bulk concentration (C_b) of solid/liquid monomers, C_i and C_r are the solubility of particle.

$$J = \frac{4\pi Dr\ (r + \delta)}{\delta}(C_b - C_i)$$

As J is irrespective of x due to steady state of solute diffusion, the integration of C_x from (r + δ) to r gives equation:

$$J = 4\pi Dr\ (C_b - C_i)$$

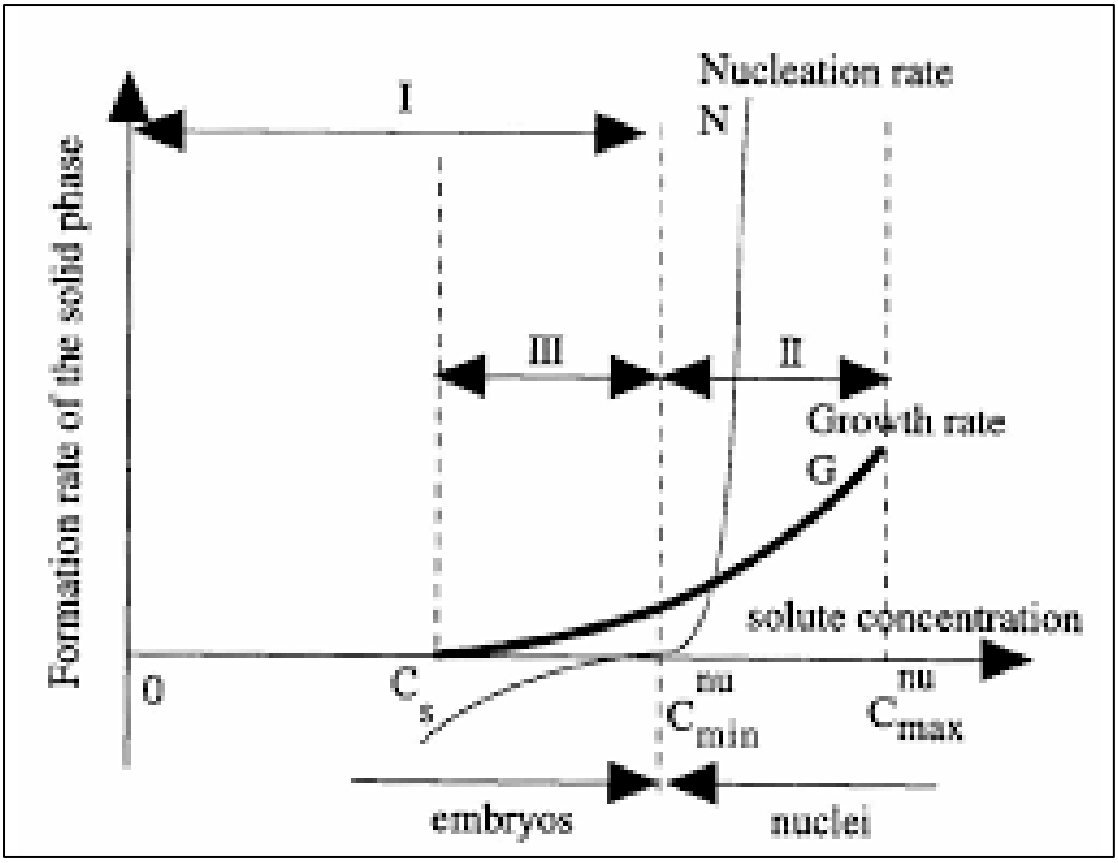

Fig.1.10. Growth of nanoparticles in terms of nucleation rate.

The equivalent equation can be used for the kinetics of surface reaction k. Rate of reaction does not depend on the size of the particles.

$$J = 4\pi r^2 k\,(C_i - C_r)$$

So it is clearly shown from the above equation that, there are two surface parameters either the monomer diffusion on the surface or rate of reaction of monomer on the surface. If limiting parameter is diffusion then variation in size of particle with time is given by the given equation:

$$\frac{dr}{dt} = \frac{Dv}{r}(C_b - C_r)$$

Correspondingly if the limiting parameter is the surface reaction then:

$$\frac{dr}{dt} = kr(C_b - C_t)$$

But when the growth of particle is not dependent on the both limiting parameter, then increase in particle radius with time is represented as:

$$\frac{dr}{dt} = \frac{Dv(Cb - Ci)}{r + \frac{D}{k}}$$

It is well understood that solubility of nanoparticles is dependent on the particle size and Gibb's- Thompson equation, a spherical nanoparticle has chemical potential $\Delta\mu = 2\gamma v/r$. Then C_r is the solubility of particle as a function of r, where v is the molar volume of bulk crystal and C_b is the concentration of bulk concentration of solution.

$$C_r = C_b \, exp\left(\frac{2\gamma v}{r k_B T}\right)$$

For the growth of nanoparticle which is already expressed, can be formed by the combination of equation as given by the above equations:

$$\frac{dr^*}{d\tau} = \frac{S - exp\left(\frac{1}{r_{cap}}\right)}{r_{cap} + K}$$

Where, all the constants are described as follows:

$$r_{cap} = \frac{RT}{2\gamma v} r$$

$$\tau = \frac{{k_B}^2 T^2 D C_b}{4\gamma^2 v} t$$

$$K = \frac{k_B T D}{2\gamma v k}$$

In the given equation $2\gamma v/k_BT$ is the length of capillary and K is known as Damkohler constant. This constant demonstrates the reaction is diffusion or dependent on the rate. If D <<1, then nuclear diffusion is independent on the surface reaction.

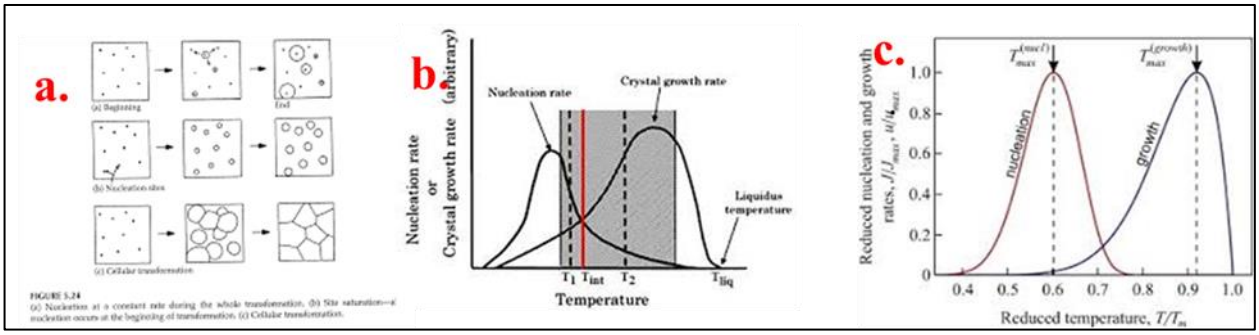

Fig.1.11. Rate of nucleation as a function of temperature of crystal growth.

1.2. Theory of nucleation and growth

A number of theories have been represented to describe the method of nucleation and growth of nanoparticles in solution phase.

1.2.1. La Mer mechanism

This method was first described by the La Mer et al. in the preparation of sulfur sol colloids from homogenous aqueous medium experiment in 1950.[80-81] They explained the nucleation and growth conceptually by separating in two stages. Firstly, to produce free sulfur sol from decomposition, solid thio-sulphate, and sulfur sol are formed in solution. For the better understanding of nucleation and growth by La Mer method, it can be categorized into three categories. First category comprising the free monomers concentration in solution, second stage involved the burst nucleation of monomers, which incomparably decrease the free monomer in solution. The rate has been determined by the slowest step of this nucleation and after this there is no

nucleation occurs due to minimization of concentration of monomers at this point and finally in third category, growth of particle occurring at controlled diffusion of monomer in solution. All the three categories can be represented by extrapolation of concentration of monomer with time function. An excellent example of this has been described in case of silver halides.[82]

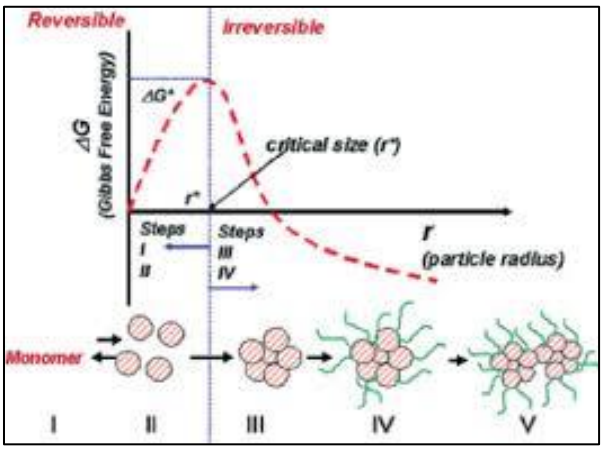

Fig.1.12. La Mer schematic.

1.2.2. Ostwald ripening and digestive ripening

This is consider as the method of synthesis of growth initiated by the variation in solubility of nanoparticles dependent on their size and can be easily explained by Gibbs-Thompson equation. Because of high surface energy and solubility of smaller particles in solution, these are re-dissolved and allow the formation of larger particles. The mathematical explanation of Ostwald ripening mechanism in closed system is defined by Lifschitz, Slyozov and Wagner.[83-84] Digestive ripening and Ostwald ripening mechanism are reverse to each other. Digestive ripening is more efficient than the Ostwald ripening. According to digestive ripening system, the growth of smaller particles is due to the destruction of larger one and it is better explained by the Lee et al. where related Gibb's Thompson relation is applicable.

1.2.3. Finke-Watzky mechanism

This mechanism can be explained in two step where nucleation and growth occur simultaneously.[85] In first step, relaxed but continuous nucleation occurs while in second self-catalytic growth takes place which is not controlled by the nucleation process.[86]

$A \rightarrow B$

$A + B \rightarrow 2B$

This mechanism was realized by the reduction of transition metal salt through hydrogen which was explained by the reduction of cyclohexane.[87]

1.3. Factors affecting the growth of nanoparticles

1.3.1. Effect of pH

For the measurement of growth rate of materials with chemical route in solution phase, the pH value of solution plays an important role in the production of final product. For e.g. the effect of pH on the ZnO nanostructures has been carefully measured before and after the growth. G. Amin et al. reported the synthesis of high density nanostructures in solution phase at $pH_{initial}$ (6.6) in 5 hrs. This experiment indicates in this medium only rod like structure can be developed. Rising the pH from 6.6 to 8, the morphology of ZnO nanostructure materials change from rod like to tetrapod.[88] This can be described by the specialty of hydroxide ion concentration in the initial solution, providing the growth in anisotropic directions. On increasing the pH upto 9.1 the growth rate further increased, due to rising in the concentration of hydroxide ion, which provides a flower like pattern of ZnO nanostructures with thick

arms in solution phase. On further rising the pH from 9.1 to 12, sea urchins like nanostructures of ZnO, with a needle length and diameter of ~50 nm is synthesized. Parallel surface morphological nanostructures were achieved at a pH of 12.5 because of the formation of tetrahydroxyzincate(II) $[Zn(OH)_4]^{-2}$ intermediates in reaction medium. However in acidic medium, large 2-D rods were formed at pH < 4.6, no growth was achieved when pH value was dropped by the addition of HCl, because of the fact that etching is dominating over the growth.

1.3.2. Effect of concentration

It is well known that raising or lowering the concentration of precursor of chemical reactors, ultimately affects the final products. G. Amin et al. reported that the growth of ZnO nanoparticles in aqueous medium, have found the micro-rod like structure at high concentration of precursor reactant,[89] at very low concentration, have obtained the nanowires and nanorods of ZnO nanostructures.[90] This suggested a good control over the chemical reactants that can be applied to improve the direct resistor over the dimension of ZnO nanostructures. So from this conclusion more research has been studied the effect of precursor concentration on the concentration of nanostructures at constant pH value. On varying the concentration of precursor density, diameter and length of synthesized nanostructure varies, at higher concentration produced at micro sized ZnO nanostructures with densely packed along c axis. Zhu et al. had fabricated the ZnO based core/shell nanostructure by applying 5 mM precursor with a shorter time by modifying the aqueous solution.[91]

1.3.3. Effect of temperature

The effect of temperature has an importance over that influence of formation of nanostructures just advantageous to pH and concentration. The synthesis of nanostructure materials by physical method involves the highest temperature (350 °C) but chemical process involves the temperature as usually less than physical method. Under the most circumstances the fabrication of nanoparticles using in green nanotechnology needs temperature lower than 100 °C or room temperature. The temperature of precursor reaction medium controls the nature of synthesized nanostructures.[92]

1.4. Semiconductor nanostructures

These have gaining attention due to cause of its shape and size dependent photo-physical and photochemical properties in various branches of chemistry, physics and material sciences, which differentiate it from the bulk semiconductor. They adopt several geometrical properties due to its electronic structure that can exhibit their conductor, semiconductor and insulator properties. The use of semiconducting nanostructures in opto-electrical device makes it a special class of material. These nanomaterials have technological potential for application in various areas as light emitting diodes and photo detectors, lasers,[93] photovoltaic solar cells,[111] photocatalyst for water splitting or dye degradation,[94-95] and biomedical field,[96-97] etc. For example most of the nanostructures have been used as a catalyst for industrial applications like oxides as active phase, promoter and support. The various types of semiconductors with their band-gap values are listed as:

Semiconductor	Band gap energy, (eV)
Diamond	5.4
Cu_2O	2.172
CuO	1.20
ZnS	3.6
TiO_2	3.03
SnO_2	3.54
ZnO	3.36
CdSe	1.70
WO_3	2.76
Si	1.170
Fe_2O_3	2.3
PbS	0.286
PbSe	1.65
ZrO_2	3.87
Ge	0.744
CdS	3.42
Ag-Au NPs	3.75
Ce-Ru NPs	2.76
Ni NPs	3.45

1.4.1. Fundamental theory of semiconductors

In a photoactive semiconductor a number of terms like valence band (VB), conduction band (CB), traps sites and Fermi level are used. In materials, bands are allowed energy states in which electrons can occupy in their states. The highest

energy band filled by electrons are called valence band while the empty energy level, next to valence band is known as conduction band. Semiconductors have clearly separated bands than that of metal. The energy difference between the top of valence band and the bottom of conduction band is called band gap energy (E_g).

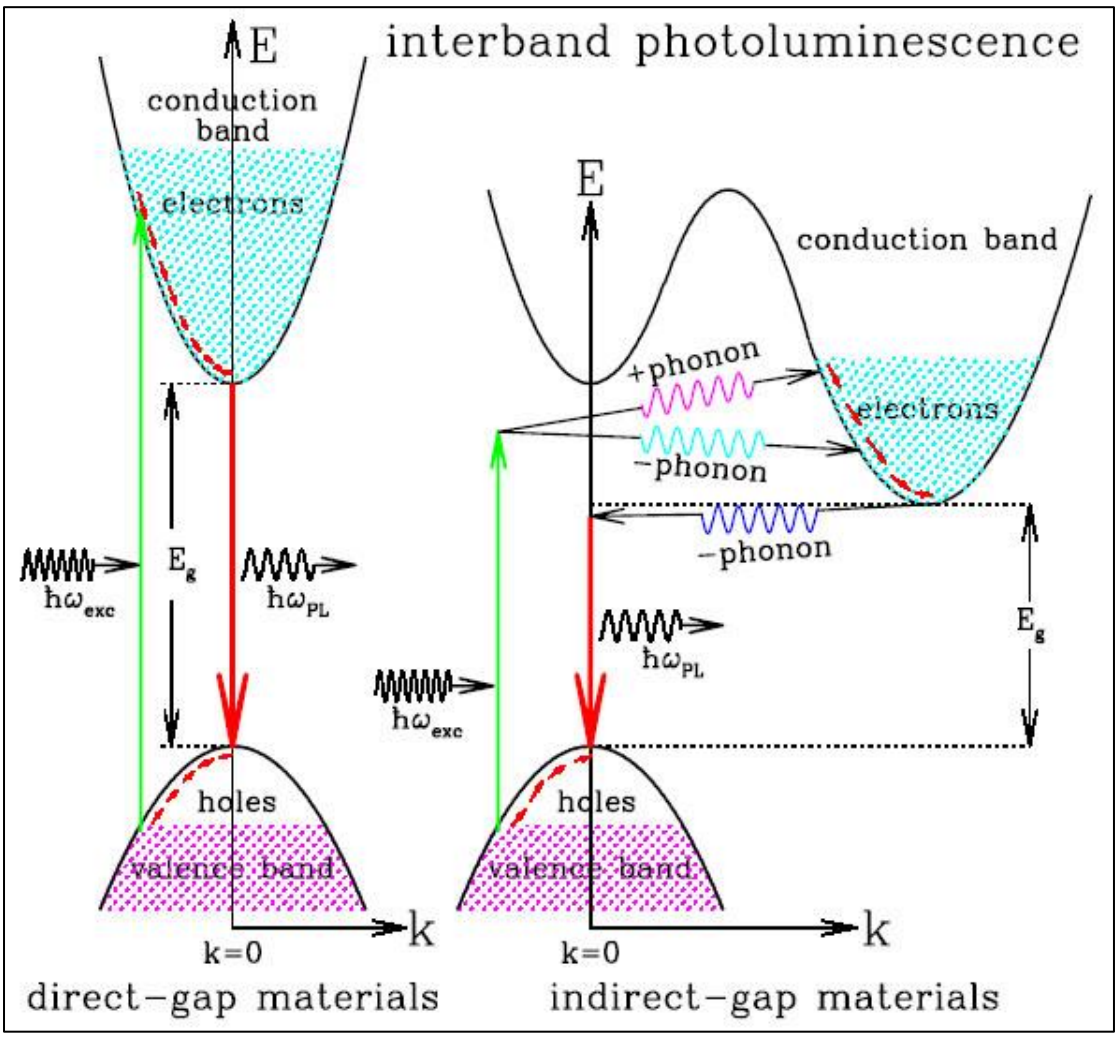

Fig.1.13. Reprsentation of band diagram in semiconductor.

On the behalf of band structure, the band gap energy is classified into two types, direct and indirect band gaps. For, direct band gap semiconductors, the minimum energy state of conduction band and maximum state of valence band occur at momentum at k = 0 (k is a wave vector).[98] For, direct band gap can be estimated in samples like ZnO, SnO_2, SnS_2 and CdS respectively. In case of indirect band gap

semiconductors, minimum state of conduction band and maximum state of valence band are not at same k value,[98] e.g. Ge, Si, GeS etc. The Fermi level is a probability distribution curve that represents 50 % probability of locating an electron at a given energy level. For n type semiconductor such as ZnO, the Fermi level is closed to conduction band.

A semiconductor demonstrates the process of photo illumination. The radiation of light have more energy compared to band gap of semiconductor, that excite the electron from valence band to next energy level conduction band leaving behind the same number of hole in valence band and generate one electron hole pair known as exciton. The recombination of exciton must be prohibited for the photocatalyzed reaction. For e.g. ZnO has a wide band gap than semiconducting materials and hence yield e-h pairs on illumination of ultraviolet light. The presence of electrons and holes are responsible for the redox activities at the semiconducting surface. Photo generated electron hole pairs are also delocalized in semiconductor. These locations are called trap sites. The electron-hole can undergo fast recombination results in decreasing the effectiveness of semiconductor. The number of photo generated electrons in ZnO is dictated by ability of surrounding to scavenge electrons and holes and recombination between photo-generated electron hole pairs.

$$ZnO + h\nu \rightarrow ZnO\ (e^{-}\text{-}h^{+})$$

$$h^{+} + H_2O \rightarrow OH^{\cdot} + H^{+}$$

$$h^{+} + OH^{\cdot} \rightarrow OH^{\cdot}$$

$$e^{-} + O_2 \rightarrow O_2^{-\cdot}$$

1.4.2. Quantization effect

The size of nano-conducting materials which are conducting to its Bohr exciton radius,[99] corresponds to regime of quantum confinement, for which the spatial

extent of electronic wave function is comparable with the dot size. The excite Bohr radius describe the electronic excitation in microscopic and bulk semiconducting materials determined by the strength of coulombic interactions of electron-hole pairs. Due to geometrical constraints, electron ambience causes the existence of particle boundaries and retort to modification in size of particle by adjusting their energy (discretization of energy level). The systematic mechanism is known as quantum size effect and it is very well played role in Quantum dots (QDs). As the particle size goes nearer to exciton Bohr radius, the wave function of electron and hole are confined in nanoparticles and charge carrier (electron and or hole), and kinetic energy enhances. So it can be explained as a major reason, for the change in absorbance edge in higher energy with reduction in size, known as blue shift in absorption spectrum.

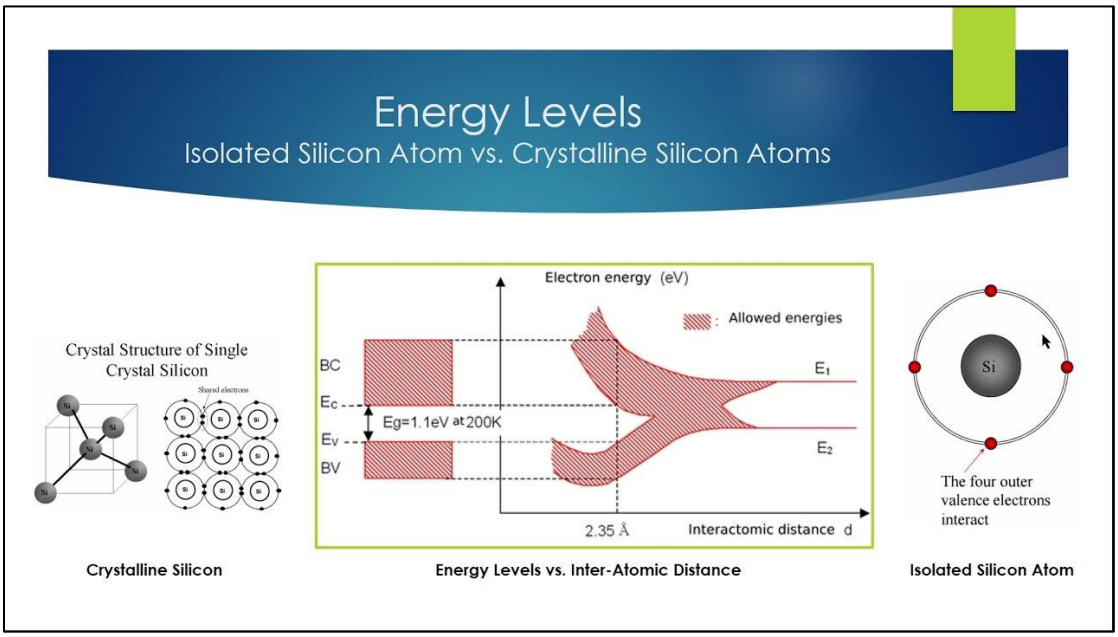

Fig.1.14. Representation of band gap analysis in semiconductor.

Semiconducting nanomaterials exhibit distinctive size dependent properties (quantization effect) that adjust its photochemical, photophysical, photochromic and optical applications.[22] Both the huge (ZnO, TiO_2, SnO_2) and small band gap exhibit

this property (CdSe, CdS). So due to quantization effect the initiation of charge, separation, retention and transfer across semiconductor and its surroundings are strongly concerned.[100-102] The existence of surface bound species involves surrounding electrolytes, sensitizers, like semiconductors, metal and dyes, plays an active role in determining the mechanism of charge transfer taking place at semiconductor and surrounding species interface. An irradiation of photon leads to charge separation in semiconducting nanostructures followed by electron and hole transfer to the surroundings dictated by the energetic of the surroundings. Further the defects or vacancies are created in semiconductors largely due to method involved in their synthesis. These defects plays vital role in their photo-electrochemical and photo-catalytic behavior of semiconductor.

The abnormality in physical and chemical behavior is due to three main reasons viz. the size of particle is equivalent to Bohr radius of exciton in metal semiconductors. It controls optical, luminescence and redox properties of semiconductors. The atoms present on the surface operate a considerable fraction of total number of atoms in nanostructures. And in last the comparable size of nanoparticles as size of molecules. This measures the peculiarities in the kinetics of chemical process on the surface of nanostructures. Since date the nanoparticles of ZnO, TiO_2, Fe_2O_3, SiO_2, MoS_2, CdS, HgS, GaP, Cd_3P_2, BiI_3, PbI_2 and other semiconductors have been synthesized and investigated.

1.4.3. Effective Mass Approximation

The quantum size effects are understood on the basis of effective mass approximation (EMA)[103-104] and empirical tight binding method (ETBM)[105-106] as aside from first principle calculations.

1.4.4. Anti-carcinomas activities of nanoparticles

A huge amount of literature is vastly describing the metallic nanoparticles to be diagnosed against anticancerous activities. Metallic nanostructures have tremendously different physicochemical properties than their bulk. The nanoparticles due to their pore size and surface area are regarded as a best drug for the treatment of various fatalities including cancer. This approach is proved to be a best way for the recognition of nanoparticles as specific drug for the protection, cure and treatment of fatality caused by this disastrous disease. The advantage of this treatment be developed as a separate sub-branch nano-organobiocatalysis as a branch under consideration of nanotechnology. A number of effective procedures like MTT, SRB, Glutathione, MMP, ROS, DNA damage analysis are seen out in cell lines by administered micro molar dosages of nanoparticles.

1.4.4.1. Palladium nanoparticles

Since few decades, identification of new cytotoxic compounds led to the beginning of new therapeutic compounds to diagnose a variety of carcinomas. It is noteworthy that less than 40 agents were used routinely in clinical stage over 600,000 compounds in testing phase due to limitation of their application as an anticarcinomous drugs.[107] The application of various anticarcinomous drugs used to diagnose carcinomas is limited due to their severe side defects like cis-platin has several undesirable effects on patients suffering from carcinomas due to their haphazard toxicity to brain, drug resistance, low stability and low solubility in physiological media. These disadvantages caused an improvement in the synthesis of novel derivatives with an anticarcinomous activity.[108, 109] Many palladium complexes were synthesized and characterized because of their morphological resemblances with

platinum based drugs and their anticarcinomous properties, like less renal toxicity.[110-112] Chelating ligands with nitrogen, sulphur and oxygen containing donor groups such as phenanthroline derivatives, N-Heterocyclic carbenes, and Schiff bases enhance the activity of DPN@LAA_PEG.[113] The activity is also increased using lipophilic ligands which less by improved transferring through cell membranes.[114] 2, 2'bipyridine (bpy) as NN-donor chelating ligands can form a planar complex with transition metal moieties and act as DNA intercalator.[114, 115-116] Metal complexes containing lipophilic ligands bind to DNA which favors via non-covalent interaction such as Vander walls and hydrophobic forces. Since recent decades considerable attention has been drawn, directed toward 8-Hydroquinoline (8Q) and derivatives because of diversity in their biological properties such as antifungal, antibiotic and antibacterial efficiency.[117-118] Recently transition metal complexes containing 8Q derivatives have been reported and used in anticarcinomous activity.[117, 119, 120-122] Interaction studies of small molecules with DNA are important for the investigation and the morphology and function of DNA and designing of novel drug effective against anticarcinomous activity. Molecules can bind with DNA via three types of non-covalent interactions like electrostatic binding, metal groove binding, and intercalation binding modes.[123-124] The drug-protein interaction with blood stream, serum and plasma may cause the formation of a drug-protein complex that greatly influences the distribution, toxicity and metabolism of drugs in the body. Albumin is most numerous plant proteins in class mammals with diverse function in the transportation of substances and in metabolism and distribution of exogenous and endogenous molecules.[125-127] Bovine serum albumin (BSA) is mainly selected as an adequate protein model for drug-protein interaction, due to its low cost, availability, morphological resemblances with human serum albumin and high bonding sites to metal complexes.[128-132]

Among the noble metal nanoparticles, dendritic Pd NPs capped by PEG and stabilized by L-Ascorbic acid (DPN@LAA_PEG) is most widely used in diverse biological applications. Particularly palladium nanosheets covered highly mesoporous silica NPs composites were found to particularly deliver the drug and affect carcinomatous cells.[133] Likewise, palladium complexes containing sulphone and other flexible linkages and chloro group possess efficient activity against malignant cells.[134] DPNs supported on mesoporous silica SBA-15 and MSU-2 is found to show better activity against carcinomatous cell lines when compared to other metal based complexes supported on mesoporous silica.[135] Recent decades are witnessing the interest for transition metal complexes bearing planar extended aromatic ligands has tremendously risen due to their application as a probe capable to utilize the nucleic acid structure. Palladium based electrocatalysts have been explored and developed the diverse morphology and structure[136] by various synthesis technologies including hydrothermal/solvothermal synthesis,[137] template method,[138-139] galvanic replacement,[140] reverse micro emulsion method[140] and electrochemical deposition.[141] A number of eminent scientists, researchers in the global era has witnessed the formation of DPN@LAA_PEG via numerous synthetic approaches. Ziba Sorinezami et al. have shown new ultrasonic-assisted palladium nanoparticles as in vitro evaluation of cytotoxicity and DNA/BSA binding proteins.[116] Yanru Yin et al. demonstrated the synthesis of palladium nanoparticles and their elecrtocatalytic properties, insight in to the role of polypyrollidone.[142] K.I. Dhanlekshmi et al. demonstrated photocatalytic activity and DNA binding studies of Pd@SiO_2 core shell nanoparticles in vitro.[143] Preeti Dauthal et al. demonstrated biosynthesis of palladium nanoparticles using *Delonix regia* leaf extract and their catalytic activity nitro-aromatics hydrogenation.[144] Stefanos Mourdikoudis et al. prepared highly porous

palladium nanodendrimers via wet chemical synthesis, electron tomography and catalytic activity.[145] Hijiang Jang et al. demonstrated graphene-templated synthesis of palladium nanoplates as novel electrocatalyst for direct methanol fuel cell.[146] Stefano Cataneo et al. has synthesized the highly uniform and composition controlled gold-palladium supported nanoparticles in continuous flow.[147]

1.4.4.2. Iron nanoparticles

Since recent decades iron and iron oxide nanoparticles have shown special attention in medicines, including in contrast agents, biosensors and carcinomas treatment.[148-150] A number of methods have been reported for optimization of these nanoparticles for particle size distribution, morphology and crystallinity.[151-153] Recent decades are witnessed, the synthesis of iron and iron oxide nanoparticles in effective catalytic activity, omitting of unwanted reaction, performance under mild environment and diverse sort of stereo selectivity in a chemical reaction, hydrolysis, oxidation-reduction and esterification.[154-155] Nanoparticles doped with vitamins, and enzymes are extensively suited for biomedical assays, food or pharmaceutical industry considering their substrate specificity, green synthetic approach and ease of production.[156-157] Hydrolase group of enzymes like lipases, triacylglycerol acyl hydrolase are a remarkable enzyme that catalyzes the plethora of process of esterification, hydrolysis and trans-esterification of the compounds establishing the most sparked biocatalyst for industrial applications.[158-159] In comparison with traditional chemical catalysis, enzyme doped materials can meet the environment and economical wants for their sustainable development. The employment of enzymes and vitamins as an alternative to chemical catalysts promotes green processes due to their unique presence including mild reaction condition, biodegradability, high

specificity, low toxicity and catalytic efficiency.[160-161] The immobilization of enzymes, vitamins onto various supports has much more potential in biological applications because it provides a facile separation of reaction media for repeated use and minimizes the contamination of products.[162-166] However one of the drawbacks of the immobilization process is their mass transfer limitations imposed by some matrices. So the developing, nano doped inorganic carriers would be an effective approach for substrate diffusion limitations.[167-170] Moreover, immobilization process improved the catalytic importance of enzymes due to decreasing aggregation to the favourable environment and enhancing the 3D- crystallization of the enzymes which might protect it again auto-proteolysis and denaturing agents.[171-172] Nanoparticles prepared using plant extract are the best-suited method to effective against the diagnosis of carcinomas of various organs.

1.4.4.3. Copper nanoparticles

The nanoscale precursors of copper and its alloys have been used in catalysis e.g. gas shift catalysis and gas detoxification catalysis.[173] The preparation of copper nanoparticles with controllable size, shape and morphological pattern is vital to be an effective catalyst. Such abilities fasten the use of copper nanoparticles as the precursor of reaction that is predominantly dominated to gold, silver and platinum nanoparticles. There is a number of methods to prepare nanoparticles regarding shape control specificity to control their shape and size effectively.[174] Due to the presence of propensity to get oxidize, a key issue is to prepare nanoparticles with controllable morphological pattern.[175] Recent literature reveals that limited attempts have been used to prepare copper nanoparticles with controllable shape, size and other morphological and surface properties.[176] Previous reports on the synthesis of copper

nano's have witnessed the organic encapsulation in organic phase,[177] encapsulation of thiol as capping agent[178] and thermal decomposition.[179] Copper nanoparticles prepared by the above required method has either limited to their size monodispersity or their susceptibility to getting oxidized.[180,181]

Pileni et al. has reported a chemical reduction of copper ion prepared by the sonochemical method in mixed reverse micelles to produce nanocrytals with different shapes and sizes.[182] The shape of the formed nanoparticles was agreed with a concentration of reducing agents. Low concentration dosed to a spherical shape and high dosage led to truncated, elongated, cubes, etc. Yanhuwei et al. has demonstrated the synthesis of stable, low polydispersity copper nanoparticles and nanorods estimated for their antifungal, anticarcinomatic and catalytic properties.[183] The literature survey witnessed the synthesis of nanostructures with controllable shape and size at the cardio of modern technology and is important their application in optics, bio-detection and catalysis.[184, 185-196] Dunying Deng et al. has demonstrated the aqueous phase synthesis and conducting film fabrication at low sintering temperature of copper nanoparticles.[197] The literature surveyed to a new application of metallic nanoparticles offer the possibility of developing new products and paved the way for new applications. The electronic industry has detected the surface effects and small size effects for this approach. Recently a considerable influence has been directed to develop conducting copper nano-inks for printable electronics plastic substrates.[198-199, 200-203] N. Arul Dhas et al. has synthesized, characterized copper nanoparticles by using thermal reduction and sonochemical reduction of copper(II) hydrazine carboxylate $Cu(N_2H_3COO)_2 \cdot 2H_2O$ in an aqueous medium.[204-205] Derrick Mott et al. prepared size control and shaped copper nanoparticles using control reaction temperature and capping agents with different alloy in organic solvents.[206-208]

1.4.4.4. Nickel nanoparticles

Nickel nanoparticles (Ni NPs) have received enormous attention due to their unique property in thermal, magnetic, electrical and chemical applications. They possess an exceptional capacity for catalysis, super capacitors, additives in oil, magnetic media for bio-chemicals and many other applications.[209] For economic, ecological and energy-saving reasons, recycled polyethene terephthalate was used instead of virgin materials. Based on the previous reports the properties of recycled polyethene terephthalate did not differ from those of virgin polyethene terephthalate.[210] A number of eminent philosophers, academicians and scientists are in approach to prepare a number of nickel nanoparticles (Ni NPs) for their best characterisation in a field to diagnose a number of various pathological activities like antitumor, antimalarial and antiphagocytic applications. H. Yin et al. has proposed the effect of particle size and surface coating on the cytotoxicity of nickel ferrite.[211] Cristina Espace et al. have proposed the toxicity and developmental defects of different sizes and shaped nickel nanoparticle in Zebrafish.[212] Angel Ezhilarazi et al. has reported the green synthesis of NiO nanoparticles using *Moringa oleifera* extract and their biomedical applications, the cytotoxicity effect of nanoparticles against HT-29 cancer cells.[213] Masanori Horie et al. have proposed ultrafine NiO particles induce cytotoxicity in vitro by cellular uptake and subsequent Ni(II) release. Elham S. Aazam et al. have proposed the synthesis of copper/ nickel nanoparticles using newly synthesized Schiff-base metal complexes and their cytotoxicity and catalytic activities.[214] Mohan Prasath Mani et al. proposed the green synthesis of nickel oxide particles and its integration into polyurethane scaffold matrix ornamented with ground nut oil for bone tissue engineering.[215] Bahareh Moazzenchi et al. has proposed the click electroless plating of nickel nanoparticles on polyester fabric, electrical

conductivity, magnetic and EMI shielding properties.[216] Fatemeh Mohammad khani et al. proposed the microwave absorption and photocatalytic properties of magnetic nickel nanoparticles/recycled nickel nanofibres web.[218] Bushra Bashir et al. has proposed the copper substituted nickel ferrite nanoparticles anchored on graphene sheet as an electrode materials for super capacitors fabrication.[219] Jyoti Chaudhari et al. has prepared the synthesis and biological function of nickel and copper nanoparticles.[220] So inspiring from the above literature the Ni NPs has been prepared with a mesoporous range were synthesized by using the sonochemical method. The mesoporous range of Ni NPs was prepared by using the grafting with polyethylene glycol (PEG) and coating of L-Ascorbic acid added on the nickel coordinated complete to obtain a homogenous solution.[221-224] The Ni NPs grafted polyethylene glycol (PEG) and coated on L-Ascorbic acid (LAA) were finally fabricated by the thermal spinning.[225-229] Further the morphological characterisation with like size estimation analysis and further biological adaptability has been estimated against breast carcinoma cell lines MCF-7.[230-233]

1.4.4.5. Silver and Gold nanocomposite

Silver and gold nanocomposites are widely used for the industrial and biomedical applications.[234] However, several studies revealed that nanocomposites cause injuries to a biological system.[235-240] Till then little has been known concerning the interaction of nanocomposites with living cells.[241-243] Nanocomposites have small sizes to cellular components or proteins and thus may bypass the natural barriers, such as cell membranes, possibly returning in harm to living cells.[244-247] Therefore, further understanding is necessary considering that these nanocomposites may cause adverse effects on living cells.[248-251] Silver and gold nanoparticles are two versatile constituents in biomedical and immunological applications. Gold nanoparticles (Au

NPs) can easily bind with amine and thiol group that has enabled the surface modification with amino acids[252] and DNA.[253-257] On this approach, gold nanoparticles (Au NPs) are widely used for cell tracers,[258] biodiagnostics,[259] transfection vectors,[260-265] drug delivery,[266] and biosensing.[267] For the biocompatibility of the clinical application of gold nanoparticles (Au NPs) is crucial. Au NPs with size range from 14-100 nm were taken up into mammalian cells and did not indicates any cytotoxicity.[268-273] The kinetics of cellular uptake was demonstrated to depend on the physical dimension of gold nanoparticles (Au NPs). Connor et al. reported that gold nanoparticles (Au NPs) in a diameter range of 18 nm containing a variety of surface modifiers were taken up by cells without causing cytotoxicity.[274] Au NPs in range of 3.5 nm capped by lysine or poly (L-lysine) were found to be bio-compatible and not-immunogenic.[275-281] Pernod et al. reported that the presence of intracellular Au NPs in a size range of 13 nm reduced actin stress fibers and induced major adverse effects on cell viability. Goodman et al. demonstrated that cationic Au NPs were moderately toxic whereas anionic Au NPs were nontoxic.[282] The cytotoxicity of Au NPs was variously described as toxic and nontoxic depending on size, concentration, surface modification and surface charge. The remarkable anti-immunological activity of Ag NPs is a major advantage for the development of products. For medical treatment, Ag NPs were coated on or embedded in the wound dressings, contraceptive devices, surgical instrument and bone-prosthesis.[283-289] Since the applications of Ag NPs become more widespread in medicines, the exposure of Ag NPs in the body increases and the consequent toxicological issues becomes important. Several studies report that Ag NPs significantly decreased the functions of mitochondria and induced cell-necrosis and apoptosis for several cell types.[290-296] However, research into the interaction of Ag NPs with cells has been limited.

1.5. Objectives of present work

In view of recent reports on nanoparticles and composites, author has extended the research work on synthesis and anti-carcinomas activities of some selected nanoparticles/nanocomposites

The main objectives of research work include:

- Synthesis of nanoparticles, nanostructures and nanocomposites by wet chemical methods using co-precipitation/sonochemical approach.
- Characterization of nanomaterials by various physico-chemical, spectral and electron microscopy techniques like UV-visible spectroscopy, FTIR analysis, XRD analysis, SEM, FESEM and TEM, Raman spectroscopy analysis for the morphology of the formed nanoparticles, particle size distribution, Zeta potential analysis, BET surface analysis for their pore size calculation.
- And in last, the prepared nanomaterials are treated with cancerous cell line passage analysis to examine the effectiveness of nanostructure materials as drug at various concentrations to confirm their cytotoxicity; IC_{50} value, SRB analysis, Glutathione treatment, mitochondrial membrane potential, (MMP), DNA damage and Apoptosis.

References

1. Toumey, C., Plenty of room, plenty of history. *Nature nanotechnology* 2009, 4, (12), 783.
2. Shetty, N. J.; Swati, P.; David, K., Nanorobots: Future in dentistry. *The Saudi dental journal* 2013, 25, (2), 49-52.
3. Drexler, K. E., *Engines of creation*. Anchor: 1986.
4. Eric Drexler, K., Nanosystems: molecular machinery, manufacturing, and computation. In New York: John Wiley & Sons: 1992.
5. Mazzola, L., Commercializing nanotechnology. *Nature Biotechnology* 2003, 21, (10), 1137-1143.
6. Ozin, G. A., Nanochemistry: synthesis in diminishing dimensions. *Advanced Materials* 1992, 4, (10), 612-649.
7. Tavakoli, A.; Sohrabi, M.; Kargari, A., A review of methods for synthesis of nanostructured metals with emphasis on iron compounds. *chemical papers* 2007, 61, (3), 151-170.
8. Whitesides, G. M., The'right'size in nanobiotechnology. *Nature Biotechnology* 2003, 21, (10), 1161-1165.
9. Moriarty, P., Nanostructured materials. *Reports on Progress in Physics* 2001, 64, (3), 297.
10. Edelstein, A. S.; Cammaratra, R., *Nanomaterials: synthesis, properties and applications*. CRC press: 1998.
11. Li, C.; Shuford, K. L.; Park, Q. H.; Cai, W.; Li, Y.; Lee, E. J.; Cho, S. O., High-yield synthesis of single-crystalline gold nano-octahedra. *Angewandte Chemie International Edition* 2007, 46, (18), 3264-3268.

12. Hitkari, G. Preparation, Properties and Applications of Chemically Synthesized Semiconducting Nanostructures. Department of Applied Chemistry, School for Physical Sciences, Babasaheb …, 2018.

13. Xia, Y.; Yang, P.; Sun, Y.; Wu, Y.; Mayers, B.; Gates, B.; Yin, Y.; Kim, F.; Yan, H., One-dimensional nanostructures: synthesis, characterization, and applications. *Advanced Materials* 2003, 15, (5), 353-389.

14. Zhai, T.; Yao, J., *One-dimensional nanostructures: principles and applications*. John Wiley & Sons: 2012.

15. Rao, C. N. R.; Müller, A.; Cheetham, A. K., *The chemistry of nanomaterials: synthesis, properties and applications*. John Wiley & Sons: 2006.

16. Novoselov, K., Nobel lecture: Graphene: Materials in the flatland. *Reviews of Modern Physics* 2011, 83, (3), 837.

17. Ramakrishna Matte, H.; Gomathi, A.; Manna, A. K.; Late, D. J.; Datta, R.; Pati, S. K.; Rao, C., MoS2 and WS2 analogues of graphene. *Angewandte Chemie International Edition* 2010, 49, (24), 4059-4062.

18. Liu, W.-T., Nanoparticles and their biological and environmental applications. *Journal of bioscience and bioengineering* 2006, 102, (1), 1-7.

19. Dunphy Guzmán, K. A.; Taylor, M. R.; Banfield, J. F., Environmental risks of nanotechnology: National nanotechnology initiative funding, 2000− 2004. In ACS Publications: 2006.

20. Radushkevich, L.; Lukyanovich, V. á., O strukture ugleroda, obrazujucegosja pri termiceskom razlozenii okisi ugleroda na zeleznom kontakte. *Zurn Fisic Chim* 1952, 26, (1), 88-95.

21. Odom, T. W.; Huang, J.-L.; Kim, P.; Lieber, C. M., Structure and electronic properties of carbon nanotubes. In ACS Publications: 2000.

22. Baughman, R. H.; Zakhidov, A. A.; De Heer, W. A., Carbon nanotubes--the route toward applications. *Science* 2002, 297, (5582), 787-792.

23. Kontos, A.; Katsanaki, A.; Maggos, T.; Likodimos, V.; Ghicov, A.; Kim, D.; Kunze, J.; Vasilakos, C.; Schmuki, P.; Falaras, P., Photocatalytic degradation of gas pollutants on self-assembled titania nanotubes. *Chemical Physics Letters* 2010, 490, (1-3), 58-62.

24. Dresselhaus, M. S.; Dresselhaus, G.; Eklund, P.; Rao, A., Carbon nanotubes. In *The physics of fullerene-based and fullerene-related materials*, Springer: 2000; pp 331-379.

25. Wakabayashi, K.; Fujita, M.; Ajiki, H.; Sigrist, M., Electronic and magnetic properties of nanographite ribbons. *Physical Review B* 1999, 59, (12), 8271.

26. Ruffieux, P.; Wang, S.; Yang, B.; Sánchez-Sánchez, C.; Liu, J.; Dienel, T.; Talirz, L.; Shinde, P.; Pignedoli, C. A.; Passerone, D., On-surface synthesis of graphene nanoribbons with zigzag edge topology. *Nature* 2016, 531, (7595), 489.

27. Dai, L.; Deng, H.; Mao, F.; Zang, J., The recent advances of research on p-type ZnO thin film. *Journal of Materials Science: Materials in Electronics* 2008, 19, (8-9), 727-734.

28. Huang, J.; Xu, Z.; Zhao, S.; Li, Y.; Zhang, F.; Song, L.; Wang, Y.; Xu, X., Organic/inorganic heterostructures for enhanced electroluminescence. *Solid state communications* 2007, 142, (7), 417-420.

29. Willander, M.; Zhao, Q.; Hu, Q.-H.; Klason, P.; Kuzmin, V.; Al-Hilli, S.; Nur, O.; Lozovik, Y. E., Fundamentals and properties of zinc oxide nanostructures: optical and sensing applications. *Superlattices and Microstructures* 2008, 43, (4), 352-361.

30. Hau, S. K.; Yip, H.-L.; Ma, H.; Jen, A. K.-Y., High performance ambient processed inverted polymer solar cells through interfacial modification with a fullerene self-assembled monolayer. *Applied Physics Letters* 2008, 93, (23), 441.

31. Singh, J.; Im, J.; Whitten, J. E.; Soares, J. W.; Steeves, D. M., Encapsulation of zinc oxide nanorods and nanoparticles. *Langmuir* 2009, 25, (17), 9947-9953.

32. Wöll, C., The chemistry and physics of zinc oxide surfaces. *Progress in Surface Science* 2007, 82, (2-3), 55-120.

33. Wang, Z. L., Splendid one-dimensional nanostructures of zinc oxide: a new nanomaterial family for nanotechnology. *Acs Nano* 2008, 2, (10), 1987-1992.

34. Saravanan, R.; Karthikeyan, N.; Gupta, V.; Thirumal, E.; Thangadurai, P.; Narayanan, V.; Stephen, A., ZnO/Ag nanocomposite: an efficient catalyst for degradation studies of textile effluents under visible light. *Materials Science and Engineering: C* 2013, 33, (4), 2235-2244.

35. Saravanan, R.; Khan, M. M.; Gupta, V. K.; Mosquera, E.; Gracia, F.; Narayanan, V.; Stephen, A., ZnO/Ag/CdO nanocomposite for visible light-induced photocatalytic degradation of industrial textile effluents. *Journal of colloid and interface science* 2015, 452, 126-133.

36. Saravanan, R.; Gupta, V.; Narayanan, V.; Stephen, A., Visible light degradation of textile effluent using novel catalyst ZnO/γ-Mn2O3. *Journal of the Taiwan Institute of Chemical Engineers* 2014, 45, (4), 1910-1917.

37. Eskizeybek, V.; Sarı, F.; Gülce, H.; Gülce, A.; Avcı, A., Preparation of the new polyaniline/ZnO nanocomposite and its photocatalytic activity for degradation of methylene blue and malachite green dyes under UV and natural

sun lights irradiations. *Applied Catalysis B: Environmental* 2012, 119, 197-206.

38. Gui, Y.; Yuan, J.; Wang, W.; Zhao, J.; Tian, J.; Xie, B., Facile solvothermal synthesis and gas sensitivity of graphene/WO3 nanocomposites. *Materials* 2014, 7, (6), 4587-4600.

39. Schaefer, H.-E., *Nanoscience: the science of the small in physics, engineering, chemistry, biology and medicine*. Springer Science & Business Media: 2010.

40. Alivisatos, A. P., Perspectives on the physical chemistry of semiconductor nanocrystals. *The Journal of Physical Chemistry* 1996, 100, (31), 13226-13239.

41. Murray, C.; Norris, D. J.; Bawendi, M. G., Synthesis and characterization of nearly monodisperse CdE (E= sulfur, selenium, tellurium) semiconductor nanocrystallites. *Journal of the American Chemical Society* 1993, 115, (19), 8706-8715.

42. Nirmal, M.; Brus, L., Luminescence photophysics in semiconductor nanocrystals. *Accounts of chemical research* 1999, 32, (5), 407-414.

43. Alivisatos, A. P., Nanocrystals: building blocks for modern materials design. *Endeavour* 1997, 21, (2), 56-60.

44. Bailey, R. E.; Nie, S., Alloyed semiconductor quantum dots: tuning the optical properties without changing the particle size. *Journal of the American Chemical Society* 2003, 125, (23), 7100-7106.

45. Sahana, M.; Sudakar, C.; Dixit, A.; Thakur, J.; Naik, R.; Naik, V., Quantum confinement effects and band gap engineering of SnO2 nanocrystals in a MgO matrix. *Acta materialia* 2012, 60, (3), 1072-1078.

46. Xu, X.; Zhuang, J.; Wang, X., SnO2 quantum dots and quantum wires: controllable synthesis, self-assembled 2D architectures, and gas-sensing properties. *Journal of the American Chemical Society* 2008, 130, (37), 12527-12535.

47. Zhu, H.; Yang, D.; Yu, G.; Zhang, H.; Yao, K., A simple hydrothermal route for synthesizing SnO2 quantum dots. *Nanotechnology* 2006, 17, (9), 2386.

48. Xi, G.; Ye, J., Ultrathin SnO2 nanorods: template-and surfactant-free solution phase synthesis, growth mechanism, optical, gas-sensing, and surface adsorption properties. *Inorganic chemistry* 2010, 49, (5), 2302-2309.

49. Hawthorne, M. F., The role of chemistry in the development of boron neutron capture therapy of cancer. *Angewandte Chemie International Edition in English* 1993, 32, (7), 950-984.

50. Bielinska, A.; Kukowska-Latallo, J. F.; Johnson, J.; Tomalia, D. A.; Baker Jr, J. R., Regulation of in vitro gene expression using antisense oligonucleotides or antisense expression plasmids transfected using starburst PAMAM dendrimers. *Nucleic acids research* 1996, 24, (11), 2176-2182.

51. Coşkun, S. Mekanik Alaşımlama Yöntemiyle Üretilmiş W-sic Ve W-sic-y2o3 Kompozitlerinin Geliştirilmesi Ve Karakterizasyonu. Fen Bilimleri Enstitüsü, 2006.

52. Matsui, I., Nanoparticles for electronic device applications: a brief review. *Journal of chemical engineering of Japan* 2005, 38, (8), 535-546.

53. Allsopp, M.; Walters, A.; Santillo, D., Nanotechnologies and nanomaterials in electrical and electronic goods: A review of uses and health concerns. *Greenpeace Research Laboratories, London* 2007.

54. Barbaro, P.; Liguori, F., *Heterogenized homogeneous catalysts for fine chemicals production: materials and processes*. Springer Science & Business Media: 2010; Vol. 33.

55. Klabunde, K. J.; Mulukutla, R. S., Chemical and catalytic aspects of nanocrystals. *Nanoscale Materials in Chemistry* 2001, 223-259.

56. Pierre, A. C.; Pajonk, G. M., Chemistry of aerogels and their applications. *Chemical reviews* 2002, 102, (11), 4243-4266.

57. Lu, Z.-l.; Lindner, E.; Mayer, H. A., Applications of sol− gel-processed interphase catalysts. *Chemical reviews* 2002, 102, (10), 3543-3578.

58. Schwarz, J. A.; Contescu, C.; Contescu, A., Methods for preparation of catalytic materials. *Chemical reviews* 1995, 95, (3), 477-510.

59. Hench, L. L.; West, J. K., The sol-gel process. *Chemical reviews* 1990, 90, (1), 33-72.

60. Wight, A.; Davis, M., Design and preparation of organic− inorganic hybrid catalysts. *Chemical reviews* 2002, 102, (10), 3589-3614.

61. Armstrong, G.; Armstrong, A. R.; Canales, J.; Bruce, P. G., Nanotubes with the TiO 2-B structure. *Chemical Communications* 2005, (19), 2454-2456.

62. Dong, R.; Jiang, S.; Li, Z.; Chen, Z.; Zhang, H.; Jin, C., Superhydrophilic TiO2 nanorod films with variable morphology grown on different substrates. *Materials letters* 2015, 152, 151-154.

63. Liu, B.; Aydil, E. S., Growth of oriented single-crystalline rutile TiO2 nanorods on transparent conducting substrates for dye-sensitized solar cells. *Journal of the American Chemical Society* 2009, 131, (11), 3985-3990.

64. Xie, Y.; Xia, C.; Du, H.; Wang, W., Enhanced electrochemical performance of polyaniline/carbon/titanium nitride nanowire array for flexible supercapacitor. *Journal of Power Sources* 2015, 286, 561-570.

65. Ge, M.; Cao, C.; Huang, J.; Li, S.; Chen, Z.; Zhang, K.-Q.; Al-Deyab, S.; Lai, Y., A review of one-dimensional TiO 2 nanostructured materials for environmental and energy applications. *Journal of Materials Chemistry A* 2016, 4, (18), 6772-6801.

66. Mascolo, M. C.; Pei, Y.; Ring, T. A., Room temperature co-precipitation synthesis of magnetite nanoparticles in a large pH window with different bases. *Materials* 2013, 6, (12), 5549-5567.

67. Kumar, K.; Chitkara, M.; Sandhu, I. S.; Mehta, D.; Kumar, S., Photocatalytic and magnetic properties of Zn1− xCrxO nanocomposites prepared by a co-precipitation method. *Materials Science in Semiconductor Processing* 2015, 30, 142-151.

68. Hou, W.-x.; Wang, Z., Structural and magnetic properties of Ni0. 15Mg0. 1Cu0. 3Zn0. 45Fe2O4 ferrite prepared by NaOH-precipitation method. *Materials Science and Engineering: B* 2015, 199, 57-61.

69. Casbeer, E.; Sharma, V. K.; Li, X.-Z., Synthesis and photocatalytic activity of ferrites under visible light: a review. *Separation and Purification Technology* 2012, 87, 1-14.

70. Meskin, P. E.; Ivanov, V. K.; Barantchikov, A. E.; Churagulov, B. R.; Tretyakov, Y. D., Ultrasonically assisted hydrothermal synthesis of nanocrystalline ZrO2, TiO2, NiFe2O4 and Ni0. 5Zn0. 5Fe2O4 powders. *Ultrasonics sonochemistry* 2006, 13, (1), 47-53.

71. Li, J. R.; Tang, Z. L.; Zhang, Z. T. In *Converting Industrial TiO2 into Titanate Nanotubes by Simple Sonochemical-Hydrothermal Processing*, Key Engineering Materials, 2005; Trans Tech Publ: 2005; pp 651-654.

72. Jia, Q.; Que, W.; Zhang, J., Heterogeneous solvothermal synthesis of one-dimensional titania nanostructures on transparent conductive glasses. *physica status solidi (a)* 2011, 208, (10), 2313-2316.

73. Nam, C. T.; Falconer, J. L.; Yang, W.-D., Morphology, structure and adsorption of titanate nanotubes prepared using a solvothermal method. *Materials Research Bulletin* 2014, 51, 49-55.

74. Xu, J.; Ge, J.-P.; Li, Y.-D., Solvothermal synthesis of monodisperse PbSe nanocrystals. *The Journal of Physical Chemistry B* 2006, 110, (6), 2497-2501.

75. Mullin, J. W., *Crystallization*. Elsevier: 2001.

76. Puntes, V. F.; Zanchet, D.; Erdonmez, C. K.; Alivisatos, A. P., Synthesis of hcp-Co nanodisks. *Journal of the American Chemical Society* 2002, 124, (43), 12874-12880.

77. Robinson, I.; Zacchini, S.; Tung, L. D.; Maenosono, S.; Thanh, N. T., Synthesis and characterization of magnetic nanoalloys from bimetallic carbonyl clusters. *Chemistry of Materials* 2009, 21, (13), 3021-3026.

78. Kwon, S. G.; Hyeon, T., Formation mechanisms of uniform nanocrystals via hot-injection and heat-up methods. *Small* 2011, 7, (19), 2685-2702.

79. Sugimoto, T., *Monodispersed particles*. Elsevier: 2019.

80. LaMer, V. K.; Dinegar, R. H., Theory, production and mechanism of formation of monodispersed hydrosols. *Journal of the American Chemical Society* 1950, 72, (11), 4847-4854.

81. Mer, V. K. L., Nucleation in phase transitions. *Industrial & Engineering Chemistry* 1952, 44, (6), 1270-1277.

82. Sugimoto, T.; Shiba, F.; Sekiguchi, T.; Itoh, H., Spontaneous nucleation of monodisperse silver halide particles from homogeneous gelatin solution I: silver chloride. *Colloids and Surfaces A: Physicochemical and Engineering Aspects* 2000, 164, (2-3), 183-203.

83. Lifshitz, I. M.; Slyozov, V. V., The kinetics of precipitation from supersaturated solid solutions. *Journal of physics and chemistry of solids* 1961, 19, (1-2), 35-50.

84. Wagner, C., Theorie der alterung von niederschlägen durch umlösen (Ostwald-reifung). *Zeitschrift für Elektrochemie, Berichte der Bunsengesellschaft für physikalische Chemie* 1961, 65, (7-8), 581-591.

85. Watzky, M. A.; Finke, R. G., Transition metal nanocluster formation kinetic and mechanistic studies. A new mechanism when hydrogen is the reductant: slow, continuous nucleation and fast autocatalytic surface growth. *Journal of the American Chemical Society* 1997, 119, (43), 10382-10400.

86. Zhang, R.; Khalizov, A.; Wang, L.; Hu, M.; Xu, W., Nucleation and growth of nanoparticles in the atmosphere. *Chemical reviews* 2012, 112, (3), 1957-2011.

87. Thanh, N. T.; Maclean, N.; Mahiddine, S., Mechanisms of nucleation and growth of nanoparticles in solution. *Chemical reviews* 2014, 114, (15), 7610-7630.

88. Amin, G.; Asif, M.; Zainelabdin, A.; Zaman, S.; Nur, O.; Willander, M., Influence of pH, precursor concentration, growth time, and temperature on the morphology of ZnO nanostructures grown by the hydrothermal method. *Journal of Nanomaterials* 2011, 2011.

89. Vayssieres, L.; Keis, K.; Lindquist, S.-E.; Hagfeldt, A., Purpose-built anisotropic metal oxide material: 3D highly oriented microrod array of ZnO. *The Journal of Physical Chemistry B* 2001, 105, (17), 3350-3352.

90. Vayssieres, L., Growth of arrayed nanorods and nanowires of ZnO from aqueous solutions. *Advanced Materials* 2003, 15, (5), 464-466.

91. Zhu, Y.; Fan, D.; Shen, W., A general chemical conversion route to synthesize various ZnO-based core/shell structures. *The Journal of Physical Chemistry C* 2008, 112, (28), 10402-10406.

92. Rai, A.; Singh, A.; Ahmad, A.; Sastry, M., Role of halide ions and temperature on the morphology of biologically synthesized gold nanotriangles. *Langmuir* 2006, 22, (2), 736-741.

93. Kim, S.; Nah, J.; Jo, I.; Shahrjerdi, D.; Colombo, L.; Yao, Z.; Tutuc, E.; Banerjee, S. K., Realization of a high mobility dual-gated graphene field-effect transistor with Al 2 O 3 dielectric. *Applied Physics Letters* 2009, 94, (6), 062107.

94. Tong, H.; Ouyang, S.; Bi, Y.; Umezawa, N.; Oshikiri, M.; Ye, J., Nano-photocatalytic materials: possibilities and challenges. *Advanced Materials* 2012, 24, (2), 229-251.

95. Sasikala, R.; Shirole, A. R.; Sudarsan, V.; Girija, K. G.; Rao, R.; Sudakar, C.; Bharadwaj, S. R., Improved photocatalytic activity of indium doped cadmium sulfide dispersed on zirconia. *Journal of Materials Chemistry* 2011, 21, (41), 16566-16573.

96. Alivisatos, P., The use of nanocrystals in biological detection. *Nature Biotechnology* 2004, 22, (1), 47-52.

97. Pradhan, N.; Peng, X., Efficient and color-tunable Mn-doped ZnSe nanocrystal emitters: control of optical performance via greener synthetic chemistry. *Journal of the American Chemical Society* 2007, 129, (11), 3339-3347.

98. Rogach, A. L.; Franzl, T.; Klar, T. A.; Feldmann, J.; Gaponik, N.; Lesnyak, V.; Shavel, A.; Eychmüller, A.; Rakovich, Y. P.; Donegan, J. F., Aqueous synthesis of thiol-capped CdTe nanocrystals: state-of-the-art. *The Journal of Physical Chemistry C* 2007, 111, (40), 14628-14637.

99. Henderson, E. J.; Hessel, C. M.; Veinot, J. G., Synthesis and photoluminescent properties of size-controlled germanium nanocrystals from phenyl trichlorogermane-derived polymers. *Journal of the American Chemical Society* 2008, 130, (11), 3624-3632.

100. Zhang, J. Z., Ultrafast studies of electron dynamics in semiconductor and metal colloidal nanoparticles: effects of size and surface. *Accounts of chemical research* 1997, 30, (10), 423-429.

101. Peter, L. M., Dynamic aspects of semiconductor photoelectrochemistry. *Chemical reviews* 1990, 90, (5), 753-769.

102. Suarez, R.; Nair, P.; Kamat, P. V., Photoelectrochemical behavior of Bi2S3 nanoclusters and nanostructured thin films. *Langmuir* 1998, 14, (12), 3236-3241.

103. Efros, A. L.; Efros, A. L., Interband absorption of light in a semiconductor sphere. *Soviet Physics Semiconductors-Ussr* 1982, 16, (7), 772-775.

104. Brus, L. E., A simple model for the ionization potential, electron affinity, and aqueous redox potentials of small semiconductor crystallites. *The Journal of chemical physics* 1983, 79, (11), 5566-5571.

105. Lippens, P.; Lannoo, M., Calculation of the band gap for small CdS and ZnS crystallites. *Physical Review B* 1989, 39, (15), 10935.

106. Lippens, P.; Lannoo, M., Comparison between calculated and experimental values of the lowest excited electronic state of small CdSe crystallites. *Physical Review B* 1990, 41, (9), 6079.

107. Schwartsmann, G.; Winograd, B.; Pinedo, H., The main steps in the development of anticancer agents. *Radiotherapy and oncology* 1988, 12, (4), 301-313.

108. Dahm, G.; Bailly, C.; Karmazin, L.; Bellemin-Laponnaz, S., Synthesis, structural characterization and in vitro anti-cancer activity of functionalized N-heterocyclic carbene platinum and palladium complexes. *Journal of Organometallic Chemistry* 2015, 794, 115-124.

109. Hadjikakou, S. K.; Hadjiliadis, N., Antiproliferative and anti-tumor activity of organotin compounds. *Coordination Chemistry Reviews* 2009, 253, (1-2), 235-249.

110. Aminzadeh, M.; Mansouri-Torshizi, H.; Modarresi-Alam, A. R., 2, 2′-bipyridine coplanar with coordination square of Pd (II) nonyldithiocarbamato antitumor complex interacting with DNA in two distinct steps. *Journal of Biomolecular Structure and Dynamics* 2017, 35, (11), 2301-2313.

111. Hacıoğlu, D.; Erdöl, H., Developments and current approaches in the treatment of pterygium. *International ophthalmology* 2017, 37, (4), 1073-1081.

112. Sorinezami, Z.; Mansouri-Torshizi, H.; Aminzadeh, M.; Ghahghaei, A.; Jamgohari, N.; Heidari Majd, M., Synthesis of new ultrasonic-assisted palladium oxide nanoparticles: an in vitro evaluation on cytotoxicity and

DNA/BSA binding properties. *Journal of Biomolecular Structure and Dynamics* 2019, 1-13.

113. Bathaie, S. Z.; Bolhasani, A.; Hoshyar, R.; Ranjbar, B.; Sabouni, F.; Moosavi-Movahedi, A.-A., Interaction of saffron carotenoids as anticancer compounds with ctDNA, Oligo (dG. dC) 15, and Oligo (dA. dT) 15. *DNA and cell biology* 2007, 26, (8), 533-540.

114. Eizadi-Mood, N.; Sabzghabaee, A. M.; Gheshlaghi, F.; Yaraghi, A., Amitraz poisoning treatment: still supportive? *Iranian journal of pharmaceutical research: IJPR* 2011, 10, (1), 155.

115. Long, S. P.; Marshall-Colon, A.; Zhu, X.-G., Meeting the global food demand of the future by engineering crop photosynthesis and yield potential. *Cell* 2015, 161, (1), 56-66.

116. Mansouri-Torshizi, H.; Rezaei, E.; Kamranfar, F.; Majd, M. H., Investigating the apoptosis ability of ethylenediamine 8-hydroxyquinolinato palladium (II) complex. *Advanced pharmaceutical bulletin* 2016, 6, (3), 449.

117. Tomás-Mendivil, E.; Suarez, F. J.; Diez, J.; Cadierno, V., An efficient ruthenium (IV) catalyst for the selective hydration of nitriles to amides in water under mild conditions. *Chemical Communications* 2014, 50, (68), 9661-9664.

118. Mahamoud, A.; Chevalier, J.; Davin-Regli, A.; Barbe, J.; Pages, J., Curr. Drug Targ. 2006, 7, 843. b) OA Philips. *Curr. Op. Invest. Drugs* 2005, 6, 768.

119. Sahu, K. B.; Ghosh, S.; Banerjee, M.; Maity, A.; Mondal, S.; Paira, R.; Saha, P.; Naskar, S.; Hazra, A.; Banerjee, S., Synthesis and in vitro study of antibacterial, antifungal activities of some novel bisquinolines. *Medicinal Chemistry Research* 2013, 22, (1), 94-104.

120. Mansouri-Torshizi, H.; Saeidifar, M.; Rezaei-Behbehani, G.; Divsalar, A.; Saboury, A., DNA Binding Studies and Cytotoxicity of Ethylenediamine 8-Hydroxyquinolinato Palladium (II) Chloride. *Journal of the Chinese Chemical Society* 2010, 57, (6), 1299-1308.

121. Sorinezami, Z.; Mansouri-Torshizi, H.; Ghanbari, B., Synthesis of PdO nanoparticles: Crystal structure, DNA binding, and cytotoxicity of a new hydroxyl-quinolinato-palladium complex. *Inorganic and Nano-Metal Chemistry* 2017, 47, (4), 500-508.

122. Ayyadurai, N.; Prabhu, N. S.; Deepankumar, K.; Jang, Y. J.; Chitrapriya, N.; Song, E.; Lee, N.; Kim, S. K.; Kim, B.-G.; Soundrarajan, N., Bioconjugation of L-3, 4-dihydroxyphenylalanine containing protein with a polysaccharide. *Bioconjugate chemistry* 2011, 22, (4), 551-555.

123. Cao, H.; Pan, M.; Kang, Y.; Xia, Q.; Li, X.; Zhao, X.; Shi, R.; Lou, J.; Zhou, M.; Kuwana, M., Clinical manifestations of dermatomyositis and clinically amyopathic dermatomyositis patients with positive expression of anti–melanoma differentiation–associated gene 5 antibody. *Arthritis care & research* 2012, 64, (10), 1602-1610.

124. Luo, Z.; Shi, X.; Hu, Q.; Zhao, B.; Huang, M., Structural evidence of perfluorooctane sulfonate transport by human serum albumin. *Chemical research in toxicology* 2012, 25, (5), 990-992.

125. Sun, J.-K.; Sun, F.; Wang, X.; Yuan, S.-T.; Zheng, S.-Y.; Mu, X.-W., Risk factors and prognosis of hypoalbuminemia in surgical septic patients. *PeerJ* 2015, 3, e1267.

126. Shahraki, S.; Shiri, F.; Majd, M. H.; Razmara, Z., Comparative study on the anticancer activities and binding properties of a hetero metal binuclear

complex [Co (dipic) 2Ni (OH2) 5]· 2H2O (dipic= dipicolinate) with two carrier proteins. *Journal of pharmaceutical and biomedical analysis* 2017, 145, 273-282.

127. Ghalandari, B.; Divsalar, A.; Saboury, A. A.; Haertlé, T.; Parivar, K.; Bazl, R.; Eslami-Moghadam, M.; Amanlou, M., Spectroscopic and theoretical investigation of oxali–palladium interactions with β-lactoglobulin. *Spectrochimica Acta Part A: Molecular and Biomolecular Spectroscopy* 2014, 118, 1038-1046.

128. Blauvelt, A.; Reich, K.; Tsai, T.-F.; Tyring, S.; Vanaclocha, F.; Kingo, K.; Ziv, M.; Pinter, A.; Vender, R.; Hugot, S., Secukinumab is superior to ustekinumab in clearing skin of subjects with moderate-to-severe plaque psoriasis up to 1 year: results from the CLEAR study. *Journal of the American Academy of Dermatology* 2017, 76, (1), 60-69. e9.

129. Shahraki, S.; Shiri, F.; Saeidifar, M., Synthesis, characterization, in silico ADMET prediction, and protein binding analysis of a novel zinc (II) Schiff-base complex: Application of multi-spectroscopic and computational techniques. *Journal of Biomolecular Structure and Dynamics* 2018, 36, (7), 1666-1680.

130. Shiri, F.; Shahraki, S.; Shahriari, S., Mechanistic understanding and binding analysis of a novel Schiff base palladium (II) complex with β-lactoglobulin and human serum albumin. *Journal of Molecular Liquids* 2018, 262, 218-229.

131. Wang, X.; Herting, G.; Wallinder, I. O.; Blomberg, E., Adsorption of bovine serum albumin on silver surfaces enhances the release of silver at pH neutral conditions. *Physical Chemistry Chemical Physics* 2015, 17, (28), 18524-18534.

132. Fang, W.; Tang, S.; Liu, P.; Fang, X.; Gong, J.; Zheng, N., Pd Nanosheet-Covered Hollow Mesoporous Silica Nanoparticles as a Platform for the Chemo-Photothermal Treatment of Cancer Cells. *small* 2012, 8, (24), 3816-3822.

133. Elhusseiny, A. F.; Hassan, H. H., Antimicrobial and antitumor activity of platinum and palladium complexes of novel spherical aramides nanoparticles containing flexibilizing linkages: Structure–property relationship. *Spectrochimica Acta Part A: Molecular and Biomolecular Spectroscopy* 2013, 103, 232-245.

134. Balbín, A.; Gaballo, F.; Ceballos-Torres, J.; Prashar, S.; Fajardo, M.; Kaluđerović, G. N.; Gómez-Ruiz, S., Dual application of Pd nanoparticles supported on mesoporous silica SBA-15 and MSU-2: Supported catalysts for C–C coupling reactions and cytotoxic agents against human cancer cell lines. *RSC Advances* 2014, 4, (97), 54775-54787.

135. Hoel, D. G.; Berwick, M.; de Gruijl, F. R.; Holick, M. F., The risks and benefits of sun exposure 2016. *Dermato-endocrinology* 2016, 8, (1), e1248325.

136. Tarushi, A.; Kakoulidou, C.; Raptopoulou, C. P.; Psycharis, V.; Kessissoglou, D. P.; Zoi, I.; Papadopoulos, A. N.; Psomas, G., Zinc complexes of diflunisal: Synthesis, characterization, structure, antioxidant activity, and in vitro and in silico study of the interaction with DNA and albumins. *Journal of inorganic biochemistry* 2017, 170, 85-97.

137. Song, H.-M.; Zink, J. I., Hard Pd Nanorods in the Soft Surfactant Mixture of CTAB and Pluronics: Seedless Synthesis and Their Self-Assembly. *Langmuir* 2018, 34, (14), 4271-4281.

138. Guo, P.; Zhang, G.; Yu, J.; Li, H.; Zhao, X., Controlled synthesis, magnetic and photocatalytic properties of hollow spheres and colloidal nanocrystal clusters of manganese ferrite. *Colloids and Surfaces A: Physicochemical and Engineering Aspects* 2012, 395, 168-174.

139. Jin, M.; Zhang, H.; Xie, Z.; Xia, Y., Palladium nanocrystals enclosed by {100} and {111} facets in controlled proportions and their catalytic activities for formic acid oxidation. *Energy & Environmental Science* 2012, 5, (4), 6352-6357.

140. Gao, C.; Zhang, Q.; Lu, Z.; Yin, Y., Templated synthesis of metal nanorods in silica nanotubes. *Journal of the American Chemical Society* 2011, 133, (49), 19706-19709.

141. Sutter, E.; Jungjohann, K.; Bliznakov, S.; Courty, A.; Maisonhaute, E.; Tenney, S.; Sutter, P., In situ liquid-cell electron microscopy of silver–palladium galvanic replacement reactions on silver nanoparticles. *Nature communications* 2014, 5, 4946.

142. Yin, Y.; Ma, N.; Xue, J.; Wang, G.; Liu, S.; Li, H.; Guo, P., Insights into the role of poly (vinylpyrrolidone) in the synthesis of palladium nanoparticles and their electrocatalytic properties. *Langmuir* 2019, 35, (3), 787-795.

143. Dhanalekshmi, K.; Sangeetha, K.; Meena, K.; Magesan, P.; Manikandan, A.; Jayamoorthy, K., Photodynamic activity and DNA binding studies of Pd@ SiO2 core-shell nanoparticles in vitro. *Photodiagnosis and photodynamic therapy* 2019, 26, 79-84.

144. Dauthal, P.; Mukhopadhyay, M., Biosynthesis of palladium nanoparticles using Delonix regia leaf extract and its catalytic activity for nitro-aromatics

hydrogenation. *Industrial & Engineering Chemistry Research* 2013, 52, (51), 18131-18139.

145. Mourdikoudis, S.; Montes-García, V.; Rodal-Cedeira, S.; Winckelmans, N.; Pérez-Juste, I.; Wu, H.; Bals, S.; Pérez-Juste, J.; Pastoriza-Santos, I., Highly porous palladium nanodendrites: wet-chemical synthesis, electron tomography and catalytic activity. *Dalton Transactions* 2019, 48, (11), 3758-3767.

146. Yang, H.; Geng, L.; Zhang, Y.; Chang, G.; Zhang, Z.; Liu, X.; Lei, M.; He, Y., Graphene-templated synthesis of palladium nanoplates as novel electrocatalyst for direct methanol fuel cell. *Applied Surface Science* 2019, 466, 385-392.

147. Nemamcha, A.; Rehspringer, J.-L.; Khatmi, D., Synthesis of palladium nanoparticles by sonochemical reduction of palladium (II) nitrate in aqueous solution. *The Journal of Physical Chemistry B* 2006, 110, (1), 383-387.

148. Himpsel, F.; Ortega, J.; Mankey, G.; Willis, R., Magnetic nanostructures. *Advances in physics* 1998, 47, (4), 511-597.

153. Estelrich, J.; Escribano, E.; Queralt, J.; Busquets, M., Iron oxide nanoparticles for magnetically-guided and magnetically-responsive drug delivery. *International journal of molecular sciences* 2015, 16, (4), 8070-8101.

149. Sun, S.; Zeng, H., Size-controlled synthesis of magnetite nanoparticles. *Journal of the American Chemical Society* 2002, 124, (28), 8204-8205.

150. Ismail, R. A.; Sulaiman, G. M.; Abdulrahman, S. A., Preparation of iron oxide nanoparticles by laser ablation in DMF under effect of external magnetic field. *International Journal of Modern Physics B* 2016, 30, (17), 1650094.

151. Sodipo, B. K.; Aziz, A. A., Recent advances in synthesis and surface modification of superparamagnetic iron oxide nanoparticles with silica. *Journal of Magnetism and Magnetic Materials* 2016, 416, 275-291.

152. Fei, L.; Jing-Han, Z.; Yang-Long, H.; Song, G., Chemical synthesis of magnetic nanocrystals: Recent progress. *Chinese Physics B* 2013, 22, (10), 107503.

153. Luckarift, H. R.; Spain, J. C.; Naik, R. R.; Stone, M. O., Enzyme immobilization in a biomimetic silica support. *Nature biotechnology* 2004, 22, (2), 211.

154. Mateo, C.; Palomo, J. M.; Fernandez-Lorente, G.; Guisan, J. M.; Fernandez-Lafuente, R., Improvement of enzyme activity, stability and selectivity via immobilization techniques. *Enzyme and microbial technology* 2007, 40, (6), 1451-1463.

155. Wandrey, C.; Liese, A.; Kihumbu, D., Industrial biocatalysis: past, present, and future. *Organic Process Research & Development* 2000, 4, (4), 286-290.

156. Jacques, P.; Béchet, M.; Bigan, M.; Caly, D.; Chataigné, G.; Coutte, F.; Flahaut, C.; Heuson, E.; Leclère, V.; Lecouturier, D., High-throughput strategies for the discovery and engineering of enzymes for biocatalysis. *Bioprocess and biosystems engineering* 2017, 40, (2), 161-180.

157. Husain, Q., Nanosupport bound lipases their stability and applications. *Biointerface Research in Applied Chemistry* 2017, 7, (6), 2194-2216.

158. Asmat, S.; Husain, Q.; Azam, A., Lipase immobilization on facile synthesized polyaniline-coated silver-functionalized graphene oxide nanocomposites as novel biocatalysts: stability and activity insights. *RSC Advances* 2017, 7, (9), 5019-5029.

159. Misson, M.; Zhang, H.; Jin, B., Nanobiocatalyst advancements and bioprocessing applications. *Journal of the Royal Society Interface* 2015, 12, (102), 20140891.

160. Wu, X.; Yang, C.; Ge, J., Green synthesis of enzyme/metal-organic framework composites with high stability in protein denaturing solvents. *Bioresources and bioprocessing* 2017, 4, (1), 24.

161. DiCosimo, R.; McAuliffe, J.; Poulose, A. J.; Bohlmann, G., Industrial use of immobilized enzymes. *Chemical Society Reviews* 2013, 42, (15), 6437-6474.

162. Wu, X.; Hou, M.; Ge, J., Metal–organic frameworks and inorganic nanoflowers: a type of emerging inorganic crystal nanocarrier for enzyme immobilization. *Catalysis Science & Technology* 2015, 5, (12), 5077-5085.

163. Amirbandeh, M.; Taheri-Kafrani, A., Immobilization of glucoamylase on triazine-functionalized Fe3O4/graphene oxide nanocomposite: Improved stability and reusability. *International journal of biological macromolecules* 2016, 93, 1183-1191.

164. Klein, M. P.; Hackenhaar, C. R.; Lorenzoni, A. S.; Rodrigues, R. C.; Costa, T. M.; Ninow, J. L.; Hertz, P. F., Chitosan crosslinked with genipin as support matrix for application in food process: Support characterization and β-d-galactosidase immobilization. *Carbohydrate polymers* 2016, 137, 184-190.

166. Lorenzoni, A. S.; Aydos, L. F.; Klein, M. P.; Rodrigues, R. C.; Hertz, P. F., Fructooligosaccharides synthesis by highly stable immobilized β-fructofuranosidase from Aspergillus aculeatus. *Carbohydrate polymers* 2014, 103, 193-197.

167. Schroeder, M. M.; Wang, Q.; Badieyan, S.; Chen, Z.; Marsh, E. N. G., Effect of surface crowding and surface hydrophilicity on the activity, stability and molecular orientation of a covalently tethered enzyme. *Langmuir* 2017, 33, (28), 7152-7159.

168. Zhang, C.; Wang, X.; Hou, M.; Li, X.; Wu, X.; Ge, J., Immobilization on metal–organic framework engenders high sensitivity for enzymatic electrochemical detection. *ACS applied materials & interfaces* 2017, 9, (16), 13831-13836.

169. Wu, X.; Ge, J.; Yang, C.; Hou, M.; Liu, Z., Facile synthesis of multiple enzyme-containing metal–organic frameworks in a biomolecule-friendly environment. *Chemical Communications* 2015, 51, (69), 13408-13411.

170. Ge, J.; Lei, J.; Zare, R. N., Protein–inorganic hybrid nanoflowers. *Nature nanotechnology* 2012, 7, (7), 428.

171. Cruz-Izquierdo, Á.; Picó, E. A.; López, C.; Serra, J. L.; Llama, M. J., Magnetic cross-linked enzyme aggregates (mCLEAs) of Candida antarctica lipase: an efficient and stable biocatalyst for biodiesel synthesis. *PLoS ONE* 2014, 9, (12), e115202.

172. Cui, J.; Ren, S.; Lin, T.; Feng, Y.; Jia, S., Shielding effects of Fe3+-tannic acid nanocoatings for immobilized enzyme on magnetic Fe3O4@ silica core shell nanosphere. *Chemical Engineering Journal* 2018, 343, 629-637.

173. Mott, D.; Galkowski, J.; Wang, L.; Luo, J.; Zhong, C.-J., Synthesis of size-controlled and shaped copper nanoparticles. *Langmuir* 2007, 23, (10), 5740-5745.

174. Chen, S.; Sommers, J. M., Alkanethiolate-protected copper nanoparticles: spectroscopy, electrochemistry, and solid-state morphological evolution. *The Journal of Physical Chemistry B* 2001, 105, (37), 8816-8820.

175. Kim, Y. H.; Kang, Y. S.; Lee, W. J.; Jo, B. G.; Jeong, J. H., Synthesis of Cu nanoparticles prepared by using thermal decomposition of Cu-oleate complex. *Molecular Crystals and Liquid Crystals* 2006, 445, (1), 231/[521]-238/[528].

176. Sun, S.; Murray, C., Weller. D.; Folks, L.; Moser, A. *Science* 2000, 287, 1989.

208. Salzemann, C.; Lisiecki, I.; Urban, J.; Pileni, M.-P., Anisotropic copper nanocrystals synthesized in a supersaturated medium: Nanocrystal growth. *Langmuir* 2004, 20, (26), 11772-11777.

177. Wei, Y.; Chen, S.; Kowalczyk, B.; Huda, S.; Gray, T. P.; Grzybowski, B. A., Synthesis of stable, low-dispersity copper nanoparticles and nanorods and their antifungal and catalytic properties. *The Journal of Physical Chemistry C* 2010, 114, (37), 15612-15616.

178. Peng, X.; Manna, L.; Yang, W.; Wickham, J.; Scher, E.; Kadavanich, A.; Alivisatos, A. P., Shape control of CdSe nanocrystals. *Nature* 2000, 404, (6773), 59.

179. Burda, C.; Chen, X.; Narayanan, R.; El-Sayed, M. A., Chemistry and properties of nanocrystals of different shapes. *Chemical reviews* 2005, 105, (4), 1025-1102.

180. Jin, R.; Cao, Y. C.; Hao, E.; Métraux, G. S.; Schatz, G. C.; Mirkin, C. A., Controlling anisotropic nanoparticle growth through plasmon excitation. *Nature* 2003, 425, (6957), 487.

181. Stuchinskaya, T.; Moreno, M.; Cook, M. J.; Edwards, D. R.; Russell, D. A., Targeted photodynamic therapy of breast cancer cells using antibody–phthalocyanine–gold nanoparticle conjugates. *Photochemical & Photobiological Sciences* 2011, 10, (5), 822-831.

182. Haes, A. J.; Van Duyne, R. P., A nanoscale optical biosensor: sensitivity and selectivity of an approach based on the localized surface plasmon resonance spectroscopy of triangular silver nanoparticles. *Journal of the American Chemical Society* 2002, 124, (35), 10596-10604.

183. Joo, S. H.; Park, J. Y.; Tsung, C.-K.; Yamada, Y.; Yang, P.; Somorjai, G. A., Thermally stable Pt/mesoporous silica core–shell nanocatalysts for high-temperature reactions. *Nature materials* 2009, 8, (2), 126.

184. Lee, I.; Delbecq, F.; Morales, R.; Albiter, M. A.; Zaera, F., Tuning selectivity in catalysis by controlling particle shape. *Nature materials* 2009, 8, (2), 132.

185. Xie, J.; Lee, J. Y.; Wang, D. I.; Ting, Y. P., Identification of active biomolecules in the high-yield synthesis of single-crystalline gold nanoplates in algal solutions. *small* 2007, 3, (4), 672-682.

186. Shen, C.; Hui, C.; Yang, T.; Xiao, C.; Tian, J.; Bao, L.; Chen, S.; Ding, H.; Gao, H., Monodisperse noble-metal nanoparticles and their surface enhanced Raman scattering properties. *Chemistry of Materials* 2008, 20, (22), 6939-6944.

187. Li, Y. G.; Lu, D.; Wong, C., *Electrical conductive adhesives with nanotechnologies*. Springer Science & Business Media: 2009.

188. Li, D.; Sutton, D.; Burgess, A.; Graham, D.; Calvert, P. D., Conductive copper and nickel lines via reactive inkjet printing. *Journal of Materials Chemistry* 2009, 19, (22), 3719-3724.

189. Ko, S. H.; Pan, H.; Grigoropoulos, C. P.; Luscombe, C. K.; Fréchet, J. M.; Poulikakos, D., All-inkjet-printed flexible electronics fabrication on a polymer substrate by low-temperature high-resolution selective laser sintering of metal nanoparticles. *Nanotechnology* 2007, 18, (34), 345202.

190. Hon, K.; Li, L.; Hutchings, I., Direct writing technology—Advances and developments. *CIRP Annals* 2008, 57, (2), 601-620.

191. Schmid, G., *Clusters and colloids: from theory to applications*. John Wiley & Sons: 2008.

192. Gates, B., Supported metal clusters: synthesis, structure, and catalysis. *Chemical reviews* 1995, 95, (3), 511-522.

193. Sun, S.; Fullerton, E. E.; Weller, D.; Murray, C., Compositionally controlled FePt nanoparticle materials. *IEEE Transactions on magnetics* 2001, 37, (4), 1239-1243.

194. Luo, J.; Maye, M. M.; Petkov, V.; Kariuki, N. N.; Wang, L.; Njoki, P.; Mott, D.; Lin, Y.; Zhong, C.-J., Phase properties of carbon-supported gold− platinum nanoparticles with different bimetallic compositions. *Chemistry of Materials* 2005, 17, (12), 3086-3091.

195. Jana, N. R.; Gearheart, L.; Murphy, C. J., Wet chemical synthesis of high aspect ratio cylindrical gold nanorods. *The Journal of Physical Chemistry B* 2001, 105, (19), 4065-4067.

196. Monteiro, A. A. d. S.; Richter, A. R.; Maciel, J. d. S.; Feitosa, J. P. A.; Paula, H. C. B.; de Paula, M.; Célia, R., Effect of chemical modification on the solubility and swelling of microspheres based on carboxymethyl cashew gum and chitosan. *Polímeros* 2015, 25, (SPE), 31-39.

197. Umer, A.; Naveed, S.; Ramzan, N.; Rafique, M. S.; Imran, M., A green method for the synthesis of copper nanoparticles using L-ascorbic acid. *Matéria (Rio de Janeiro)* 2014, 19, (3), 197-203.

198. Panigrahi, S.; Kundu, S.; Ghosh, S. K.; Nath, S.; Praharaj, S.; Basu, S.; Pal, T., Selective one-pot synthesis of copper nanorods under surfactantless condition. *Polyhedron* 2006, 25, (5), 1263-1269.

199. Wang, H.; Imura, M.; Malgras, V.; Li, C.; Wang, L.; Yamauchi, Y., A Solution Phase Synthesis of Dendritic Platinum Nanoelectrocatalysts with the

Assistance of Polyoxyethylene Nonylphenyl Ether. *Journal of Inorganic and Organometallic Polymers and Materials* 2015, 25, (2), 245-250.

200. Jardim, K. V.; Joanitti, G. A.; Azevedo, R. B.; Parize, A. L., Physico-chemical characterization and cytotoxicity evaluation of curcumin loaded in chitosan/chondroitin sulfate nanoparticles. *Materials Science and Engineering: C* 2015, 56, 294-304.

201. Wunderbaldinger, P.; Josephson, L.; Weissleder, R., Tat peptide directs enhanced clearance and hepatic permeability of magnetic nanoparticles. *Bioconjugate chemistry* 2002, 13, (2), 264-268.

202. Larson, D. R.; Zipfel, W. R.; Williams, R. M.; Clark, S. W.; Bruchez, M. P.; Wise, F. W.; Webb, W. W., Water-soluble quantum dots for multiphoton fluorescence imaging in vivo. *Science* 2003, 300, (5624), 1434-1436.

203. Nah, J.-W.; Paek, Y.-W.; Jeong, Y.-I.; Kim, D.-W.; Cho, C.-S.; Kim, S.-H.; Kim, M.-Y., Clonazepam release from poly (DL-lactide-co-glycolide) nanoparticles prepared by dialysis method. *Archives of pharmacal research* 1998, 21, (4), 418-422.

204. Williams, J.; Lansdown, R.; Sweitzer, R.; Romanowski, M.; LaBell, R.; Ramaswami, R.; Unger, E., Nanoparticle drug delivery system for intravenous delivery of topoisomerase inhibitors. *Journal of Controlled Release* 2003, 91, (1-2), 167-172.

205. Brannon-Peppas, L.; Blanchette, J. O., Nanoparticle and targeted systems for cancer therapy. *Advanced drug delivery reviews* 2004, 56, (11), 1649-1659.

206. Bellocq, N. C.; Pun, S. H.; Jensen, G. S.; Davis, M. E., Transferrin-containing, cyclodextrin polymer-based particles for tumor-targeted gene delivery. *Bioconjugate chemistry* 2003, 14, (6), 1122-1132.

207. Benns, J.; Kim, S., Tailoring new gene delivery designs for specific targets. *Journal of drug targeting* 2000, 8, (1), 1-12.

208. Kong, G.; Braun, R. D.; Dewhirst, M. W., Hyperthermia enables tumor-specific nanoparticle delivery: effect of particle size. *Cancer research* 2000, 60, (16), 4440-4445.

209. Riboh, J. C.; Haes, A. J.; McFarland, A. D.; Ranjit Yonzon, C.; Van Duyne, R. P., A nanoscale optical biosensor: real-time immunoassay in physiological buffer enabled by improved nanoparticle adhesion. *The Journal of Physical Chemistry B* 2003, 107, (8), 1772-1780.

210. Hoet, P. H.; Nemmar, A.; Nemery, B., Health impact of nanomaterials? *Nature Biotechnology* 2004, 22, (1), 19-19.

211. Giles, J., Size matters when it comes to safety, report warns. *Nature* 2004, 430, (7000), 599-600.

212. Colvin, V. L., The potential environmental impact of engineered nanomaterials. *Nature Biotechnology* 2003, 21, (10), 1166-1170.

213. Vestal, C. R.; Zhang, Z. J., Effects of surface coordination chemistry on the magnetic properties of MnFe2O4 spinel ferrite nanoparticles. *Journal of the American Chemical Society* 2003, 125, (32), 9828-9833.

214. Mangeney, C.; Ferrage, F.; Aujard, I.; Marchi-Artzner, V.; Jullien, L.; Ouari, O.; Rékaï, E. D.; Laschewsky, A.; Vikholm, I.; Sadowski, J. W., Synthesis and properties of water-soluble gold colloids covalently derivatized with neutral polymer monolayers. *Journal of the American Chemical Society* 2002, 124, (20), 5811-5821.

215. Mayya, K. S.; Schoeler, B.; Caruso, F., Preparation and organization of nanoscale polyelectrolyte-coated gold nanoparticles. *Advanced Functional Materials* 2003, 13, (3), 183-188.

216. Derfus, A. M.; Chan, W. C.; Bhatia, S. N., Probing the cytotoxicity of semiconductor quantum dots. *Nano letters* 2004, 4, (1), 11-18.

217. Sayes, C. M.; Fortner, J. D.; Guo, W.; Lyon, D.; Boyd, A. M.; Ausman, K. D.; Tao, Y. J.; Sitharaman, B.; Wilson, L. J.; Hughes, J. B., The differential cytotoxicity of water-soluble fullerenes. *Nano letters* 2004, 4, (10), 1881-1887.

218. Hilger, I.; Frühauf, S.; Linß, W.; Hiergeist, R.; Andrä, W.; Hergt, R.; Kaiser, W. A., Cytotoxicity of selected magnetic fluids on human adenocarcinoma cells. *Journal of magnetism and magnetic materials* 2003, 261, (1-2), 7-12.

219. Ferrando, R.; Jellinek, J.; Johnston, R. L., Nanoalloys: from theory to applications of alloy clusters and nanoparticles. *Chemical reviews* 2008, 108, (3), 845-910.

220. Lee, H. J.; Song, J. Y.; Kim, B. S., Biological synthesis of copper nanoparticles using Magnolia kobus leaf extract and their antibacterial activity. *Journal of Chemical Technology & Biotechnology* 2013, 88, (11), 1971-1977.

221. Argueta-Figueroa, L.; Morales-Luckie, R. A.; Scougall-Vilchis, R. J.; Olea-Mejía, O. F., Synthesis, characterization and antibacterial activity of copper, nickel and bimetallic Cu–Ni nanoparticles for potential use in dental materials. *Progress in Natural Science: Materials International* 2014, 24, (4), 321-328.

222. Mohammadkhani, F.; Montazer, M.; Latifi, M., Microwave absorption and photocatalytic properties of magnetic nickel nanoparticles/recycled PET

nanofibers web. *The Journal of The Textile Institute* 2019, 110, (11), 1606-1614.

223. Yin, H.; Too, H.; Chow, G., The effects of particle size and surface coating on the cytotoxicity of nickel ferrite. *Biomaterials* 2005, 26, (29), 5818-5826.

224. Ispas, C.; Andreescu, D.; Patel, A.; Goia, D. V.; Andreescu, S.; Wallace, K. N., Toxicity and developmental defects of different sizes and shape nickel nanoparticles in zebrafish. *Environmental science & technology* 2009, 43, (16), 6349-6356.

225. Ezhilarasi, A. A.; Vijaya, J. J.; Kaviyarasu, K.; Maaza, M.; Ayeshamariam, A.; Kennedy, L. J., Green synthesis of NiO nanoparticles using Moringa oleifera extract and their biomedical applications: Cytotoxicity effect of nanoparticles against HT-29 cancer cells. *Journal of Photochemistry and Photobiology B: Biology* 2016, 164, 352-360.

226. Aazam, E. S.; El-Said, W. A., Synthesis of copper/nickel nanoparticles using newly synthesized Schiff-base metals complexes and their cytotoxicity/catalytic activities. *Bioorganic chemistry* 2014, 57, 5-12.

227. Mani, M. P.; Jaganathan, S. K.; Md Khudzari, A. Z.; Ismail, A. F., Green synthesis of nickel oxide particles and its integration into polyurethane scaffold matrix ornamented with groundnut oil for bone tissue engineering. *International Journal of Polymer Analysis and Characterization* 2019, 24, (7), 571-583.

228. Moazzenchi, B.; Montazer, M., Click electroless plating of nickel nanoparticles on polyester fabric: Electrical conductivity, magnetic and EMI shielding properties. *Colloids and Surfaces A: Physicochemical and Engineering Aspects* 2019, 571, 110-124.

229. Bashir, B.; Rahman, A.; Sabeeh, H.; Khan, M. A.; Aboud, M. F. A.; Warsi, M. F.; Shakir, I.; Agboola, P. O.; Shahid, M., Copper substituted nickel ferrite nanoparticles anchored onto the graphene sheets as electrode materials for supercapacitors fabrication. *Ceramics International* 2019, 45, (6), 6759-6766.

230. Chaudhary, J.; Tailor, G.; Yadav, B.; Michael, O., Synthesis and biological function of Nickel and Copper nanoparticles. *Heliyon* 2019, 5, (6), e01878.

231. Selvakannan, P.; Mandal, S.; Phadtare, S.; Gole, A.; Pasricha, R.; Adyanthaya, S.; Sastry, M., Water-dispersible tryptophan-protected gold nanoparticles prepared by the spontaneous reduction of aqueous chloroaurate ions by the amino acid. *Journal of Colloid and Interface Science* 2004, 269, (1), 97-102.

232. Gearheart, L. A.; Ploehn, H. J.; Murphy, C. J., Oligonucleotide adsorption to gold nanoparticles: a surface-enhanced Raman spectroscopy study of intrinsically bent DNA. *The Journal of Physical Chemistry B* 2001, 105, (50), 12609-12615.

233. Yi, H.; Leunissen, J. L.; Shi, G.-M.; Gutekunst, C.-A.; Hersch, S. M., A novel procedure for pre-embedding double immunogold–silver labeling at the ultrastructural level. *Journal of Histochemistry & Cytochemistry* 2001, 49, (3), 279-283.

234. Storhoff, J. J.; Lazarides, A. A.; Mucic, R. C.; Mirkin, C. A.; Letsinger, R. L.; Schatz, G. C., What controls the optical properties of DNA-linked gold nanoparticle assemblies? *Journal of the American Chemical Society* 2000, 122, (19), 4640-4650.

235. Sandhu, K. K.; McIntosh, C. M.; Simard, J. M.; Smith, S. W.; Rotello, V. M., Gold nanoparticle-mediated transfection of mammalian cells. *Bioconjugate chemistry* 2002, 13, (1), 3-6.

236. O'Brien, J.; Lummis, S. C., An improved method of preparing microcarriers for biolistic transfection. *Brain research protocols* 2002, 10, (1), 12-15.

237. Voskerician, G.; Shive, M. S.; Shawgo, R. S.; Von Recum, H.; Anderson, J. M.; Cima, M. J.; Langer, R., Biocompatibility and biofouling of MEMS drug delivery devices. *biomaterials* 2003, 24, (11), 1959-1967.

238. Olofsson, L.; Rindzevicius, T.; Pfeiffer, I.; Käll, M.; Höök, F., Surface-based gold-nanoparticle sensor for specific and quantitative DNA hybridization detection. *Langmuir* 2003, 19, (24), 10414-10419.

239. Chithrani, B. D.; Ghazani, A. A.; Chan, W. C., Determining the size and shape dependence of gold nanoparticle uptake into mammalian cells. *Nano letters* 2006, 6, (4), 662-668.

240. Connor, E. E.; Mwamuka, J.; Gole, A.; Murphy, C. J.; Wyatt, M. D., Gold nanoparticles are taken up by human cells but do not cause acute cytotoxicity. *small* 2005, 1, (3), 325-327.

241. Pernodet, N.; Fang, X.; Sun, Y.; Bakhtina, A.; Ramakrishnan, A.; Sokolov, J.; Ulman, A.; Rafailovich, M., Adverse effects of citrate/gold nanoparticles on human dermal fibroblasts. *small* 2006, 2, (6), 766-773.

242. Shukla, R.; Bansal, V.; Chaudhary, M.; Basu, A.; Bhonde, R. R.; Sastry, M., Biocompatibility of gold nanoparticles and their endocytotic fate inside the cellular compartment: a microscopic overview. *Langmuir* 2005, 21, (23), 10644-10654.

243. Moaddab, S.; Ahari, H.; Shahbazzadeh, D.; Motallebi, A. A.; Anvar, A. A.; Rahman-Nya, J.; Shokrgozar, M. R., Toxicity study of nanosilver (nanocid?) on osteoblast cancer cell line. *International Nano Letters* 2011, 1, (1), 11.

244. Cheng, D.; Yang, J.; Zhao, Y., Antibacterial materials of silver nanoparticles application in medical appliances and appliances for daily use. *Chin Med Equip J* 2004, 4, 26-32.

245. Cohen, M. S.; Stern, J. M.; Vanni, A. J.; Kelley, R. S.; Baumgart, E.; Field, D.; Libertino, J. A.; Summerhayes, I. C., In vitro analysis of a nanocrystalline silver-coated surgical mesh. *Surgical infections* 2007, 8, (3), 397-404.

246. Alt, V.; Bechert, T.; Steinrücke, P.; Wagener, M.; Seidel, P.; Dingeldein, E.; Domann, E.; Schnettler, R., An in vitro assessment of the antibacterial properties and cytotoxicity of nanoparticulate silver bone cement. *biomaterials* 2004, 25, (18), 4383-4391.

247. Hussain, S.; Hess, K.; Gearhart, J.; Geiss, K.; Schlager, J., In vitro toxicity of nanoparticles in BRL 3A rat liver cells. *Toxicology in vitro* 2005, 19, (7), 975-983.

248. Hussain, S. M.; Javorina, A. K.; Schrand, A. M.; Duhart, H. M.; Ali, S. F.; Schlager, J. J., The interaction of manganese nanoparticles with PC-12 cells induces dopamine depletion. *Toxicological sciences* 2006, 92, (2), 456-463.

249. Elhalawany, N.; Awad, M. A.; Zahran, M. K., Synthesis, characterization, optical and electrical properties of novel highly dendritic polythiophene nanocomposites with silver and/or gold. *Journal of Materials Science: Materials in Electronics* 2018, 29, (11), 8970-8977.

250. Ak, M.; Toppare, L., Synthesis of star-shaped pyrrole and thiophene functionalized monomers and optoelectrochemical properties of corresponding copolymers. *Materials Chemistry and physics* 2009, 114, (2-3), 789-794.

251. Chronakis, I. S.; Grapenson, S.; Jakob, A., Conductive polypyrrole nanofibers via electrospinning: electrical and morphological properties. *Polymer* 2006, 47, (5), 1597-1603.

252. Banerjee, M.; Sharma, S.; Chattopadhyay, A.; Ghosh, S. S., Enhanced antibacterial activity of bimetallic gold-silver core–shell nanoparticles at low silver concentration. *Nanoscale* 2011, 3, (12), 5120-5125.

253. Chen, J.; Wang, D.; Xi, J.; Au, L.; Siekkinen, A.; Warsen, A.; Li, Z.-Y.; Zhang, H.; Xia, Y.; Li, X., Immuno gold nanocages with tailored optical properties for targeted photothermal destruction of cancer cells. *Nano letters* 2007, 7, (5), 1318-1322.

254. Wang, X.; Peng, X.; Zhang, Y.; Ni, J.; Au, C.-t.; Jiang, L., Efficient ammonia synthesis over a core–shell Ru/CeO 2 catalyst with a tunable CeO 2 size: DFT calculations and XAS spectroscopy studies. *Inorganic Chemistry Frontiers* 2019, 6, (2), 396-406.

255. Inoue, Y.; Kitano, M.; Kishida, K.; Abe, H.; Niwa, Y.; Sasase, M.; Fujita, Y.; Ishikawa, H.; Yokoyama, T.; Hara, M., Efficient and stable ammonia synthesis by self-organized flat Ru nanoparticles on calcium amide. *ACS Catalysis* 2016, 6, (11), 7577-7584.

256. Lezau, A.; Skadtchenko, B.; Trudeau, M.; Antonelli, D., Mesoporous Ta oxide reduced with bis (toluene) Ti: electronic properties and mechanistic considerations of nitrogen cleavage on the low valent surface. *Dalton Transactions* 2003, (21), 4115-4120.

257. Gao, W.; Wang, P.; Guo, J.; Chang, F.; He, T.; Wang, Q.; Wu, G.; Chen, P., Barium hydride-mediated nitrogen transfer and hydrogenation for ammonia synthesis: a case study of cobalt. *ACS Catalysis* 2017, 7, (5), 3654-3661.

258. Lin, B.; Guo, Y.; Liu, R.; Wang, X.; Ni, J.; Lin, J.; Jiang, L., Preparation of a highly efficient carbon-supported ruthenium catalyst by carbon monoxide treatment. *Industrial & Engineering Chemistry Research* 2018, 57, (8), 2819-2828.

259. Kitano, M.; Inoue, Y.; Yamazaki, Y.; Hayashi, F.; Kanbara, S.; Matsuishi, S.; Yokoyama, T.; Kim, S.-W.; Hara, M.; Hosono, H., Ammonia synthesis using a stable electride as an electron donor and reversible hydrogen store. *Nature chemistry* 2012, 4, (11), 934.

260. Lu, Y.; Li, J.; Tada, T.; Toda, Y.; Ueda, S.; Yokoyama, T.; Kitano, M.; Hosono, H., Water durable electride Y5Si3: Electronic structure and catalytic activity for ammonia synthesis. *Journal of the American Chemical Society* 2016, 138, (12), 3970-3973.

261. Kitano, M.; Kanbara, S.; Inoue, Y.; Kuganathan, N.; Sushko, P. V.; Yokoyama, T.; Hara, M.; Hosono, H., Electride support boosts nitrogen dissociation over ruthenium catalyst and shifts the bottleneck in ammonia synthesis. *Nature communications* 2015, 6, 6731.

262. Liu, H., *Ammonia synthesis catalysts: innovation and practice*. World Scientific: 2013.

263. Lin, B.; Liu, Y.; Heng, L.; Wang, X.; Ni, J.; Lin, J.; Jiang, L., Morphology effect of ceria on the catalytic performances of Ru/CeO2 catalysts for ammonia synthesis. *Industrial & Engineering Chemistry Research* 2018, 57, (28), 9127-9135.

264. Ogura, Y.; Sato, K.; Miyahara, S.-i.; Kawano, Y.; Toriyama, T.; Yamamoto, T.; Matsumura, S.; Hosokawa, S.; Nagaoka, K., Efficient ammonia synthesis

over a Ru/La 0.5 Ce 0.5 O 1.75 catalyst pre-reduced at high temperature. *Chemical science* 2018, 9, (8), 2230-2237.

265. Hara, M.; Kitano, M.; Hosono, H., Ru-loaded C12A7: e–electride as a catalyst for ammonia synthesis. *ACS Catalysis* 2017, 7, (4), 2313-2324.

266. Doh, H.; Kim, H. Y.; Kim, G. S.; Cha, J.; Park, H. S.; Ham, H. C.; Yoon, S. P.; Han, J.; Nam, S. W.; Song, K. H., Influence of Cation Substitutions Based on ABO3 Perovskite Materials, Sr1–x Y x Ti1–y Ru y O3− δ, on Ammonia Dehydrogenation. *ACS Sustainable Chemistry & Engineering* 2017, 5, (10), 9370-9379.

267. Wang, Z.; Liu, B.; Lin, J., Highly effective perovskite-type BaZrO3 supported Ru catalyst for ammonia synthesis. *Applied Catalysis A: General* 2013, 458, 130-136.

268. Zeinalipour-Yazdi, C. D.; Hargreaves, J. S.; Catlow, C. R. A., Nitrogen activation in a Mars–van Krevelen mechanism for ammonia synthesis on Co3Mo3N. *The Journal of Physical Chemistry C* 2015, 119, (51), 28368-28376.

269. Ma, Z.; Zhao, S.; Pei, X.; Xiong, X.; Hu, B., New insights into the support morphology-dependent ammonia synthesis activity of Ru/CeO 2 catalysts. *Catalysis Science & Technology* 2017, 7, (1), 191-199.

270. Szmigiel, D.; Bielawa, H.; Kurtz, M.; Hinrichsen, O.; Muhler, M.; Raróg, W.; Jodzis, S.; Kowalczyk, Z.; Znak, L.; Zieliński, J., The kinetics of ammonia synthesis over ruthenium-based catalysts: The role of barium and cesium. *Journal of Catalysis* 2002, 205, (1), 205-212.

271. Luo, X.; Wang, R.; Ni, J.; Lin, J.; Lin, B.; Xu, X.; Wei, K., Effect of La 2 O 3 on Ru/CeO 2-La 2 O 3 catalyst for ammonia synthesis. *Catalysis letters* 2009, 133, (3-4), 382.

272. Lin, J.; Zhang, L.; Wang, Z.; Ni, J.; Wang, R.; Wei, K., The effect of Ag as a promoter for Ru/CeO2 catalysts in ammonia synthesis. *Journal of Molecular Catalysis A: Chemical* 2013, 366, 375-379.

273. Liu, W.; Wang, W.; Tang, K.; Guo, J.; Ren, Y.; Wang, S.; Feng, L.; Yang, Y., The promoting influence of nickel species in the controllable synthesis and catalytic properties of nickel–ceria catalysts. *Catalysis Science & Technology* 2016, 6, (7), 2427-2434.

274. Liu, X.; Park, M.; Kim, M. G.; Gupta, S.; Wu, G.; Cho, J., Integrating NiCo alloys with their oxides as efficient bifunctional cathode catalysts for rechargeable zinc–air batteries. *Angewandte Chemie International Edition* 2015, 54, (33), 9654-9658.

275. Patake, V.; Lokhande, C.; Joo, O. S., Electrodeposited ruthenium oxide thin films for supercapacitor: Effect of surface treatments. *Applied Surface Science* 2009, 255, (7), 4192-4196.

276. Brezesinski, T.; Wang, J.; Tolbert, S. H.; Dunn, B., Ordered mesoporous α-MoO 3 with iso-oriented nanocrystalline walls for thin-film pseudocapacitors. *Nature materials* 2010, 9, (2), 146.

277. Zhao, D.-D.; Bao, S.-J.; Zhou, W.-J.; Li, H.-L., Preparation of hexagonal nanoporous nickel hydroxide film and its application for electrochemical capacitor. *Electrochemistry communications* 2007, 9, (5), 869-874.

278. Kim, I.-H.; Kim, K.-B., Electrochemical characterization of hydrous ruthenium oxide thin-film electrodes for electrochemical capacitor

applications. *Journal of The Electrochemical Society* 2006, 153, (2), A383-A389.

279. Sugimoto, W.; Yokoshima, K.; Murakami, Y.; Takasu, Y., Charge storage mechanism of nanostructured anhydrous and hydrous ruthenium-based oxides. *Electrochimica Acta* 2006, 52, (4), 1742-1748.

280. Augustyn, V.; Simon, P.; Dunn, B., Pseudocapacitive oxide materials for high-rate electrochemical energy storage. *Energy & Environmental Science* 2014, 7, (5), 1597-1614.

281. Dubal, D. P.; Chodankar, N. R.; Holze, R.; Kim, D. H.; Gomez-Romero, P., Ultrathin Mesoporous RuCo2O4 Nanoflakes: An Advanced Electrode for High-Performance Asymmetric Supercapacitors. *ChemSusChem* 2017, 10, (8), 1771-1782.

282. Bi, R.-R.; Wu, X.-L.; Cao, F.-F.; Jiang, L.-Y.; Guo, Y.-G.; Wan, L.-J., Highly dispersed RuO2 nanoparticles on carbon nanotubes: facile synthesis and enhanced supercapacitance performance. *The Journal of Physical Chemistry C* 2010, 114, (6), 2448-2451.

283. Rakhi, R.; Chen, W.; Hedhili, M. N.; Cha, D.; Alshareef, H. N., Enhanced rate performance of mesoporous Co3O4 nanosheet supercapacitor electrodes by hydrous RuO2 nanoparticle decoration. *ACS applied materials & interfaces* 2014, 6, (6), 4196-4206.

284. Liang, J.; Tan, H.; Xiao, C.; Zhou, G.; Guo, S.; Ding, S., Hydroxyl-riched halloysite clay nanotubes serving as substrate of NiO nanosheets for high-performance supercapacitor. *Journal of Power Sources* 2015, 285, 210-216.

285. Nair, D. P.; Sakthivel, T.; Nivea, R.; Eshow, J. S.; Gunasekaran, V., Effect of surfactants on electrochemical properties of vanadium-pentoxide nanoparticles

synthesized via hydrothermal method. *Journal of nanoscience and nanotechnology* 2015, 15, (6), 4392-4397.

286. Hu, Z.; Zu, L.; Jiang, Y.; Lian, H.; Liu, Y.; Li, Z.; Chen, F.; Wang, X.; Cui, X., High specific capacitance of polyaniline/mesoporous manganese dioxide composite using Ki-H2SO4 electrolyte. *Polymers* 2015, 7, (10), 1939-1953.

287. Lei, B.-H.; Kong, Q.; Yang, Z.; Yang, Y.; Wang, Y.; Pan, S., Hierarchized band gap and enhanced optical responses of trivalent rare-earth metal nitrates due to (d–p) π conjugation interactions. *Journal of Materials Chemistry C* 2016, 4, (26), 6295-6301.

288. Zhao, G.; Yang, F.; Chen, Z.; Liu, Q.; Ji, Y.; Zhang, Y.; Niu, Z.; Mao, J.; Bao, X.; Hu, P., Metal/oxide interfacial effects on the selective oxidation of primary alcohols. *Nature communications* 2017, 8, 14039.

289. Cargnello, M.; Doan-Nguyen, V. V.; Gordon, T. R.; Diaz, R. E.; Stach, E. A.; Gorte, R. J.; Fornasiero, P.; Murray, C. B., Control of metal nanocrystal size reveals metal-support interface role for ceria catalysts. *Science* 2013, 341, (6147), 771-773.

290. Mao, M.; Lv, H.; Li, Y.; Yang, Y.; Zeng, M.; Li, N.; Zhao, X., Metal support interaction in Pt nanoparticles partially confined in the mesopores of microsized mesoporous CeO2 for highly efficient purification of volatile organic compounds. *ACS Catalysis* 2015, 6, (1), 418-427.

291. Yen, H.; Seo, Y.; Kaliaguine, S.; Kleitz, F., Role of metal–support interactions, particle size, and metal–metal synergy in CuNi nanocatalysts for H2 generation. *ACS Catalysis* 2015, 5, (9), 5505-5511.

292. Deng, W.; Zhang, H.; Wu, X.; Li, R.; Zhang, Q.; Wang, Y., Oxidative conversion of lignin and lignin model compounds catalyzed by CeO 2-supported Pd nanoparticles. *Green Chemistry* 2015, 17, (11), 5009-5018.

293. Pesce, M. A.; Bodourian, S. H., Evaluation of a fluorescence polarization immunoassay procedure for quantitation of methotrexate. *Therapeutic drug monitoring* 1986, 8, (1), 115-121.

294. Liu, X.; Liu, J.; Huang, Y.; Zhao, R.; Liu, G.; Chen, Y., Determination of methotrexate in human serum by high-performance liquid chromatography combined with pseudo template molecularly imprinted polymer. *Journal of Chromatography A* 2009, 1216, (44), 7533-7538.

295. Kuo, C. Y.; Chiou, S. S.; Wu, S. M., Solid-phase extraction and large-volume sample stacking with an electroosmotic flow pump in capillary electrophoresis for determination of methotrexate and its metabolites in human plasma. *Electrophoresis* 2006, 27, (14), 2905-2909.

296. Barbieri, A.; Sabatini, L.; Indiveri, P.; Bonfiglioli, R.; Lodi, V.; Violante, F. S., Simultaneous determination of low levels of methotrexate and cyclophosphamide in human urine by micro liquid chromatography/ electrospray ionization tandem mass spectrometry. *Rapid Communications in Mass Spectrometry: An International Journal Devoted to the Rapid Dissemination of Up-to-the-Minute Research in Mass Spectrometry* 2006, 20, (12), 1889-1893.

Chapter 2

Characterization Techniques, Materials and Methods

This chapter incudes a number of characterization techniques used for the identification of nanostructures/ nanoparticles and nanocomposite materials. The crystallinity, phase with lattice strain and purity of materials are examined via X-ray diffraction analysis, morphological characterization via SEM, FESEM and TEM analysis, surface area measurement with BET analysis, SERS analysis to determine the shift in frequency, absorbance value has been detected with UV/Visible spectroscopy and functional groups presence has been analyzed with FTIR spectrometer and dynamic light scattering-zeta potential for particle size analysis and surface charge on surface of nanoparticles. The formed nanoparticles/nanostructures and nanocomposite materials have been tested for the degree of cytotoxicity against carcinomatous cell lines.

Instruments are proved as a warrior in the field of experimentation, which help in established key role for sworded their importance.

Characterization techniques, materials and methods

2.1. General experimental methods and techniques

All the basic materials employed for the fabrication of nanostructure materials were of analytical grade, purchased from the Sigma Aldrich, Fisher Scientific and Merck India chemical supplier, and were used without further chemical purification. The details of tentative method, accepted analytical process, materials required, application of cytotoxicity application etc. are defined in this chapter.

2.2. Materials required

Palladium chloride ($PdCl_2$), Copper chloride ($CuCl_2$), Iron sulphate ($FeSO_4.7H_2O$), Nickel chloride ($NiCl_2.6H_2O$), Silver chloride (AgCl) and gold chloride ($AuCl_3$), polyethylene glycol (PEG), L-Ascorbic acid (LAA), deionized water etc.

For cytotoxicity measurement there is requirement of 10 % (w/v) TCA, 1 % (v/v) acetic acid, 0.057 % SRB in 1 % (v/v) acetic acid, 10 mM un-buffered Tris base solution.

2.3. Analytical methods

2.3.1. UV-visible spectroscopy

The UV-visible spectroscopy is commonly known as adsorption or reflectance spectroscopy and has shown its absorbance in ultraviolet visible spectral region. Amongst all techniques, it is considered as one of the best technique to determine electronic structure of free atom or colloidal form of nanostructure materials in frequent and in most simple way. This technique is correlative to the fluorescence

spectroscopy, in that fluorescence measures spectroscopic transition from excited to the ground state, at the same time adsorption deals with adsorption from ground to an excited state. When an electromagnetic radiation passage over the free or colloidal state of material, a fraction of radiation absorbed, by virtue of energy absorption, atoms or molecules excite from ground to first excited state giving absorption spectrum. The fraction of radiation that is absorbed has energy that is equal to path difference between the ground state and first excited state known as band energy. When the energy of incident light ($h\nu$) is greater than that of band gap (E_g) of semiconductor ($h\nu > E_g$) then valence band excite into the conduction band and the percentage of light absorbed by the particular semiconductor depends on the transition probability of electrons between the valence and conduction band. The probability strongly depends on the semiconductor band structure. The optical properties or optical absorption of the nanostructure semiconductor material can also be demonstrated by the UV-visible spectroscopy via the intercommunication between electromagnetic radiation and semiconducting materials. The optical absorption phenomenon is responsible for electronic transition in semiconductor material through interband and intraband transition, or via impurity and lattice defects. The first type of optical phenomenon involves the absorption of photons which involves the energy greater or equal than band gap energy of a semiconductor. This type of optical absorption is called the process of fundamental edge or interband absorption. The fundamental absorption edge energy is determined by the semiconductor band gap. The fundamental or interband absorption band phenomenon is typically followed by an electronic transition through the forbidden gap, correspondingly excess electron hole pairs are generated in semiconducting nanostructures. The absorption coefficient is commonly very large because of interband transition.[1-2]

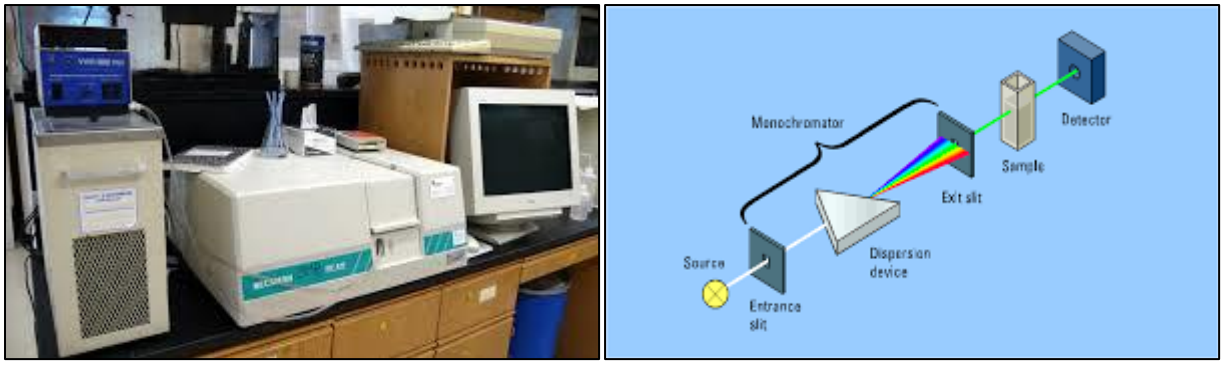

Fig.2.1. Image of UV-visible spectroscopy

The absorption band changes into very small, when the energy of electromagnetic radiation drops lower the band energy of semiconductor. In this circumstance, another type of optical absorption takes place which is the result of electronic structure within the allowed energy state in semiconductor material and is known as free carrier absorption process. Absorption of photons with energy underneath the band gap energy of semiconductor may also lead to an electronic transition from localized impurity state to the conduction or valence band states.[3]

The relation between the absorbance and concentration has been explained by the Beer-Lambert law[4] as:

$$T = \frac{I}{I_0}$$

$$A = log\left(\frac{I_0}{I}\right) = log\left(\frac{1}{T}\right) = \epsilon cl$$

Where T is the transmittance, I_0 is the intensity of incident light, I is the intensity of transmitted light, A is absorbance, ϵ is molar extinction coefficient, l is the path length and c is the concentration.

The schematic presentation of UV-visible spectrophotometer contains source (hydrogen/deuterium, tungsten/halogen discharge lamp), wavelength selector (diffraction gratings), sample, solvent and detector. A beam of monochromatic light is

divided into two beams, one of the fragments light is passed through the specimen and other passed to reference cell, two beams are collected to detectors when they are analyzed. The optical absorption and transmission spectra are recorded using a Carry-100 UV-visible spectrophotometer in 200-800 nm range.

2.3.2. Fourier Transform Infrared spectroscopy (FTIR)

This is the most broadly used technique for the characterization of nanostructures. It is the most widespread characterization technique to investigate the IR spectra, absorbed by the sample, when it kept in path of IR radiation source.[5] The infrared spectrum performs only when the vibration amongst the bonded atoms provide a permanent change in electric dipole moment of molecule or material. It is well understood that more polar the bond, more intense will be the IR spectrum arising from the vibration of bond. The information concerning structure, symmetry, bond length, inter and intra molecular interactions etc., are obtained from IR spectra. Therefore IR spectroscopy is operating to recognize the type of bond between atoms of a molecule and consequently identifies functional groups like –OH, COOH, NH_2 and CH_2 etc. The intensity and spectral position of IR absorption allow the identification of structure of molecule. Solid, liquid and gaseous samples can be characterized by this technique.

The entire infrared spectrum of polyatomic molecule can be divided into the functional group region and fingerprint region. The functional group region is generally considered as 4000 to 1500 cm^{-1} while fingerprint region has been ranges from 1500 to 400 cm^{-1}. The fingerprint region[6] involves usually bending vibrations that are characteristics of entire molecule or fragments of molecule and are used for the identification. The functional group region mainly includes stretching vibration that is localized and characteristics of typical functional groups found in organic

molecules.[6] These are not very useful to confirm its identity, but provide useful information about the components of sample.

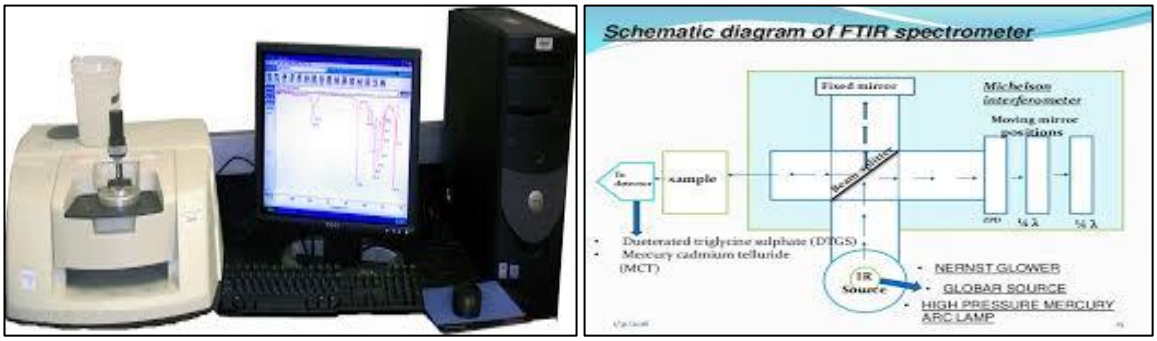

Fig.2.2. Image of FTIR instrument.

IR spectroscopic technique mostly encloses a source, a monochromator and detector. IR source provide a high radiation energy output in IR region. The most frequently used source in the production of IR is Nernst Glower and Glober.[7] The deuterated triglycerine sulfates (DTGS), L-alanine doped deuterated triglycerine sulfate (DLaTGS), mercury cadmium telluride (MCT) are generally used detectors in IR spectroscopy. DTGS detectors have significantly lesser sensitivity as compared to MCT detectors, which have to be cooled typically using liquid nitrogen. The basic description of source, monochromator, filters and detectors has defined by Colthen et al. In FTIR spectral analysis, the dispersive device, prism and monochromators are replaced by interferometer. The beam splitter splits the radiation into two beams that are reflected back from mirror to beam splitter. The recombined beam at beam splitter provides interference. If a beam passes through the sample, absorption cause gaps in frequency distribution: one mirror of the interferometer is moved towards and away from the splitter at a constant speed. The detector sees time domain signals (interferogram), which convert to frequency domain by Fourier transform using software and computer. It is faster and sensitive system than the older dispersive

instruments. FTIR measurement has high resolution, high signal to noise ratio and higher accuracy.

2.3.3. Powder X-ray diffraction

The powder X-ray crystallography is an important non-destructive analytical technique for investigation of chemical and physical features of nanostructure materials, to explore atoms in crystalline phase and interatomic distances and angles etc. It also endows evidence about the preferred crystal orientation and phase and other structural constraints such as average particle size, crystallographic unit cell, crystal defect and crystallinity.[8-9] In this characteristic technique, a beam of accelerated electrons colloid with metal target to produce X-rays. In this procedure inner electron moves down to fill vacancy and emit X-rays. X-rays have wavelength in angstrom (Å), which is the characteristic range of distance inner atoms in crystalline solids. The beam of X-ray have similar wavelength that interacts on a material (single crystalline or amorphous powder) of the nanostructure under investigation.

Fig.2.3. Image of XRD instrument

The diffraction pattern is the outcome of interaction among the X-rays and inner electrons of atoms. On behalf of arrangement of atoms, retardation between the scattered rays is profitable, when path between the two diffracted rays is different from an integral number of wavelengths. The situation is illustrated by the Bragg's equation and is given by[10]:

$$n\lambda = 2d\,Sin\theta$$

Where, n is an integer quantity, λ is the wavelength of X-ray, d is the space between the planes in atomic lattice, θ is the diffracted angle between X-rays and atomic planes. This law represents a relationship between wavelength of incident X-ray, diffraction angle and lattice distance in crystalline material. The diffracted X-ray from the material is then perceived, refined and counted. By scanning the material through a range of 2θ angle, all possible diffraction directions of lattice should be obtained because of random orientation of powdered sample. The conversion of lattice peaks to d-spacing allows identification of samples because each sample has a set of unique d- spacing with joint committee on powder diffraction standard (JCPDS).

Applications

The mean size of crystalline material can be calculated by adopting the full width half maxima (FWHM) of diffraction peaks by applying the Scherrer's equation[11] is given by:

$$D = \frac{0.91\lambda}{\beta \cos\theta}$$

Where 0.91 is the value of shape factor, λ is the wavelength of X-ray which is 1.5406 nm for the CuKα, β is the FWHM of diffraction peaks, measured in radians and θ is Bragg's angle.

The bond length and volume was calculated from the unit cell for the prepared material with the help of given equation[12]:

$$L = \sqrt{\frac{a^2}{3} + \left(\frac{1}{2} - z^2\right)c}$$

$$z = \frac{a^2}{3c^2} + \frac{1}{4}$$

$$V = 0.866a^2c$$

Where a and c are lattice parameters that are determined by the following expression[13]:

$$\frac{1}{d^2} = \frac{4}{3}\left(\frac{h^2 + hk + k^2}{a^2}\right) + \frac{l^2}{c^2}$$

The microstrain, (ϵ) present in the material also be calculated by using the following relation[14]:

$$\epsilon = \frac{\beta Cos\theta}{4}$$

The dislocation density, (δ) in the nanoparticle was estimated by the Williamson and Smallman equation[15]:

$$\delta = \frac{n}{D^2}$$

Where n is constant usually close to one.

2.3.4. Transmission Electron Microscopy

It is a powerful technique, developed in 1930 for obtaining the information of morphology, size, crystal structure, and defect structure of the prepared material.[16] It is direct and most advanced most important technique for imaging the nanostructure

materials. The energy of electron for imaging and diffraction pattern decided by the de' Broglie wavelength i.e. $\lambda = h/p$, where h is a Plank's constant and p is the momentum of electron. In an experimental pattern, a thin sample typically less than 200 nm, is bombarded by the high energy level (few hundred keV) and focused electrons of very short wavelength emitted from the tungsten filament at the top of cylindrical column of height of about 2 m.[17-18] These bombarded electrons scattered or backscattered elastically or in-elastically or produce many interactions between the fast electron and atomic electron. An image is formed from the electron, transmitted through the sample, the image is stretched and focused onto an imaging device such as fluorescent screen or on a layer of photographic film and detected by a detector such as CCD (charge couple device) camera. The back scattered electron give diffraction pattern to obtaining the information of structure of materials, including perfect crystal and defect structures. The preference of electron diffraction over other methods i.e. X-rays or neutrons are due to the generation of extremely short wavelength (2 pm), the strong atomic scattering and more capability to scrutinize insignificant volume of matter (10 nm).[19]

When we consider the schematic ray diagram of the TEM analyzer, an electron gun (electron source) generated electron beam, and confined through the condenser lens, passes the condenser aperture and strikes the sample, which is ultra-thin and most of un-scattered electrons are transmitted through the materials with some undergoing deflection as a result of elastic and inelastic scattering. The scattered and un-scattered electrons are then recombined through the objective lens forming either a first intermediate image or a diffraction pattern in back focal plane. The image of diffraction pattern will be further magnified by an intermediate lens, and by altering the projector lens, an enlarged image or diffraction pattern will be focused and

projected on the fluorescent screen or reduced on a digital camera (CCD). TEM microscopy has dominance over other, because it can't obtain the image of sample but diffraction pattern also, which be enable to make crystal structure analysis of the sample. So using diffraction analysis one can find the size dependent changes in lattice parameters, defects etc. in sample. It is also possible to analyze single particles of very small dimension (nanometer).

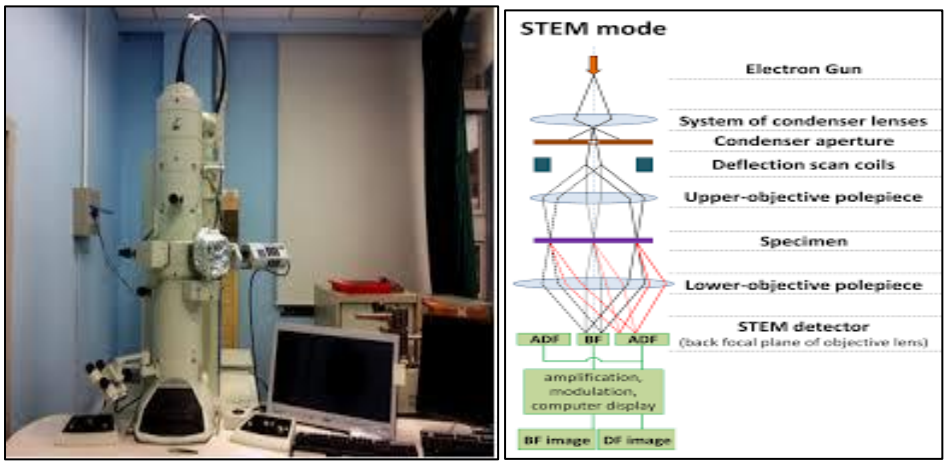

Fig.2.4. Image of TEM instrument.

High resolution TEM is capable of providing the atomic resolution lattice images. In case of HRTEM images are formed because of phase difference in scattered electrons waves through a thin specimen. The emergence of HRTEM has allowed the direct reconstruction of Bragg's differential electron beams to create an interference pattern.[20]

2.3.5. Scanning Electron Microscopy

It is frequently used characterization technique that applied to beam of electrons to obtain high enlargement of three dimensional images for the morphological and topographical studies of material and surface on a micrometer and sub-micrometer scale. It can also provide information about the elemental composition of sample by

an additional part of this technique known as electron dispersive X-ray spectroscopy (EDS).

In the experimental process, the electron beam of high intensity generated from the electron gun,[21-22] passes through the electromagnetic lenses and strikes a point on the sample, the molecules in the materials are strikes on sample, and excites to high energy level, because of the number of effective collision between generated electron beams and atoms in the molecules of materials will occur, which causes the production of secondary electrons. Many secondary electrons are created by inelastic interactions between incident electrons and weakly bound conduction band electron in atom of samples. Secondary electrons possess very small kinetic energy (5 eV). Hence, average distance that a secondary electrons travels in solid is less than 2 nm. Apart from secondary electrons, backscattered electrons, characteristic X-rays and various energy of photons are also produced.[23] Backscattered electrons are also generated by elastic interaction (diffraction angle > 90) between the incident electrons and nucleus of atom in sample. High energy backscattered electrons can penetrate deeper than secondary electrons in solid sample. The penetration depth is strongly dependent on the specimen's atomic number (Z), decreases with increasing (Z). The secondary as well as backscattered electrons have comparatively low energy and can conveniently gather by detector. The detectors tallies the number of electrons released from the specimen and resulting pattern produces a three dimensional image of morphology and topography of the sample on the screen of the detector. Compositional analysis of the material may also be achieved by observing X-ray produced by the interaction of electron and interaction specimen. Scanning takes place at lower pressure so that electrons are not scattered by gas molecules inside the chamber.

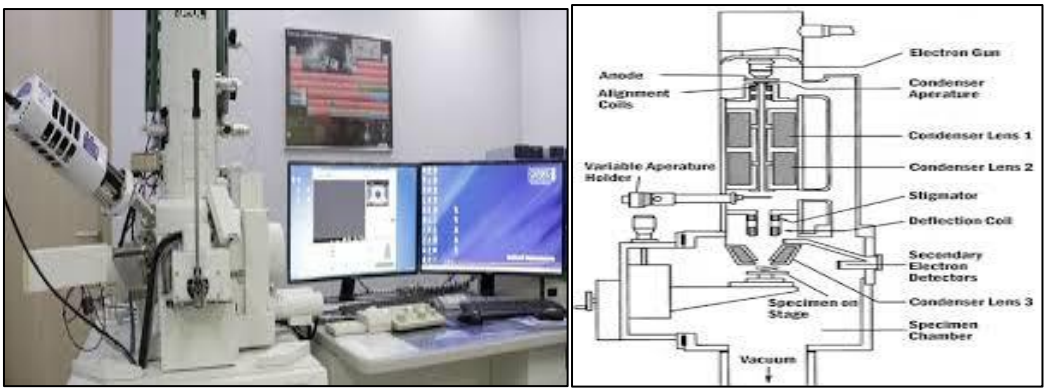

Fig.2.5. Image of SEM instrument

2.3.6. Brunauer Emmett Taylor (BET) surface analysis

This method is applied to recognize the physical adsorption of gas molecules[24] on the surface of nanostructure materials and assist as a fundamental technique for an estimation of surface area analysis of nanoparticles expressed in m^2/g per unit volume. The BET method is applied to multilayer adsorption of materials and commonly used those gases which do not react to the surface on nanoparticle materials act as adsorbate for the measurement of specific surface area. Nitrogen gas is specially used as adsorbate for the surface inquiry by BET method. The tenet of BET surface area examination is an augmentation of Langmuir theory based on adsorption theory of monolayer to multilayer adsorption with some hypothesis such as gas molecules adsorb on materials with infinite layers and adsorb gas molecules can interact with adjacent layers only. The BET equation can be represented as:

$$\frac{1}{\{v(p_0/p) - 1\}} = \frac{(c - 1)}{v_m c}\frac{p}{p_0} + \frac{1}{v_m c}$$

Where p is the equilibrium pressure, p_0 is the saturation pressure of nitrogen gas as adsorbate at a temperature of adsorption, v is the total quantity of gas adsorbed, v_m is the quantity of gas adsorbed on monolayer and c is the BET constant, which can be expressed as:

$$c = exp\left(\frac{E1 - E2}{RT}\right)$$

Where E_1 represents the adsorption of heat on the first layer and E_2 is for second and higher layer. So from an equation of adsorption isotherm graph is plotted between $\frac{1}{\{v(p_0/p) - 1\}}$against $\frac{p}{p_0}$. This plot is known as BET plot. To obtain linear graph, the value of p/p_0 is $0.05<p/p_0<0.35$. From this, the value of slope (S) and intercept (I) measure the gas quantity (v_m) of adsorbed monolayer gas and BET constant, c used following equation.

$$v_m = \frac{1}{S + I}$$

$$c = 1 + \frac{S}{I}$$

The total area (S_{total}) and specific surface area (S_{BET}) is measure with the help of the following equation:

$$S_{total} = \frac{v_m N s}{V}$$

$$S_{BET} = \frac{S_{total}}{a}$$

Where v_m is the volume unit, N is the Avogadro's number, s is the cross section surface area of adsorbed gas and V is the molar volume of adsorbate gas amount in nanomaterials.

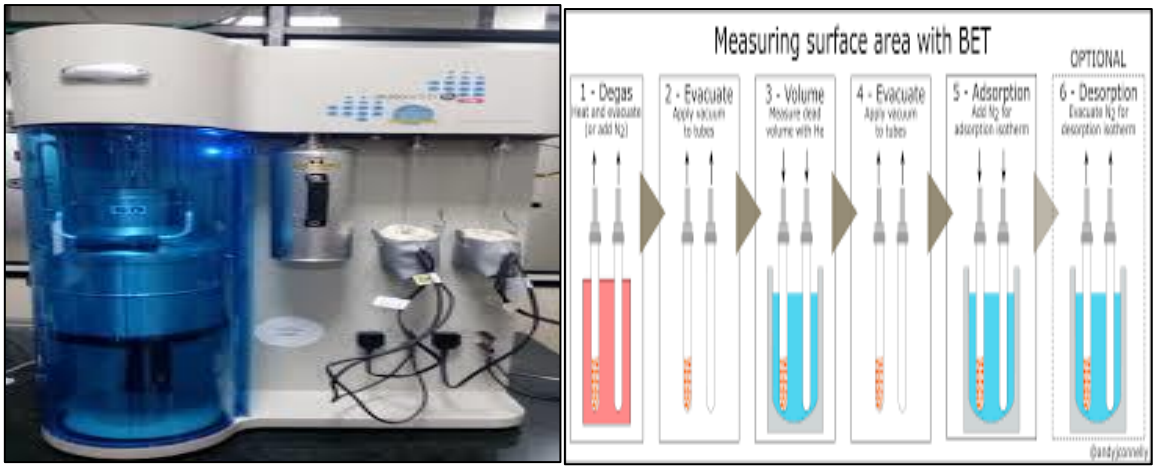

Fig.2.6. Images of BET instrument.

Barrett-Joyner-Halenda (BJH) measurement can also be applied to calculate the pore size and specific pore volume by adopting adsorption and desorption method.

2.3.7. Surface Enhanced Raman spectroscopy (SERS)

The surface enhanced Raman spectroscopy (SERS) is a powerful technique for investigating the chemical reaction on metal nanoparticles surface.[8-10] In past few years, number of bi-functional nano-hybrids,[11-13] and nano-assemblies[14-15] with both SERS and catalytic activity have been reported. SERS detection of catalysis is limited to very few models, including the prominent reaction of 4-nitrothiophenol (4-NTP) and 4-aminothiophenol (4-ATP).[16-19] As a surface sensitive and molecule specific method.[20-21] SERS monitoring of catalysis should not only focus on model reaction but also find applications in NP catalyzed Suzuki reaction to answer the fundamental question of whether the catalyst is homogenous and heterogeneous. The Raman scattering has been prescribed by the German physicist A. Smekel in 1923. It was observed by C.V. Raman and K.S. Krishnan in 1928. The Indian Scientist C.V Raman won the Noble Prize in Physics in 1930 for his work on the scattering of light and for the discovery of Raman Effect.

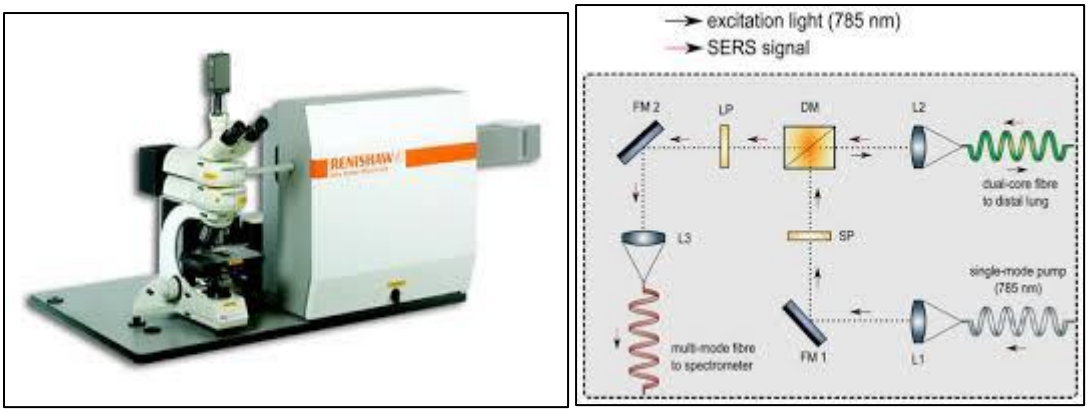

Fig.2.7. Image of Raman instrument

This theory stated that when a molecule, excited to the higher unstable vibrational state, returns to the original vibrational state, we get Rayleigh scattering. If it returns to a different vibrational state, which gives rise to Raman scattering (Stokes lines).[25] When the molecules initially in first excited vibration state is promoted to higher unstable vibrational state and return to ground state, this again gives rise to Raman scattering (anti-Stokes lines).[26] This the Raman spectrum of a molecule consist of Stokes and anti-Stokes lines, situated symmetrically about the Rayleigh line.

The Rayleigh line is far more intense than Stokes lines which in turn have greater intensity than the anti-stokes lines.[27] The anti-stokes lines are difficult to observe in conventional Raman spectroscopy because they correspond to the return of the molecule from unstable excited vibrational state to the ground state and initially there are very molecules in the excited vibrational state.[28]

$$E' - E = h(\nu' - \nu) = h\Delta\nu_{Raman} = hc\Delta\bar{\nu}_{Raman}$$

The shift in frequency, (v-v') is called Raman shift. It falls in range of 100-4000 cm^{-1} for vibrational energy changes. These values are similar for rotational energy changes. Since $\bar{\nu} = 1/\lambda$, we have[29]:

$$\bar{v}(cm^{-1}) = \frac{10^8}{\lambda}(\AA)$$

Hence Raman shift (in cm^{-1}) is given by[30]:

$$\Delta\bar{v}_{Raman}(cm^{-1}) = \frac{10^8}{\lambda_{exc}}(\AA) - \frac{10^8}{\lambda_{Raman}}(\AA)$$

Where λ_{exc} is the wavelength correspond to the exciting (incident) frequency.

2.3.8 Dynamic Light Scattering (DLS) @ Zeta potential

The standard technique used to analyze the measurement of polydisperse samples has completed via intensity-intensity autocorrelation function of scattered light, described in terms of distribution of decay rates. It provides a method of distribution and information about the dispersed particles, their ranges and peaks intensity. However, the method doesn't permit the independent determination of a long time baseline of the intensity correlation function and can lead to inconsistent results when different data are included. The different version of the methods is compared by analysis of data for polydisperse- vesicle samples.

The dynamic light scattering (DLS) technique measures motion optically by recording the scattered light signal at a fixed angle. These particles are illuminated with a monochromatic coherent light source (laser) and light scattered by particles is recorded.

Principles

Several backlight systems dominate the power requirement of battery-operated handheld devices with the color thin filmed transistor (TFT), liquid crystal display (LCD). The introduction of dynamic light scattering analysis (DLS) of the backlight

with an appropriate image concentration provides an effective analysis for the determination of the size of materials in terms of their polydispersity index (PDI) value. The particles size of the dispersed particles has been elucidating from the given formulae:

$$D = \frac{kT}{3\pi\eta dP}$$

Where k is Boltzmann's constant, T is absolute temperature, η is viscosity.

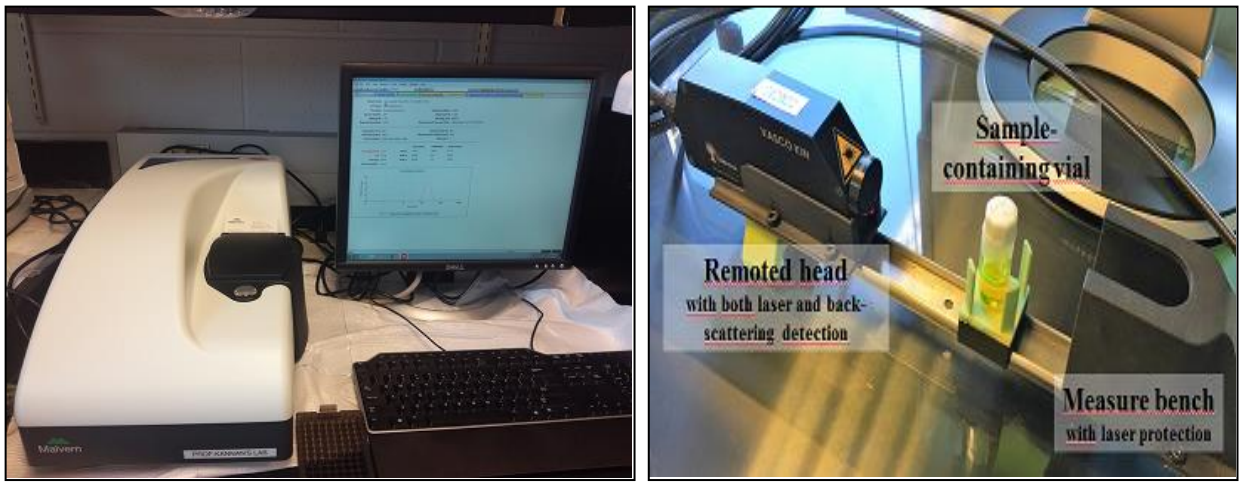

Fig.2.8. Dynamic Light Scattering (DLS) @ Zeta potential

Zeta potential

This method describes the measurement of electrostatic potential at the electrical double layer surrounding around nanoparticles solution. This is referred to zeta potential analysis. Nanoparticles have value in range of -10 mV to + 10 mV are approximately neutral. Nanoparticles having zeta value greater than +30 mV and lesser than -30 mV are completely cationic and anionic respectively. Since most cellular membranes are negatively charged, zeta potential can affect a nanoparticle's tendency to permeate membranes, with cationic particles displaying more toxicity than associated with cell disruption.

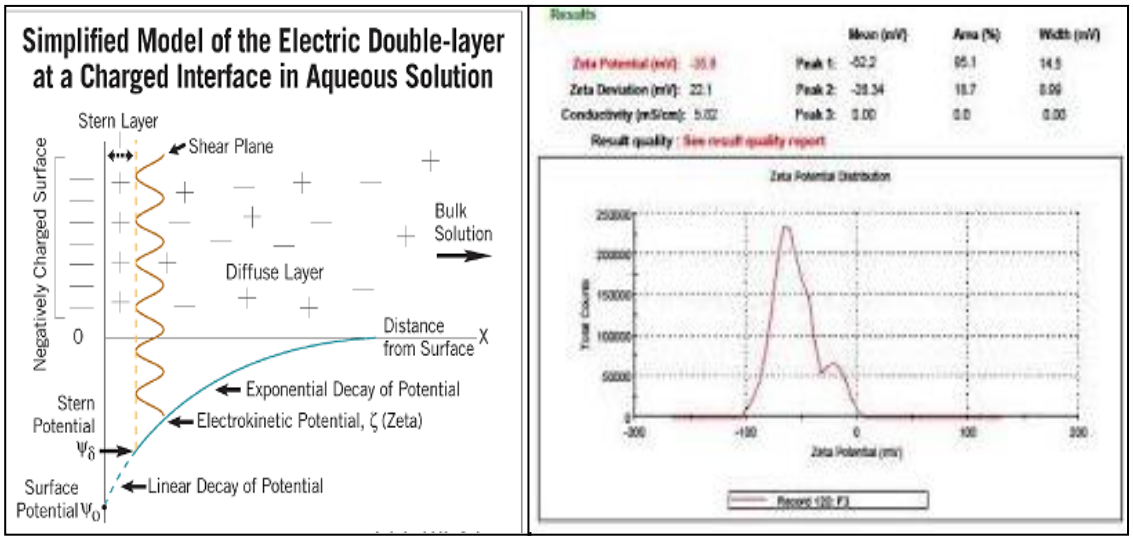

Fig.2.9. Zeta potential analysis.

References

1. Takahashi, K.; Yoshikawa, A.; Sandhu, A., Wide bandgap semiconductors. *Springer-Verlag Berlin Heidelberg*. **2007**, 239.
2. Bass, M.; DeCusatis, C.; Enoch, J.; Lakshminarayanan, V.; Li, G.; Macdonald, C.; Mahajan, V.; Van Stryland, E., *Handbook of optics, Volume II: Design, fabrication and testing, sources and detectors, radiometry and photometry*. McGraw-Hill, Inc.: 2009.
3. Kalt, H.; Hetterich, M., *Optics of Semiconductors and their Nanostructures*. Springer Science & Business Media: 2013; Vol. 146.
4. Workman Jr, J.; Springsteen, A., *Applied spectroscopy: a compact reference for practitioners*. Academic Press: 1998.
5. Kendall, D. N., Applied infrared spectroscopy. **1966**.
6. Hausdorff, H. In *Analysis of polymers by infrared spectroscopy*, Analytical chemistry, 1951; AMER CHEMICAL SOC 1155 16TH ST, NW, WASHINGTON, DC 20036: 1951; pp 683-683.
7. Colthup, N.; Daly, L.; Wiberley, S., Introduction to infrared and Raman spectroscopy, Acad. *Press, New York* **1964**.
8. Als-Nielsen, J.; McMorrow, D., *Elements of modern X-ray physics*. John Wiley & Sons: 2011.
9. Bowen, D. K.; Tanner, B. K., *High resolution X-ray diffractometry and topography*. CRC press: 1998.
10. Kittel, C.; McEuen, P., *Introduction to solid state physics*. Wiley New York: 1996; Vol. 8.
11. Pandey, G.; Dixit, S., Growth mechanism and optical properties determination of CdS nanostructures. *The Journal of Physical Chemistry C* **2011,** 115, (36), 17633-17642.

12. Othman, A.; Ali, M. A.; Ibrahim, E.; Osman, M., Influence of Cu doping on structural, morphological, photoluminescence, and electrical properties of ZnO nanostructures synthesized by ice-bath assisted sonochemical method. *Journal of Alloys and Compounds* **2016,** 683, 399-411.

13. Hitkari, G.; Singh, S.; Pandey, G., Structural, optical and photocatalytic study of ZnO and ZnO–ZnS synthesized by chemical method. *Nano-Structures & Nano-Objects* **2017,** 12, 1-9.

14. Shannon, R. D., Revised effective ionic radii and systematic studies of interatomic distances in halides and chalcogenides. *Acta crystallographica section A: crystal physics, diffraction, theoretical and general crystallography* **1976,** 32, (5), 751-767.

15. Kumar, S.; Sharma, P.; Sharma, V., CdS nanofilms: synthesis and the role of annealing on structural and optical properties. *journal of Applied Physics* **2012,** 111, (4), 043519.

16. Klimov, V. I., *Semiconductor and metal nanocrystals: synthesis and electronic and optical properties*. CRC Press: 2003.

17. Fultz, B.; Howe, J. M., *Transmission electron microscopy and diffractometry of materials*. Springer Science & Business Media: 2012.

18. Kohl, H.; Reimer, L., *Transmission electron microscopy: physics of image formation*. Springer: 2008.

19. Bendersky, L. A.; Gayle, F. W., Electron diffraction using transmission electron microscopy. *Journal of research of the National Institute of Standards and Technology* **2001,** 106, (6), 997.

20. Goodhew, P. J.; Humphreys, J., *Electron microscopy and analysis*. CRC Press: 2000.

21. Reimer, L., Scanning electron microscopy: physics of image formation and microanalysis. In IOP Publishing: 2000.

22. Lee, R. E., *Scanning electron microscopy and X-ray microanalysis*. 1993.

23. Vernon-Parry, K., Scanning electron microscopy: an introduction. *III-Vs Review* **2000,** 13, (4), 40-44.

24. Brunauer, S.; Emmett, P. H.; Teller, E., Adsorption of gases in multimolecular layers. *Journal of the American Chemical Society* **1938,** 60, (2), 309-319.

25. Stiles, P. L.; Dieringer, J. A.; Shah, N. C.; Van Duyne, R. P., Surface-enhanced Raman spectroscopy. *Annu. Rev. Anal. Chem.* **2008,** 1, 601-626.

26. Xie, W.; Schlücker, S., Surface-enhanced Raman spectroscopic detection of molecular chemo-and plasmo-catalysis on noble metal nanoparticles. *Chemical Communications* **2018,** 54, (19), 2326-2336.

27. Zong, C.; Xu, M.; Xu, L.-J.; Wei, T.; Ma, X.; Zheng, X.-S.; Hu, R.; Ren, B., Surface-enhanced Raman spectroscopy for bioanalysis: reliability and challenges. *Chemical reviews* **2018,** 118, (10), 4946-4980.

28. Heck, K. N.; Janesko, B. G.; Scuseria, G. E.; Halas, N. J.; Wong, M. S., Observing metal-catalyzed chemical reactions in situ using surface-enhanced Raman spectroscopy on Pd− Au nanoshells. *Journal of the American Chemical Society* **2008,** 130, (49), 16592-16600.

29. Xie, W.; Herrmann, C.; Kömpe, K.; Haase, M.; Schlücker, S., Synthesis of bifunctional Au/Pt/Au core/shell nanoraspberries for in situ SERS monitoring of platinum-catalyzed reactions. *Journal of the American Chemical Society* **2011,** 133, (48), 19302-19305.

30. Taladriz-Blanco, P.; Rodríguez-Lorenzo, L.; Sanles-Sobrido, M.; Hervés, P.; Correa-Duarte, M. A.; Alvarez-Puebla, R. A.; Liz-Marzán, L. M., SERS study of the controllable release of nitric oxide from aromatic nitrosothiols on bimetallic, bifunctional nanoparticles supported on carbon nanotubes. *ACS applied materials & interfaces* **2009,** 1, (1), 56-59.

Chapter 3

Effect of Reaction Temperature on Shape Evolution of Palladium Nanoparticles and Their Cytotoxicity against A-549 Lung Cancer Cells

Effect of reaction temperature on shape evolution of palladium nanoparticles and their cytotoxicity against A-549 lung cancer cells

Abstract

Different shapes and sizes palladium nanoparticles (Pd NPs) have been synthesized by reducing potassium tetrachloropalladinate(II) by L-ascorbic acid (AA) in aqueous solution phase in the presence of an amphiphilic nonionic surfactant poly ethylene glycol (PEG) via sonochemical method. Materials have been characterized by XRD, SEM, TEM, EDX, FTIR, SERS, particle's distribution and zeta potential studies. Truncated octahedron/fivefold twinned pentagonal rods are formed at room temperature (25 °C) while hexagonal/trigonal plates are formed at 65 °C. XRD results show evolution of anisotropically grown, phase pure and well crystalline face centered cubic (fcc) Pd NPs at both temperatures. FTIR and SERS studies revealed adsorption of ascorbic acid (AA) and poly ethylene glycol (PEG) at NP's surface. Particle's size distribution graph indicates formation of particles having wide size distribution while the zeta potential particle's surface is negatively charged and stable. The truncated octahedron/fivefold twinned pentagonal rods shaped Pd NPs, formed at room temperature while thermally stable and kinetically controlled hexagonal/trigonal plate-like Pd NPs have been evolved at higher temperature 65 °C. The obtained Pd NPs has a high surface area and narrow pore size distribution. To predict protein reactivity of Pd cluster, docking has been done with DNA and lung cancer effective proteins. The cytotoxicity of the Pd NPs has been screened on human lung cancer cells A-549 at 37 °C. The biological adaptability exhibited by Pd NPs has opened a pathway in biochemical applications.

Keywords: Pd nanoparticles; electron microscopy; BET; XRD; docking; cytotoxicity.

3.1. Introduction

In the last few decades, mesoporous materials have gained enormous attention of various scientists globally in both industry and academia because of their high surface area, tunable pore size, uniform and narrow pore size distribution.[1-2] On account of these properties, mesoporous and nanoporous materials have shown high demand in various fields such as energy storage[3], catalysis[4,5] and biomedical applications.[6,7] In the past, desired shapes nanoparticles, like spherical, films, rods, tubes etc., with mesoporous structures have been prepared by soft template method like self-assembly of micelles.[8] On the other hand, in hard template method, the targeted materials are deposited in the confined spaces of a template with the desired morphology.[9] Since soft template method is simple and easy approach, hence it is favourable for the generation of desired shapes nanoparticles using low molecular weight molecules like Brij 58, PEG etc. and high molecular weight amphiphilic molecules, e.g. triblock copolymers as pore-directing agents.

In recent years nanotechnology has shown enormous potential in the biomedical field as therapeutic mediators for many diseases, including cancer.[10] In this regard, metal nanostructures have shown great interest due to their size, structure versatility, and optoelectronic properties.[11] Since the introduction of catalytic converters in the USA in 1975 and in Europe in 1986 (Wiseman and Zereini 2009), platinum group metals have shown increasing demands particularly in the area of electronics and catalysis. The latest research demonstrate that palladium (Pd) nanoparticles have widely been used in catalysis, (e.g. oxidation/reduction of methanol,[12] stereochemical oxidation of ethanol,[13] redox organic reactions,[14,15] sensors for detection of various analytes,[16] hydrogen generation/storage, methane combustion, supercapacitors, lithium-ion batteries and in biomedical applications.[17]

Kyubin Shim *et al.* synthesized dendritic platinum nanoparticles and demonstrated their cytotoxicities against human embryonic kidney cells.[18] Unciti-Broceta *et al.* demonstrated that the prodrugs 5-fluoro-1-propargyluracil[19] and N-4-propargyloxycarbonylgemcitabine[20] are independently harmless, however, when separately combined with Pd(0)-glycol-polystyrene resin these prodrugs exhibited anti-proliferation properties compared to the unmodified drug in colorectal and pancreatic cancer cells. However one of the major limitations, in the case of metallic NPs is their nonspecific untargeted toxicity. Huang *et al.* used ultra-thin (1.8 nm) hexagonal Pd nanosheet with 41 nm edge for cancer photothermal therapy (PT). The nanosheets were able to kill 100 % liver cancer cells after 5 minutes irradiation of 808 nm laser, showing size dependant and tunable absorption peaks in the NIR region and exhibited high biocompatibility in the absence of irradiation. More interestingly, these Pd nanosheets exhibited better photo-stability than Au and Ag nanostructures.[21] Balbin *et al.* reported high cytotoxicity of mesoporous silica-supported Pd NPs against four human cancer cell lines, simultaneously displaying catalytic activity for C-C bond formation via Suzuki-Miyaura cross-coupling between small molecules.[22] Pranesh Kumar *et al.* prepared (polylactic-co-glycolic acid)- loaded nanoparticles betulinic acid for improved treatment of hepatic cancer and showed in vitro and in vivo evaluation.[23] Several structural modifications have been proposed to improve biomedical efficiency of Pd nanoparticles.[22,24] Porous Pd nanoparticles(22.8 nm) were also recently reported as attractive PT agents with PT conversion efficiency as high as 93.4%, which is comparable to typical Au nanorods.[25]

There is high interest to expand the applicability of Pd nanoparticles, therefore it is highly desirable to synthesize shape and size-controlled Pd NPs for excellent performance in biomedical applications. Generation Pd nanoparticles using amphiphilic molecules (non-ionic surfactants) via sonochemical process is a novel

and rapid approach to tune the kinetics of the reaction. In this investigation, mesoporous Pd nanoparticles have been prepared via sonochemical route and their cytotoxicity has been screened by using the culture of human lung cancer cells A-549.

3.2 Materials and Methods

3.2.1 Materials

Analytical reagent grade potassium tetrachloropalladinate (II) (K_2PdCl_4), polyethylene glycol (PEG) and L-ascorbic acid (AA, $C_6H_8O_6$) were purchased from Sigma-Aldrich and used without further purification. De-ionized water and ethanol were used as solvents in this study.

3.2.2 Synthesis

In the two different vessels, 10 mL solutions of 0.1 M K_2PdCl_4 were prepared, and 10 mL aqueous 0.1 M ascorbic acid (AA) solutions were added to each vessel. Further, 1 mL of 50 mg/L aqueous PEG solutions were added to each reaction mixtures. The two solution mixtures were reacted at room temperature and 65 $^{\circ}$C, respectively, for 30 minutes with thorough ultra-sonication (220-240V, 50-60Hz). After the reactions, the products were collected by centrifugation and washed several times with de-ionized water and ethanol to remove residual surfactant and excess reactants.

3.2.3 Characterization

The X-ray diffraction patterns of the obtained products were recorded on Pananalytical's X'Pert Pro X-ray diffractometer in the 2θ range 10 to 80° with a step size of 0.025°. Scanning electron microscope (SEM) images of the materials were observed on JEOL 6490 LB equipment at operating electrical energy of 3 kV.

Particles shapes and sizes of the materials were further examined on JEOL-2100 transmission electron microscope (TEM). The zeta potential of Pd nanoparticles (formed at room temperature) was measured using a Zetasizer ZS90 (Nano series Malvern Instrument) at room temperature. Dispersion of nanoparticles was sonicated for 20 minutes and diluted to make a solution with concentration 80 µg/mL in phosphate buffer saline (pH = 7.4). The particle size and size distribution were carried out on a Zetasizer ZS90 (Nano series Malvern Instrument). SERS spectrum of Pd nanoparticles, formed at room temperature, was recorded on NSCOM/Raman/ Confocal/AFM used for UV/lithography (200 nm) and near field imaging of features as small as 100 nm Raman spectra and imaging for an excitation wavelength of 532 nm with an extinction coefficient of 8000 $M^{-1}cm^{-1}$. FTIR spectra of the products have been recorded on Perkin Elmer Spectrum two instrument. UV/Vis data were collected on a Shimadzu UV-3600 spectrophotometer. Brunauer-Emmett-Teller (BET) analysis of the materials was recorded on Belsorp-mini II instrument.

3.2.4 Cytotoxicity Test

The culture of A-549 human lung cancer cells (~ 100000 cell mL^{-1}) were taken in 10 % fetal bovine serum (FBS)-supplemented Dulbecco's Modified Eagle's Medium (DMEM) in a 24-well microtitre plate. Different amounts of Pd NPs (formed at room temperature) were suspended in deionized water to make solutions with concentration from 10 to 60 µg mL^{-1}. Homogenization of each solution was carried out with an ultrasonic processor (LABSONIC® M, Sartorius Stedim Biotech GmbH) for 15 minutes and added separately to cultures, keeping one blank as reference. The cultures were incubated for 24 hours in an incubator with 5 % CO_2 in a humid atmosphere at 37 °C. After incubation, the cells were removed from the culture by

trypsinisation and washed a coupled by Dulbecco's phosphate-buffered saline (PBS; pH: 7.4) to remove the residual presence of serum. The cells were again suspended in PBS, and aliquots of 20 µL were prepared from all the cultures. Equal amounts (v/v) of pre-filtered 0.4 % trypan blue stain added to the aliquots, and were put aside to settle for 1 minute. To determine the cell viability, the samples were observed on an inverted microscope in a Fuchs-Rosenthal Haemocytometer. The results of cytotoxicity were expressed by plotting cell viability histogram and curve and analyzed by IC_{50} value.

3.3. Results and Discussion

3.3.1. Characterization of Pd nanoparticles

When the solution containing $[PdCl_4]^{2-}$ complexions were treated with AA at room temperature, the solution turned black within 30 minutes, indicating a reduction of $[PdCl_4]^{2-}$ complex ions is completed in this period. This reaction was monitored by UV-visible absorption spectroscopy experiment shown in Figure 3.1. Before formation of Pd NPs, absorption band corresponding to the Pd complex was clearly detected at 424 nm, which completely disappeared after reaction, indicating that the complex ions are changed from Pd^{+2} to Pd(0) owing to their reduction by AA.[13] Moreover, the spectrum of the sample shows broad continuous absorptions in the UV-visible range which is characteristic of the reduced Pd NPs as reported earlier.[26] On increasing reaction temperature at 65 °C virtually no alteration in spectral profile has been observed. The yield of this reaction was approximately 91.84 %.

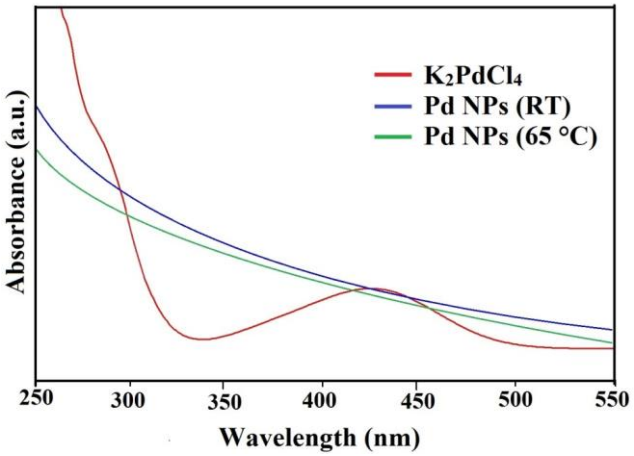

Fig. 3.1 UV-visible absorption spectra of K_2PdCl_4 and Pd NPs synthesized at room temperature (RT) and at 65 °C.

To observe the adsorption of organic molecules on the surface of Pd nanoparticles, FTIR spectra of the formed nanoparticles (at room temperature) were carried out in liquid phase as well as in solid phase (Figure 3.2 a). In the liquid phase FTIR spectrum (Figure 3.2 b) the intense peak at 3425 cm^{-1} is corresponding to O-H stretching of water molecules/-OH groups. The peak at 1634 cm^{-1} is due to the C=C stretching frequency of AA. Red shifting of C=C stretching frequency (compared to 1665 cm^{-1} in pure AA) is due to adsorption of L-Ascorbic acid on the nanoparticle's surface.[27] The peak at 1452 cm^{-1} is due to $-CH_2$ scissoring, at 964 cm^{-1} is due to $-CH_2$ wagging, at 1029 cm^{-1} is due to $-CH_2$ rocking and at 1268 cm^{-1} is due to C-O-C antisymmetric stretching vibration of adsorbed PEG at particle's surface.[28] Other peaks at 651 and 458 cm^{-1} correspond to the vibration of adsorbed AA nanoparticle's surface.

In the solid phase FTIR spectrum (Figure 3.2 b) the intensity of peaks is much decreased compared to those in the solution phase. Many peaks have been disappeared while the intensity of a few peaks has been increased. The increased intensity peaks at 2927 cm^{-1} and 2853 cm^{-1} is due to $-CH_2$ stretching vibration while

peak at 1452 cm^{-1} is due to CH_2 scissoring of alkyl chains of adsorbed PEG. Position of these peaks is much decreased compared to those of pure PEG[28] due to adsorption at nanoparticle's surface. Although peaks correspond to $–CH_2$ stretching do not appear in Figure 2 a, however, a small hump is visible at 2927 cm^{-1} probably due to preferential adsorption of AA at nanoparticle's surface in liquid phase.

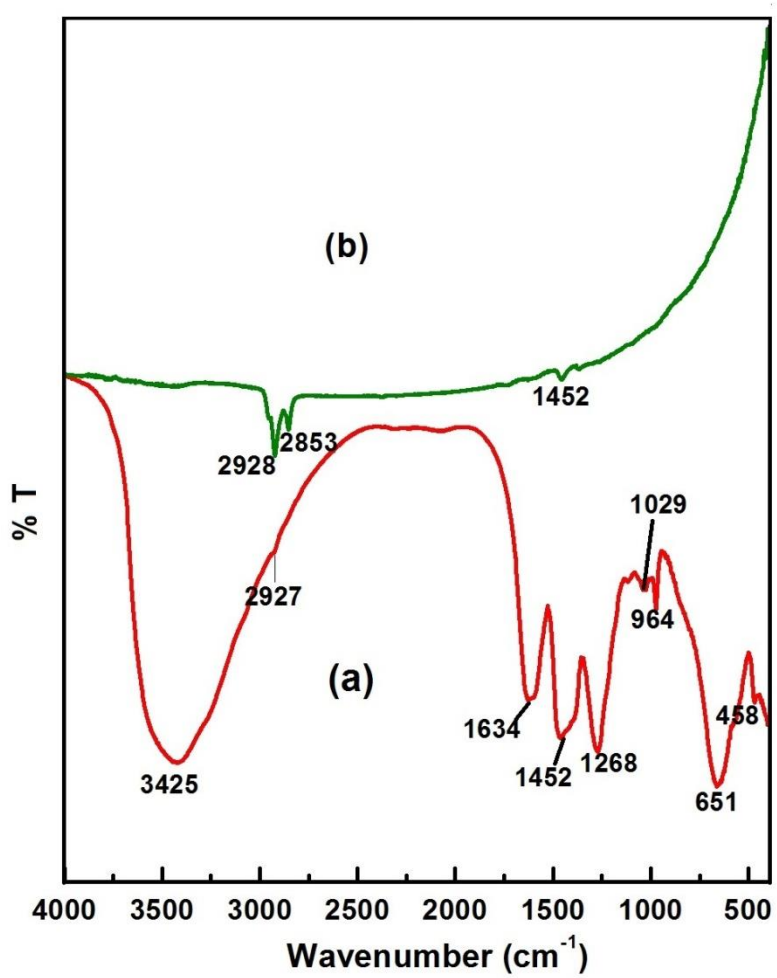

Fig. 3.2 FTIR spectra of Pd NPs formed at room temperature (a) in solution phase and (b) in solid phase.

Further vibrational analysis of Pd nanoparticles (formed at room temperature) was carried out by Raman measurement, which shows very strong, few broad and weak background peaks. Intensity versus Raman shift graph was plotted to take 20 mM Pd NPs, grafted with PEG and coated with AA (Figure 3.3). In the SERS

spectrum, the strong peaks at 480 and 633 cm^{-1} are due to ascorbic acid, while the peak at 278 cm^{-1} is probably due to υ (Pd…O) vibration.[29] The bands at 1076, 1170 and 1516 cm^{-1} are due to (C-O-H bend), CH_2 rocking and CH_2 scissoring.[30]

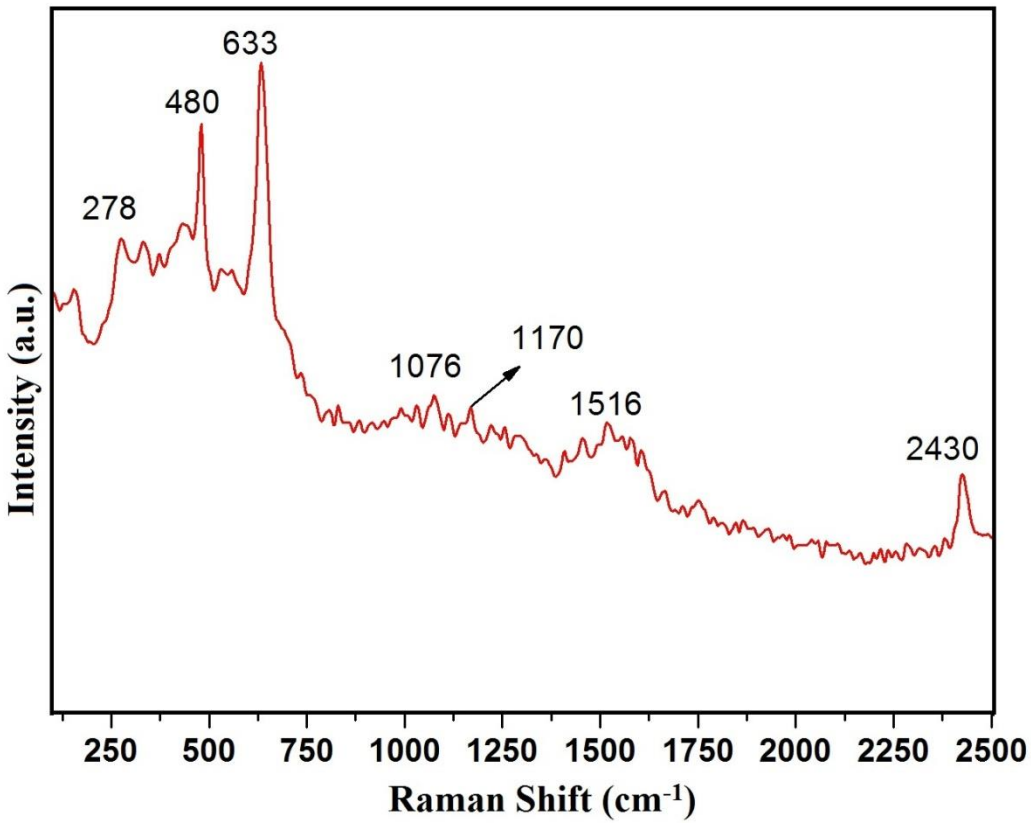

Fig. 3.3 SERS spectra of Pd NPs synthesized at room temperature.

The structural and morphological investigation of above-synthesized materials has been performed using SEM and TEM analysis. Different shapes and sizes Pd nanoparticles have been formed at room temperature and at 65 °C. When the $[PdCl_4]^{2-}$ complex ions were treated with AA in PEG medium at room temperature, truncated octahedron/fivefold twinned pentagonal rod-like Pd NPs have been formed on 30 minutes of reaction. In the SEM images (Figure 3.4 a & b) and the TEM image (Figure 3.4 c), 8-10 nm edge length truncated octahedron/fivefold twinned pentagonal rod-like Pd nanoparticles observed. The size of nanostructures varies in the range of 20-50 nm. In the corresponding EDX pattern (Figure 3.4 d) the only peak due to Pd

observed indicating the formation of phase pure Pd NPs. When reaction temperature was increased at 65 °C, keeping reaction time same i.e. 30 minutes, 17-20 nm edge length hexagonal/trigonal plates are formed. In the SEM image (Figure 3.5 a), although structures seem to be plate-like, however in the corresponding TEM image (Figure 3.5 b) hexagonal/trigonal plates like structures are visible.

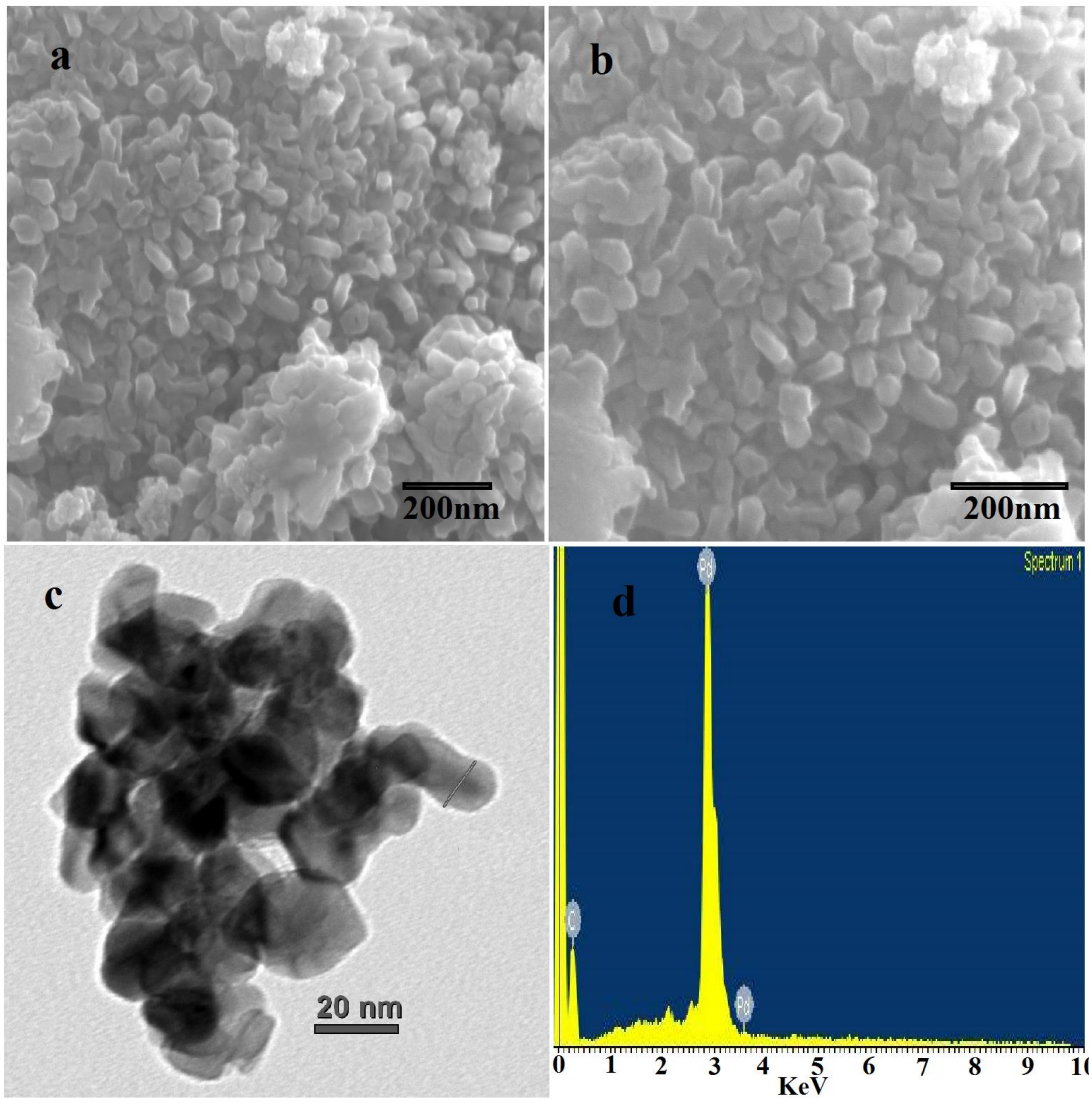

Fig. 3.4 (a,b) SEM images, (c) TEM image and (d) EDX spectrum of Pd NPs synthesized at room temperature.

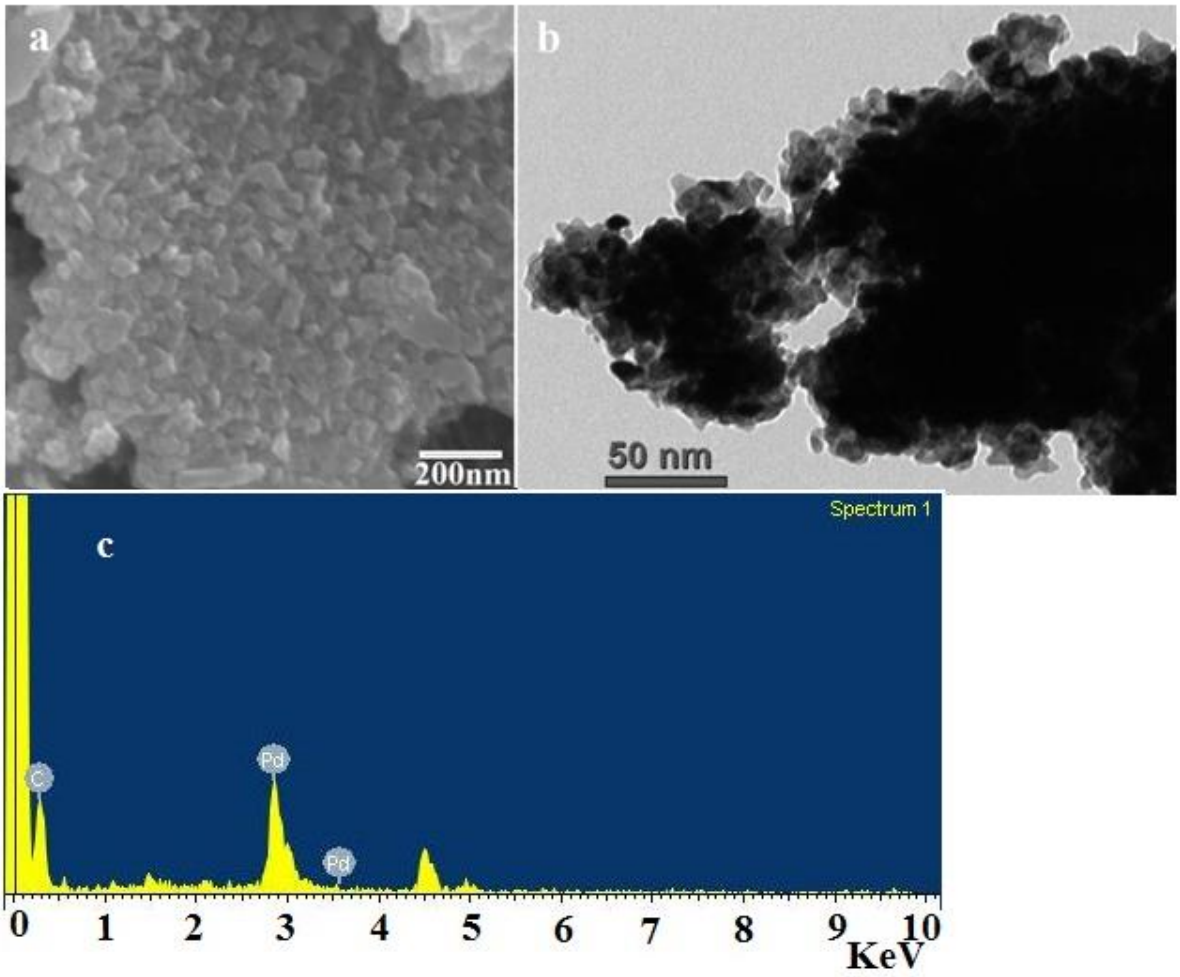

Fig. 3.5 (a) SEM image, (b) TEM image and (c) EDX spectrum of Pd NPs synthesized at 65 °C.

The particle size and size distribution analysis of Pd NPs, formed at room temperature were carried out to by plotting particle's size distribution curve (Figure 3.6). The curve indicates that the size of particles is distributed in a range of 20-60 nm while the maximum population falls at 40 nm. Zeta potential analysis is an effective technique for determining the surface charge of nanoparticles in colloidal solution and hence predicts their stability. The zeta potential curve of the Pd nanoparticles dispersion (formed at room temperature) was measured in the range of -100 to +100 mV (Figure 3.7). The obtained zeta potential value (-13 mV) indicates that the surface of nanoparticles is negatively charged and thus maintains their stability.

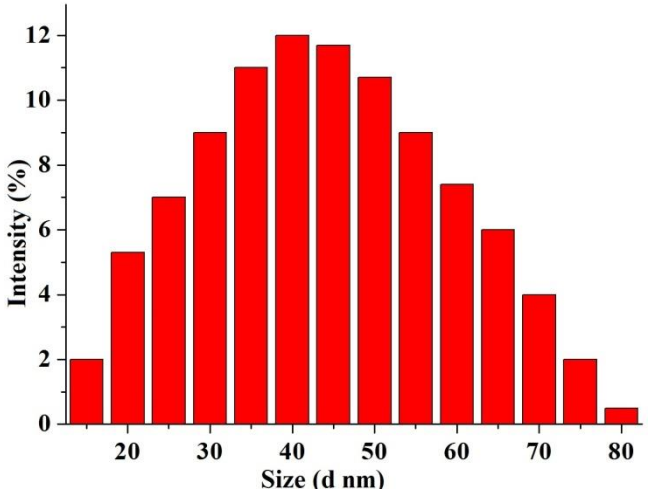

Fig. 3.6 Particle's size distribution of Pd nanoparticles formed at room temperature.

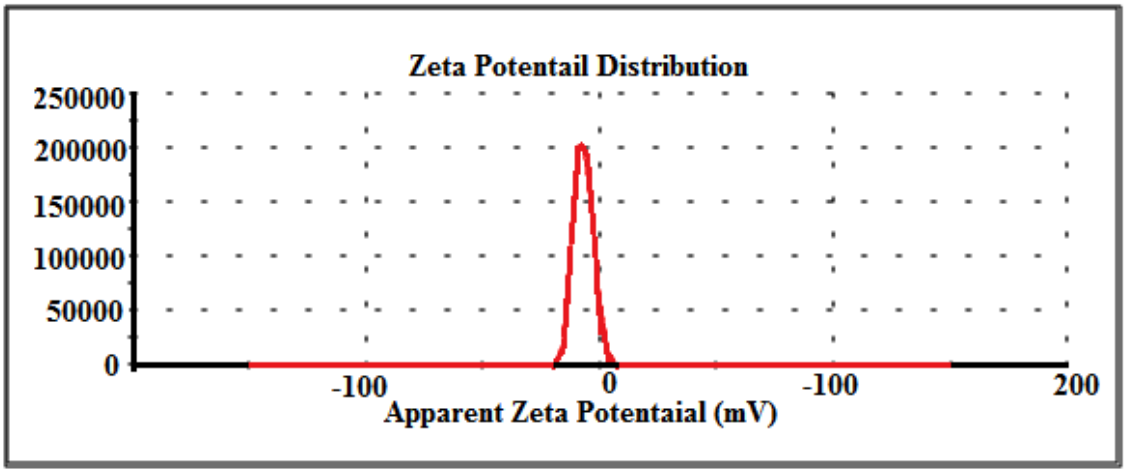

Fig. 3.7 Zeta potential distribution curve of Pd nanoparticles formed at room temperature.

The phase and crystallinity of Pd NPs were investigated by wide-angle XRD measurement. In the XRD pattern of the Pd NPs (formed at room temperature and at 65 °C), peaks observes at 2θ positions 40.26, 45.78, 68.67, 79.87 and 88.85°, corresponding to the reflection of (111), (200), (220), (311) and (222) planes of crystalline Pd NPs (Figure 3.8 a-b). These XRD patterns indicate the formation of phase pure face centered cubic (fcc) Pd NPs (JCPDS file No. 461043). The weak

intensity peak at 27° in XRD pattern of Pd NPs formed at 65 °C is due to the presence of residual PEG moieties.[31] Furthermore, the obtained XRD peaks are intense and broadened, indicating the formation of good crystalline and small size Pd nanoparticles.[18] The average crystallite size (D) has been determined from the Debye-Scherrer formula:

$$D = \frac{0.9\lambda}{\beta \cos\theta}$$

Where D is the crystallites size (in nm), λ the wavelength (in nm), β is the full width at half maxima (FWHM) and θ is the Bragg's diffraction angle. Crystallites size of Pd NPs synthesized at room temperature (RT) and at 65 °C, corresponding to different planes determined by above formula of has been shown in Figure 2 b. From the graph it has been found that crystallites size corresponding to (111) and (222) planes are larger than that of rest of the planes at both temperatures, indicating orientation of Pd NPs preferentially towards {111} facet and particles growth took place anisotropic in shape at both temperatures.[32] Further the particles size determined is smaller than those of TEM and particles size distribution analyses probably due to wide size distribution of particles.

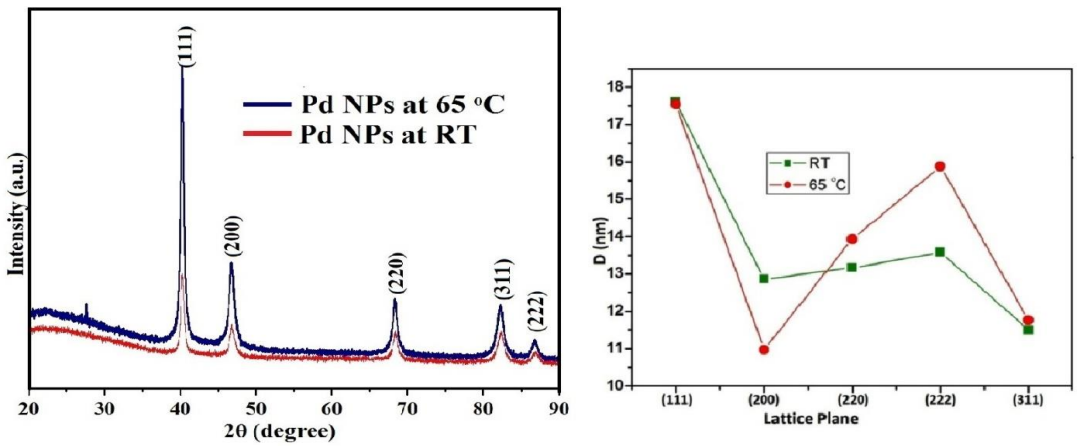

Fig. 3.8 (a) XRD patterns and (b) crystallites size corresponding to different planes determined by Debye-Scherrer formula of Pd NPs synthesized at room temperature (RT) and at 65 °C.

Nitrogen adsorption/desorption isotherm plots have been used to evaluate pore diameter (*Dp*) and the surface area (*S*) of the Pd NPs formed at room temperature. From the Barrett-Joyner-Halenda (BJH) method, an average pore diameter of DPNs has been found to be 24.29 nm (Figure 3.9 a). This result is indicative of its porous structure containing mesopores. The specific surface area obtained by the Brunauer-Emmett-Teller (BET) method[33] (Figure 3.9 b) was approximately 19.44 m^2g^{-1}. Such high surface area of Pd NPs indicates the presence of more catalytic sites.

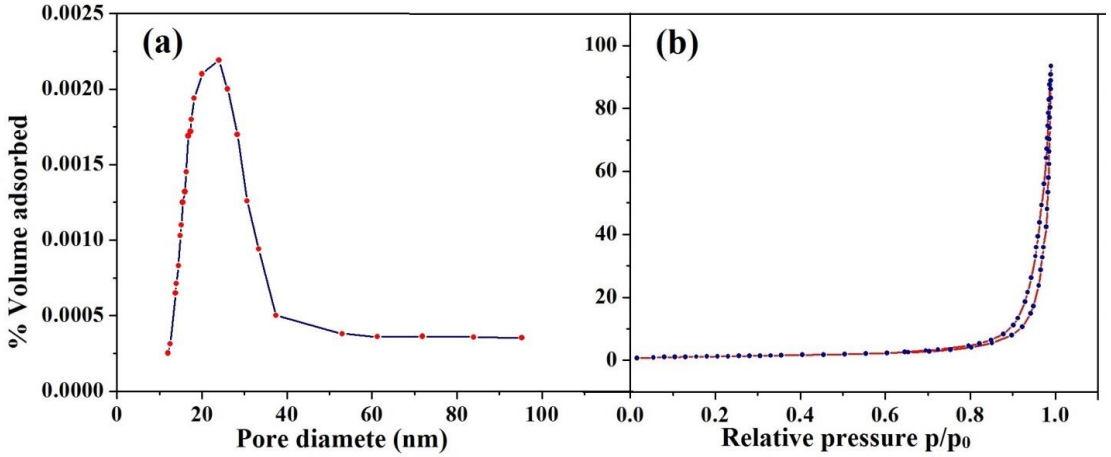

Fig. 3.9 BJH plot (a) and N_2 adsorption-desorption isotherm (b) of Pd NPs synthesized at room temperature.

It is well understood that the shape, size, surface area and charge of nanostructure affect the biological cell membrane interaction and thus decide their biological applications.[34] It is reported that cellular uptake of Pd nanoparticles are shape-dependent apart from surface charge because of membrane binding energy barriers during endocytosis predominantly responsible for shape effect.[35] Hence a better understanding of shape evolution Pd nanoparticles would aid the development of physicochemical and reaction parameters for generation of Pd nanoparticles for effective biochemical applications.

The inside atoms of face centered cubic metals (eg. Pd) have coordination number (CN) 12 while the atoms at the various low index surfaces (eg. {111}, {100} and {110}) have the CN of 9, 8 and 7 respectively. The planar density of three surfaces increases in the order {111} > {100} > {110}, hence the surface energy increases in the order $\gamma_{\{111\}} < \gamma_{\{100\}} < \gamma_{\{110\}}$.[36,37] When aqueous solution of K_2PdCl_4 was treated with ascorbic acid in presence of surfactant PEG, Pd^{+2} ion is readily reduced to Pd(0) owing to reaction.

$$Pd^{+2} + AA\ (C_6H_8O_6) \rightarrow C_6H_6O_6 + Pd(0) + 2H^{+}.$$

Here $[PdCl_4]^{-2}$ reduction takes place using AA as reductant via sonication. It is supposed that Pd nanoparticles evolved following three steps; supersaturation of monomers, burnt nucleation and controlled growth according to the LaMer method.[38] In the prevailing reaction conditions when monomer concentration increased steadily and reaches to stage of the critical point of supersaturation, small clusters spontaneously separates decreasing the monomer concentration by nucleation. Now concentration of monomer decreases below critical concentration and available monomer henceforth used for particle growth, however, during the nucleation period, particle growth may also take place simultaneously.[39] Thus to control size broadening of particles, a short nucleation span and controlled growth kinetics should be maintained which can be achieved by the presence of adsorbate, additives or surfactant in the reaction medium.

When K_2PdCl_4 is reduced by AA in an aqueous medium in presence of PEG, truncated octahedron/fivefold twinned pentagonal rod-like polyhedral structures enclosed by {111} and {100} mixed facets are formed because {111} is the most stable facet followed by {100} and then {110}. From stability point of view only

{111} facet terminating shapes like octahedral and tetrahedral seed should be formed during nucleation stage, however according to Wulff's theory, since octahedron and tetrahedron have larger surface area than the cube per unit volume, the truncated octahedron, known as Wulff's polyhedron nucleated as the most stable speed in order to minimize both surface area and interfacial face energy.[40] On increasing reaction temperature at 65 °C the concentration of monomer increases, thus the rate of reaction increases. Now among two facets {111} and {100} of a octahedron, {111} surface grows more rapidly than {100} because of availability of higher monomer concentration at elevated temperature. Thus thermodynamically stable and kinetically controlled hexagonal/trigonal plate-like Pd NPs have been evolved at higher temperature 65 °C.

3.3.2. Molecular Docking Studies of Palladium clusters with DNA

3.3.2.1. Computational Details

Dataset

DNA

The PDB format file of DNA sequences with PDB ID 1BNA was downloaded from RCSB Protein Data Bank.[41] Ligands and water molecules were removed from DNA sequence using CHIMERA.[42]

Drugs

The structure of Pd cluster was taken after optimization. Fig.3.10 shows the chemical structure of the cluster.

3.3.2.2. Molecular Docking

AutoDock 4.2 was used for molecular docking simulations using Lamarckian Genetic Algorithm (LGA).[43] Docking was performed using DNA sequences as a rigid receptor molecule, whereas Pd cluster was treated as a flexible ligand. The receptor and ligand files were prepared for docking using AutoDock Tools (ADT).[44] The grid box size was set at 50-50 and 100 A˚ for x, y and z respectively, and the grid centre was set to 14.748, 20.984 and 8.809 for x, y and z respectively. The Gasteiger charges were added to the complex by AutoDock Tools (ADT) before performing docking calculations. Lamarckian genetic algorithms, as implemented in Auto Dock, were employed to perform blind docking calculations. For metal, modifications were done in the parameter file to include Pd. The lowest energy docked confirmation, according to the AutoDock scoring function, was selected as the binding mode (Figure 3.10).

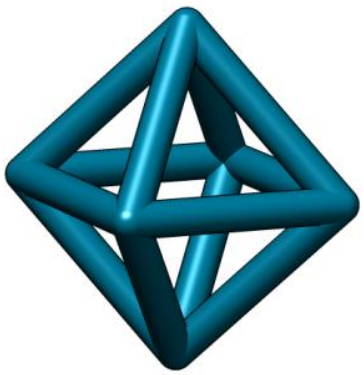

Fig.3.10 Three dimensional structure of Pd-cluster.

3.3.2.3. Result

The figure shows the Minor groove binding of Pd-cluster with 1BNA present in lung cancer A549 cell lines. Pd cluster binds in the minor groove of the DNA sequences concluding that cluster is minor groove binder. The computationally calculated binding energy is -0.14 kcal/mol, which indicates this it is an effective drug against cancer cells (Figure 3.11).

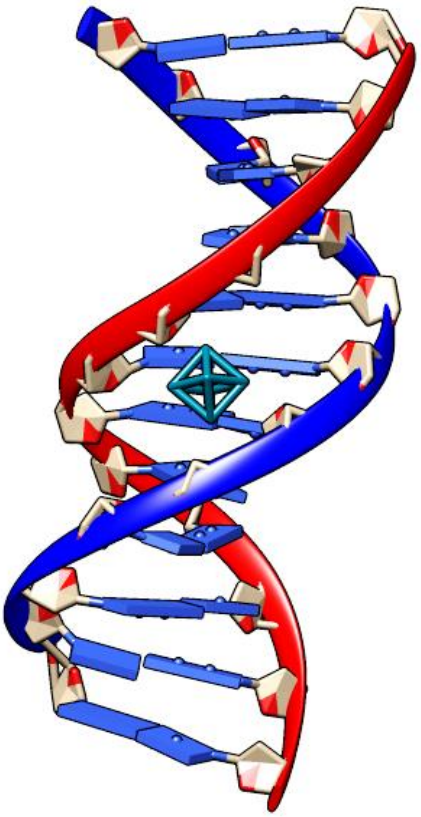

Fig.3.11 Minor groove binding of Pd-cluster with 1BNA.

3.3.3. Molecular Docking Studies of Palladium clusters with Lung Cancer proteins

3.3.3.1. Computational Details

Dataset

DNA

The PDB format file of proteins with PDB ID 2ITW, 2ITX, 2ITY, 2J6M and 4LQM were downloaded from RCSB Protein Data Bank.[45] These are crystal structures of the EGFR kinase domain. Mutations in the EGFR kinase are a cause of non-small-cell lung cancer.[44] Ligands and water molecules were removed from each protein using CHIMERA.[46]

Drugs

The structure of Pd cluster was taken after optimization. Figure 3.10 shows the chemical structure of the cluster.

3.3.3.2. Molecular Docking

AutoDock4.2 was used for molecular docking simulations using Lamarckian Genetic Algorithm (LGA).[43] The docking was performed using Protein as a rigid receptor molecule, whereas Pd cluster was treated as a flexible ligand. The receptor and ligand files were prepared for docking using Auto Dock Tools (ADT).[44] Grid boxes of various dimensions were used to prepare grid maps using Auto-Grid for each protein. The Gasteiger charges were added to the complex by Auto Dock Tools (ADT) before performing docking calculations. Lamarckian genetic algorithms, as implemented in Auto Dock, were employed to perform blind docking calculations. All other parameters were default settings. For metals, modifications were done in the parameter file to include Pd. According to the Auto Dock scoring function, the lowest energy docked conformation was selected as the binding mode.

3.3.3.3. Result

The computationally calculated binding energies of all protein-drug complexes are given in Table 1. From the tabulated data it is very much clear that binding energies of all EGFR proteins with Pd cluster are of the same range. The binding modes and geometrical orientation of all compounds were almost identical; suggesting that all the inhibitors occupied a common cavity in the receptor. The lowest binding energy is with 2ITY complex. Molecular Docking gives the best and stable conformations of the ligand with proteins in the receptor active pocket. Figure 3.12 shows interaction of the ligand with proteins.

In silico studies revealed the entire synthesized molecule showed good binding energy toward the target protein. Pd cluster binds in the pocket of the proteins (Table1).

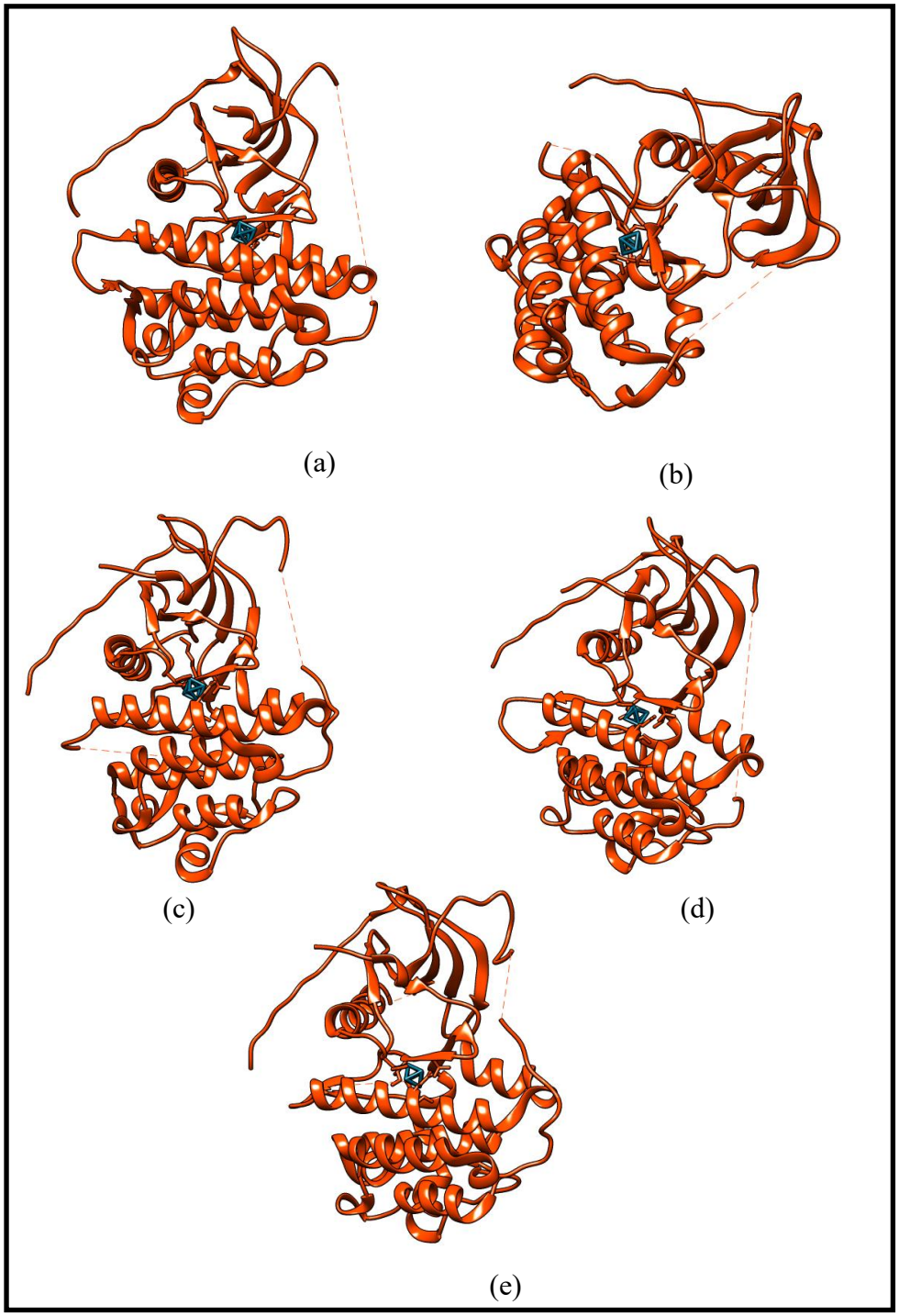

Fig.3.12 Interaction of Ag-Au cluster with (a) 2ITW (b) 2ITX (c) 2ITY (d) 2J6M (e) 4LQM.

Table1 Binding energies of protein-drug complexes

S.No	Proteins	Binding energies(Kcal/mol)
1	2ITW	-0.44
2	2ITX	-0.46
3	2ITY	-0.48
4	2J6M	-0.42
5	4LQM	-0.44

3.3.4. Cytotoxicity

With a view of the above fact, it is also necessary to observe the use of Pd nanoparticles (formed at room temperature) in biochemical system, we performed the cytotoxicity effects using A-549 human lung cancer cells. The cytotoxicity result was analyzed by plotting viability histogram curve, and IC_{50} values. As per data obtained from Figure 3.15, the positive control i.e. Adriamycin kills all the cytotoxic cells at 10 µg/ml concentration indicating that our cell culture experiment moved to a positive direction in all respects.[47] It is found that the cell viability is dose-dependent manner with noticeable changes in shape and size from 10-30 µg/ml concentrations (Figure 3.13, 3.14).[48] The observed IC_{50} is ≤10 µg/ml, indicating good therapeutic efficacy in the biological system i.e. against lungs carcinoma. This action may be due to the cytotoxic effect of the palladium nanoparticle on the DNA (shown in docking experiment in Fig. 3.11).[49] Cell viability decreased according to increase the concentration, which implies that our synthesized compound may be active against lung cancer which is beneficial for future drug design perspectives.[50]

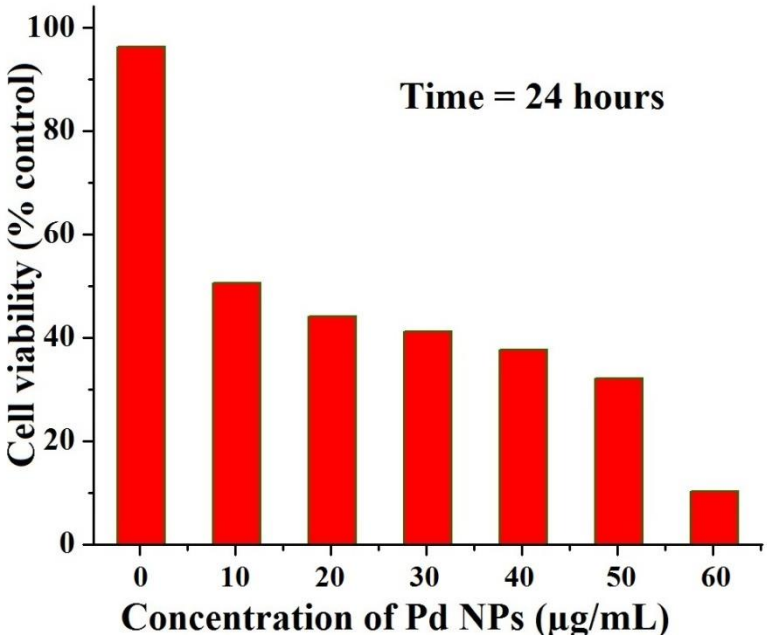

Fig. 3.13 Effect of dose of Pd NPs (synthesized at room temperature) on cell viability of A-549 human lung cancer cells.

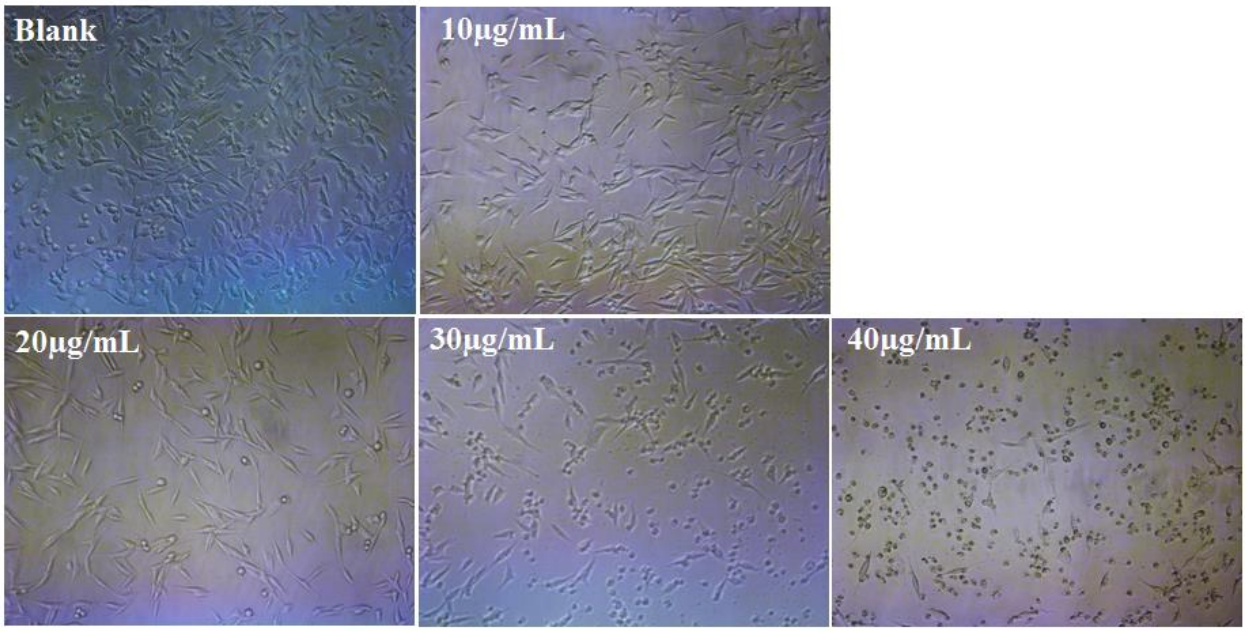

Fig. 3.14 Cell viability curve: Effect of dose of Pd NPs (synthesized at room temperature) on A-549 human lung cancer cells.

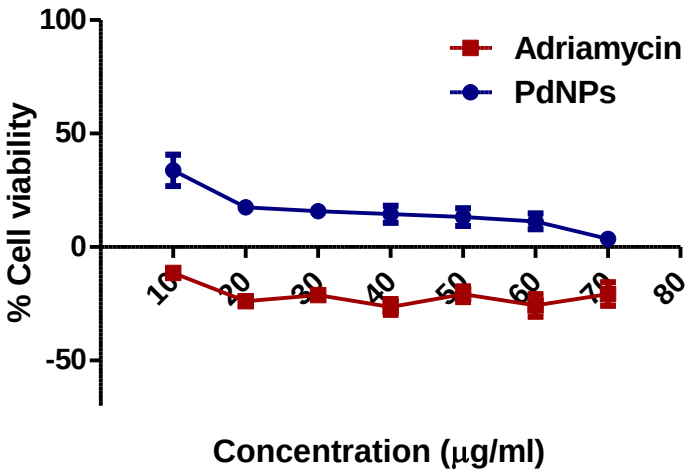

Fig. 3.15 Cell viability curve: Effect of dose of Pd NPs (synthesized at room temperature) and Adriamycin on A-549 human lung cancer cells.

Conclusion

In summary, we have successfully synthesized different shapes and sizes Pd nanoparticles, like 8-10 nm edge length truncated octahedron/fivefold twinned pentagonal rods and 17-20 nm edge length hexagonal/trigonal plates in aqueous solution phase by reducing K_2PdCl_4 with ascorbic acid in the presence of surfactant PEG via sonochemical method at room temperature. XRD study revealed particles growth took place anisotropically at both temperatures. FTIR and SERS studies revealed adsorption of AA and PEG at NP's surface. The particle's size distribution graph indicates formation of particles having wide size distribution while the zeta potential value -13 mV indicated that the particle's surface is negatively charged and hence stable. The truncated octahedron/fivefold twinned pentagonal rods shaped Pd NPs, formed at room temperature while thermally stable and kinetically controlled hexagonal/trigonal plate-like Pd NPs have been evolved at a higher temperature 65 °C. The obtained Pd NPs has a high surface area and narrow pore size distribution. The computationally calculated binding energy indicates this Pd cluster is an effective

drug against cancer cells. The lowest binding energy is with 2ITY complex. Molecular Docking gives the best and stable conformations of the ligand with proteins in the receptor active pocket. Biochemically, the effect of PD NPs on A-549 human lung cancer cells exhibited that cytotoxicity is dependent on the dose of NPs. The results described here indicate much potential for use of these NPs in biomedical applications.

References

1. Shen, L.; Che, Q.; Li, H.; Zhang, X., Mesoporous NiCo2O4 nanowire arrays grown on carbon textiles as binder-free flexible electrodes for energy storage. *Adv. Funct. Mater.* **2014,** *24*, 2630-2637.
2. Wang, Y.; Zhang, J.; Wang, X.; Antonietti, M.; Li, H., Boron-and fluorine-containing mesoporous carbon nitride polymers: metal-free catalysts for cyclohexane oxidation. *Angew. Chem. Int. Ed.* **2010,** *49*, 3356-3359.
3. Malgras, V.; Ataee-Esfahani, H.; Wang, H.; Jiang, B.; Li, C.; Wu, K. C. W.; Kim, J. H.; Yamauchi, Y., Nanoarchitectures for mesoporous metals. *Adv. Mater.* **2016,** *28*, 993-1010.
4. Deng, Y.; Wei, J.; Sun, Z.; Zhao, D., Large-pore ordered mesoporous materials templated from non-Pluronic amphiphilic block copolymers. *Chem. Soc. Rev.* **2013,** *42*, 4054-4070.
5. Khalafi, Tariq.; Buazar, F.; Ghanemi, K. Phycosynthesis and enhanced photocatalytic activity of zinc oxide nanoparticles toward organosulfur pollutants. *Sci. Rep.* **2019**, *9*, 6866.
6. Mourdikoudis, S.; Chirea, M.; Altantzis, T.; Pastoriza-Santos, I.; Pérez-Juste, J.; Silva, F.; Bals, S.; Liz-Marzán, L. M., Dimethylformamide-mediated synthesis of water-soluble platinum nanodendrites for ethanol oxidation electrocatalysis. *Nanoscale* **2013,** *5*, 4776-4784.
7. Gholizadeh, Safikhani, B.; Buazar, F.; Hosseini, S. M.; Mousavi, S. M. Enhanced antibacterial activity, mechanical and physical properties of alginate/hydroxyapatite bionanocomposite film. *Int. J. Biol. Macromol.* **2018**, *116*, 786-792.

8. Hitkari, G.; Singh, S.; Pandey, G., Structural, optical and photocatalytic study of ZnO and ZnO–ZnS synthesized by chemical method. *Nano-Struct. & Nano-Object* **2017,** 12, 1-9.

9. Wang, L.; Nemoto, Y.; Yamauchi, Y., Direct synthesis of spatially-controlled Pt-on-Pd bimetallic nanodendrites with superior electrocatalytic activity. *J. Am. Chem. Soc.* **2011,** *133*, 9674-9677.

10. Daniel, M.-C.; Astruc, D., Gold nanoparticles: assembly, supramolecular chemistry, quantum-size-related properties, and applications toward biology, catalysis, and nanotechnology. *Chem. Rev.* **2004,** *104*, 293-346.

11. Reddy, L. H.; Arias, J. L.; Nicolas, J.; Couvreur, P., Magnetic nanoparticles: design and characterization, toxicity and biocompatibility, pharmaceutical and biomedical applications. *Chem. Rev.* **2012,** *112*, 5818-5878.

12. Wang, L.; Yamauchi, Y., Metallic nanocages: synthesis of bimetallic Pt–Pd hollow nanoparticles with dendritic shells by selective chemical etching. *J. Am. Chem. Soc.* **2013,** *135*, 16762-16765.

13. Li, C.; Yamauchi, Y., Facile solution synthesis of Ag@ Pt core–shell nanoparticles with dendritic Pt shells. *Phys. Chem. Chem. Phys.* **2013,** *15*, 3490-3496.

14. Wang, L.; Wang, H.; Nemoto, Y.; Yamauchi, Y., Rapid and efficient synthesis of platinum nanodendrites with high surface area by chemical reduction with formic acid. *Chem. Mater.* **2010,** *22*, 2835-2841.

15. Xia, B. Y.; Wu, H. B.; Li, N.; Yan, Y.; Lou, X. W.; Wang, X., One-pot synthesis of Pt–Co alloy nanowire assemblies with tunable composition and enhanced electrocatalytic properties. *Angew. Chem. Int. Ed.* **2015,** *54*, 3797-3801.

16. Pelka, J.; Gehrke, H.; Esselen, M.; Türk, M.; Crone, M.; Bräse, S.; Muller, T.; Blank, H.; Send, W.; Zibat, V., Cellular uptake of platinum nanoparticles in human colon carcinoma cells and their impact on cellular redox systems and DNA integrity. *Chem. Res. Toxicol.* **2009,** *22*, 649-659.
17. Weiss, J. T.; Dawson, J. C.; Fraser, C.; Rybski, W.; Torres-Sánchez, C.; Bradley, M.; Patton, E. E.; Carragher, N. O.; Unciti-Broceta, A., Development and bioorthogonal activation of palladium-labile prodrugs of gemcitabine. *J. Med. Chem.* **2014,** *57*, 5395-5404.
18. Shim, K.; Kim, J.; Heo, Y. U.; Jiang, B.; Li, C.; Shahabuddin, M.; Wu, K. C. W.; Hossain, M. S. A.; Yamauchi, Y.; Kim, J. H., Synthesis and cytotoxicity of dendritic platinum nanoparticles with HEK-293 cells. *Chem.–As. J.* **2017,** *12*, 21-26.
19. Weiss, J. T.; Dawson, J. C.; Macleod, K. G.; Rybski, W.; Fraser, C.; Torres-Sánchez, C.; Patton, E. E.; Bradley, M.; Carragher, N. O.; Unciti-Broceta, A., Extracellular palladium-catalysed dealkylation of 5-fluoro-1-propargyl-uracil as a bioorthogonally activated prodrug approach. *Nat. Commun.* **2014,** *5*, 3277.
20. Weiss, J. T.; Fraser, C.; Rubio-Ruiz, B.; Myers, S. H.; Crispin, R.; Dawson, J. C.; Brunton, V. G.; Patton, E. E.; Carragher, N. O.; Unciti-Broceta, A., N-alkynyl derivatives of 5-fluorouracil: susceptibility to palladium-mediated dealkylation and toxigenicity in cancer cell culture. *Front. Chem.* **2014,** *2*, 56.
21. Huang, X.; Tang, S.; Mu, X.; Dai, Y.; Chen, G.; Zhou, Z.; Ruan, F.; Yang, Z.; Zheng, N., Freestanding palladium nanosheets with plasmonic and catalytic properties. *Nat. Nanotech.* **2011,** *6*, 28.

22. Balbín, A.; Gaballo, F.; Ceballos-Torres, J.; Prashar, S.; Fajardo, M.; Kaluđerović, G. N.; Gómez-Ruiz, S., Dual application of Pd nanoparticles supported on mesoporous silica SBA-15 and MSU-2: Supported catalysts for C–C coupling reactions and cytotoxic agents against human cancer cell lines. *RSC Adv.* **2014,** *4*, 54775-54787.

23. Kumar, P.; Singh, A. K.; Raj, V.; Rai, A.; Keshari, A. K.; Kumar, D.; Maity, B.; Prakash, A.; Maiti, S.; Saha, S., Poly (lactic-co-glycolic acid)-loaded nanoparticles of betulinic acid for improved treatment of hepatic cancer: characterization, in vitro and in vivo evaluations. *Int. J. Nanomed.* **2018**, *13*, 975-990.

24. Tang, S.; Huang, X.; Zheng, N., Silica coating improves the efficacy of Pd nanosheets for photothermal therapy of cancer cells using near infrared laser. *Chem. Commun.* **2011,** *47*, 3948-3950.

25. Xiao, J.-W.; Fan, S.-X.; Wang, F.; Sun, L.-D.; Zheng, X.-Y.; Yan, C.-H., Porous Pd nanoparticles with high photothermal conversion efficiency for efficient ablation of cancer cells. *Nanoscale* **2014,** *6*, 4345-4351.

26. Henglein, A.;Colloidal Palladium Nanoparticles: Reduction of Pd(II) by H2; Pd Core Au Shell Ag Shell Particles. *J. Phys. Chem. B,* **2000,** *104,* 6683-6685**.**

27. Sreeja, V.; Jayaprabha, K.; Joy, P., Water-dispersible ascorbic-acid-coated magnetite nanoparticles for contrast enhancement in MRI. *Appl. Nanosci.* **2015,** *5, 435*-441.

28. Dutta, J., Synthesis and characterization of γ-irradiated PVA/PEG/CaCl2 hydrogel for wound dressing. *Am. J. Chem.* **2012,** *2*, 6-11.

29. Li, J.-J.; An, H.-Q.; Zhu, J.; Zhao, J.-W. Detecting glucose by using the Raman scattering of oxidized ascorbic acid: The effect of graphene oxide–gold nanorod hybrid. *Sens. Actuat. B: Chem.* **2016,** *235*, 663-669.

30. Boca, S.; Rugina, D.; Pintea, A.; Leopold, N.; Astilean, S. Designing gold nanoparticle-ensembles as surface enhanced Raman scattering tags inside human retinal cells. *J Nanotechnol.* **2012,** *2012*, 1–10.

31. Shanthi, K.; Vimala, K.; Gopi, D.; Kannan, S., Fabrication of a pH responsive DOX conjugated PEGylated palladium nanoparticle mediated drug delivery system: an in vitro and in vivo evaluation. *RSC Adv.* **2015,** *5*, 44998-45014.

32. Navaladian, S.; Viswanathan, B; Varadarajan, T. K.; Viswanath, R. P. A Rapid Synthesis of Oriented Palladium Nanoparticles by UV Irradiation. *Nanoscale Res. Lett.* **2009**, *4*,181–186.

33. Hitkari, G.; Singh, S.; Pandey, G. Photoluminescence behaviour and Visible light photocatalytic degradation of methyl orange using ZnO, ZnO/ZnS and ZnO/ZnS/α-Fe_2O_3 nanocomposites. *Trans. Nonferrous Met. Soc. China* **2018**, *28*, 1386-1396.

34. Chen, M.; Wu, B.; Yang, J.; Zheng, N., Small Adsorbate-Assisted shape control of Pd and Pt nanocrystals. *Adv. Mater.* **2012,** *24*, 862-879.

35. Xie, X., Liao, J., Shao, X., Li, Q., Lin, Y.: The effect of shape on cellular uptake of gold nanoparticles in the forms of stars, rods, and triangles. Scientific Reports **7**, 3827 (2017).

36. Chen, A.; Ostrom, C., Palladium-Based Nanomaterials: Synthesis and Electrochemical Applications: *Chem. Rev.* **2015**, *115*, 11999−12044.

37. Vitos, L.; Ruban, A.; Skriver, H. L.; Kollar, J., The surface energy of metals. *Surf. Sci.* **1998,** *411*, 186-202.

38. LaMer, V. K.; Dinegar, R. H., Theory, production and mechanism of formation of monodispersed hydrosols. *J. Am. Chem. Soc.* **1950,** *72*, 4847-4854.

39. Buazar, F.; Sweidi, S.; Badri, M.; Kroushawi, F. Biofabrication of highly pure copper oxide nanoparticles using wheat seed extract and their catalytic activity: a mechanistic approach. *Green Process. Synth.* **2019**, *8*, 691-702.

40. Pimpinelli, A., Villain, J.: Physics of crystal growth, Cambridge University Press, Cambridge, 1998.

41. Marcon, V.; Raos, G., Free energies of molecular crystal surfaces by computer simulation: Application to tetrathiophene. *J. Am. Chem. Soc.* **2006,** *128*, 1408-1409.

42. Berman, H. M.; Bourne, P. E.; Westbrook, J.; Zardecki, C., The protein data bank. In *Protein Structure*, CRC Press: 2003; pp 394-410.

43. Krug, J., Four lectures on the physics of crystal growth. *Physica A: Statist. Mech. Appl.* **2002,** *313*, 47-82.

44. Pettersen, E. F.; Goddard, T. D.; Huang, C. C.; Couch, G. S.; Greenblatt, D. M.; Meng, E. C.; Ferrin, T. E., UCSF Chimera-a visualization system for exploratory research and analysis. *J. Comp. Chem.* **2004,** *25*, 1605-1612.

45. Morris, G. M.; Huey, R.; Lindstrom, W.; Sanner, M. F.; Belew, R. K.; Goodsell, D. S.; Olson, A. J., AutoDock4 and AutoDockTools4: Automated docking with selective receptor flexibility. *J. Comp. Chem.* **2009,** *30*, 2785-2791.

46. Chen, B. Y.; Bandyopadhyay, S. In *A statistical model of overlapping volume in ligand binding cavities*, 2011 IEEE International Conference on

Bioinformatics and Biomedicine Workshops (BIBMW), 2011; IEEE: 2011; pp 424-431.

47. Bridot, J.-L.; Faure, A.-C.; Laurent, S.; Riviere, C.; Billotey, C.; Hiba, B.; Janier, M.; Josserand, V.; Coll, J.-L.; Vander Elst, L., Hybrid gadolinium oxide nanoparticles: multimodal contrast agents for in vivo imaging. *J. Am. Chem. Soc.* **2007,** *129*, 5076-5084.
48. Berman, H.; Henrick, K.; Nakamura, H., Announcing the worldwide protein data bank. *Nat. Struct. Mol. Biol.* **2003,** *10*, 980.
49. Wang, H.; Imura, M.; Malgras, V.; Li, C.; Wang, L.; Yamauchi, Y., A Solution Phase Synthesis of Dendritic Platinum Nanoelectrocatalysts with the Assistance of Polyoxyethylene Nonylphenyl Ether. *J. Inorg. Organomet. Polym. Mater.* **2015,** *25*, 245-250.
50. Sorinezami, Z.; Mansouri-Torshizi, H.; Aminzadeh, M.; Ghahghaei, A.; Jamgohari, N.; Heidari Majd, M., Synthesis of new ultrasonic-assisted palladium oxide nanoparticles: an in vitro evaluation on cytotoxicity and DNA/BSA binding properties. *J. Biomol. Struct. Dyn.* **2019**, *37*, 4238-4250.

ACS OMEGA
Cite This: ACS Omega 2019, 4, 21839−21847
Article
http://pubs.acs.org/journal/acsodf

Effect of Reaction Temperature on Shape Evolution of Palladium Nanoparticles and Their Cytotoxicity against A-549 Lung Cancer Cells

Gulam Abbas,[†] Narinder Kumar,[‡] Devesh Kumar,[‡] and Gajanan Pandey*[,†]

[†]Department of Chemistry and [‡]Department of Physics, Babasaheb Bhimrao Ambedkar University, Lucknow 226025, India

ABSTRACT: Palladium nanoparticles (Pd NPs) of different shapes and sizes have been synthesized by reducing potassium tetrachloropalladinate(II) by L-ascorbic acid (AA) in an aqueous solution phase in the presence of an amphiphilic nonionic surfactant poly ethylene glycol (PEG) via a sonochemical method. Materials have been characterized by X-ray diffraction (XRD), scanning electron microscopy (SEM), transmission electron microscopy (TEM), energy dispersive X-ray soectrscopy (EDX), Fourier transform infrared (FTIR), surface-enhanced Raman spectroscopy (SERS), particle distribution, and zeta potential studies. Truncated octahedron/fivefold twinned pentagonal rods are formed at room temperature (RT) (25 °C) while hexagonal/trigonal plates are formed at 65 °C. XRD results show evolution of anisotropically grown, phase-pure, and well crystalline face-centered cubic Pd NPs at both temperatures. FTIR and SERS studies revealed adsorption of ascorbic acid (AA) and PEG at NP's surface. Particle's size distribution graph indicates formation of particles having wide size distribution while the zeta potential particle surface is negatively charged and stable. The truncated octahedron/fivefold twinned pentagonal rod-shaped Pd NPs, formed at RT, while thermally stable and kinetically controlled hexagonal/trigonal plate-like Pd NPs, evolved at higher temperature 65 °C. The obtained Pd NPs have a high surface area and narrow pore size distribution. To predict protein reactivity of the Pd cluster, docking has been done with DNA and lung cancer-effective proteins. The cytotoxicity of the Pd NPs has been screened on human lung cancer cells A-549 at 37 °C. The biological adaptability exhibited by Pd NPs has opened a pathway in biochemical applications.

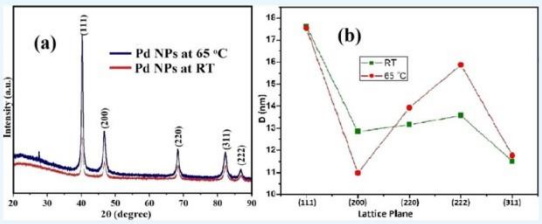

1. INTRODUCTION

In the last few decades, mesoporous materials have gained enormous attention of various scientists globally in both industry and academia because of their high surface area, tunable pore size, and uniform and narrow pore size distribution.[1,2] On account of these properties, mesoporous and nanoporous materials have shown high demand in various fields such as energy storage,[3] catalysis,[4,5] and biomedical applications.[6,7] In the past, nanoparticles of desired shapes, such as spherical, films, rods, tubes, and so forth with mesoporous structures have been prepared by a soft template method like self-assembly of micelles.[8] On the other hand, in the hard template method, the targeted materials are deposited in the confined spaces of a template with the desired morphology.[9] Because the soft template method is a simple and easy approach, hence it is favorable for the generation of desired shapes of nanoparticles using low molecular weight molecules like Brij 58, poly ethylene glycol (PEG), and so forth and high molecular weight amphiphilic molecules, for example, triblock copolymers as pore-directing agents.

In recent years nanotechnology has shown enormous potential in the biomedical field as therapeutic mediators for many diseases, including cancer.[10] In this regard, metal nanostructures have attracted great interest because of their size, structure, versatility, and optoelectronic properties.[11] Since the introduction of catalytic converters in the USA in 1975 and in Europe in 1986 (Wiseman and Zereini 2009), platinum group metals have shown increasing demands particularly in the area of electronics and catalysis. The latest research demonstrate that palladium (Pd) nanoparticles have widely been used in catalysis, (e.g., oxidation/reduction of methanol,[12] stereochemical oxidation of ethanol,[13] redox organic reactions,[14,15] sensors for detection of various analytes,[16] hydrogen generation/storage, methane combustion, supercapacitors, lithium-ion batteries, and in biomedical applications.[17] Shim et al. synthesized dendritic platinum nanoparticles and demonstrated their cytotoxicities against human embryonic kidney cells.[18] Unciti-Broceta et al. demonstrated that the prodrugs 5-fluoro-1-propargyluracil[19] and *N*-4-propargyloxycarbonylgemcitabine[20] are independently harmless; however, when separately combined with Pd(0)-glycol-polystyrene resin these prodrugs exhibited antiproliferation properties compared to the unmodified drug in colorectal and pancreatic cancer cells. However, one of the major limitations, in the case of metallic NPs is their nonspecific untargeted toxicity. Huang et al. used ultrathin (1.8 nm)

Received: August 27, 2019
Accepted: November 28, 2019
Published: December 12, 2019

DOI: 10.1021/acsomega.9b02776
ACS Omega 2019, 4, 21839−21847

Chapter 4

Efficient Anticarcinogenic Activity of α-Fe_2O_3 Nanoparticles: In-vitro and Computational Study on Human Renal Carcinoma Cells HEK-293

Efficient Anticarcinogenic Activity of α-Fe_2O_3 Nanoparticles: In-vitro and Computational Study on Human Renal Carcinoma Cells HEK-293

Abstract

The present study has witnessed the synthesis of α-Fe_2O_3 NPs using polyethylene glycol (PEG) as a surfactant and L-ascorbic acid (LAA) as a stabilizer. The product has been characterized by UV-visible absorption spectroscopy, FTIR, Dynamic Light Scattering, particle size distribution analysis, X-ray diffraction analysis, TEM, FESEM, EDX and BET, which show formation of variable size and shape, mesoporous, PEG-coated α-Fe_2O_3 NPs (LAA@IONP-PEG) with β-FeOOH as an impurity. The present work emphasizes upon an anti-cancer study of LAA@IONP-PEG against renal carcinoma HEK-293 human embryonic kidney cell lines. The study suggests that LAA@IONP-PEG is a promising material against renal carcinoma HEK-293 human embryonic kidney cell lines. The docking study has confirmed anti-proliferative action of NPs through binding affinity with renal carcinoma molecular targets. The synthesized NPs show the synergistic effect with Axitinib as an anti-cancer drug effective against renal carcinoma cell lines. ROS and 1,1-diphenyl-2-picrylhydrazine (DPPH) free radical scavenging assay have shown the antioxidant capability of synthesized NPs. The efficient biocatalytic activity of LAA@IONP-PEG prescribes its use as one of the best suited drugs for the future perspectives against fatal renal carcinoma and thus it is reckoned that synthesized NPs will have persistent utilization in different field of medical applications.

Keywords: PEG-coated α-Fe_2O_3NPs; HEK-293; renal carcinoma; docking; XRD

4.1. Introduction

Renal carcinoma is one of the most frequently diagnosed malignancies in men, which causes mobility and mortality globally [1]. To improve the efficacy of cancer therapy and to minimize its hazardous impacts on healthy tissues and organs, new treatment methods are urgently needed. Since recent decades, nanotechnology and its interdisciplinary fields are emerging as the best tool to diagnose several diseases fatal to mankind and causing problems to the environment. Synthesis of nanoparticles has gained attention in the field of a wide variety of biomedical applications like hyperthermia, gene or drug delivery, magnetic resonance imaging (MRI) and *in vivo* cell tracking [2,3]. It has been reported that cytotoxicity depends on the nanoparticle size, shape, its structure and morphology [4,5]. The small size of such particles means that they are able to more easily evade the immune system of the body and penetrate cellular membranes to come into close proximity to sensitive biological components [6] Generally, the cytotoxicity of nanoparticles results due to cations on the surface of the metal oxides, which generate harmful free radical species catalytically within the cytoplasm [7] and are then able to chemically attack sensitive cellular components. Thus increased free radical concentrations can lead to apoptosis [8] or can responsible for potential carcinogenesis [9].

Due to structural imperfection and uncompensated spins, magnetic nanomaterials exhibit induced permanent magnetic moments on the surface of the particles [10]. The surface uncompensated exchange couplings at the surface modify the magnetic properties, [11]. Although several associated issues like aggregation, toxic states of the nanoparticles, surface functionalization, poor durability etc. restrain the use of bare magnetic nanoparticles, however, these problems can be addressed by

coating magnetic nanoparticles with non-magnetic materials like polymers, organic monolayers, enzymes etc. [12-14]. Such coated magnetic nanoparticles have added advantage in the biomedical field due to easy separation and sensitivity to a magnetic field [15].

Iron oxide nanoparticles exhibited exceptional features in catalysis by reducing unwanted reactions, good selectivity, the requirement of the mild environment in various examples like hydrolysis, esterification, and redox reactions [16,17]. In case of biocatalytic applications, for example inhibition of proliferation and differentiation effect on morphology, functionality and death, little is reported that analyzes the chemical reaction on the surface of nanoparticles as a source of cytotoxicity [18,19]. It has been reported that α-Fe_2O_3 is highly biocompatible and it has potential free radical scavenging behaviour, which is attributed due to spinel defects of tetrahedrally coordinated Fe sites (T-defects) on their surface [20]. In many cases, this problem is addressed by shielding or binding the highly reactive surface of these particles with some organic macromolecules to scavenge reactive oxygen species (ROS) generated from ionizing radiation [21].

Several efforts have been performed on the synthesis of nano-biocatalysts, which are effective against fatal carcinoma and drug-dosage ability of enzymes using grafted nanoparticles [22-27]. Due to their mesoporous nature, PEG-coated iron oxide NPs have drawn particular attention in medicines, including in contrast agents, biosensors and anti-carcinomas treatment [28]. Zhongwen Chen *et al*. demonstrated pH-dependent dual enzyme-like activity of iron oxide nanoparticles and their concentration-dependent cytotoxicity on human glioma U 251 cells [29]. Leila Gholami *et al*. reported green facile synthesis of low toxic superparamagnetic iron oxide nanoparticles, (SPIONs) and their cytotoxic effect towards Neuro2A and

HUVEC cell lines [30]. R. Abhinayaa *et al*. reported synthesis of cytotoxic consequences of halloysite nanotube/iron oxide nanocomposite and iron oxide nanoparticles upon interaction with bacterial, noncancerous and cancerous cell lines [31]. In an excellent work, Dean Cardillo and co-workers demonstrated morphological and structural defects dependent cytotoxicity of hematite nanoparticles against MDCK cell lines [4].

Inspiring from the above works, the present investigation deals synthesis and characterization of PEG-coated and L-Ascorbic acid grafted α-Fe_2O_3 NPs (LAA@IONP-PEG) as an effective anti-carcinogenic agent against HEK-293 human embryonic kidney cell lines.

4.2. Experimental section

4.2.1. Materials

DMEM (Gibco Invitrogen), Trypsin (0.25%, Gibco Invitrogen), FBS US Origin (Gibco Invitrogen), Trypan Blue (Gibco Invitrogen), DPBS (Gibco Invitrogen) FBS, Iron(III) chloride ($FeCl_3$), potassium chloride (KCl), polyethyleneglycol (PEG) and L-ascorbic acid (LAA) were purchased from Sigma Aldrich and used without further purification.

4.2.2. Synthesis

In a typical procedure, aqueous solutions of potassium hexachloroiron(III) [$K_3(FeCl)_6$] and L-ascorbic acid reacted in the presence of an amphiphilic nonionic surfactant PEG at 37 °C to produce iron oxide nanoparticles in its stable oxidation state. In the first step, aqueous solutions of $FeCl_3$ and KCl in a 1:3 ratio (dissolved in de-ionized water) were mixed for 6 hours with continuous magnetic stirring at room

temperature to produce coordinate complex $K_3[FeCl_6]$. For synthesis of iron oxide nanoparticles, 30 mL of 20 mM of the complex $K_3[FeCl_6]$, 30 mL of 0.l M L-ascorbic acid and 6 mg/mL of PEG (surfactant) were taken in a vessel and mixed thoroughly on a magnetic stirring at 37 °C for one hour. Thus formed dark reddish-brown solution was sonicated for 1 hour at 37 °C temperature, centrifuged at 10000 rpm for 20 minutes, washed several times with de-ionized water to remove excess surfactant and other contaminants and dried in a microwave oven.

4.2.3. Instrumental techniques

The UV-visible absorption spectrum of the material was recorded on Shimadzu UV-3600 spectrophotometer in the range 200-700 nm while surface coating and adsorption of PEG and L-ascorbic acid have been examined by Fourier Transform Infrared spectral study, recorded on Perkin Elmer Spectrum II instrument. FESEM and EDX analyses were carried out on JEOL 6490 LB equipment at an operating voltage of 15 kV. The particles sized distribution was measured by Horiba Scientific Nanopartica (SZ100Z). The zeta potential of iron oxide nanomaterial was measured using Zetasizer ZS90 (Nano series Malvern Instrument) at room temperature. The dispersion of nanoparticles was sonicated for 20 minutes and diluted to make solution concentration 80 µg/mL in phosphate buffer saline (pH = 7.4). Nitrogen adsorption-desorption and pore-size diameter have been estimated by Belsorp mini-II instrument. Transmission electron microscopy images of the material were recorded using JEOL-2100 equipment. X-ray diffraction pattern of the material was recorded on Pananalytical's X'Pert Pro X-ray diffractometer in the 2θ range 10 to 80° at a scanning rate of 2° per minute using CuKα radiation at a wavelength of 1.54059A°. CO_2 Incubator (Eppendorf Galaxy 170), Fluorescent Microscope (Carl Zeiss),

Refrigerated Centrifuge (Thermo scientific), and Hemocytometer were used for in-vitro cell line assay.

4.2.4. Docking

The docking studies of LAA@IONP-PEG was performed with anticancer molecular targets, namely PPARγ (PDB:2PRG) and GLUT1 (PDB:1SUK), using AUTODOCK 1.5.4. Before docking study, the active site domain was determined through LogP active site recognizer. The grid box was set according to the best configuration of the active site amino acid sequence [32,33]. The binding affinities (kcal/mole) and the count of probable hydrogen bonds were also evaluated.

4.2.5. In vitro cell line assay

MTT [3-(4,5-Dimethylthiazol-2-yl)-2,5-diphenyl tetrazolium bromide] viability assay was performed as per protocol reported earlier in the literature. Briefly, HEK-293 cells were seeded in 96-wells plate (5.0×10^3cells/well) and kept for 24 h. The cells were treated with 200 µL of varying concentrations of LAA@IONP-PEG (15-60 µg/mL) and the samples were incubated in a humid condition of CO_2 at 37 °C. After 24 h, 50 µL of MTT solution (1 mg/mL) was added to each well and incubated for another 4 h. Then, the media and excess MTT were removed and 150 µL of dimethyl sulfoxide (DMSO) was also added. The absorbance was recorded at 570 nm using the Infinite M200 microplate reader (Tecan Group Ltd., Mannedorf, Switzerland). Samples containing media with and without cells were also analyzed and labelled as 'control' and 'blank', respectively. All the experiments were performed in triplicates. The final organic solvent concentration was 0.3% (v/v). Cell survival (% of control) was calculated relative to untreated control cells.

4.2.6. Determination of Reactive Oxygen Species (ROS)

100 µL suspension of LAA@IONP-PEG was incubated with a MIC concentration at 37 °C for 2 h, thereafter 20 µL (20 µM) of H_2 DCFDA (cellular ROS assay kit) solution was added to the resulting mixture. The fluorescent intensity was measured on spectrophotometer Biotek Synergy HT with an excitation and emission wavelength of 480 and 520 nm, respectively, at time tenure of 30 minutes. An untreated sample suspension was used as a control. The experiment was completed in triplicate.

4.2.7. Radical scavenging analysis

The reducing ability of LAA@IONP-PEG was done using 1,1-Diphenyl-2-picryl hydrazine radical, (DPPH) assay analysis. For antioxidant ability, 3 mL of DPPH (0.0004 %) was added to1 mL aliquot of samples having concentration 15, 30, 45, and 60 µg/mL. The prepared solution was put in rest for half an hour in the darkroom and UV-visible spectra were recorded at 517 nm. The value of percentage inhibition was determined using the formula as:

$$\% \text{ Inhibition (DPPH radicals)} = [(A_c - A_t) / A_t] * 100$$

Where A_t stands to an absorbance of the control sample and A_t, the absorbance of the test sample.

4.3. Results and discussion

4.3.1. Structural studies of LAA@IONP-PEG

UV-visible absorption spectroscopy was performed to observe the formation of LAA@IONP-PEG. The sample was dispersed in de-ionized water and measurement was carried out in the range of 200-700 nm (Fig. 4.1 a). The graph

shows a peak at 429 nm, which is characteristic of LAA@IONP-PEG, wherein iron is coordinated [34,35].

FTIR spectral analysis of LAA@IONP-PEG was carried out in the range of 400-4000 cm^{-1} region at room temperature to analyze the interaction of IONPs with functional groups of L-ascorbic acid and polyethylene glycol (Fig. 4.1 b). The graph shows a broad absorption peak at 3429 cm^{-1} due to -OH stretching of the carboxyl group [36]. The broadness of this peak indicated the presence of hydrogen bonding between LAA-PEG-iron oxide nanoparticles. The peak at 1728 and 1634 cm^{-1} are due to C=O of five-membered lactone ring and C=C stretching of ascorbic acid, respectively. These peaks are red-shifted compared to those of pure ascorbic acid (at 1750 and 1655 cm^{-1}, respectively of C=O and C=C) due to its adsorption on the nanoparticle's surface. The strong peak at 1089 cm^{-1} is due to C-O stretching, peaks at 1406, and 1357 cm^{-1} are due to $–CH_2$ scissoring and wagging while the peaks at 2942 and 2888 cm^{-1} are due to stretching vibrations of PEG [37]. The peak at 946 cm^{-1} is due to out of plane bending vibration C-H of PEG. Moreover, small intensity peaks in the far IR region at 591 and 472 cm^{-1}corresponds to Fe-O vibration modes of α-Fe_2O_3 [38] while peaks at 811, 706 and 627 cm^{-1} are due to vibrations of β-FeOOH (Fig. 4.1 c) [39].

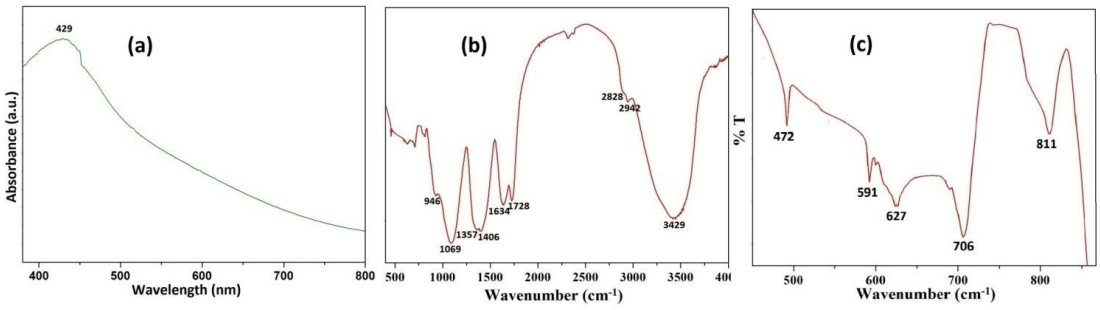

Fig. 4.1.UV-visible spectrum (a), FTIR spectrum (b) and high resolution peaks in far IR region (c) of LAA@IONP-PEG

The particle size analysis of formed LAA@IONP-PEG was analyzed by particle size distribution curve shown in Fig. 4.2 a. The curve shows that the size of particles is distributed in a range of 70-100 nm while the maximum population falls at 83 nm. The zeta-potential analysis (ζ) of nanoparticles at -23±8 mV Fig. 4.2 b shows that the surface of nanoparticles is negatively charged, which maintains their stability [40].

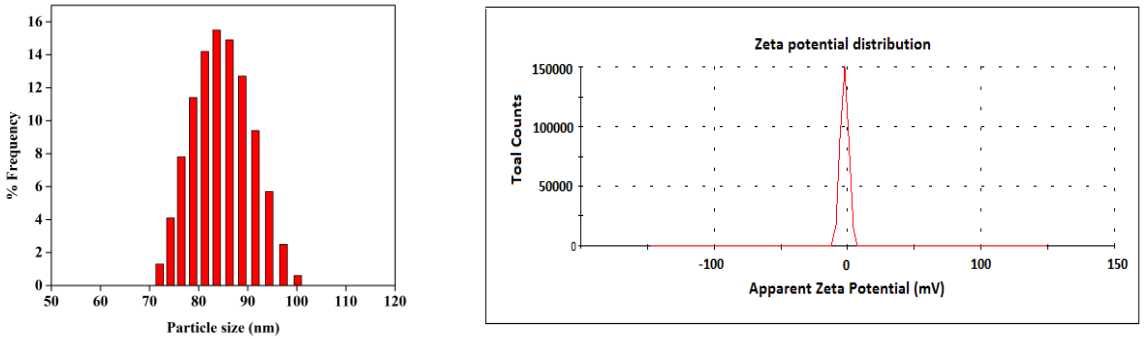

Fig. 4.2 a-b. Particle's size distribution and Zeta potential curve of LAA@IONP-PEG

The size and morphology of as-synthesized LAA@IONP-PEG NPs were analyzed using field emission scanning electron microscopy (FESEM) and the representative images are shown in Fig. 4.3 a-c. In the FESEM images, variable shapes like sphere, ellipsoid, rod, chain and closed rings have been observed. In the corresponding EDX spectrum, the peaks of O and Fe have been found (Fig. 4.3 d). The weight percentage of the O and Fe in the EDX spectrum has been estimated to be 29.82 and 60.18 % respectively, indicating the formation of α-Fe_2O_3 mainly in this experiment [41].

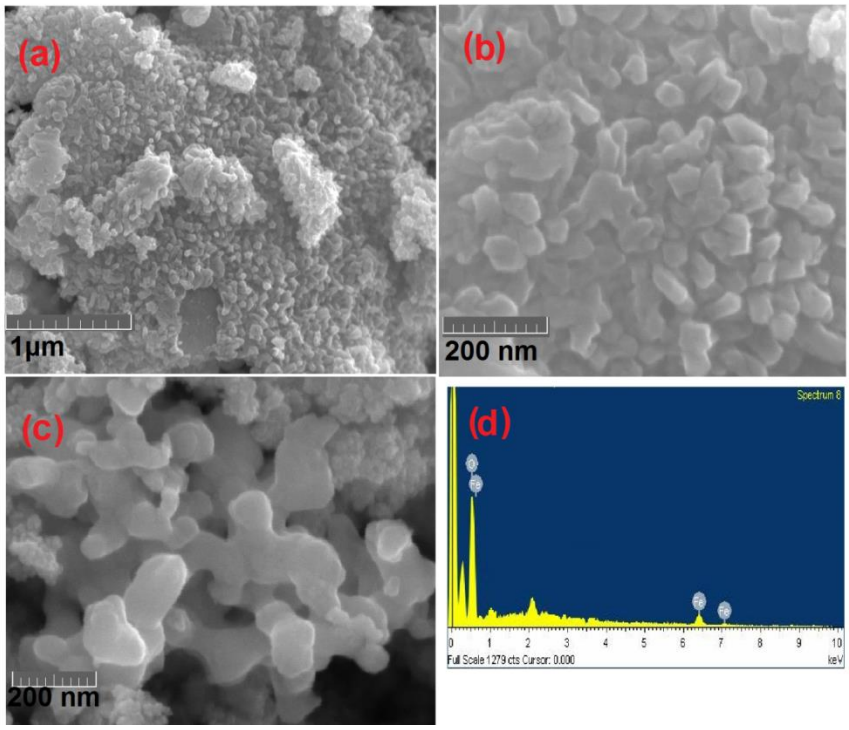

Fig. 4.3. FESEM images (a-c) and EDX pattern (d) of LAA@IONP-PEG

The structural features of LAA@IONP-PEG NPs have further been examined by TEM analyses shown in Fig. 4.4 a-d. In the TEM images, 30-70 nm diameter spherical/ellipsoidal structures and few rod/chain like variable structures (70-600 nm long, 50-70 nm wide) have been observed. Chain-like structures have been evolved in variable length and shape: small to long and ring-like chains, showing granular agglomerates with particle width in the range of 60 ± 10 nm. The addition of surfactant PEG led to a slight increase in the size of the prepared NPs, as the average diameter of such nanostructure was increased as proven by dynamic light scattering analysis (DLS) measurement. From the physical interpretation of the TEM micrograph, it seems that the size of NPs increases after binding with PEG, which is indicative of PEG coating on-to the surface of nanoparticles. In the FTIR spectral analyses, it has been found that LAA-PEG molecules are attached via M-O interaction; hence increase in size and shape of nanoparticles is obvious in

LAA@IONP-PEG. These results are also in good agreement with X-ray diffraction analysis.

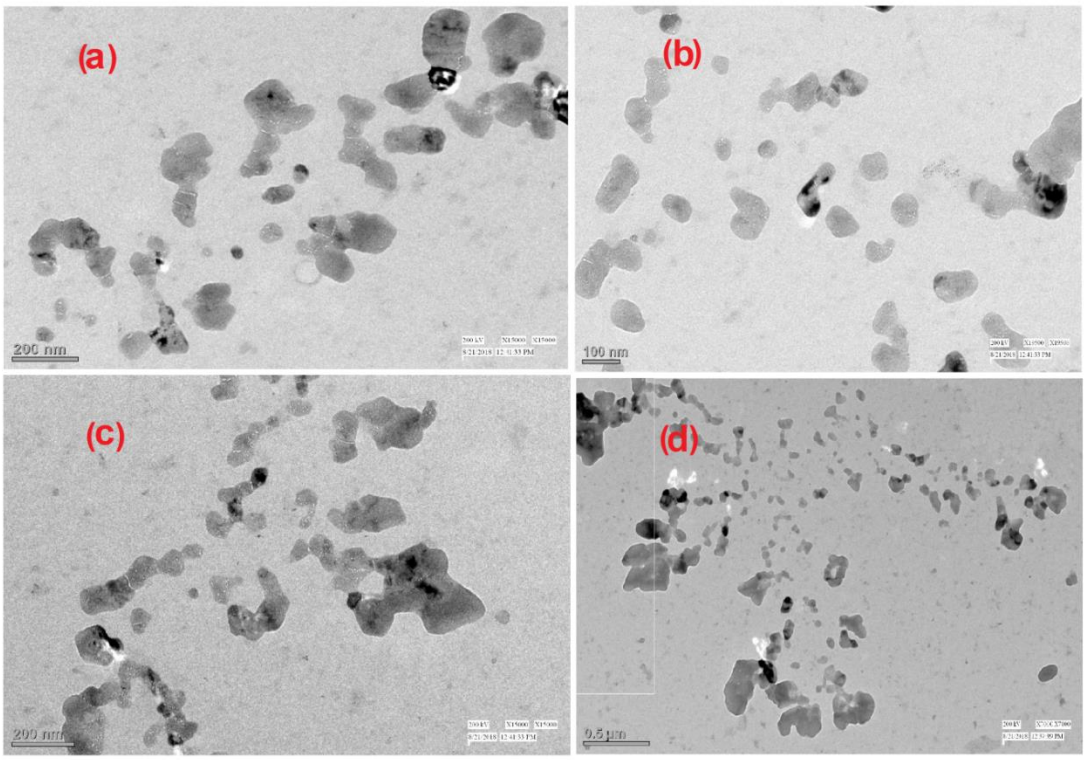

Fig.4.4. TEM images of LAA@IONP-PEG (a-d)

The crystal phase and purity of LAA@IONP-PEG were analyzed using X-ray diffraction analysis shown in Fig. 4.5. In the diffraction pattern, the peaks at 2θ value 32.1, 35.4, 40.9, 48.2, 54.1, 57.4, 62.9, 64.6 and 73.4 are correspond to planes (Miller indices; (hkl)) of (104), (110), (113), (024), (116), (112), (214), (300) and (1010) respectively, which indicate the formation of α-Fe_2O_3(JCPDS card no. 33-0664), as reported earlier [42]. Minor peaks observed at 2θ values 45.7 and 69.1 correspond to planes (Miller indices; (hkl)) of (411) and (312) of β-FeOOH (JCPDS card no. 34-1266) showing the presence of alkaganeite as an impurity. Peaks in diffraction patterns are intense and broadened, indicating formation of well crystalline and small size particles. The mean crystallite size can be determined by Scherrer's formula, considering that the XRD line broadening caused due to decreasing crystallite size

[43]. The obtained mean crystallite's size by this formula is the size perpendicular to a given plane (hkl) [44]. It is known that the 104 plan is related to the near basal plane (a-axis); the calculated mean crystallite size corresponds to the crystallite dimensions in the c-axis direction [45]. The narrower the 104 lines, the more elongated the crystal along the c-axis. Inverse relation has been applied for 110 planes i.e. as the FWHM of the 110 line increases , the crystal is thinner in the a-axis direction. The full width half maximum (FWHM) of the two lines (104) and (110) [46] corrected for the instrumental line broadening have been used to determine crystallite's size and found to be 234 and 31 nm respectively of the (104) and (110) lines which are in agreement with values obtained in TEM results.

β-FeOOH nanoparticles are known to be an intermediate phase that gradually transforms into the α-Fe_2O_3 phase in a suitable environment [47-49]. The presence of suitable additives like surfactants and stabilizers assist the evolution of α-Fe_2O_3 with specific shape and size. β-FeOOH is a slight metastable phase; the decrease of surface energy is supposed to be driving force for transformation of β-FeOOH into α-Fe_2O_3 phase. Ostwald rule suggests a competition between kinetics, reversible thermodynamics, and irreversible thermodynamics. As the reaction proceeded with magnetic stirring at 37 °C, the required thermal energy gets available for β-FeOOH bonds breaking, and therefore its dissolution commences leading to the formation of Fe^{3+} ions at the surface of β-FeOOH. Now more stable α-Fe_2O_3 seeds nucleate and concentration of Fe^{3+} ions decreased. This forced dissolution of β-FeOOH, provides more Fe^{3+} ions, and therefore the growth of α-Fe_2O_3 particles takes place rapidly. Now surfactant PEG and stabilizer LAA present in reaction medium ensure the evolution of stable α-Fe_2O_3 with specific shape and size during one hour of reaction time [50].

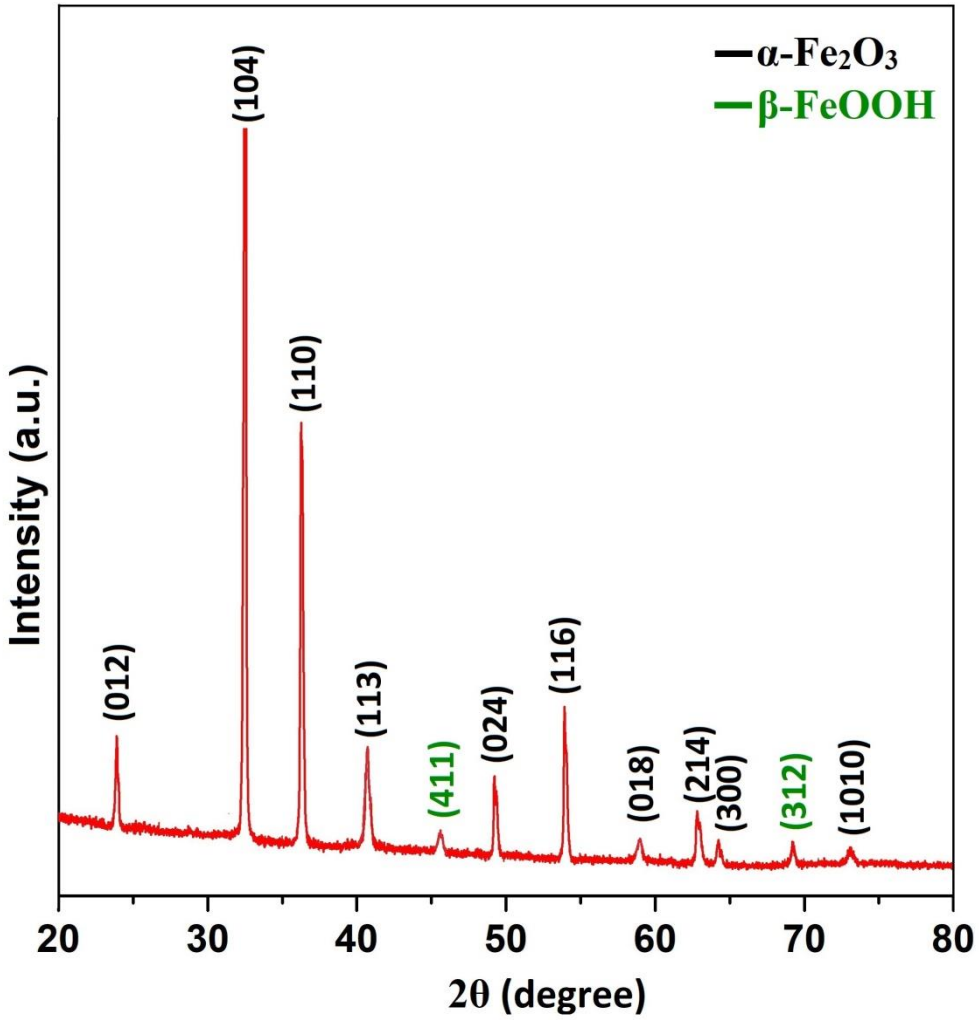

Fig.4.5. XRD pattern of LAA@IONP-PEG

Nitrogen adsorption/desorption isotherm plots have been utilized to determine pore diameter (*Dp*) and the surface area (*S*) of PEG-coated α-Fe_2O_3 NPs. Barrett-Joyner-Halenda (BJH) method was applied to estimate the average pore diameter and found to be 14 nm (Fig. 4.6 a). The specific surface area derived from the Brunauer-Emmett-Teller (BET) method was found to be 48.37 m^2g^{-1} (Fig. 4.6 b). The high surface area of NPs indicates the presence of more catalytic sites and thus expected to show high catalytic properties [51].

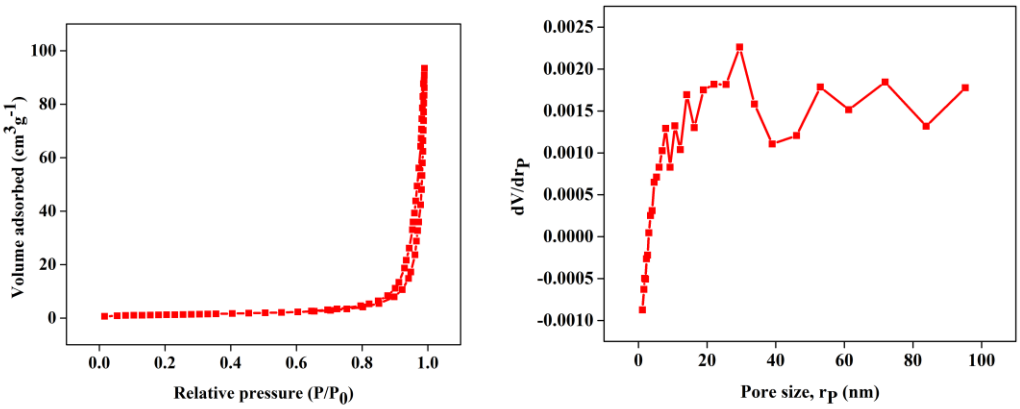

Fig. 4.6 a-b. N_2 adsorption-desorption isotherm of Pore size analysis of LAA@IONP-PEG

4.3.2. Docking Studies

The docking studies are performed via renal carcinomas cell lines PDBs on the molecular target of amino acid tyrosine, glutamine, threonine, etc. with LAA@IONP-PEG nanoparticles and evaluation of their binding affinities and number of probable hydrogen bonds are estimated. The docking images of the compound with an analyzed compound have been docked amino acids with an energy content of -6.1 kcal/mol (Human MRP protein, 12IRJ @ two hydrogen bond), -8.1 kcal/mol (Human MRP8, IMR8@ one hydrogen bond), -7.9 kcal/mol (KGA, 3VOZ@ two hydrogen bonds) (Fig. 4.7).

Target With PDB ID	Binding Energy (kcal/ mol)	Image of autodock 1.5.6	Amino acids involved in Interactions	H-Bonds
Human MRP14 1IRJ	-6.1	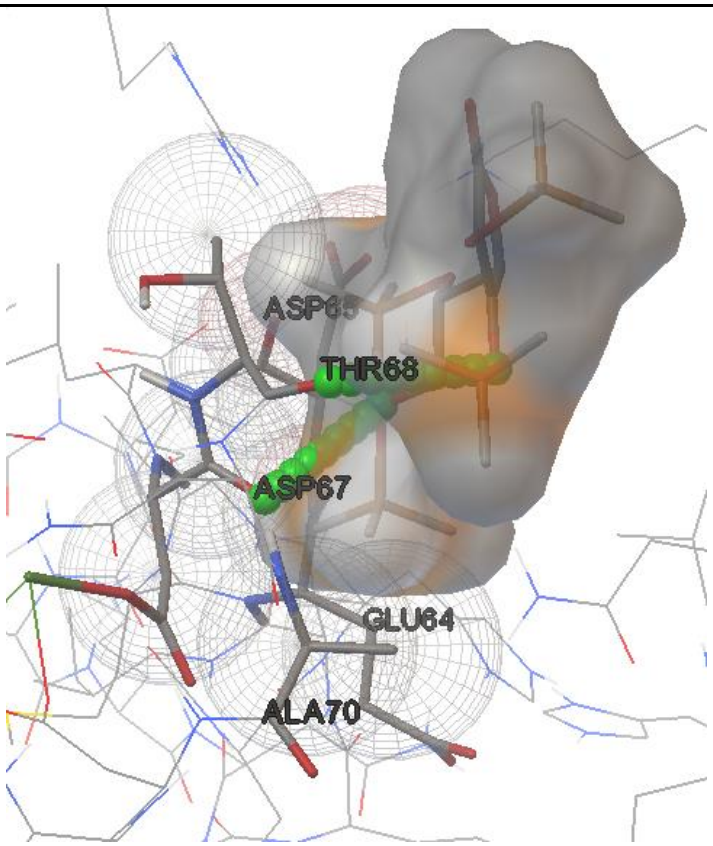	ASP65, THR68, ASP67, GLU64, ALA70	2
Human MRP8 1MR8	-8.3	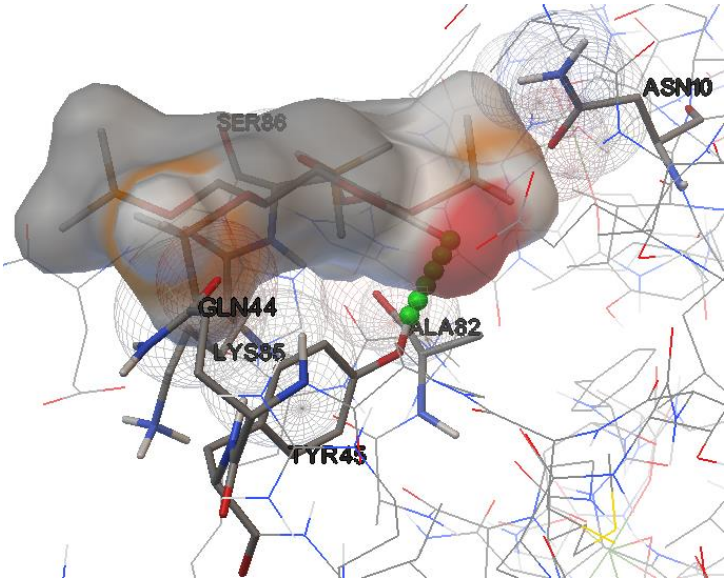	SER86, ASN10, GLN44, ALA82, LYS85, TYR45	1

KGA 3VOZ	**-7.9**	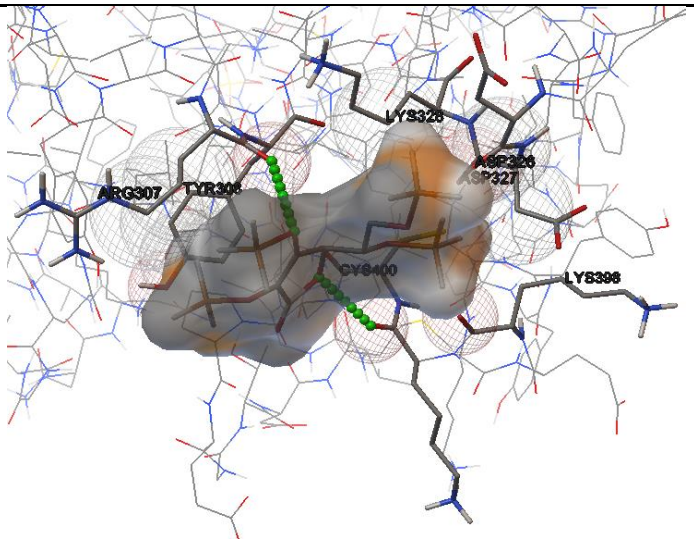	**ARG307, TYR308, LYS328, ASP326, ASP327, CYS400, LYS398**	**2**

Fig.4.7. Binding affinity of α-Fe_2O_3 with target proteins. Docking studies were performed using AUTODOCK 1.5.6

4.3.3. Molecular Docking studies of iron oxide clusters with proteins

Molecular docking is one of the crucial techniques, and it is a very useful tool for designing and computational calculations for the interaction of drugs and macromolecules. It is a method that predicts the preferred orientation of one molecule to others when a stable complex is formed by the interaction of the two. Here the iron oxide cluster is docked with DNA, proteins, and binding energy has been reported.

4.3.3.1. Computational Details

Dataset

Protein

The Protein Data Bank (PDB) format file of proteins with PDB ID's 1NOW, 2ING, 2ITX, 2ITY, 4C6C, 6D96 and 1BNA were downloaded from RCSB Protein

Data Bank [52]. The first two proteins PDBs 1NOW and 2ING are the crystal structure of breast cancer protein BRCA2 [53,54]. 3rd and 4th proteins are crystal structures of the EGFR kinase domain. Mutations in the EGFR kinase are cause of non-small-cell lung cancer [55]. 4C6C and 6D96 are the crystal structure of proteins present in Human Embryonic Kidney HEK-293 cell lines [56]. The last PDB id 1BNA is the structure of B-type DNA [57]. DNA present in the human body is mostly B-type. Using CHIMERA software, ligands and water molecules were removed from each protein [58].

4.3.3.2. Drugs

The nanocluster has optimized by Gaussian 09 software package [59]. This α-Fe_2O_3 cluster is optimized with the DFT method using B3LYP at the Def2tzvp level. The structure of the α-Fe_2O_3 cluster was taken after optimization. 3-D image of the chemical structure of the cluster is given in Fig. 4.8.

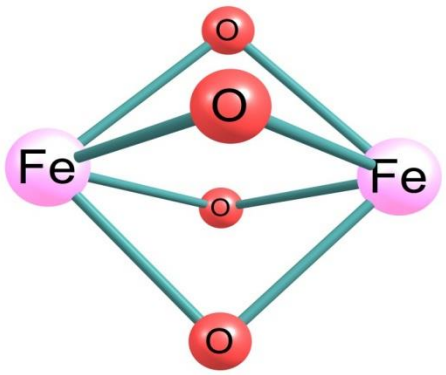

Fig. 4.8. Three dimensional structure of iron oxide cluster

4.3.3.3. Molecular Docking

Molecular Docking is done using software Autodock4.2 [60]. Lamarckian Genetic Algorithm is implemented for the task at hand. The proteins were taken as the

macromolecule and the iron oxide cluster as the ligand. Both macromolecule and ligand were prepared for docking. Water molecules were deleted from macromolecule. For Auto grid, macromolecule was contained in grid boxes. Grid boxes of appropriate dimensions were prepared for each protein. The number of LGA runs was set to 20. Kollman and Gasteiger charges were added to the complex by Auto Dock Tools (ADT) [61]. The complex is modified and adjusted for blind docking. The docked pose with the highest docking score was selected as the binding mode of the system.

4.4. Results and Discussion

The computationally calculated binding energies of all protein-drug complexes are given in Table 1. From the tabulated data, it is very much clear that binding energies of all proteins with the iron oxide cluster are of the same range. All of the obtained energies are negative, showing that the complex system is stable. The binding modes and geometrical orientation of all compounds were almost identical, suggesting that all the inhibitors occupied a common cavity in the receptor. For the proteins of the same type, the ligand binds in the same active pocket. The interactions are non-bonded. The lowest binding energy is with the 2ING complex. Molecular Docking gives the best and stable conformations of the ligand with proteins in the receptor active pocket. For each category of protein, the active pocket is shown with the one with better binding energy with iron oxide cluster. Fig. 4.9 shows the stable complex and interaction of the ligand with proteins.

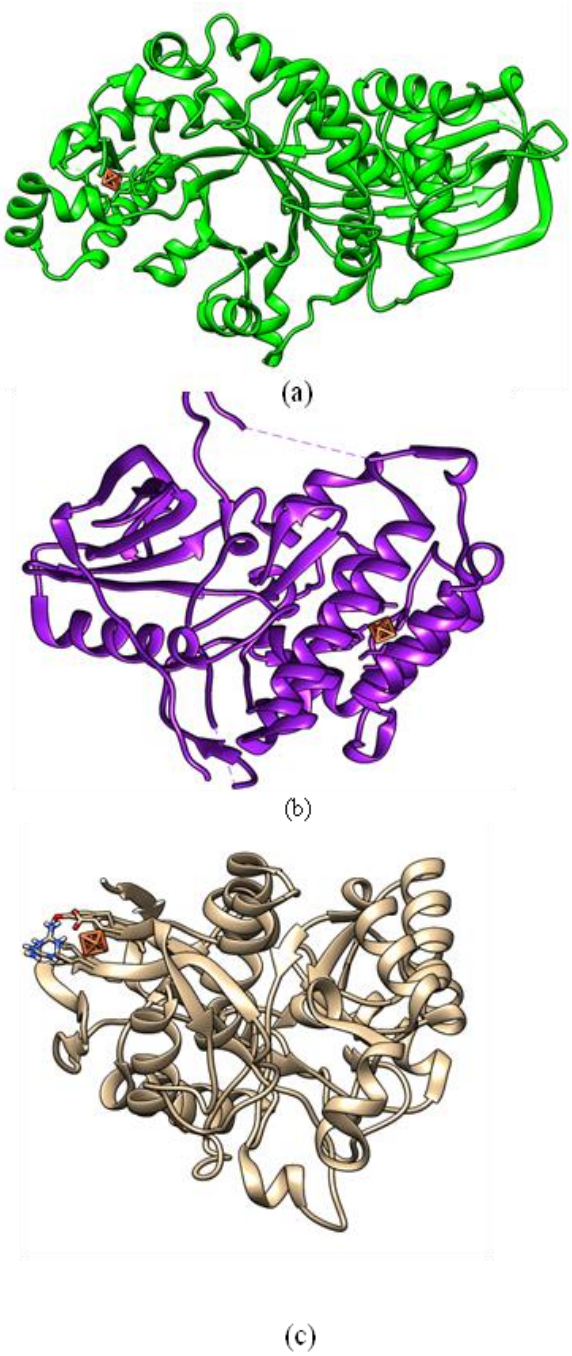

Fig.4.9. Docked complex of (a) 1NOW with cluster (b) 2ITX with cluster(c) 4C6Cwith cluster

The result of binding with DNA shows low interaction. Cluster binds in the minor groove of DNA. The binding energy with 1BNA comes out to be -0.09 kcal/mol, which is very less. It shows that the cluster has very less effect on DNA (Fig. 4.10).

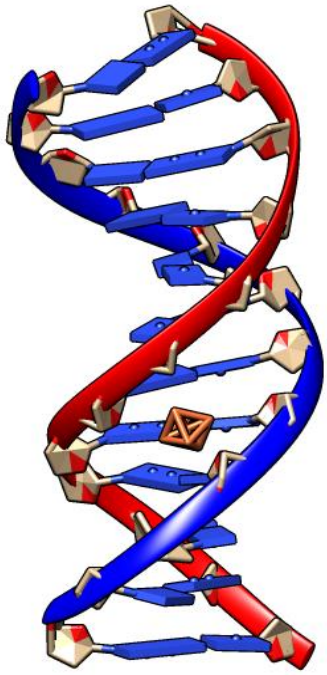

Fig. 4.10. Interaction of cluster with 1BNA

In silico studies revealed the entire synthesized molecule showed good binding energy toward the target protein.

4.4.1. Cytotoxicity test

The MTT assay was performed to check cytotoxicity of synthesized LAA@IONP-PEG NPs against renal carcinoma HEK-293 human embryonic kidney cell lines. The results were analyzed by plotting percentage cell viability *verses* concentration graph, the histogram curve and IC_{50} value (Fig. 4.11 a-c). It is obvious from the graph that the synthesized material LAA@IONP-PEG inhibited HEK-293 in a dose-dependent manner. The inhibition property of the iron oxide NPs was found out up-to the highest dose concentration. Axitinib showed 100 % inhibition at lower concentration i.e. 15 μg/mL which signified the positive direction of MTT cytotoxicity assay and our synthesized compounds has good inhibitory property.

However, the inhibitory action was slightly lower than that of Axitinib. The calculated IC_{50} was near about 40 µg/mL (IC_{50} value ≤ 40 µg/mL), indicating good therapeutic efficacy in the biological system i.e., against renal carcinoma HEK-293 human embryonic cell lines. This action may be due to the anti-cancer cytotoxic effect of LAA@IONP-PEG on DNA (as shown in *in silico* docking analysis in Fig. 4.10). Cell viability decreases with an increase in concentration implies that the synthesized LAA@IONP-PEG may be active against renal carcinoma, which is beneficial in future drug design perspective. For 24 hours incubation period at 37 °C temperature, a significant abatement has been observed in the treated cell lines at an increased concentration of 15-60 µg/mL concentration.

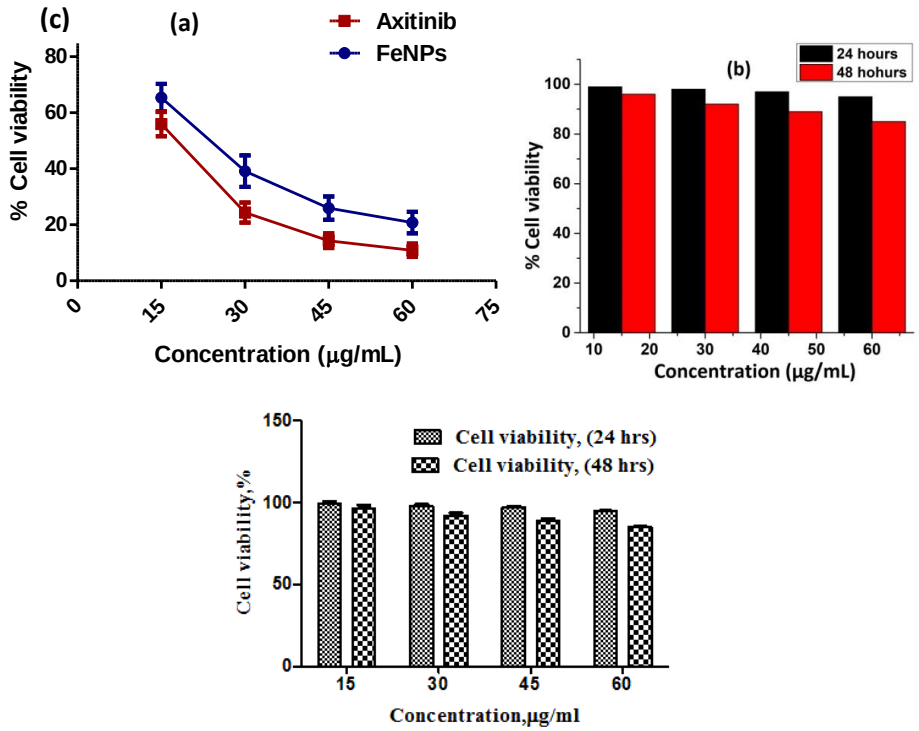

Fig.4.11. Percentage cell viability of LAA@IONP-PEG against HEK-293with Axitinib (a), cytotoxicity of LAA@IONP-PEG against HEK-293 for 24 and 48 hours (b) and IC_{98}, IC_{92} values of LAA@IONP-PEG against HEK-293 T cell lines at 24 and 48 hours (c)

Microscopic observation of cells with LAA@IONP-PEG at an increased concentration was done with an appropriate control (Fig. S7, S8). Treatment of renal carcinoma HEK-293 human embryonic kidney cell lines with LAA@IONP-PEG inhibited proliferation of cell lines in a time-dependent and dose-dependent manner. The morphology seems to be lost effectively with the treatment of LAA@IONP-PEG at higher concentrations and debris is collected at a concentration range of 45-60 µg/mL with the destruction of cells (Fig 4.12). Anti-cancer cytotoxicity analyzed at the above concentration for 48 hours gives a prominent result with certain accuracy (Fig. S8). The cytotoxicity of HEK-293 T cell lines has also analyzed which has a lower value of cell abatement death, ($IC_{92} \leq 30$ µg mL^{-1}) that shows that it is somehow less harmless to normal cells.

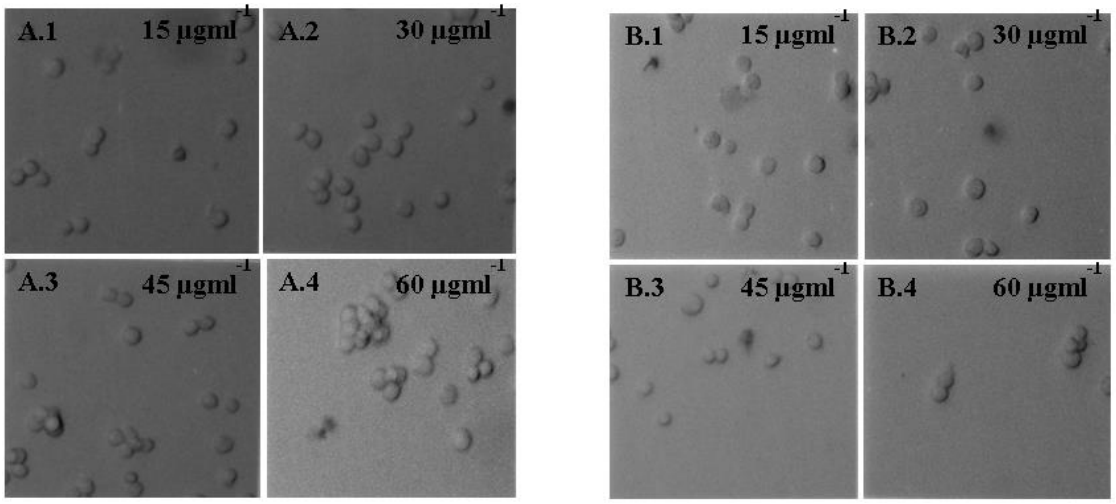

Fig. 4.12. Microscopic images of LAA@IONP-PEG against HEK-293 at different concentration for 24 hours (A.1-A.4) and for 48 hours (B.1-B.4).

Physico-chemical properties, such as size, shape, surface chemistry and dose play key role in inducing toxicity of iron oxide nanoparticles [4,5]. High cytotoxicity of the LAA@IONP-PEG is attributed to its small size and possibly due to the presence of adsorbed PEG and stabilizer L-ascorbic acid over hematite nanoparticles

surface. The cellular response to the nanoparticle could be due to different surface reactivity modulated by the presence of cytotoxic surface defects [62]. XRD results show that stable α-Fe_2O_3 phase formed due to dissolution of metastable β-FeOOH. Forced dissolution of β-FeOOH, provide more Fe^{3+} ions, and therefore the growth of α-Fe_2O_3 particles took place in this experiment, however β-FeOOH phase still remained as an impurity along with α-Fe_2O_3 phase. Presence of β-FeOOH as impurity induced surface defects in α-Fe_2O_3 lattice and catalytic iron break the homeostasis by promoting free radical production through Fenton/or Haber-Weiss reaction [63,64]. LAA@IONP-PEG induce reactive oxygen species (ROS) production [65] and activate redox-sensitive signaling cascades [66], attacking proteins and nucleic acids, leading to cytotoxicity effect [67].

Later ROS and free radical scavenging assay like 1,1-diphenyl-2-picrylhydrazine (DPPH), assay have also been performed during our experiment to check antioxidant capabilities [68]. The antioxidant assay showed that nanoparticles have a good scavenging property of oxygen species (Fig. 4.13. a-b) [55]. All the assays collectively suggested that our compound inhibited oxygen radicals in a dose-dependent manner. It is well established that free radicals generated during cancerous condition damage the normal tissue system. The scavenging ability of nanoparticles indicated the antioxidant property. The antioxidant ability of LAA@IONP-PEG further suggested that it has a tremendous role during the cancerogenic condition [69]. Therefore, it may be concluded that our synthesized nanoparticles may be a good antioxidant agent during the cancerous condition of the cell.

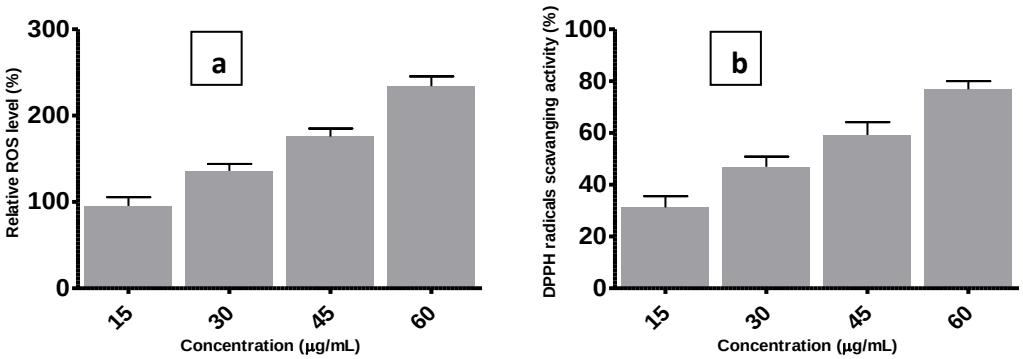

Fig. 4.13. ROS analysis (a) and DPPH analysis (b) of LAA@IONP-PEG against HEK-293 cell lines.

Conclusion

Synthesis of PEG-coated and L-ascorbic acid stabilized mesoporous α-Fe_2O_3 NPs (LAA@IONP-PEG) has been achieved in the sonochemical assisted method using aqueous solution mixture of complex $K_3[FeCl_6]$, PEG and L-ascorbic acid. LAA@IONP-PEG have been evolved in varieties of shapes and size as revealed in TEM, FESEM, EDX, UV-visible, FTIR, XRD and BET studies. Initially formed metastable β-FeOOH transformed into a stable α-Fe_2O_3 phase during the reaction at 37 °C. The anti-cancer study of LAA@IONP-PEG against renal carcinoma HEK-293 human embryonic kidney cell lines study suggests that high surface area with a large number of active sites mesoporous α-Fe_2O_3nanoparticles are well suited anti-cancer agent and serve as promising candidate for treatment of renal carcinoma HEK-293 human embryonic kidney cell lines. Docking study has confirmed the anti-proliferative action of NPs through binding affinity with renal carcinoma molecular targets. The synthesized NPs show a synergistic effect with Axitinib as an anti-cancer drug effective against renal carcinoma cell lines. Cytotoxicity and IC_{50} analysis led to detailed changes in the enzyme structure. The nanoparticles sample may be a good antioxidant agent during the cancerous condition of a cell. The results from the experimental and theoretic studies served as a valuable anti-cancer tool against renal carcinoma drug therapy in future.

References

1. Höglund, M.; Gisselsson, D.; Soller, M.; Hansen, G. B.; Elfving, P.; Mitelman, F., Dissecting karyotypic patterns in renal cell carcinoma: an analysis of the accumulated cytogenetic data. *Cancer genetics and cytogenetics* 2004, 153, (1), 1-9. https://doi.org/10.1016/j.cancergencyto.2003.12.019
2. Pankhurst, Q. A.; Connolly, J.; Jones, S. K.; Dobson, J., Applications of magnetic nanoparticles in biomedicine. *Journal of Physics D: Applied Physics* 2003, 36, (13), R167. https://doi.org/10.1088/0022-3727/36/13/201
3. Berry, C. C., Progress in functionalization of magnetic nanoparticles for applications in biomedicine. *Journal of Physics D: Applied Physics* 2009, 42, (22), 224003. https://doi.org/10.1088/0022-3727/42/22/224003
4. Cardillo, D.; Tehei, M.; Hossain, M. S.; Islam, M. M.; Bogusz, K.; Shi, D.; Mitchell, D.; Lerch, M.; Rosenfeld, A.; Corde, S. p., Synthesis-dependent surface defects and morphology of hematite nanoparticles and their effect on cytotoxicity in vitro. *ACS applied materials & interfaces* 2016, 8, (9), 5867-5876. https://doi.org/10.1021/acsami.5b12065
5. Dutta, B.; Shetake, N. G.; Gawali, S. L.; Barick, B.; Barick, K.; Babu, P.; Pandey, B.; Priyadarsini, K.; Hassan, P., PEG mediated shape-selective synthesis of cubic Fe3O4 nanoparticles for cancer therapeutics. *Journal of Alloys and Compounds* 2018, 737, 347-355. https://doi.org/10.1016/j.jallcom.2017.12.028
6. Li, S.-D.; Huang, L., Pharmacokinetics and biodistribution of nanoparticles. *Molecular pharmaceutics* 2008, 5, (4), 496-504. https://doi.org/10.1021/mp800049w

7. Raghupathi, K. R.; Koodali, R. T.; Manna, A. C., Size-dependent bacterial growth inhibition and mechanism of antibacterial activity of zinc oxide nanoparticles. *Langmuir* 2011, 27, (7), 4020-4028. https://doi.org/10.1021/la104825u

8. Sharma, V.; Anderson, D.; Dhawan, A., Zinc oxide nanoparticles induce oxidative DNA damage and ROS-triggered mitochondria mediated apoptosis in human liver cells (HepG2). *Apoptosis* 2012, 17, (8), 852-870. https://doi.org/10.1007/s10495-012-0705-6

9. Federico, A.; Morgillo, F.; Tuccillo, C.; Ciardiello, F.; Loguercio, C., Chronic inflammation and oxidative stress in human carcinogenesis. *International journal of cancer* 2007, 121, (11), 2381-2386. https://doi.org/10.1002/ijc.23192

10. Wagner, J.; Autenrieth, T.; Hempelmann, R., Core shell particles consisting of cobalt ferrite and silica as model ferrofluids [CoFe2O4–SiO2 core shell particles]. *Journal of magnetism and magnetic materials* 2002, 252, 4-6. https://doi.org/10.1016/S0304-8853(02)00729-1

11. Tronc, E.; Ezzir, A.; Cherkaoui, R.; Chanéac, C.; Nogues, M.; Kachkachi, H.; Fiorani, D.; Testa, A.; Greneche, J.; Jolivet, J., Surface-related properties of γ-Fe2O3 nanoparticles. *Journal of magnetism and magnetic materials* 2000, 221, (1-2), 63-79. https://doi.org/10.1016/S0304-8853(00)00369-3

12. Gupta, A. K.; Gupta, M., Synthesis and surface engineering of iron oxide nanoparticles for biomedical applications. *Biomaterials* 2005, 26, (18), 3995-4021. https://doi.org/10.1016/j.biomaterials.2004.10.012

13. McBain, S. C.; Yiu, H. H.; Dobson, J., Magnetic nanoparticles for gene and drug delivery. *International Journal of Nanomedicine* 2008, 3, (2), 169. http//doi: 10.2147/ijn.s1608

14. Nicolás, P.; Saleta, M.; Troiani, H.; Zysler, R.; Lassalle, V.; Ferreira, M. L., Preparation of iron oxide nanoparticles stabilized with biomolecules: experimental and mechanistic issues. *Acta biomaterialia* 2013, 9, (1), 4754-4762. https://doi.org/10.1016/j.actbio.2012.09.040

15. Issa, B.; Obaidat, I. M.; Albiss, B. A.; Haik, Y., Magnetic nanoparticles: surface effects and properties related to biomedicine applications. *International journal of molecular sciences* 2013, 14, (11), 21266-21305. https://doi.org/10.3390/ijms141121266

16. Hall, M.; Bommarius, A. S., Enantioenriched compounds via enzyme-catalyzed redox reactions. *Chemical reviews* 2011, 111, (7), 4088-4110. https://doi.org/10.1021/cr200013n

17. Herrmann, A., Controlled release of volatiles under mild reaction conditions: from nature to everyday products. *Angewandte Chemie International Edition* 2007, 46, (31), 5836-5863. https://doi.org/10.1002/anie.200700264

18. Soenen, S. J.; Nuytten, N.; De Meyer, S. F.; De Smedt, S. C.; De Cuyper, M., High intracellular iron oxide nanoparticle concentrations affect cellular cytoskeleton and focal adhesion kinase-mediated signaling. *Small* 2010, 6, (7), 832-842. https://doi.org/10.1002/smll.200902084

19. Ankamwar, B.; Lai, T.; Huang, J.; Liu, R.; Hsiao, M.; Chen, C.; Hwu, Y., Biocompatibility of Fe3O4 nanoparticles evaluated by in vitro cytotoxicity assays using normal, glia and breast cancer cells. *Nanotechnology* 2010, 21, (7), 075102. https://doi.org/10.1088/0957-4484/21/7/075102

20. Chernyshova, I.; Hochella Jr, M.; Madden, A., Size-dependent structural transformations of hematite nanoparticles. 1. Phase transition. *Physical Chemistry Chemical Physics* 2007, 9, (14), 1736-1750. https://doi.org/10.1186/1743-8977-10-46

21. Na, H. B.; Palui, G.; Rosenberg, J. T.; Ji, X.; Grant, S. C.; Mattoussi, H., Multidentate catechol-based polyethylene glycol oligomers provide enhanced stability and biocompatibility to iron oxide nanoparticles. *Acs Nano* 2012, 6, (1), 389-399. https://doi.org/10.1021/nn203735b

22. Abbas, G.; Kumar, N.; Kumar, D.; Pandey, G., Effect of Reaction Temperature on Shape Evolution of Palladium Nanoparticles and Their Cytotoxicity against A-549 Lung Cancer Cells. *ACS omega* 2019, 4, (26), 21839-21847. https://doi.org/10.1021/acsomega.9b02776

23. Asmat, S.; Husain, Q., A robust nanobiocatalyst based on high performance lipase immobilized to novel synthesised poly (o-toluidine) functionalized magnetic nanocomposite: Sterling stability and application. *Materials Science and Engineering: C* 2019, 99, 25-36. https://doi.org/10.1016/j.msec.2019.01.070

24. Soozanipour, A.; Taheri-Kafrani, A.; Barkhori, M.; Nasrollahzadeh, M., Preparation of a stable and robust nanobiocatalyst by efficiently immobilizing of pectinase onto cyanuric chloride-functionalized chitosan grafted magnetic nanoparticles. *Journal of colloid and interface science* 2019, 536, 261-270. https://doi.org/10.1016/j.jcis.2018.10.053

25. Joshi, R.; Sharma, R.; Kuila, A., Lipase production from Fusarium incarnatum KU377454 and its immobilization using Fe3O4 NPs for application in waste cooking oil degradation. *Bioresource Technology Reports* 2019, 5, 134-140. https://doi.org/10.1016/j.biteb.2019.01.005

26. Kashefi, S.; Borghei, S. M.; Mahmoodi, N. M., Superparamagnetic enzyme-graphene oxide magnetic nanocomposite as an environmentally friendly biocatalyst: Synthesis and biodegradation of dye using response surface methodology. *Microchemical Journal* 2019, 145, 547-558. https://doi.org/10.1016/j.microc.2018.11.023

27. Mahmoudi, M.; Laurent, S.; Shokrgozar, M. A.; Hosseinkhani, M., Toxicity evaluations of superparamagnetic iron oxide nanoparticles: cell "vision" versus physicochemical properties of nanoparticles. *Acs Nano* 2011, 5, (9), 7263-7276. https://doi.org/10.1021/nn2021088

28. Mohanta, S. C.; Saha, A.; Devi, P. S., PEGylated iron oxide nanoparticles for pH responsive drug delivery application. *Materials Today: Proceedings* 2018, 5, (3), 9715-9725. https://doi.org/10.1016/j.matpr.2017.10.158

29. Chen, Z.; Yin, J.-J.; Zhou, Y.-T.; Zhang, Y.; Song, L.; Song, M.; Hu, S.; Gu, N., Dual enzyme-like activities of iron oxide nanoparticles and their implication for diminishing cytotoxicity. *Acs Nano* 2012, 6, (5), 4001-4012. https://doi.org/10.1021/nn300291r

30. Gholami, L.; Oskuee, R. K.; Tafaghodi, M.; Farkhani, A. R.; Darroudi, M., Green facile synthesis of low-toxic superparamagnetic iron oxide nanoparticles (SPIONs) and their cytotoxicity effects toward Neuro2A and HUVEC cell lines. *Ceramics International* 2018, 44, (8), 9263-9268. https://doi.org/10.1016/j.ceramint.2018.02.137

31. Abhinayaa, R.; Jeevitha, G.; Mangalaraj, D.; Ponpandian, N.; Vidhya, K.; Angayarkanni, J., Cytotoxic consequences of Halloysite nanotube/iron oxide nanocomposite and iron oxide nanoparticles upon interaction with bacterial, non-cancerous and cancerous cells. *Colloids and Surfaces B: Biointerfaces* 2018, 169, 395-403. https://doi.org/10.1016/j.colsurfb.2018.05.040

32. Lee, K. W.; Briggs, J. M., Molecular modeling study of the editing active site of Escherichia coli leucyl-tRNA synthetase: Two amino acid binding sites in the editing domain. *Proteins: Structure, Function, and Bioinformatics* 2004, 54, (4), 693-704. https://doi.org/10.1002/prot.10300

33. Afzelius, L.; Zamora, I.; Ridderström, M.; Andersson, T. B.; Karlén, A.; Masimirembwa, C. M., Competitive CYP2C9 inhibitors: enzyme inhibition

studies, protein homology modeling, and three-dimensional quantitative structure-activity relationship analysis. *Molecular pharmacology* 2001, 59, (4), 909-919. DOI: https://doi.org/10.1124/mol.59.4.909

34. Reem, R. C.; Solomon, E. I., Spectroscopic studies of the binuclear ferrous active site of deoxyhemerythrin: coordination number and probable bridging ligands for the native and ligand-bound forms. *Journal of the American Chemical Society* 1987, 109, (4), 1216-1226. https://doi.org/10.1021/bi4013726

35. Perera, R.; Sono, M.; Sigman, J. A.; Pfister, T. D.; Lu, Y.; Dawson, J. H., Neutral thiol as a proximal ligand to ferrous heme iron: implications for heme proteins that lose cysteine thiolate ligation on reduction. *Proceedings of the National Academy of Sciences* 2003, 100, (7), 3641-3646. http://hdl.handle.net/1808/4254

36. Kumar, A.; Ahuja, M., Carboxymethyl gum kondagogu–chitosan polyelectrolyte complex nanoparticles: Preparation and characterization. *International journal of biological macromolecules* 2013, 62, 80-84. https://doi.org/10.1016/j.ijbiomac.2013.08.035

37. Zeng-guo, F.; Sanping, Z., Synthesis and characterization of biodegradable hydrogels based on photopolymerizable acrylate-terminated CL-PEG-CL macromers with supramolecular assemblies of α-cyclodextrins. *Polymer* 2003, 44, (18), 5177-5186. https://doi.org/10.1016/S0032-3861(03)00505-6

38. Lu, L.; Li, L.; Wang, X.; Li, G., Understanding of the finite size effects on lattice vibrations and electronic transitions of nano α-Fe2O3. *The Journal of Physical Chemistry B* 2005, 109, (36), 17151-17156. https://doi.org/10.1021/jp052780+

39. Kazeminezhad, I.; Mosivand, S., Phase transition of electrooxidized Fe3O4 to γ and α-Fe2O3 nanoparticles using sintering treatment. *Acta Physica Polonica A* 2014, 125, (5), 1210-1214. https://doi.org/10.1080/15440478.2017.1361372

40. Zain, N. M.; Stapley, A. G.; Shama, G., Green synthesis of silver and copper nanoparticles using ascorbic acid and chitosan for antimicrobial applications. *Carbohydrate polymers* 2014, 112, 195-202. https://doi.org/10.1016/j.carbpol.2014.05.081

41. Hernández, A.; Maya, L.; Sánchez-Mora, E.; Sánchez, E. M., Sol-gel synthesis, characterization and photocatalytic activity of mixed oxide ZnO-Fe 2 O 3. *Journal of Sol-Gel Science and Technology* 2007, 42, (1), 71-78. https://doi.org/10.1007/s10971-006-1521-7

42. Wang, B.; Chen, J. S.; Wu, H. B.; Wang, Z.; Lou, X. W., Quasiemulsion-templated formation of α-Fe2O3 hollow spheres with enhanced lithium storage properties. Journal of the American Chemical Society 2011, 133, (43), 17146-17148. https://doi.org/10.1021/ja208346s

43. Pourghahramani, P.; Forssberg, E., Microstructure characterization of mechanically activated hematite using XRD line broadening. International Journal of Mineral Processing 2006, 79, (2), 106-119. https://doi.org/10.1016/j.minpro.2006.02.001

44. Hartridge, A.; Bhattacharya, A.; Sengupta, M.; Majumdar, C.; Das, D.; Chintalapudi, S., Crystallite size dependence on the magnetic properties of nanocrystalline magnetite powders. Journal of magnetism and magnetic materials 1997, 176, (2-3), L89-L92. https://doi.org/10.1016/S0304-8853(97)01004-4

45. Glas, J.-E., Studies on the ultrastructure of dental enamel: 1. Size and shape of the apatite crystallites as deduced from X-ray diffraction data. Journal of

ultrastructure research 1960, 3, (3), 334-344. https://doi.org/10.1016/S0022-5320(60)80020-2

46. Das, H.; Sakamoto, N.; Aono, H.; Shinozaki, K.; Suzuki, H.; Wakiya, N., Investigations of superparamagnetism in magnesium ferrite nano-sphere synthesized by ultrasonic spray pyrolysis technique for hyperthermia application. Journal of magnetism and magnetic materials 2015, 392, 91-100. https://doi.org/10.1016/j.jmmm.2015.05.029

47. Song, H.; Zhang, X.; Chen, T.; Jia, X., One-pot synthesis of bundle-like β-FeOOH nanorods and their transformation to porous α-Fe2O3 microspheres. Ceramics International 2014, 40, (10), 15595-15602. https://doi.org/10.1016/j.ceramint.2014.07.037

48. Li, M.; Li, B.; Meng, F.; Liu, J.; Yuan, Z.; Wang, C.; Liu, J., Highly sensitive and selective butanol sensors using the intermediate state nanocomposites converted from β-FeOOH to α-Fe2O3. Sensors and Actuators B: Chemical 2018, 273, 543-551. https://doi.org/10.1016/j.snb.2018.06.081

49. Almeida, T. P.; Fay, M. W.; Zhu, Y.; Brown, P. D., Hydrothermal growth mechanism of α-Fe 2 O 3 nanorods derived by near in situ analysis. Nanoscale 2010, 2, (11), 2390-2399. https://doi.org/10.1021/acs.jpcc.7b01363

50. Mohapatra, M.; Anand, S., Synthesis and applications of nano-structured iron oxides/hydroxides–a review. International Journal of Engineering, Science and Technology 2010, 2, (8). https://doi.org10.1080/19443994.2012.720411

51. Zhao, H.; Yang, J.; Wang, L.; Tian, C.; Jiang, B.; Fu, H., Fabrication of a palladium nanoparticle/graphene nanosheet hybrid via sacrifice of a copper template and its application in catalytic oxidation of formic acid. *Chemical Communications* 2011, 47, (7), 2014-2016. https://doi.org/10.1016/j.mattod.2013.01.021

52. Rose, P. W.; Prlić, A.; Altunkaya, A.; Bi, C.; Bradley, A. R.; Christie, C. H.; Costanzo, L. D.; Duarte, J. M.; Dutta, S.; Feng, Z., The RCSB protein data bank: integrative view of protein, gene and 3D structural information. *Nucleic acids research* 2016, gkw1000. https://doi.org/10.1093/nar/gkw100

53. Wilson, J. H.; Elledge, S. J., BRCA2 enters the fray. *Science* 2002, 297, (5588), 1822-1823. DOI: 10.1126/science.1077171

54. Khamkar, T.; Abhyankar, M.; Tendulkar, G.; Gopiesh Khanna, V.; Kannabiran, K., In silico molecular docking of marine drugs against cancer proteins. *Adv Chem Sci* 2013, 1, (2). https://doi.org/10.1186/s40064-016-3364-1

55. Pao, W.; Chmielecki, J., Rational, biologically based treatment of EGFR-mutant non-small-cell lung cancer. *Nature Reviews Cancer* 2010, 10, (11), 760-774. https://doi.org/10.1038/nrc2947

56. Chaudhary, S.; Pak, J. E.; Pedersen, B. P.; Bang, L. J.; Zhang, L. B.; Ngaw, S. M.; Green, R. G.; Sharma, V.; Stroud, R. M., Efficient expression screening of human membrane proteins in transiently transfected Human Embryonic Kidney 293S cells. *Methods* 2011, 55, (4), 273-280. https://doi.org/10.1016/j.ymeth.2011.08.018

57. Protas, A. V.; Popova, E. A.; Mikolaichuk, O. V.; Porozov, Y. B.; Mehtiev, A. R.; Ott, I.; Alekseev, G. V.; Kasyanenko, N. A.; Trifonov, R. E., Synthesis, DNA and BSA binding of Pd (II) and Pt (II) complexes featuring tetrazolylacetic acids and their esters. *Inorganica Chimica Acta* 2018, 473, 133-144. https://doi.org/10.1016/j.ica.2017.12.040

58. Lang, P. T.; Brozell, S. R.; Mukherjee, S.; Pettersen, E. F.; Meng, E. C.; Thomas, V.; Rizzo, R. C.; Case, D. A.; James, T. L.; Kuntz, I. D., DOCK 6: Combining techniques to model RNA–small molecule complexes. *Rna* 2009, 15, (6), 1219-1230. http:// doi:10.1261/rna.1563609

59. Hannon, F. H., Geometrical Optimization and Electronic Properties of Li on Xn Nanoclusters. *International Journal of New Technology and Research* 2017, 3, (2). https://doi.org/10.1016/j.cirp.2017.05.004

60. Yuriev, E.; Ramsland, P. A., Latest developments in molecular docking: 2010–2011 in review. *Journal of Molecular Recognition* 2013, 26, (5), 215-239. https://doi.org/10.1002/jmr.2266

61. Morris, G. M.; Lim-Wilby, M., Molecular docking. In *Molecular modeling of proteins*, Springer: 2008; pp 365-382. https://doi.org/10.1007/978-1-59745-177-2_19

62. Huber, D. L., Synthesis, properties, and applications of iron nanoparticles. *Small* 2005, 1, (5), 482-501. https://doi.org/10.1002/smll.200500006

63. Voinov, M. A.; Pagán, J. O. S.; Morrison, E.; Smirnova, T. I.; Smirnov, A. I., Surface-mediated production of hydroxyl radicals as a mechanism of iron oxide nanoparticle biotoxicity. *Journal of the American Chemical Society* 2011, 133, (1), 35-41. https://doi.org/10.1021/ja104683w

64. Stohs, S. J.; Bagchi, D., Oxidative mechanisms in the toxicity of metal ions. *Free radical biology and medicine* 1995, 18, (2), 321-336. https://doi.org/10.1016/0891-5849(94)00159-H

65. Chan, J.; Ang, S.; Ye, E.; Sullivan, M.; Zhang, J.; Lin, M., Heterogeneous photo-Fenton reaction on hematite (α-Fe 2 O 3){104},{113} and {001} surface facets. *Physical Chemistry Chemical Physics* 2015, 17, (38), 25333-25341. https://doi.org/10.1021/acs.jpcc.6b10553

66. Hao, H.; Sun, D.; Xu, Y.; Liu, P.; Zhang, G.; Sun, Y.; Gao, D., Hematite nanoplates: Controllable synthesis, gas sensing, photocatalytic and magnetic properties. *Journal of colloid and interface science* 2016, 462, 315-324. https://doi.org/10.1016/j.jcis.2015.10.012

67. Zhu, W.; Cui, X.; Wang, L.; Liu, T.; Zhang, Q., Monodisperse porous pod-like hematite: hydrothermal formation, optical absorbance, and magnetic properties. *Materials Letters* 2011, 65, (6), 1003-1006. https://doi.org/10.1016/j.matlet.2010.12.053

68. Mishra, A.; Roy, S.; Maity, S.; Yadav, R. K.; Keshari, A.; Saha, S., Antiproliferative effect of flower extracts of Spilanthes paniculata on hepatic carcinoma cells. *Int. J. Pharm. Sci* 2015, 7, 130-134. https://doi.org/10.1002/cbin.10180

69. Rai, A.; Kumar, U.; Raj, V.; Singh, A. K.; Kumar, P.; Keshari, A. K.; Kumar, D.; Maity, B.; De, A.; Samanta, A., Novel 1, 4-benzothazines obliterate COX-2 mediated JAK-2/STAT-3 signals with potential regulation of oxidative and metabolic stress during colorectal cancer. *Pharmacological research* 2018, 132, 188-203. https://doi.org/10.1016/j.phrs.2017.12.010

Materials Today Communications 26 (2021) 102175

Contents lists available at ScienceDirect

Materials Today Communications

journal homepage: www.elsevier.com/locate/mtcomm

Efficient anticarcinogenic activity of α-Fe_2O_3 nanoparticles: In-vitro and computational study on human renal carcinoma cells HEK-293

Gulam Abbas [a], Kijay Bahadur Singh [a,b], Narinder Kumar [b], Anamika Shukla [b], Devesh Kumar [b], Gajanan Pandey [a,*]

[a] Department of Chemistry, Babasaheb Bhimrao Ambedkar University, Lucknow, 226025, U.P., India
[b] Department of Physics, Babasaheb Bhimrao Ambedkar University, Lucknow, 226025, U.P., India

ARTICLE INFO

Keywords:
PEG-coated α-Fe_2O_3NPs
HEK-293
Renal carcinoma
Docking
XRD

ABSTRACT

The present study has witnessed the synthesis of α-Fe_2O_3 NPs using polyethylene glycol (PEG) as a surfactant and L-ascorbic acid (LAA) as a stabilizer. The product has been characterized by UV–vis absorption spectroscopy, FTIR, Dynamic Light Scattering, particle size distribution analysis, X-ray diffraction analysis, TEM, FESEM, EDX and BET, which show formation of variable size and shape, mesoporous, PEG-coated α-Fe_2O_3 NPs (LAA@IONP-PEG) with β-FeOOH as an impurity. The present work emphasizes upon an anti-cancer study of LAA@IONP-PEG against renal carcinoma HEK-293 human embryonic kidney cell lines. The study suggests that LAA@IONP-PEG is a promising material against renal carcinoma HEK-293 human embryonic kidney cell lines. The docking study has confirmed anti-proliferative action of NPs through binding affinity with renal carcinoma molecular targets. The synthesized NPs show the synergistic effect with Axitinib as an anti-cancer drug effective against renal carcinoma cell lines. ROS and 1,1-diphenyl-2-picrylhydrazine (DPPH) free radical scavenging assay have shown the antioxidant capability of synthesized NPs. The efficient biocatalytic activity of LAA@IONP-PEG prescribes its use as one of the best suited drugs for the future perspectives against fatal renal carcinoma and thus it is reckoned that synthesized NPs will have persistent utilization in different field of medical applications.

1. Introduction

Renal carcinoma is one of the most frequently diagnosed malignancies in men, which causes mobility and mortality globally [1]. To improve the efficacy of cancer therapy and to minimize its hazardous impacts on healthy tissues and organs, new treatment methods are urgently needed. Since recent decades, nanotechnology and its interdisciplinary fields are emerging as the best tool to diagnose several diseases fatal to mankind and causing problems to the environment. Synthesis of nanoparticles has gained attention in the field of a wide variety of biomedical applications like hyperthermia, gene or drug delivery, magnetic resonance imaging (MRI) and *in vivo* cell tracking [2,3]. It has been reported that cytotoxicity depends on the nanoparticle size, shape, its structure and morphology [4,5]. The small size of such particles means that they are able to more easily evade the immune system of the body and penetrate cellular membranes to come into close proximity to sensitive biological components [6] Generally, the cytotoxicity of nanoparticles results due to cations on the surface of the metal oxides, which generate harmful free radical species catalytically within the cytoplasm [7] and are then able to chemically attack sensitive cellular components. Thus increased free radical concentrations can lead to apoptosis [8] or can responsible for potential carcinogenesis [9].

Due to structural imperfection and uncompensated spins, magnetic nanomaterials exhibit induced permanent magnetic moments on the surface of the particles [10]. The surface uncompensated exchange couplings at the surface modify the magnetic properties, [11]. Although several associated issues like aggregation, toxic states of the nanoparticles, surface functionalization, poor durability etc. restrain the use of bare magnetic nanoparticles, however, these problems can be addressed by coating magnetic nanoparticles with non-magnetic materials like polymers, organic monolayers, enzymes etc. [12–14]. Such coated magnetic nanoparticles have added advantage in the biomedical field due to easy separation and sensitivity to a magnetic field [15].

Iron oxide nanoparticles exhibited exceptional features in catalysis by reducing unwanted reactions, good selectivity, the requirement of the mild environment in various examples like hydrolysis, esterification,

* Corresponding author.
E-mail address: pandeygajanan@rediffmail.com (G. Pandey).

https://doi.org/10.1016/j.mtcomm.2021.102175
Received 17 July 2020; Received in revised form 20 January 2021; Accepted 14 February 2021
Available online 20 February 2021
2352-4928/

Chapter 5

Synthesis of LAA@Cu_2O-PEG Nanostructures and their Cytotoxicity against Renal Carcinomas HEK-293 Human Embryonic Kidney Cell Lines

Synthesis of LAA@Cu_2O-PEG nanostructures and their cytotoxicity against renal carcinomas HEK-293 human embryonic kidney cell lines

Abstract

The present study reports sonochemical synthesis of Cu_2O nanostructures (LAA@Cu_2O-PEG nanopolyhedra) prepared by reduction of Cu(II) complex $K_3[CuCl_5]$ by L-ascorbic acid (LAA), stabilized by polyethylene glycol (PEG) and their cytotoxicity against HEK-293 Human embryonic kidney cell lines. The products have been characterizes by UV-visible spectroscopy, FTIR, XRD, SEM (EDX), FESEM, TEM, particles size distribution and BET surface area analyses exhibited formation of well crystalline, mesoporous LAA@Cu_2O-PEG polyhedral nanostructures, capped with PEG molecules. The biological analysis revealed the role of capturing protein in capping and stabilization of Cu_2O nanopolyhedra. The synthesized LAA@Cu_2O-PEG nanopolyhedra were found to have a stable zeta potential in a range of -18±0.29mV. The IC_{50} of the prepared LAA@Cu_2O-PEG nanopolyhedra against renal carcinomas HEK-293 human embryonic kidney cell lines are in the range of 15-60μM, inducing morphological changes in proteins.

Keywords: LAA@Cu_2O-PEG nanopolyhedra, L-Ascorbic acid, renal carcinomas, polyethylene glycol, cytotoxicity.

5.1 Introduction

Since recent decades, nanoparticles are witnessing their tremendous growth due to unusual physical and chemical properties which have been demonstrated intermediate states of matter.[1,2] The catalytic activity of the formed nanostructures depends on the shape, size and stabilizing agents which are dependent on preparation techniques.[3] There are a number of diverse approaches for the preparation of nanostructures as elucidated from a literature review.[4-7] Controlled chemical reduction,[4] electrochemical reduction[4] and metal vaporization[5] are included briefly to describe the methods of formation of nanostructures.[6] But most recently the sonochemical method has been emerged as the best method for the formation of novel nanostructures due to their unique properties.[7] The chemical effects of ultrasound which arise from acoustic cavitation, which involve formation, growth and an implosive growth of bubbles in liquids have produced unusual chemical environment. The major condition attained during bubble collapse has been exploited to prepare nanoscale metal,[8] metal oxide[9] and nanocomposite.[10] The ability to synthesize nanomaterials of different morphology with their shape and size is exploring their applications in the catalytic system, sensing technology, microelectronical gadgets and other important fields of nanotechnology.[11,12] The nanoscale precursors of copper and its alloys have been used in catalysis e.g. gas shift catalysis and gas detoxification catalysis.[13]

The preparation of copper oxide nanoparticles with controllable size, shape and morphological pattern is vital to be an effective catalyst. Such abilities have fastened the use copper oxide nanostructures as the precursor of reaction that is predominantly dominated to gold, silver and platinum nanoparticles. There is a number of methods to prepare nanoparticles regarding shape control specificity to

control their shape and size effectively.[14] Literature review revealed that limited attempts have been used to prepare copper oxide nanostructures with controllable shape, size and other morphological and surface properties[15-16]. Previous reports on the synthesis of copper oxide NPs have witnessed the organic encapsulation in organic phase,[13] encapsulation of thiol as capping agent[14] and thermal decomposition.[17] Copper based nanostructures prepared by the above required method has either limited to their size monodispersity or their susceptibility to getting oxidized.[18-19] The major limitation of nanoscale copper oxide particles is lack of sufficient stability because of large energy associated with their high surface area of their dispersions and therefore they have strong tendency to aggregate and form larger clusters.[20-22] The cluster formation leads to rapid sedimentation which diminishes reactivity and activity of copper oxide, associated with nanometric size.[22] To overcome this problem surfactants like SDBS, CTAB, AOT etc. have been used as stabilizers and to generate nanoparticles with uniform size.[23-24] Polymeric stabilizers like PEG is supposed to be better stabilizers for copper oxide NPs because of its suitability in biological systems.

Several studies have reported antibacterial activity of copper oxide NPs against Gram-positive bacteria, such as *B. subtilis, S. aureus* and Gram-negative bacteria such as, *P. aeruginosa* and *E. coli.*[25-29] Metallic copper as well as copper oxide nanoparticles have exhibited multitoxicity to a broad-spectrum of bacterial species, including some multi-drug resistant bacteria such as the "superbug" MRSA (methicillin-resistant *S. aureus*).[30] The growing attention on copper oxide nanoparticles is prompted by their cheaper price and abundance compared to the noble and expensive metals like gold, silver and their competent potential application as microbial agents.[27] Besides other mechanisms, mechanism of action of copper oxide NPs against microbes includes generation of oxidative stress and tendency of

copper nanoparticles to alternate between cupric, Cu(II) and cuprous, Cu(I) oxidation states, make it unique from other metal nanoparticles.[27] Especially, Cu_2O nanoparticles are widely abundant and have been reported to show lower toxicity, good environmental acceptability and remarkable broad-spectrum antibacterial and anti-superbug activity against a range of bacteria through generation of reactive oxygen species (ROS) and release of copper ions.[20-21, 31-32] Zhou et al.[21] reported remarkable antibacterial activity of Cu_2O NPs on the superbugs "*methicillin-resistant staphylococcus aureus* (MRSA)" and "*vancomycin-resistantent erococcus* (VRE)" after being loaded on ZrP nanosheet matrix. Cuprous (Cu(I)) ions from Cu_2O, have been shown to be considerably more toxic than cupric (Cu(II)) ions, due to their higher thiophilicity and cytoplasmic membrane permeability.[33]

Based on the above reports LAA@Cu_2O-PEG nanostructures have been synthesized by using amphiphilic nonionic surfactant, PEG as a surface stabilizer and L-Ascorbic acid as reducing agent in a mesoporous range. The formed LAA@Cu_2O-PEG nanopolyhedra show their surface enhancing, the property to their controllable pore size and unique polyhedral nature. The fabricated LAA@Cu_2O-PEG nanopolyhedra have been examined for cytotoxicity against HEK-293 Human embryonic kidney cell lines.

5.2. Experimental section

5.2.1. Chemicals

Copper chloride ($CuCl_2$), potassium chloride (KCl), polyethylene glycol (PEG), and L-Ascorbic acid (98%) were purchased from Sigma Aldrich chemical supplier and were used without further purification.

5.2.2. Synthesis

Aqueous solutions of $CuCl_2$ and KCl in a 1:2 molar ratio were mixed on magnetic stirring for 6-8 hours at room temperature, which led to the formation of copper coordinate complex $K_3[CuCl_5]$. For the formation of LAA@Cu_2O-PEG nanopolyhedra, 50 mL of 20 mM $K_3[CuCl_5]$, 5 mL of 1 mg/mL of PEG and 0.1 M L-Ascorbic acid were taken in a beaker and kept for 3 hours for ultrasonication. After the reaction gets completed, the precipitate was removed via centrifugation (8000 rpm for 20 min) and washed several times with deionized water and ethyl alcohol to remove excess surfactant and reducing agent. After washing with the alcohol and water the material kept it in the oven for some time to get dried.

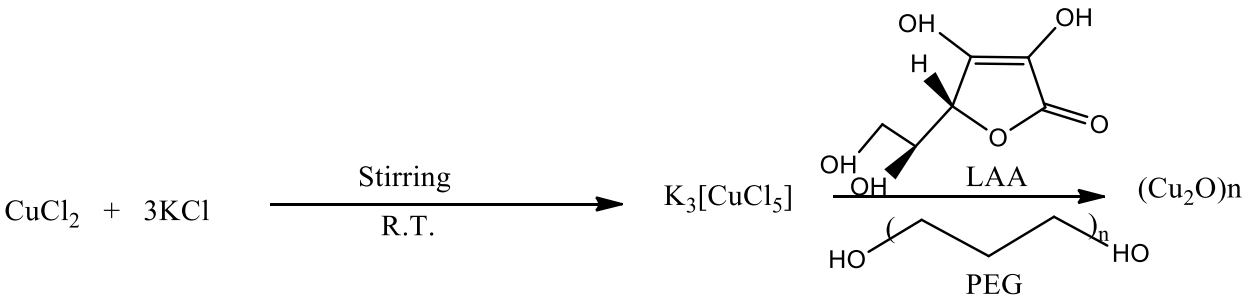

5.2.3. Instrumentation and Measurement

Detailed LAA@Cu_2O-PEG nanopolyhedra were examined through UV-visible spectrophotometry by Shimadzu UV-3600 spectrophotometer. The X-ray diffraction patterns of the obtained products were recorded on Pananalytical's X'Pert Pro X-ray diffractometer in the 2θ range 10 to 80° with a step size of 0.025°. Scanning electron microscope (SEM) images of the materials were observed on JEOL 6490 LB equipment at operating electrical energy of 3 kV. Particles shapes and sizes of the materials were further examined on JEOL-2100) transmission electron microscope (TEM). The zeta potential of Cu_2O NPs (formed at room temperature)

was measured using a Zetasizer ZS90 (Nano series Malvern Instrument) at room temperature. Dispersion of nanoparticles was sonicated for 20 minutes and diluted to make a solution with concentration 80 µg/mL in phosphate buffer saline (pH = 7.4). The particle size and size distribution were carried out on a Zetasizer ZS90 (Nano series Malvern Instrument). SERS spectrum of Cu_2O NPs, formed at room temperature, was recorded on NSCOM/Raman/Confocal/AFM used for UV/lithography (200 nm) and near field imaging of features as small as 100 nm Raman spectra and imaging for an excitation wavelength of 532 nm with an extinction coefficient of 8000 $M^{-1}cm^{-1}$. FTIR spectra of the products have been recorded on Perkin Elmer Spectrum two instrument. UV-visible data were collected on a Shimadzu UV-3600 spectrophotometer. Brunauer-Emmett-Teller (BET) analysis of the materials was recorded on Belsorp-mini II instrument.

5.3. Results and Discussion

When reducing agent L-Ascorbic acid and capping agent/stabilizer PEG were added to Cu(II) complex $K_3[CuCl_5]$ and reaction performed for 3 hours with ultrasonication, the temperature of reaction mixture slightly raised up-to 37 °C, simultaneously color of the resulting product darkened. The separated and purified product was dispersed in de-ionized water and UV-visible absorption measurement has been carried out in the range of 200-700 nm. The graph (Fig 5.1a) shows a peak at 369 nm which is a characteristic of Cu_2O nanostructures.[34] Appearance of broad continuous absorption spectrum, gradually rise in intensity from visible to ultraviolet region, suggesting complete reduction of Cu^{+2} to Cu^{+1}, which is similar to earlier reports.[15,17] The optical band gap energy of formed LAA@Cu_2O-PEG nanopolyhedra was elucidated by using Tauc's equation :

$$\alpha\hbar\upsilon = A(\hbar\upsilon - E_g)^n$$

Where α is the absorption coefficient, A is energy independent constant, ħυ is photon energy, E_g is the optical energy gap and exponent n depends on the nature of the electronic transition. The coefficient, α can be calculated using Beer-Lambert's relation:

$$\alpha = 2.303 \times \frac{A}{L}$$

Where, L is path-length and A is the absorbance. The energy-gap (E_g) value has been elucidated from the plot of $(\alpha\hbar\upsilon)^2$ and ħυ as depicted from Figure. The band gap was estimated by extrapolating of the $(\alpha\hbar\upsilon)^2 = 0$ to gives straight line. As clearly seen from Fig.1.b, the optical-band energy gap was 2.0 eV with $(\alpha\hbar\upsilon)^2$ versus ħυ for an indirect allowed transition for LAA@Cu_2O-PEG nanopolyhedra (Fig.5.1.b).

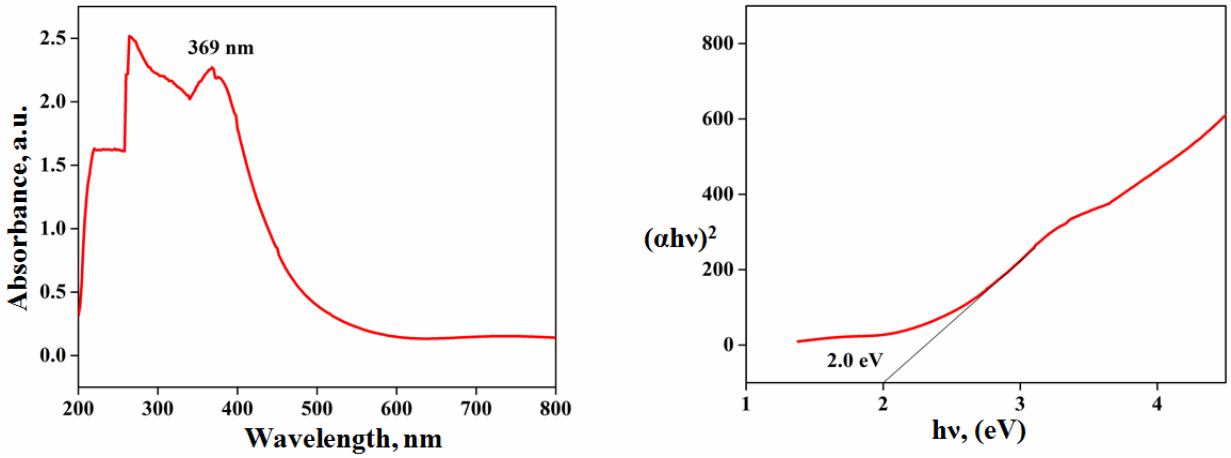

Fig. 5.1. UV-visible spectrum (a) and band gap analysis (b) of LAA@Cu_2O-PEG nanopolyhedra

In order to observe adsorption of PEG and/or L-Ascorbic acid over cuprous oxide nanopolyhedra, FTIR spectral analysis has been performed. In the FTIR spectrum (Fig.5.2) the peak at range of 3427 cm^{-1} is correspond to -OH stretching.

The peaks at 1404 and 1377 cm^{-1} are due to $–CH_2$ scissoring and wagging, while the peak at 2930 cm^{-1} and 2888 cm^{-1} are due to $–CH_2$ stretching of PEG.[35] The characteristic absorption peak at 1722 cm^{-1} is correspond to stretching vibration of C=O of five member ring and at 1092 cm^{-1} is due to C-O stretching in the of L-Ascorbic acid. The band at 1673 cm^{-1} correspond to the C=C stretching frequency of L-Ascorbic acid.[36] The peak at 926 cm^{-1} is due to out of plane bending vibration C-H of PEG. Moreover, small intensity peaks in the far IR region at 634 cm^{-1} is corresponds to Cu-O vibration mode in LAA@Cu_2O-PEG nanopolyhedra.[37]

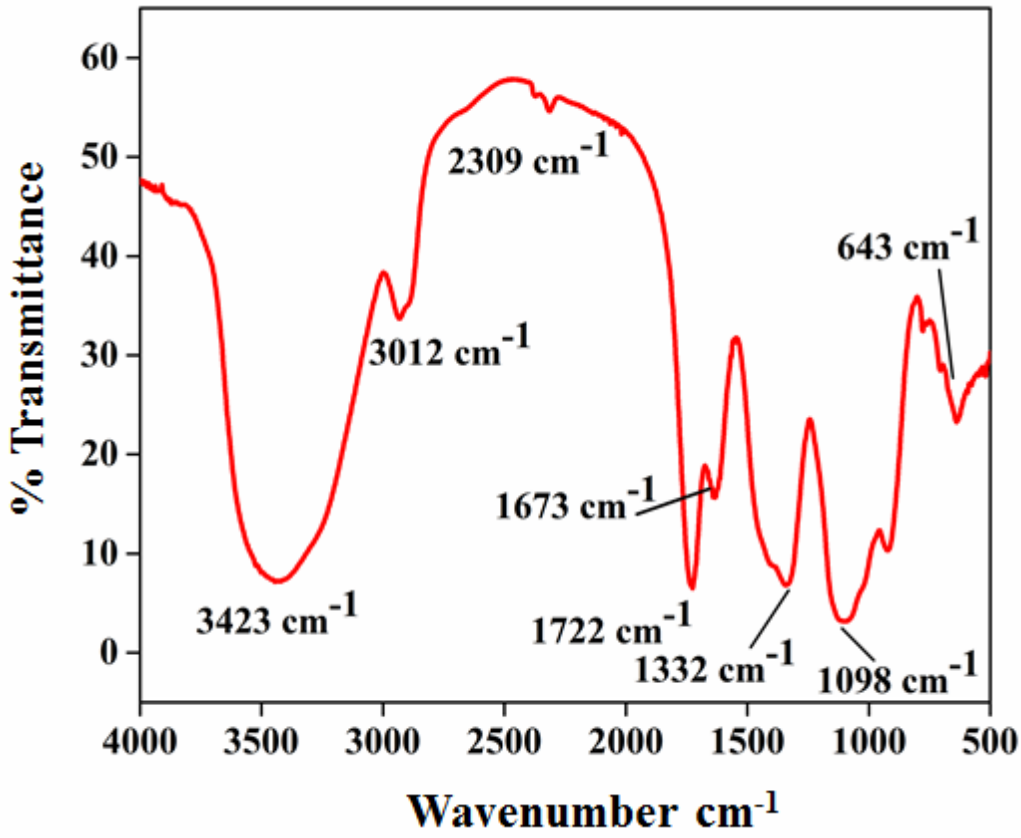

Fig. 5.2. FTIR spectrum of synthesized LAA@Cu_2O-PEG nanopolyhedra.

Vibrational analysis of LAA@Cu_2O-PEG has further been examined using Raman spectral measurement, excited at a wavelength of 532 nm with an extinction coefficient of 8000 M^{-1} cm^{-1}. The SERS spectrum of the LAA@Cu_2O-PEG (Fig. 5.3)

nanopolyhedra was obtained by plotting the intensity, (arbitrary value) versus Raman shift graph. The ascorbic acid/PEG molecular orientation on particle surface has been determined in wave numbers ranges from 400 to 3500 cm^{-1}. The band at 1569 cm^{-1} is correspond to vibrational band characteristic to C=C stretching of lactone ring of L-Ascorbic acid. Peak at 965 cm^{-1} is due to –CH bending vibration of polyethylene glycol (PEG).[38] The Surface Enhanced Raman spectroscopy (SERS) of 438 cm^{-1} is dominated by -CH stretching out of plane bending of alkanes of polyols[39] and 1967 cm^{-1} are due to C=C stretching[40] and 2449 cm^{-1}, 3173 cm^{-1} is due to –CH stretching of carboxylic group of L-Ascorbic acid.[41] Besides, the Raman scattering spectrum of Cu_2O NPs is dominated by ring deformation, ring twisting deformation and ring breathing and wagging.

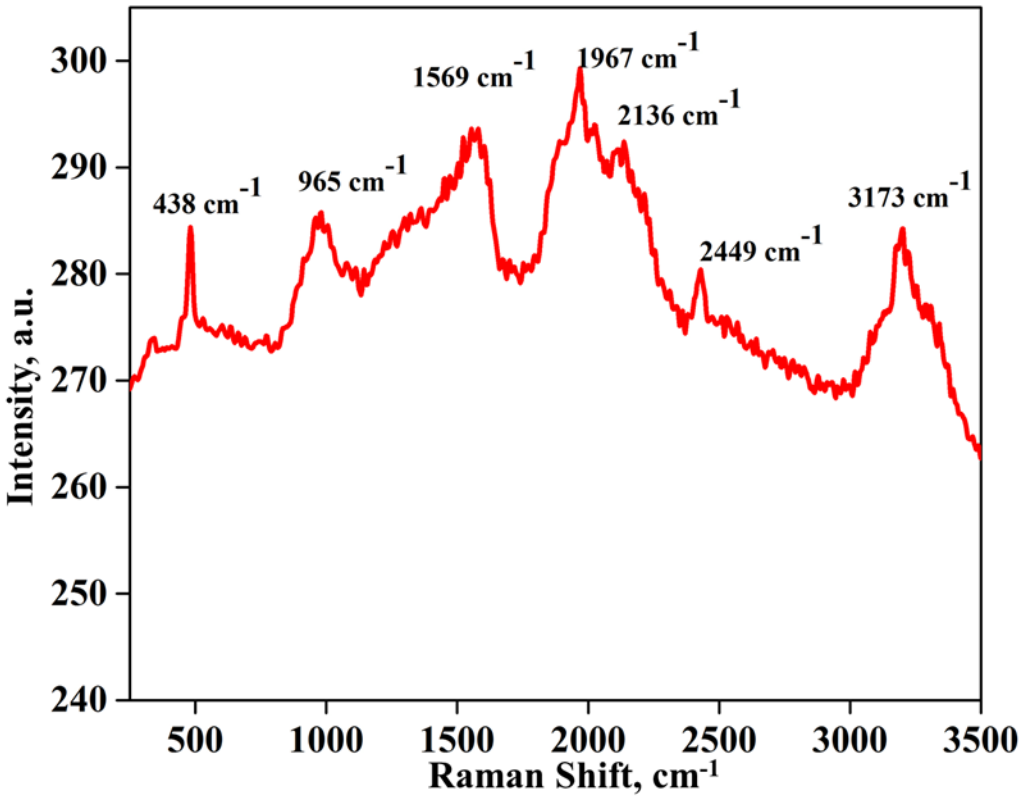

Fig.5.3. SERS/Raman analysis of LAA@Cu_2O-PEG nanopolyhedra.

From dynamic light scattering particle size of LAA@Cu_2O-PEG NPs has been determined (Fig. 5.4 a), which shows that particles size lie in the range of 15-45 nm and maximum population at 27 nm while smaller quantity present in the small aggregates in solution. The Zeta potential of synthesized LAA@Cu_2O-PEG nanopolyhedra shows a characteristic value in a negative range of -18±0.29 mV (Fig. 5.4 b), which maintains stability of NPs surface. The negative charge on particles surface is probably due to presence of anionic form L-Ascorbic acid at the NPs surface.

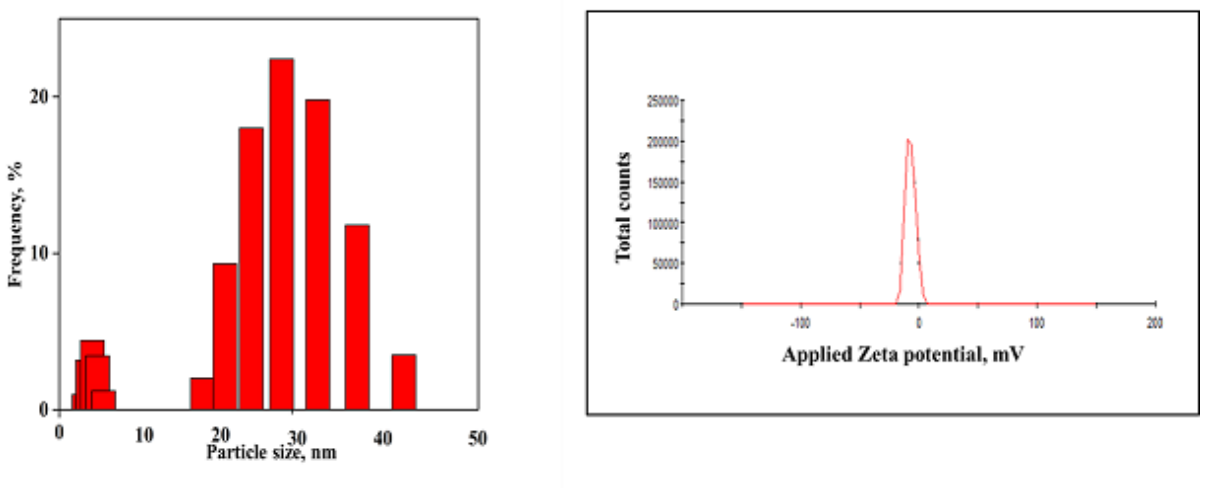

Fig. 5.4 a-b. DLS spectra of LAA@Cu_2O-PEG nanopolyhedra

The degree of crystallinity, size and structure of synthesized LAA@Cu_2O-PEG nanopolyhedra has been achieved by XRD analysis. The diffraction pattern indicates that particles have cubic arrangement of constituents (Fig. 5.5). In the XRD pattern very sharp peaks centered at 43.31,36.5, 61.9, 73.9 and 77.3° are corresponding to the reflection of (111), (200), (220), (311) and (222) planes of crystalline LAA@Cu_2O-PEG nanopolyhedra, which were assigned to their cubic crystal pattern (JCPDS file No.01-071-3631).[42-43] The peaks at 43.31 and 73° reflect

the indices of cuprous oxide nanostructure (JCPDS card no. 85-1325) with face centered cubic, (fcc) structure.[44] The broadening of the peaks represents that the synthesized LAA@Cu_2O-PEG nanopolyhedra are in the nanorange. The mean diameter of LAA@Cu_2O-PEG nanopolyhedra were estimated to be 32 nm with the full width half maximum, (FWHM) value of prominent (111) peak. The broad diffraction peaks at 39.9 clearly represent their disordered mesoporous nature calculated by using the Scherrer's formula (Fig.5.5)**.**

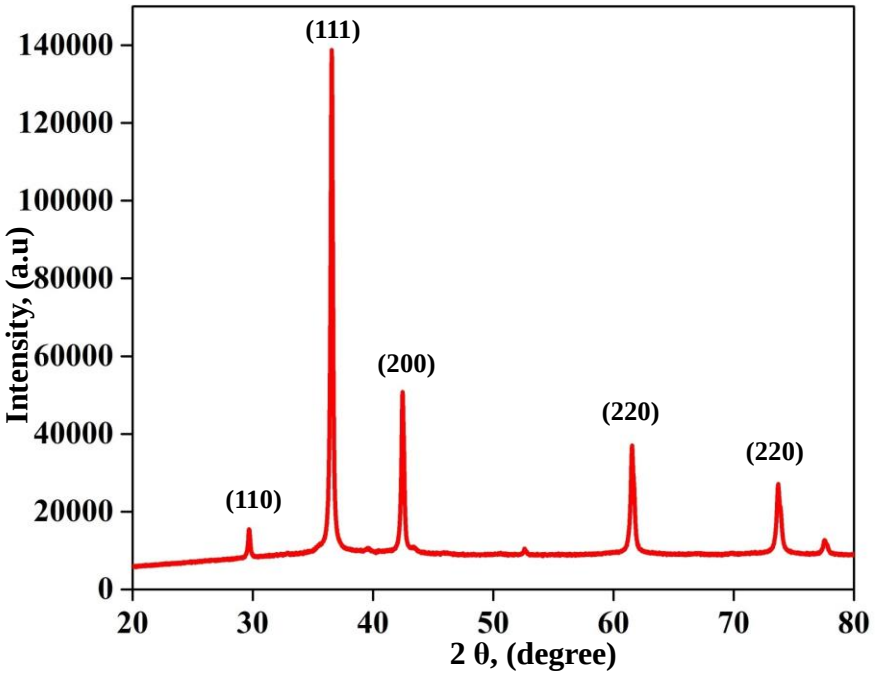

Fig.5.5. XRD analysis of LAA@Cu_2O-PEG nanopolyhedra

The porosity of LAA@Cu_2O-PEG nanopolyhedra were further estimated via N_2 adsorption-desorption isotherm. From the Barrett-Joyner-Halenda (BJH) method an average mesopore diameter of LAA@Cu_2O-PEG nanopolyhedra has been found to be 18 nm. These results were consistent with TEM observation and were indicative of mesoporous structure. The specific surface area obtained by Brunauer-Emmett-Taylor method (BET) were approximately 28 m^2/g (Fig. 5.6 a-b) observed with a mesoporous

structure having pores in diameters 2-50 nm as per IUPAC nomenclature.[45] Recent literature witnessed that the other related nanostructure materials had a smaller area in a range of 18 to 30 m^2/g.[46] In comparison of previous reports, LAA@Cu_2O-PEG nanopolyhedra had a large surface area, which contain more catalytic sites.

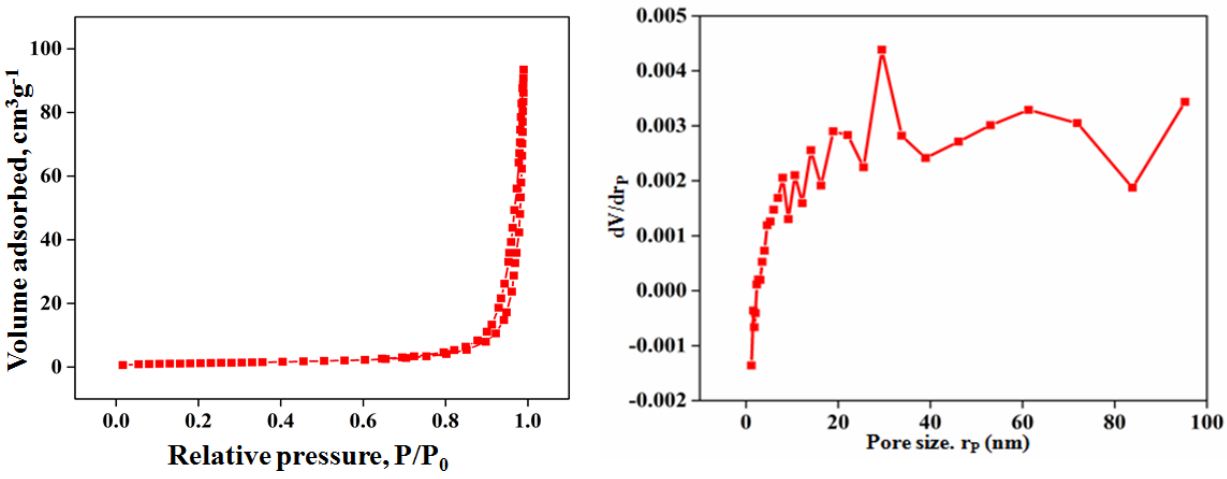

Fig.5.6. BET surface analysis (a) and BJH pore size analysis (b) of LAA@Cu_2O-PEG nanopolyhedra

The morphology, size and elemental composition of as-synthesized LAA@Cu_2O-PEG NPs were examined by SEM, FE-SEM, TEM and Energy-dispersive X-ray spectroscopy (EDX) analyses. In the SEM image (Fig. 5.7 a), the morphology and structure of particles are not clear, however in the EDS spectrum of LAA@Cu_2O-PEG confirms the presence of copper and oxygen, (Fig.5.7 b). In the FE-SEM images (Fig. 5.8 a-d) of LAA@Cu_2O-PEG uniform sized polyhedral structures are observed which assisted by sonochemical approach.[47] FE-SEM images further revealed that most of the NPs have similar shapes and sizes, indicating uniformity throughout the sample. The polyhedral shape LAA@Cu_2O-PEG have been supposed to show effective cytotoxicity against cell lines because of effective interaction in the biological cell membranes as reported erlier.[48] The TEM images

(Fig. 5.9 a-b) revealed the polyhedral LAA@Cu_2O-PEG overall dimension in the range of 20-60 nm with face diameter in the range of 10-20 nm. Previous reports also in accordance of these results in the mesoporous range and polyhedron appearance and shape.[49]

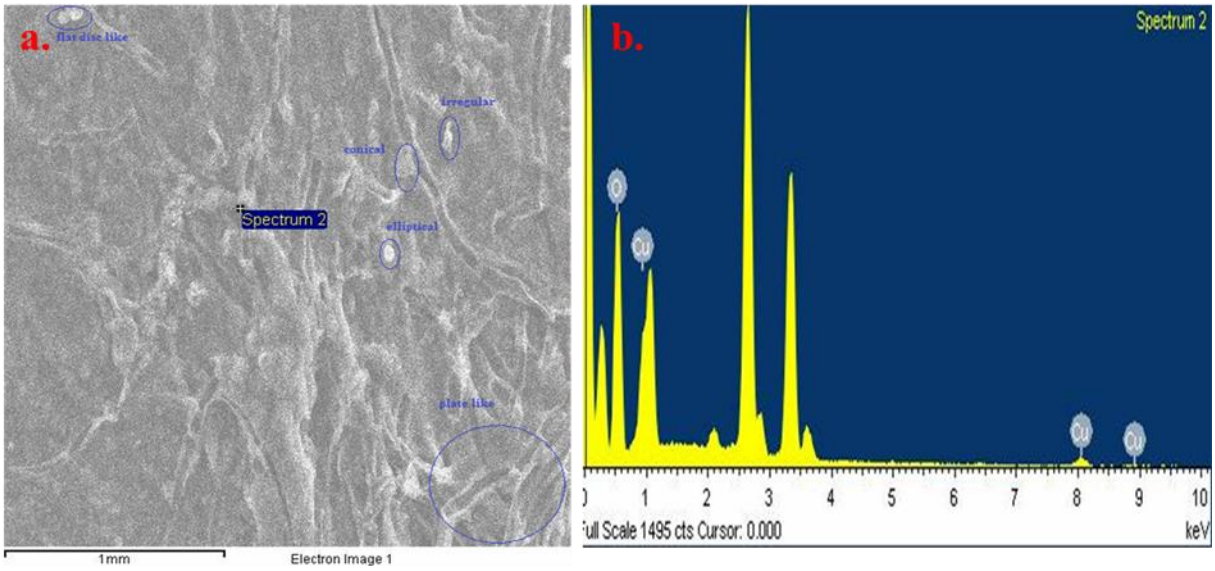

Fig.5.7. SEM image (a) and EDX spectrum (b) of LAA@Cu_2O-PEG NPs

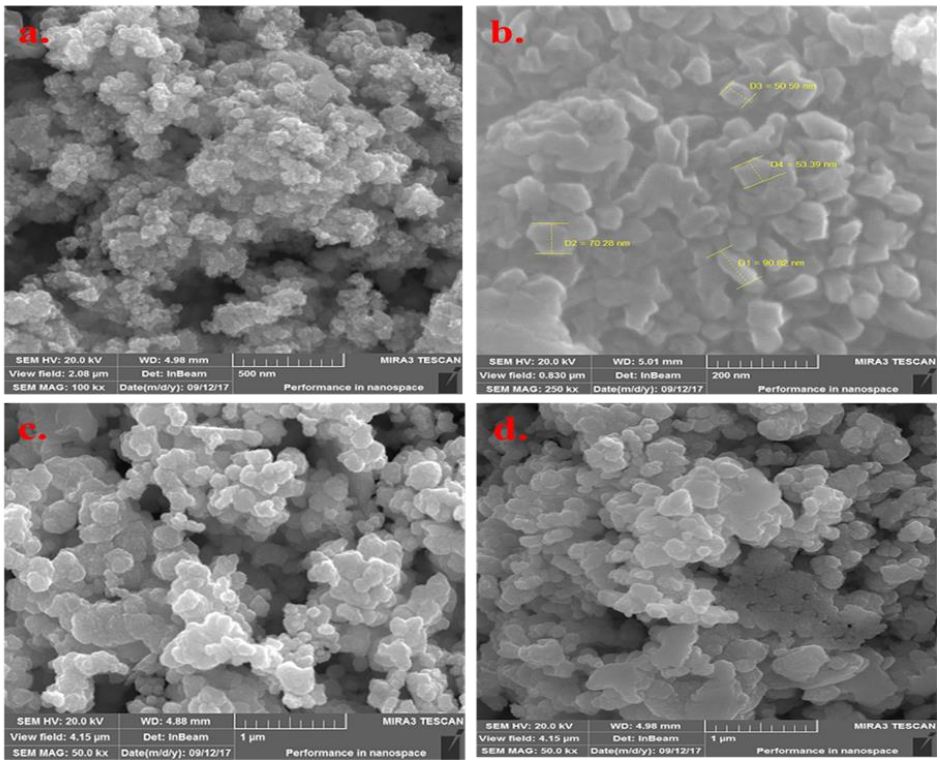

Fig.5.8 (a-d). FE-SEM images of LAA@Cu_2O-PEG nanopolyhedra.

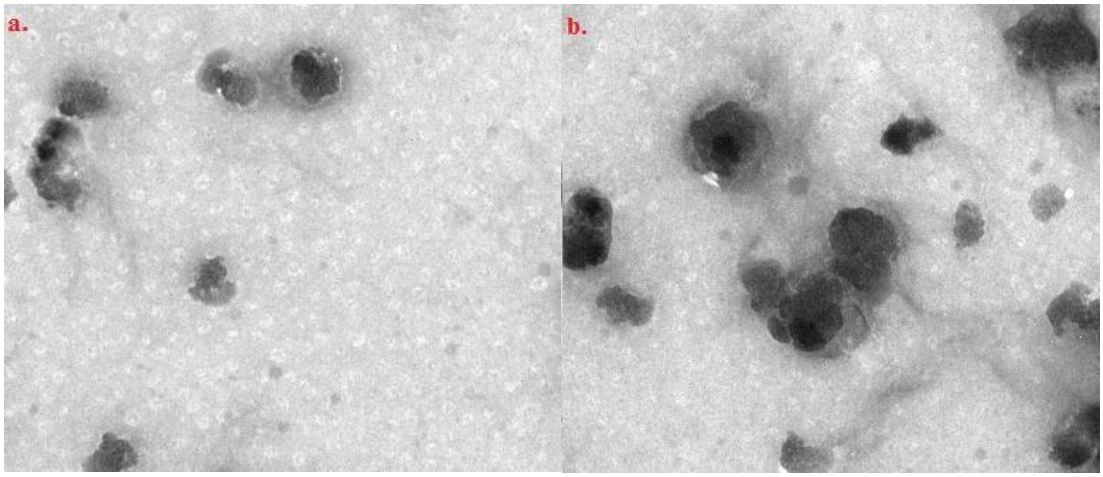

Fig. 5.9 (a-b). TEM images of LAA@Cu_2O-PEG nanopolyhedra.

5.3.1. Cytotoxicity test

Cell viability of LAA@Cu_2O-PEG nanopolyhedra with renal carcinomas HEK-293 human embryonic kidney cell lines has been determined by MTT assay in which cell was seeded in 96 well plates and incubated at a concentration of 15 to 90 µM taking one blank as reference at 37 °C temperature.[50] Control groups corresponding to untreated cells with ethanol and acetic acid applied in the formulation. The pH of the sample was adjusted to 7.4 with NaOH whenever necessary. Treatment lasted for 24 to 48 hours with 15 µL concentration, MTT addition and incubated for 3 hours at 37 °C temperature. The culture medium then aspirated and dimethylsulphoxide of 200 µL was added to the sample. The absorbance of the solution was monitored by spectrophotometer with a micro plate reader at a wavelength of 595 nm.

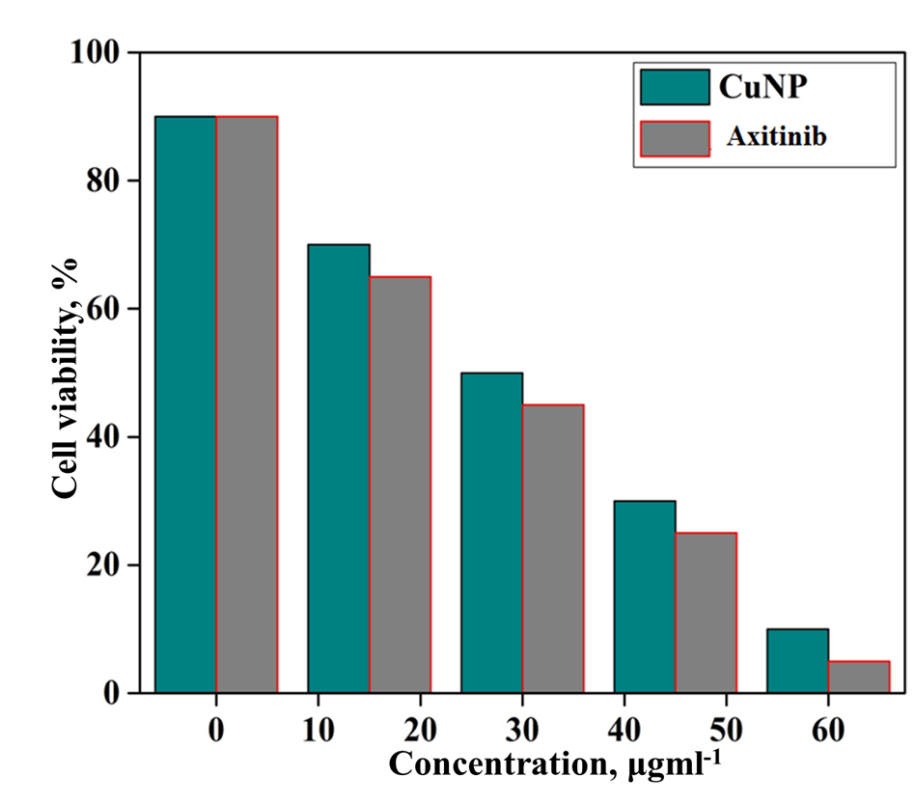

Fig.5.10.a. Cell viability analysis of LAA@Cu_2O-PEG nanopolyhedra.

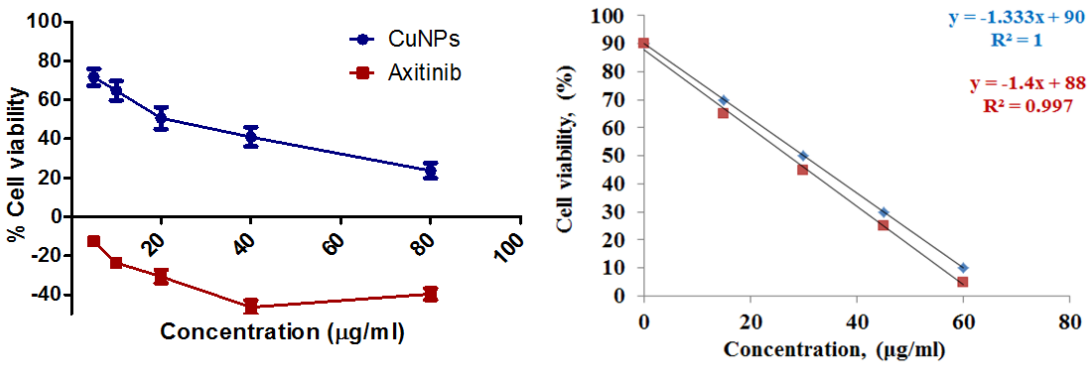

Fig.10 b. Cell viability analysis of LAA@Cu_2O-PEG nanopolyhedra

The effect of LAA@Cu_2O-PEG nanopolyhedra with renal carcinomas HEK-293 human embryonic kidney cell lines has been monitored on 24-48 hrs period at 15 to 90 µM concentration range (Fig. 5.10 a). The HEK-293 cell lines used against renal carcinomas cell lines is spontaneously arising renal tumor cell having metastatic property extensively characterized. In addition, the application was also used for

therapeutic procedures and the effect of the drug's efficacy and toxicity study of the cells.[50] The results were also consistent with NIH 3T3 cell lines for easily transfection of host and easily effective against leukemia virus propagation and transfect ion of DNA.[51] The IC_{50} value analysis at an inhibitory 50 µM concentration was found to be 30.54 (Fig. 5.10 b). The use of in vitro cytotoxicity test is the first step in the evaluation of biocompatibility of substance (Fig. 5.10 a-b).

Table 3: The cell viability after incubation with LAA@Cu_2O-PEG nanopolyhedra in comparison with other reports

Particles	Cell lines	Incubation period	Concentration	Cell viability	Ref.
Mesoporous Copper nanoparticles	HEK-293	24hrs	15-60µM	95-99	This work
Mesoporous Copper nanoparticles	HEK-293	48hrs	15-60µM	85-95	This work
Mesoporous Copper nanoparticles	HEK-293	24hrs	15-60nM	0-99	This work
Mesoporous Copper nanoparticles	HEK-293	48hrs	15-60nM	97-99	This work
Dendritic Copper nanoparticles	BT-20	24hrs	0-100µg/mL	80-98	52
Dendritic Copper nanoparticles	MCF-7	24hrs	1-8mg/mL	46-87	52
Mesoporous Copper nanoparticles	HepG-2	24hrs	1-8mg/mL	8-96	52
Apoferritin encapsulated Copper nanoparticles	HepG-2	48hrs	0-140µg/mL	80-100	52
Polyvinypyrollidone stabilized Copper nanoparticles	HepG-2	48hrs	0-140µg/mL	30-100	52
Ac-G9 dendrimer	MCF-7	24hrs	1-30nM	87-97	53

encapsulated Copper nanoparticles					
Ac-G9 dendrimer encapsulated Copper nanoparticles	HeLa	24hrs	1-30nM	85-98	54
Dendritic Copper nanoparticles	NHEKs	24hrs	0-25µg/mL	88-100	54
Dendritic Copper nanoparticles	NHEKs	24hrs	0-25µg/mL	83-100	54
Dendritic Copper nanoparticles	NHEKs	24hrs	0-25µg/mL	82-100	54
Dendritic Copper nanoparticles	A-549	24hrs	15-90 µM	80-88	55

Conclusion

In summary, LAA@Cu_2O-PEG nanopolyhedra has been synthesized via sonochemical assisted method using aqueous solution mixture of complex $K_3[FeCl_6]$, PEG and L-ascorbic acid at a temperature 37 °C. LAA@Cu_2O-PEG has been evolved polyhedral. The anti-cancer study of LAA@Cu_2O-PEG against renal carcinoma HEK-293 human embryonic kidney cell lines study suggests that high surface area with a large number of active sites nanopolyhedra are well suited anti-cancer agent and serve as promising candidate for treatment of renal carcinoma HEK-293 human embryonic kidney cell lines. The synthesized NPs show a synergistic effect with Axitinib as an anti-cancer drug effective against renal carcinoma cell lines. Cytotoxicity and IC_{50} analysis led to detailed changes in the enzyme structure. The nanoparticles sample may be a good antioxidant agent during the cancerous condition of a cell. The results from the experimental and theoretic study served as a valuable anti-cancer tool against renal carcinoma drug therapy in future.

References

1. Rao, C. R.; Kulkarni, G. U.; Thomas, P. J.; Edwards, P. P., Metal nanoparticles and their assemblies. *Chemical Society Reviews* **2000,***29* (1), 27-35.
2. Reetz, M. T.; Quaiser, S. A.; Breinbauer, R.; Tesche, B., A new strategy in heterogeneous catalysis: the design of cortex catalysts. *Angewandte Chemie International Edition in English* **1996,***34* (23-24), 2728-2730.
3. Aiken III, J. D.; Finke, R. G., A review of modern transition-metal nanoclusters: their synthesis, characterization, and applications in catalysis. *Journal of Molecular Catalysis A: Chemical* **1999,***145* (1-2), 1-44.
4. Khanna, P.; Gaikwad, S.; Adhyapak, P.; Singh, N.; Marimuthu, R., Synthesis and characterization of copper nanoparticles. *Materials Letters* **2007,***61* (25), 4711-4714.
5. Ghosh, S. K.; Kundu, S.; Mandal, M.; Pal, T., Silver and gold nanocluster catalyzed reduction of methylene blue by arsine in a micellar medium. *Langmuir* **2002,***18* (23), 8756-8760.
6. Suslick, K. S., *Ultrasound: its chemical, physical, and biological effects*. 1988.
7. Koltypin, Y.; Katabi, G., prozorov, R.; Gedanken, A. *J. Non-Cryst. Solids* **1996,***201*, 159.
8. Salkar, R.; Jeevanandam, P.; Kataby, G.; Aruna, S.; Koltypin, Y.; Palchik, O.; Gedanken, A., Elongated copper nanoparticles coated with a zwitterionic surfactant. *The Journal of Physical Chemistry B* **2000,***104* (5), 893-897.
9. Dhas, N. A.; Gedanken, A., Sonochemical synthesis of molybdenum oxide− and molybdenum carbide− silica nanocomposites. *Chemistry of Materials* **1997,***9* (12), 3144-3154.

10. Hoover, N. N.; Auten, B. J.; Chandler, B. D., Tuning supported catalyst reactivity with dendrimer-templated Pt− Cu nanoparticles. *The Journal of Physical Chemistry B* **2006,***110* (17), 8606-8612.
11. Niu, Y.; Crooks, R. M., Preparation of dendrimer-encapsulated metal nanoparticles using organic solvents. *Chemistry of Materials* **2003,***15* (18), 3463-3467.
12. Ressler, T.; Kniep, B. L.; Kasatkin, I.; Schlögl, R., The microstructure of copper zinc oxide catalysts: bridging the materials gap. *Angewandte Chemie International Edition* **2005,***44* (30), 4704-4707.
13. Mott, D.; Galkowski, J.; Wang, L.; Luo, J.; Zhong, C.-J., Synthesis of size-controlled and shaped copper nanoparticles. *Langmuir* **2007,***23* (10), 5740-5745.
14. Chen, S.; Sommers, J. M., Alkanethiolate-protected copper nanoparticles: spectroscopy, electrochemistry, and solid-state morphological evolution. *The Journal of Physical Chemistry B* **2001,***105* (37), 8816-8820.
15. Kim, Y. H.; Kang, Y. S.; Lee, W. J.; Jo, B. G.; Jeong, J. H., Synthesis of Cu nanoparticles prepared by using thermal decomposition of Cu-oleate complex. *Molecular Crystals and Liquid Crystals* **2006,***445* (1), 231/[521]-238/[528].
16. Sun, S.; Murray, C., Weller. D.; Folks, L.; Moser, A. *Science* **2000,***287*, 1989.
17. Salzemann, C.; Lisiecki, I.; Urban, J.; Pileni, M.-P., Anisotropic copper nanocrystals synthesized in a supersaturated medium: Nanocrystal growth. *Langmuir* **2004,***20* (26), 11772-11777.
18. Wei, Y.; Chen, S.; Kowalczyk, B.; Huda, S.; Gray, T. P.; Grzybowski, B. A., Synthesis of stable, low-dispersity copper nanoparticles and nanorods and their antifungal and catalytic properties. *The Journal of Physical Chemistry C* **2010,***114* (37), 15612-15616.

19. Peng, X.; Manna, L.; Yang, W.; Wickham, J.; Scher, E.; Kadavanich, A.; Alivisatos, A. P., Shape control of CdSe nanocrystals. *Nature* **2000,***404* (6773), 59.

20. Wozniak-Budych, M. J.; Przysiecka, Ł.; Maciejewska, B. M.; Wieczorek, D.; Staszak, K.; Jarek, M.; Jesionowski, T.; Jurga, S., Facile synthesis of sulfobetaine-stabilized Cu2O nanoparticles and their biomedical potential. *ACS Biomaterials Science & Engineering* **2017,***3* (12), 3183-3194.

21. Zhou, J.; Xiang, H.; Zabihi, F.; Yu, S.; Sun, B.; Zhu, M., Intriguing anti-superbug Cu 2 O@ ZrP hybrid nanosheet with enhanced antibacterial performance and weak cytotoxicity. *Nano Research* **2019,***12* (6), 1453-1460.

22. Hotze, E. M.; Phenrat, T.; Lowry, G. V., Nanoparticle aggregation: challenges to understanding transport and reactivity in the environment. *Journal of environmental quality* **2010,***39* (6), 1909-1924.

23. Usman, M. S.; El Zowalaty, M. E.; Shameli, K.; Zainuddin, N.; Salama, M.; Ibrahim, N. A., Synthesis, characterization, and antimicrobial properties of copper nanoparticles. *International journal of nanomedicine* **2013,***8*, 4467.

24. Morsy, S. M., Role of surfactants in nanotechnology and their applications. *Int. J. Curr. Microbiol. App. Sci* **2014,***3* (5), 237-260.

25. Chaudhary, R. G.; Sonkusare, V. N.; Bhusari, G. S.; Mondal, A.; Shaik, D. P.; Juneja, H. D., Microwave-mediated synthesis of spinel CuAl 2 O 4 nanocomposites for enhanced electrochemical and catalytic performance. *Research on Chemical Intermediates* **2018,***44* (3), 2039-2060.

26. Kaweeteerawat, C.; Chang, C. H.; Roy, K. R.; Liu, R.; Li, R.; Toso, D.; Fischer, H.; Ivask, A.; Ji, Z.; Zink, J. I., Cu nanoparticles have different impacts in Escherichia coli and Lactobacillus brevis than their microsized and ionic analogues. *ACS nano* **2015,***9* (7), 7215-7225.

27. Bogdanovic, U.; Vodnik, V.; Mitric, M.; Dimitrijevic, S.; Skapin, S. D.; Zunic, V.; Budimir, M.; Stoiljkovic, M., Nanomaterial with High Antimicrobial Efficacy Copper/Polyaniline Nanocomposite. *ACS applied materials & interfaces* **2015,***7* (3), 1955-1966.
28. Hsueh, Y.-H.; Tsai, P.-H.; Lin, K.-S., Ph-dependent antimicrobial properties of copper oxide nanoparticles in staphylococcus aureus. *International journal of molecular sciences* **2017,***18* (4), 793.
29. Nishino, F.; Jeem, M.; Zhang, L.; Okamoto, K.; Okabe, S.; Watanabe, S., Formation of CuO nano-flowered surfaces via submerged photo-synthesis of crystallites and their antimicrobial activity. *Scientific reports* **2017,***7* (1), 1-11.
30. Weaver, L.; Noyce, J.; Michels, H.; Keevil, C., Potential action of copper surfaces on meticillin-resistant Staphylococcus aureus. *Journal of applied microbiology* **2010,***109* (6), 2200-2205.
31. Xiong, L.; Yu, H.; Nie, C.; Xiao, Y.; Zeng, Q.; Wang, G.; Wang, B.; Lv, H.; Li, Q.; Chen, S., Size-controlled synthesis of Cu 2 O nanoparticles: size effect on antibacterial activity and application as a photocatalyst for highly efficient H 2 O 2 evolution. *RSC advances* **2017,***7* (82), 51822-51830.
32. Yang, Z.; Hao, X.; Chen, S.; Ma, Z.; Wang, W.; Wang, C.; Yue, L.; Sun, H.; Shao, Q.; Murugadoss, V., Long-term antibacterial stable reduced graphene oxide nanocomposites loaded with cuprous oxide nanoparticles. *Journal of colloid and interface science* **2019,***533*, 13-23.
33. Solioz, M., *Copper and bacteria: evolution, homeostasis and toxicity*. Springer: 2018.
34. Jana, N. R.; Gearheart, L.; Murphy, C. J., Wet chemical synthesis of high aspect ratio cylindrical gold nanorods. *The Journal of Physical Chemistry B* **2001,***105* (19), 4065-4067.

35. Zeng-guo, F.; Sanping, Z., Synthesis and characterization of biodegradable hydrogels based on photopolymerizable acrylate-terminated CL-PEG-CL macromers with supramolecular assemblies of α-cyclodextrins. *Polymer* **2003,***44* (18), 5177-5186.

36. Xiao, X.-Q.; Liu, J.-M.; Zeng, G., Joint remote state preparation of arbitrary two-and three-qubit states. *Journal of Physics B: Atomic, Molecular and Optical Physics* **2011,***44* (7), 075501.

37. Bezza, F. A.; Tichapondwa, S. M.; Chirwa, E. M., Fabrication of monodispersed copper oxide nanoparticles with potential application as antimicrobial agents. *Scientific reports* **2020,***10* (1), 1-18.

38. Edsall, J. T.; Sagall, E. L., Raman Spectra of l-Ascorbic Acid, Tetronic Acid and Related Compounds1. *Journal of the American Chemical Society* **1943,***65* (7), 1312-1316.

39. Panicker, C. Y.; Varghese, H. T.; Philip, D., FT-IR, FT-raman and SERS spectra of vitamin C. *Spectrochimica Acta Part A: Molecular and Biomolecular Spectroscopy* **2006,***65* (3-4), 802-804.

40. Yang, H.; Irudayaraj, J., Rapid determination of vitamin C by NIR, MIR and FT-Raman techniques. *Journal of Pharmacy and Pharmacology* **2002,***54* (9), 1247-1255.

41. Muniz-Miranda, M., SERS monitoring of the catalytic reduction of 4-nitrophenol on Ag-doped titania nanoparticles. *Applied Catalysis B: Environmental* **2014,***146*, 147-150.

42. Oliveira, L. M.; Nascimento, M. A.; Guimarães, Y. M.; Oliveira, A. F.; Silva, A. A.; Lopes, R. P., Removal of beta-lactams antibiotics through zero-valent copper nanoparticles. *Journal of the Brazilian Chemical Society* **2018,***29* (8), 1630-1637.

43. Ismail, M.; Gul, S.; Khan, M.; Khan, M. A.; Asiri, A. M.; Khan, S. B., Green synthesis of zerovalent copper nanoparticles for efficient reduction of toxic azo dyes congo red and methyl orange. *Green processing and synthesis* **2019,***8* (1), 135-143.

44. Salavati-Niasari, M.; Davar, F., Synthesis of copper and copper (I) oxide nanoparticles by thermal decomposition of a new precursor. *Materials letters* **2009,***63* (3-4), 441-443.

45. Rouquerol, J.; Avnir, D.; Fairbridge, C.; Everett, D.; Haynes, J.; Pernicone, N.; Ramsay, J.; Sing, K.; Unger, K., Recommendations for the characterization of porous solids (Technical Report). *Pure and Applied Chemistry* **1994,***66* (8), 1739-1758.

46. Wang, H.; Imura, M.; Malgras, V.; Li, C.; Wang, L.; Yamauchi, Y., A Solution Phase Synthesis of Dendritic Platinum Nanoelectrocatalysts with the Assistance of Polyoxyethylene Nonylphenyl Ether. *Journal of Inorganic and Organometallic Polymers and Materials* **2015,***25* (2), 245-250.

47. Liz-Marzán, L. M.; Giersig, M.; Mulvaney, P., Synthesis of nanosized gold− silica core− shell particles. *Langmuir* **1996,***12* (18), 4329-4335.

48. Abbas, G.; Kumar, N.; Kumar, D.; Pandey, G., Effect of Reaction Temperature on Shape Evolution of Palladium Nanoparticles and Their Cytotoxicity against A-549 Lung Cancer Cells. *ACS omega* **2019**.

49. Henam, S. D.; Ahmad, F.; Shah, M. A.; Parveen, S.; Wani, A. H., Microwave synthesis of nanoparticles and their antifungal activities. *Spectrochimica Acta Part A: Molecular and Biomolecular Spectroscopy* **2019,***213*, 337-341.

50. Jardim, K. V.; Joanitti, G. A.; Azevedo, R. B.; Parize, A. L., Physico-chemical characterization and cytotoxicity evaluation of curcumin loaded in chitosan/chondroitin sulfate nanoparticles. *Materials Science and Engineering: C* **2015,***56*, 294-304.

51. Landau, N.; Page, K.; Littman, D., Pseudotyping with human T-cell leukemia virus type I broadens the human immunodeficiency virus host range. *Journal of virology* **1991,***65* (1), 162-169.

52. Martinez, D. S. T.; Faria, A. F.; Berni, E.; Souza Filho, A. G.; Almeida, G.; Caloto-Oliveira, A.; Grossman, M. J.; Durrant, L. R.; Umbuzeiro, G. A.; Alves, O. L., Exploring the use of biosurfactants from Bacillus subtilis in bionanotechnology: A potential dispersing agent for carbon nanotube ecotoxicological studies. *Process Biochemistry* **2014,***49* (7), 1162-1168.

53. Kumar, B.; Smita, K.; Debut, A.; Cumbal, L., Andean Sacha Inchi (Plukenetia Volubilis L.) leaf-mediated synthesis of Cu2O nanoparticles: a low-cost approach. *Bioengineering* **2020,***7* (2), 54.

54. Kiran, G. S.; Selvin, J.; Manilal, A.; Sujith, S., Biosurfactants as green stabilizers for the biological synthesis of nanoparticles. *Critical reviews in biotechnology* **2011,***31* (4), 354-364.

55. Pang, Z.; Raudonis, R.; Glick, B. R.; Lin, T.-J.; Cheng, Z., Antibiotic resistance in Pseudomonas aeruginosa: mechanisms and alternative therapeutic strategies. *Biotechnology advances* **2019,***37* (1), 177-192.

Chapter 6

Synthesis of Nickel Nanoparticles and their Cytotoxicity against MCF-7 Breast Cancer Cell Lines

Synthesis of Nickel Nanoparticles and their Cytotoxicity against MCF-7 Breast Cancer Cell Lines

Abstract

Apart from potential applications in many fields, cytotoxicity and safety of nanoparticles has promising scientific interest. Metallic nanoparticles, such as nickel NPs have applications in sensing, catalytic and electronics etc. but their environmental and health effects are not been fully investigated. Controlled sizes and distribution nickel nanoparticles with enormous surface properties have been prepared by a novel method and cytotoxicity has been examined against cancer cell lines MCF-7 for the assessment of mortality and developmental changes. Nickel nanoparticles exposure was compared with respect to established antitumor drug. Cytotoxicity has significantly been increased when one or two layers of L-ascorbic acid and/or polyethylene glycol were deposited. Cytotoxicity and in silico studies suggested that the configuration of nanoparticles may affect cytotoxicity more and defects from Ni NPs exposure occur by biological MTT assay analysis.

Keywords: Ni NPs; Cytotoxicity; MCF-7; drug; in silico; antitumor.

6.1. Introduction

Since recent decades the emergence of biomedical applications like cell labelling,[1] drug targeting,[2] gene delivery,[3] hyperthermia therapy,[4] and biosensors,[5] nanoparticles attract increasing fundamental and technological interests. Major advances have been made in developing methods for their improved performance. In the recent years potential environmental and health impacts of Ni NPs have been highlighted.[6] The raising concern of toxicity is a typical factor for evaluating their applications especially via in vitro biological applications. It is well understood from previous literature that the reduction of particle size from macroscopic to nanometer length scale, the chemical and physical properties changed due to size and surface effects. In case of bulk materials the ratio of surface atoms to that of interior atoms in small and surface effect is insignificant. Although the particles size and surface defects control the material properties, however the surface coating may predominately affect the material properties. For example the manganese ferrite nanoparticles surface modified by benzoic acid and substituted benzoic ligands enhance biocompatibility because coated ligands led to decrease coercivity and increase saturation magnetisation up-to the size range of 10, 20 and 25 nm.[7] Changes in optical properties were reported in gold nanoparticles with different surface coatings for improved stability and water solubility.[8] Up-to what extent particle size and surface coating influence on toxicological behaviour is not clear though some reports on this issue are available.[9] Furthermore the complications in cytotoxicity studies arise when surface coating with same materials may depend on the type of synthesis and method chosen. One should therefore not assume that coated and uncoated nanoparticles would have same degree of biosafety. Often cytotoxicity

studies on nanoparticles did not include sufficient data on their surface properties. Commercialized product has also been used.

A lot of works are available in this area on noble metals, such as gold and silver due to their unique surface plasmonic properties, however less interest have been shown on economical metals like nickel etc. Recent investigation has been extended to the study of other metals like copper and nickel that could have antibacterial activity. Bimetallic Cu-Ni NPs show some features of alloys NPs that distinguish them from the pure ones.[10] Recently a number of studies have shown antibacterial activities of Ni NPs.[11] Nevertheless they have not been synthesized in aqueous solution without using surface stabilizers like polymers, ligands and salts etc. By dispersing a specific material in polymer matrix, high-performance lightweight composites can be used for individual applications. The polymer nanocomposites have been developed by multifunctional materials with low nanofiller content.[12] Nanophase materials such as fillers in the polymer matrix is generally the group of molecules with a size of 1-100 nm with specific properties different from their bulk counterparts.[13] Spherical and fibrous fillers have been added to polymer matrix to improve their effectiveness, including rheological, mechanical, thermal, flammability, calorimetric and other properties.[14] There are many composites that use different polymer matrices, filler system and treatment system to improve certain characteristics.[15] The versatile method has been prepared polymeric nanocomposites, such as *in situ* polymerisation solution being melt compounding, high shear mixing and electrospinning.[12]

Nickel nanoparticles (Ni NPs) have received enormous attention due to their unique property in thermal, magnetic, electrical and chemical applications. They possess an exceptional capacity in catalysis, supercapacitors, additives in oil,

magnetic media for biochemicals and many other applications.[12, 16] For economic, ecological and energy-saving reasons, recycled polyethylene terephthalate was used instead of virgin materials. Based on the previous reports the properties of recycled polyethylene terephthalate did not differ from those of virgin polyethylene terephthalate.[12, 17] A number of eminent philosophers, academicians and scientists are in approach to prepare a number of nickel nanoparticles (Ni NPs) for their best characterisation in a field to diagnose a number of various pathological activities like antitumor, antimalarial and antiphagocytic applications. H. Yin *et al.* proposed the effect of particle size and surface coating on the cytotoxicity of nickel ferrite.[18] Cristina Espace *et al.* have proposed the toxicity and developmental defects of different sizes and shaped nickel nanoparticle in Zebrafish.[19] G. Abbas *et al.* has prepared the shape evolution of Pd nanoparticle and their cytotoxicity against A-549 lung cancer cell lines.[20] Angel Ezhilarazi *et al.* reported the green synthesis of NiO nanoparticles using *Moringa oleifera* extract and their biomedical applications, the cytotoxicity effect of nanoparticles against HT-29 cancer cells.[21] Masanori Horie *et al.* have proposed ultrafine NiO particles induce cytotoxicity in vitro by cellular uptake and subsequent Ni(II) release. Elham S. Aazam *et al.* have proposed the synthesis of copper/nickel nanoparticles using newly synthesized Schiff-base metal complexes and their cytotoxicity and catalytic activities.[22] Mohan Prasath Mani *et al.* proposed the green synthesis of nickel oxide particles and its integration into polyurethane scaffold matrix ornamented with groundnut oil for bone tissue engineering.[23] Bahareh Moazzenchi *et al.* proposed the click electroless plating of nickel nanoparticles on polyester fabric, electrical conductivity, magnetic and EMI shielding properties.[24] Fatemeh Mohammadkhani *et al.* proposed the microwave absorption and photocatalytic properties of magnetic nickel nanoparticles/recycled

nickel nanofibres web.[12,23] Bushra Bashir *et al.* proposed the copper substituted nickel ferrite nanoparticles anchored on graphene sheet as an electrode materials for supercapacitors fabrication.[25] Jyoti Chaudhari *et al.* prepared the synthesis and biological function of nickel and copper nanoparticles.[26]

Inspiring from the above studies, polyethylene glycol (PEG) grafted L-Ascorbic acid coated Ni NPs have been prepared in mesoporous range by sonochemical method and biological adaptability has been estimated against breast carcinoma cell lines MCF-7.[27]

6.2 Experimental section

6.2.1 Chemicals

DMEM (Gibco Invitrogen), Trypsin 0.25 % (Gibco Invitrogen), FBS US Origin (Gibco Invitrogen), Trypan Blue (Gibco Invitrogen), DPBS (Gibco Invitrogen), FBS, Nickel(II) chloride ($NiCl_2$), potassium chloride (KCl), polyethylene glycol (PEG), L-Ascorbic acid (LAA) from Sigma Aldrich chemical were used in this analysis without further purification.

6.2.3 Synthesis of Ni NPs

For synthesis of Ni NPs, $K_2[NiCl_4]$ has been prepared in the first step, by mixing $NiCl_2$ and KCl in 1:2 ratio and magnetic stirring at room temperature. 50 mL aqueous solution of 0.1 M L-Ascorbic acid (LAA) was mixed with 50 mL of 20 mM $K_2[NiCl_4]$ and finally 10 mL of 1mg/mL of polyethylene glycol was mixed to above reaction mixture. The solution mixture was stirred on a magnetic stirrer for six hours for complete reaction and thereafter sonicated for 2 hours at 37 °C for proper homogenisation of the precipitate and for complete reduction of $K_2[NiCl_4]$ to Ni NPs.

The solution mixture was centrifuged at 8000 rpm for 15 minutes to separate the product. The product was washed several times with deionised water and ethyl alcohol to remove the excess amount of the surfactant and other impurities. The crystals were kept in microwave oven to remove the moisture and stored in eppendorf tube for studies.

6.2.4 Instrumentation and measurement

UV-visible analysis Ni NPs was carried out at Shimadzu UV-3600 spectrophotometer in the range 200-800 nm. The adsorption of PEG and L-Ascorbic acid on the NPs surface has been determined by FTIR spectral studies on Perkin Elmer Spectrum II instrument. SEM with EDS analyses has been recorded on model JEOL at operating voltage of 15kV. The particles sized analysis and zeta- potential has been achieved through Horiba Scientific Nanopartica, SZ100Z. Nitrogen adsorption-desorption and pore-size diameter have been estimated through Belsorp mini-II instrument. SERS analysis of the formed Ni NPs has been performed on NSOM/ Raman/Confocal/AFM used for UV/ lithography (200 nm) with near field imaging features as small as 100 nm. TEM images of the product have been estimated by JEOL-2100 apparatus. Degree of crystallinity of the formed NPs was analyzed on a Phillips X'pertdiffractometer using CuKα radiation at a wavelength of 1.54059 A°. CO_2 incubator (Eppendorf Galaxy 170), fluorescent microscope (Carl Zeiss), refrigerated centrifuge (Thermo scientific) hemocytometer were used for biological studies.

6.2.5 Molecular Docking

The molecular docking is one of the crucial techniques in molecular

modelling. It is a handy tool for the computational calculations for the molecular interaction of drugs and macromolecule. It is a suitable method for predicts the preferred orientation of one molecule to second when bound to each other to form a stable complex. Here the nickel cluster is docked with the different cancer cell proteins and calculated the binding energies. This binding energy predicts the mostly affected proteins by the nanocluster. This theoretical prediction is suitable for experimental evidence (present work).

6.2.6 Cell culture

MCF-7 (breast cancer) cell lines was cultured and maintained in Dulbecco's modification of Eagle's medium, (DMEM, provided by Advanced Reseach Lab, King George Medical University), supplemented with 10 % Foetal Bovine Serum, (FBS) and maintained at 37 °C under a humidified atmosphere at 5% CO_2. All the cells were seeded into 96 well plates at the density of 20,000 cells/well in DMEM supplemented with 10% FBS. Different concentration of particles was suspended in the serum-free medium using an ultrasonic bath for 1 hour to prevent agglomeration. After plating cells for a period of 28 hrs, the medium with 10% FBS was removed and replaced by 200 μL of particle suspension with different concentration. The control was carried out with cells treated with an equivalent volume of serum-free medium without any particles. Cells were incubated for further 40 hrs with test particles before the cell viability assay was performed.

Cytotoxicity was assessed by using an MTT (3,(4,5 dimetylthiazol-2-yl)-2, 5-diphenyltetrazolium bromide) test to measure the cytotoxicity against breast carcinomas. Plates were centrifuged at 2000 rpm to harvest total cell contents. Hundred mL of fresh media with 20 μL of 5 mg/mL MTT stain (Sigma Aldrich in

vitro cytotoxicity assay kit) was added into each well and incubated for 4 hours. The media stain was aspirated and purple color crystal was dissolved with acidic isopropyl alcohol. The absorbance in each cell was measured at 570 nm in BIO-RAD 680 microplate reader. Background absorbance was measured in a medium containing net particles (without cells) and net cells (without particles). All experiments were repeated between 5 to 15 times to ensure reproducibility. Statistical analysis was carried out using the calculation of IC_{50} with a level 95 % significance. Microscopic images show the typically observed morphologies of MCF-7 cells of control 50 % viability. In cytotoxic condition, the cell membrane was compromised and distinct cell shape was no longer visible.

6.3 Results and Discussion

To confirm the formation of Ni NPs, UV-visible absorption spectrum of synthesized material was recorded in the range of 200-800 nm which shows peak at 395 nm (Fig 6.1 a). This observation is similar to the damping effect of Ni NPs on the SPR band of noble metals as reported in case of Ni coated- Au nanorods.[28] The Band-gap analysis of Ni NPs is estimated by using the Tauc's equation.[29]

$$\alpha h\upsilon = A(h\upsilon - E_g)^n$$

where α is the absorption coefficient, $h\upsilon$ is photon energy and E_g is the bandgap, $n = 1/2$ for the direct transition. A plot of $(\alpha h\upsilon)^2$ versus $h\upsilon$, as shown in the inset of figure and linear portion of the graph is extrapolated to hυ axis to determine the bandgap. The bandgap is found to be 2.2 eV (Fig 6.1 b).

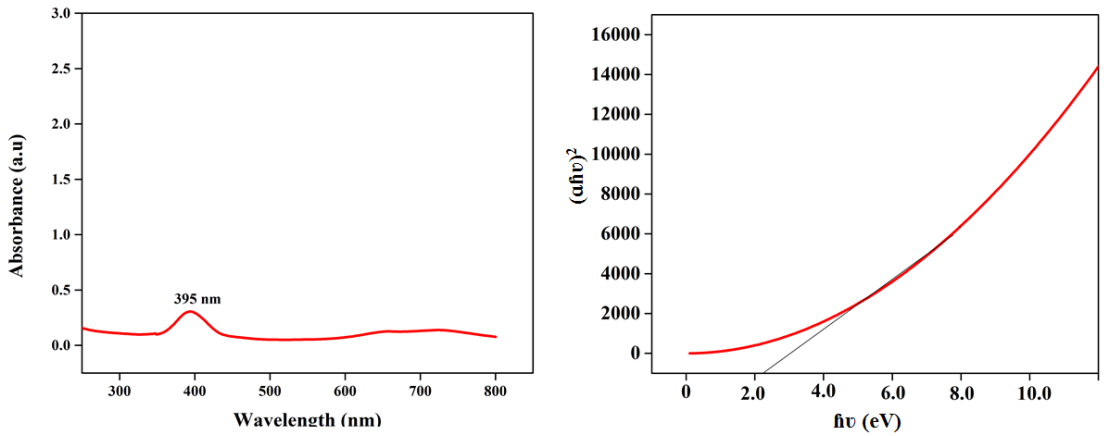

Fig.6.1. UV-visible spectrum (a) and band gap analysis (b) of Ni NPs

The prepared Ni NPs were subjected for particle size distribution which represents their size in a range of 30 to 70 nm (Fig. 6.2 a). The synthesized Ni NPs were further investigated by zeta potential measurement and the results revealed that Ni NPs shows surface charge -20.3 meV, indicating high stability at as clearly shown in Figure 6.2 b. Similar results has witnessed the synthesis of Ni NPs which be used in several biomedical applications against pathogenesis.[30]

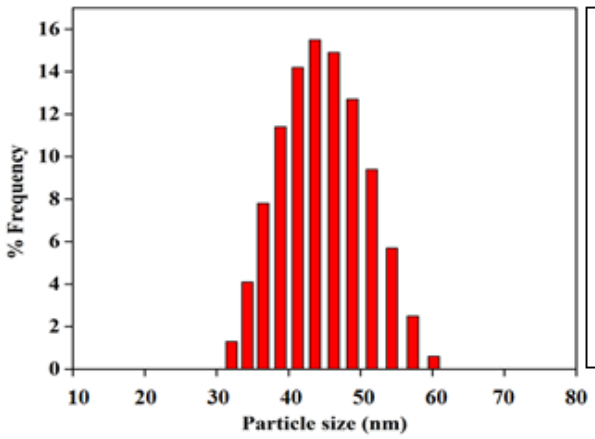

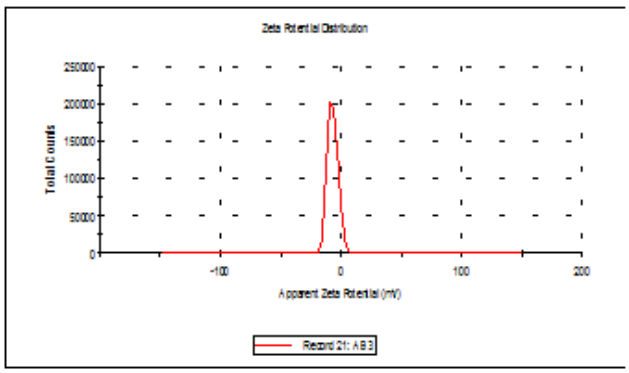

Fig.6.2 a. particle size distribution Ni NPs **Fig.6.2 b. Zeta potential of Ni NPs**

With a view to observe interaction of organic molecules of reaction mixture with Ni NPs, the FTIR spectral analysis of the Ni NPs was carried out. The graph shows an

absorption peak at 3424 cm^{-1} due to –OH stretching of carboxyl group (Fig. 6.3 a).[31] The broadness of this peak indicated the presence of hydrogen bonding between Ni NPs. The peak at 1623 cm^{-1} is due to C=C stretching of L-Ascorbic acid. This peak is red shifted compared to those of pure L-Ascorbic acid due to its adsorption on the nanoparticle's surface. The peak at 660 cm^{-1} is due to the out of plane bending vibration of –CH of PEG. The peak at 1461 cm^{-1} is due to CH_2 scissoring of alkyl chains of adsorbed PEG. Although peaks corresponding to $-CH_2$ stretching do not appear in Figure 6.3 a, however, a small hump is visible at 2927 cm^{-1} probably because of preferential adsorption of AA at nanoparticle's surface in the liquid phase. The absorption at 1256 and 661 cm^{-1} wagging transformation of trans conformation and ring C-C stretching and CH_2 rocking.[32] The room temperature Raman spectra of nickel nanoparticles, (Ni NPs) measured using 532 nm green laser beam exhibited multiple bands above 300 cm^{-1} (Fig. 6.3 b). Two vibrational bands could be seen at 479 cm^{-1} and 561 cm^{-1} are characteristic Ni-O vibration[33] indicating interaction of Ni-O-PEG. The band at 700 is correspond to adsorbed AA while the peak at 1076 cm^{-1} is due to C-O-H bending vibration.[34]

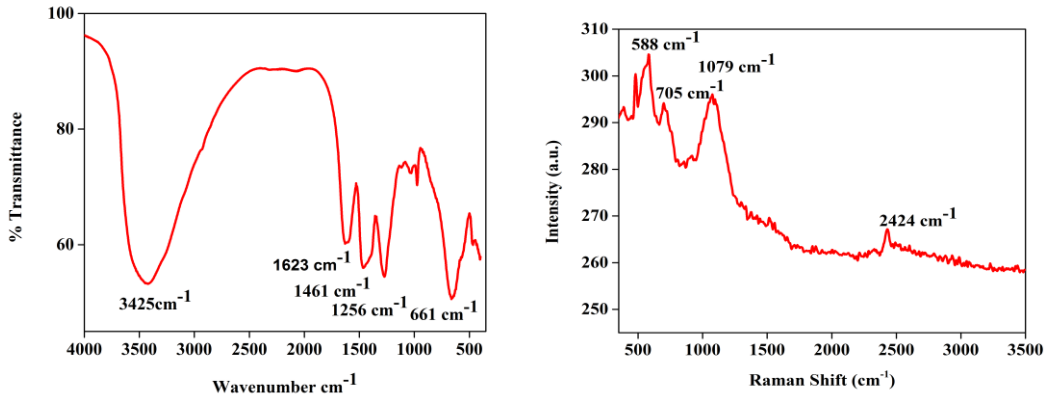

Fig. 6.3. FTIR spectrum (a) and Raman spectrum (b) of Ni NPs

X-ray diffraction analysis (Cu K_α radiation, λ=1.5418 A^o) of PEG grafted and LAA coated Ni NPs is shown in Figure 6.4. The strong diffraction peak at 28.6, 44.9, 70.1, 82 and 103.7° which are correspond (111), (200), (220), (311) and (222) respectively Bragg's reflection face-centered cubic phase without any other additional peaks, indicating that the Ni nanoparticles are single phased fcc phase. The broad diffraction peaks are indicative of the ultrafine Ni particles. [35]. Using the Scherrer's equation at 34.9° the size of synthesized nickel nanoparticles, (Ni NPs) was estimated to be 47.39 nm.[36]

$$D = \frac{k\lambda}{\beta cos\theta}$$

Where D = particle size, k = Scherrer's constant (0.94), value of λ can be derived from Bragg's equation ($n\lambda = 2dsin\theta$), λ is wavelength, β = full maxima half width, θ = diffraction angle.

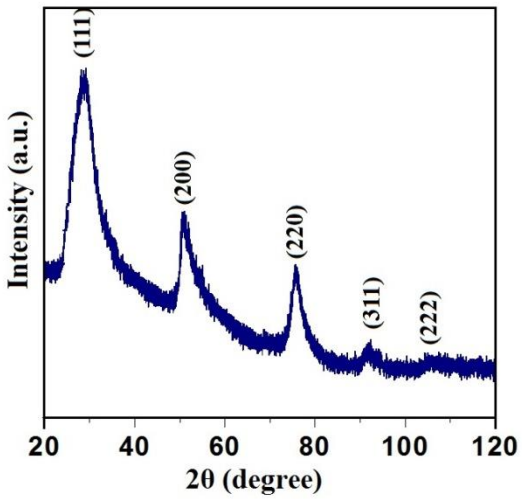

Fig. 6.4. XRD pattern of Ni NPs

The porosity of the formed Ni NPs has been determined by using N_2 adsorption-desorption isotherm. From the Barrett- Joyner-Halenda (BJH) method, an average mesopore diameter has been found to be 24 nm (Fig. 6.5 a). The specific

surface area obtained by Brunauer-Emmett-Taylor (BET) method has been determined as 53 m^2g^{-1}. Recent literature witnessed other related nanostructure of Ni NPs normally has small surface areas[37] in a range of 18 to 30 m^2g^{-1} (Fig. 6.5 b). So compared to these results Ni NPs have a relatively large surface area, which expected to have large catalytic sites.

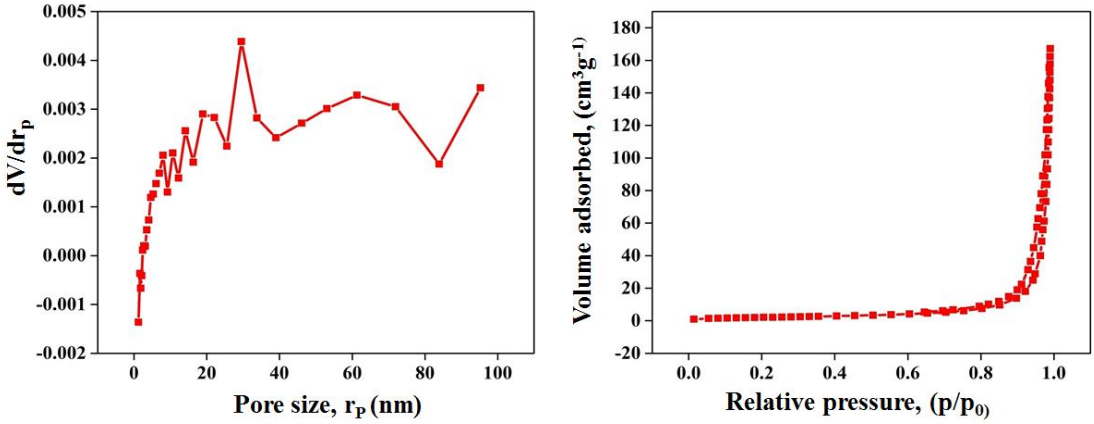

Fig. 6.5. BJH analysis (a) and BET analysis (b) of Ni NPs

The prepared Ni NPS was subjected to scanning electron microscopy for their morphological studies. The result shows that the shapes of synthesized Ni NPs have cubical shape (Fig 6.6 a-b). EDX spectrum (Fig. 6.6 c) confirms the higher presence of nickel while oxygen and carbon metals observed due to adsorbed organic molecules, and coated zirconium observed because the zirconium coating used in SEM@EDX analysis.[30] SEM images show that all the particles have nearly uniform size and well dispersed.

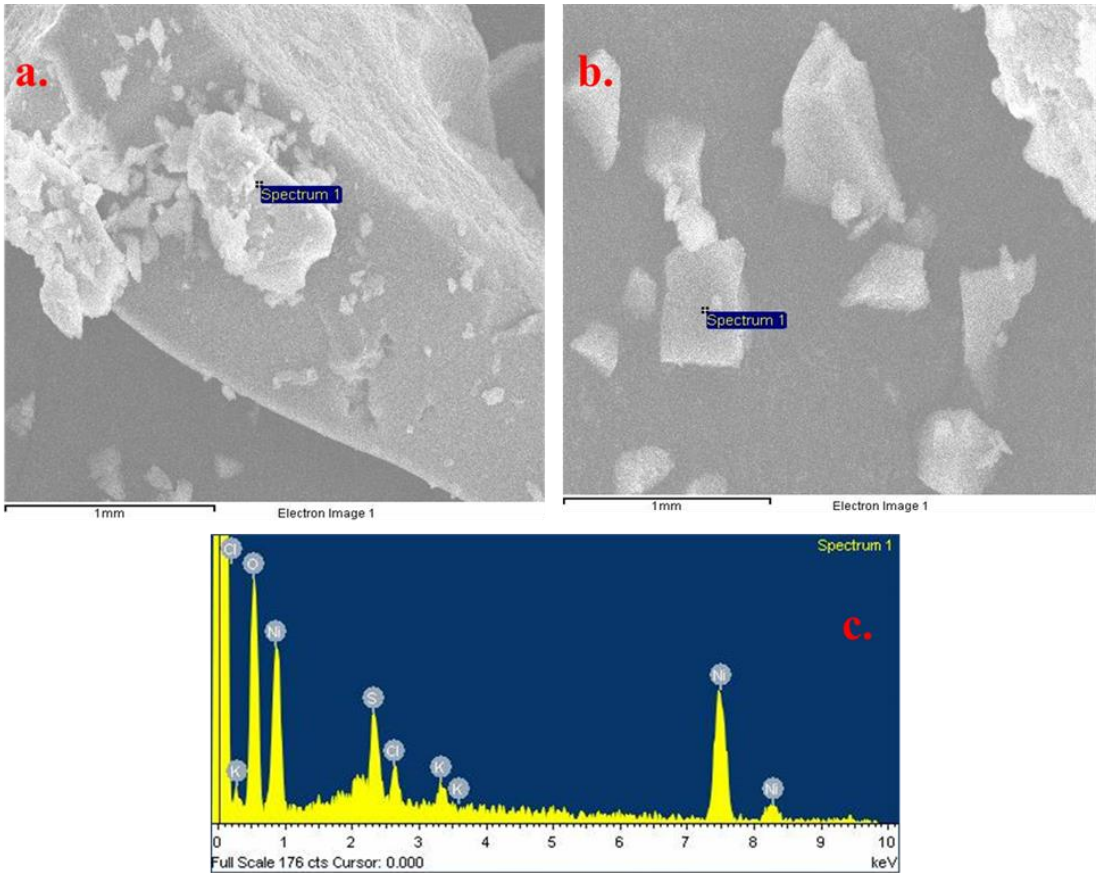

Fig.6.6 a-c. SEM and EDX analysis of Ni NPs

The FESEM analysis was used to observe high resolution view of Ni NPs. The Figure 6.7 a-d shows the FESEM images of Ni NPs. The dimension of Ni NPs is found to be 45 to 60 nm and these structure is found to be free from any type of surface cracks and infrastructure adherence.[38] The TEM micrographs depicted in Figure 6.8 a-b indicate formation of cube shape Ni NPs which further shape support the SEM and FESEM results. The size of particles varies in the range of 30-90 nm probably due to presence of PEG. However the average size obtained from the Scherrer's formula shows slight decrease from that of TEM images because of the difference in their particles size distribution.[39]

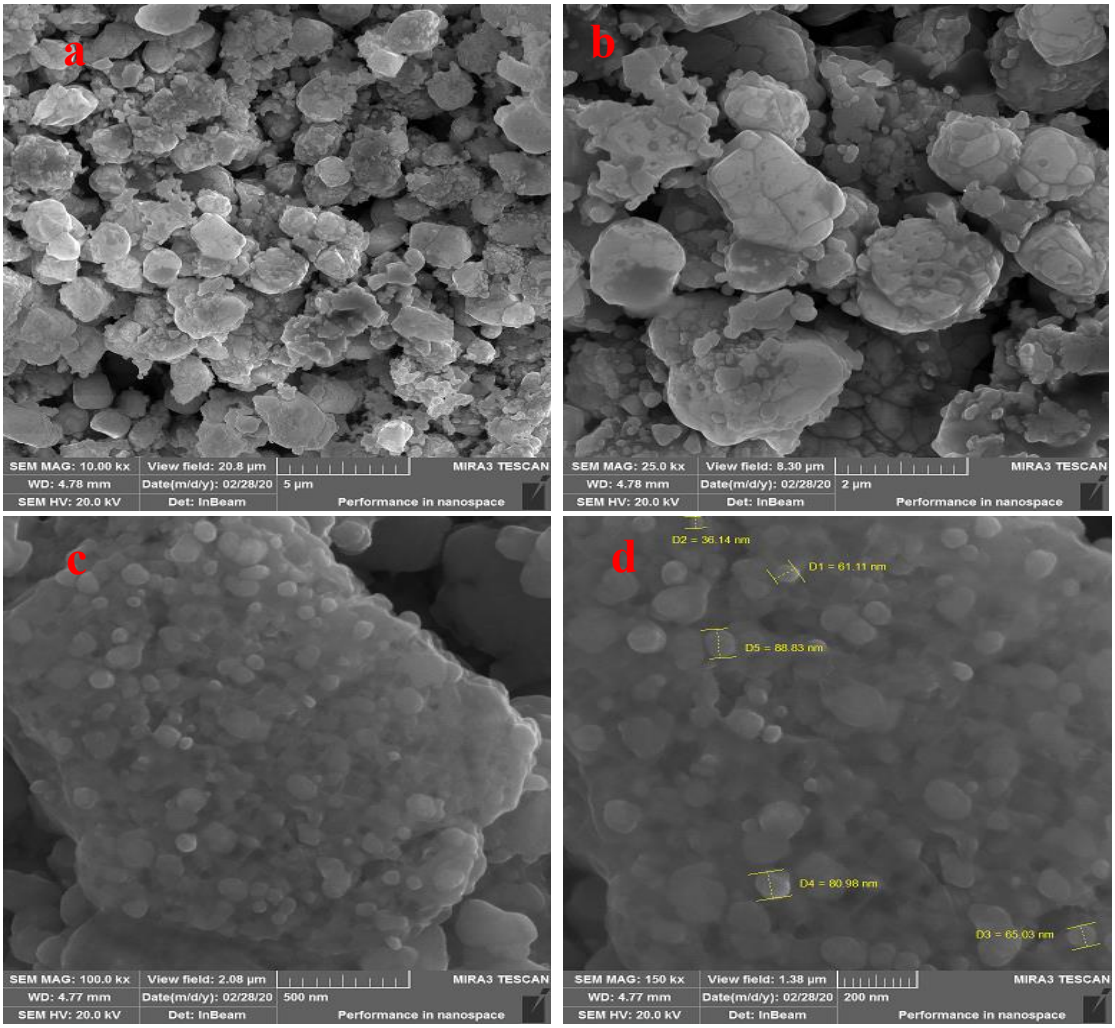

Fig.6.7.a-d FESEM analysis of Ni NPs

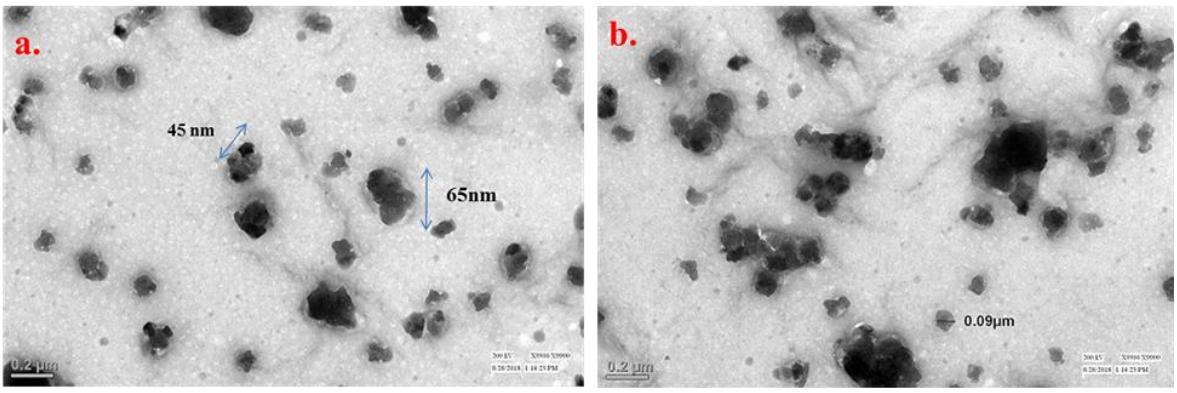

Fig.6.8.a-b. TEM analysis of Ni NPs

6.3.1. Protein and nanocluster description

The PDB format file of proteins with PDB ID 4C6C, 6D96, 2ITX, 2ITY, 1NOW, and 2ING have downloaded from RCSB Protein Data Bank[40]. The 4C6C and 6D96 PDB are the mesomorphic structure of proteins present in Human Embryonic Kidney HEK-293 cell lines.[41] The 2ITX and 2ITY proteins are the amorphous structures of the EGFR kinase domain. Mutations in the EGFR kinase are a cause of non-small-cell lung cancer.[42] The proteins PDB 1NOW and 2ING are the crystal structure of breast cancer protein BRCA2.[43] With the help of CHIMERA software[44], ligands and water molecules have removed from each protein.[44]

6.3.2. Drug

The nanocluster has optimized by the Gaussian 09 software package.[45] The nickel cluster is optimized by the DFT method B3LYP[46] at the Def2tz level.[47] The structural geometry of the Nickel cluster has taken after optimization. Figure 6.9 represents the 3-D chemical structure of the Nickel cluster.

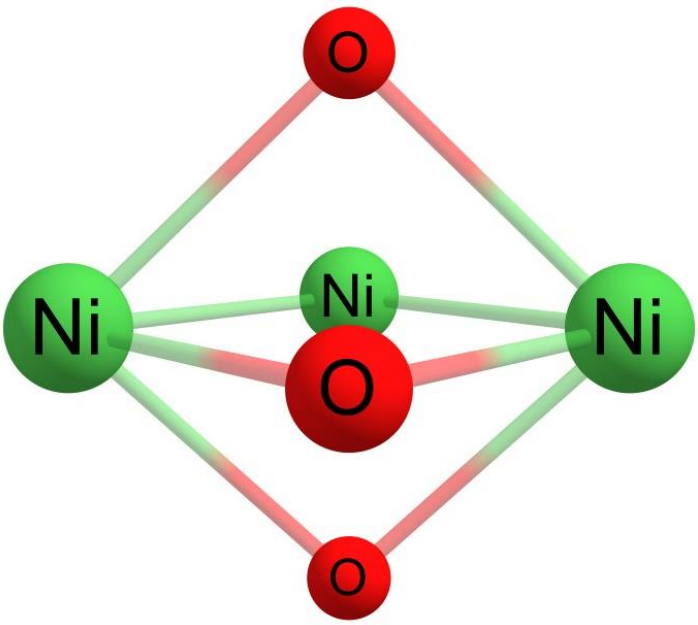

Fig.6.9.Three-dimensional structure of the Nickel cluster

6.3.3. Molecular Docking

The Molecular Docking has calculated by the Autodock4.2 software.[48] Lamarckian Genetic Algorithm (LGA) has implemented for flexible ligand and receptor docking. All the proteins have taken as the macromolecule and the Nickel cluster used as the ligand. Both macromolecule and ligand have prepared for docking. Before the docking, all the water molecules have deleted from the macromolecule. For Autogrid, macromolecule has contained in grid boxes. The Grid boxes for all the proteins are taking an appropriate dimension. The number of LGA runs set to 20. Kollman and Gasteiger charges have added to the complex by Auto Dock Tools (ADT).[49] The complex is modified and adjusted for the blind docking. The docked pose with the highest docking score has selected as the binding mode of the system.

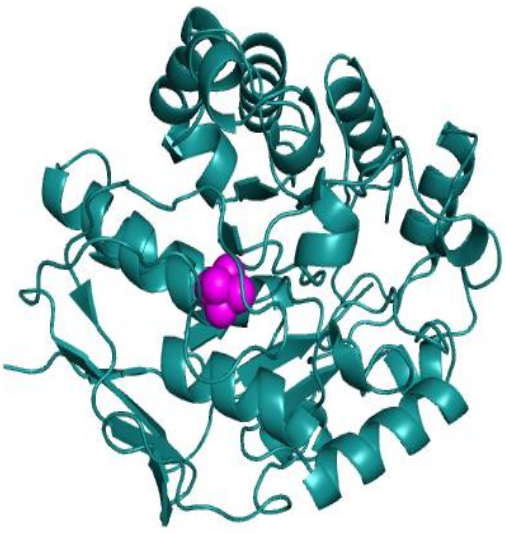

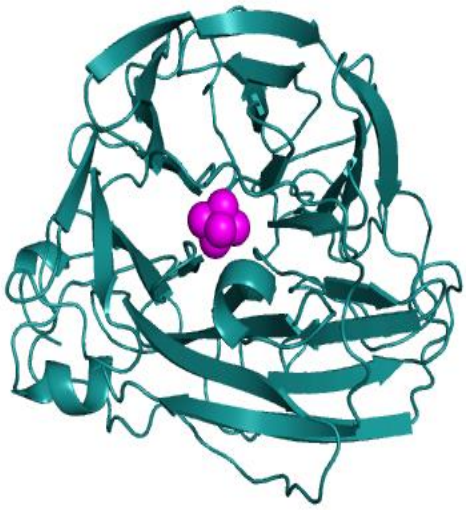

(a). 4C6C PDB docked with Ni cluster **(b). 6D96 PDB docked with Ni cluster**

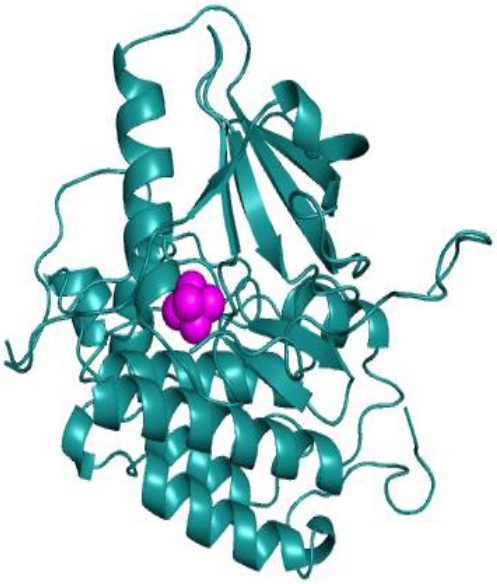

(c) 2ITX PDB docked with Ni cluster

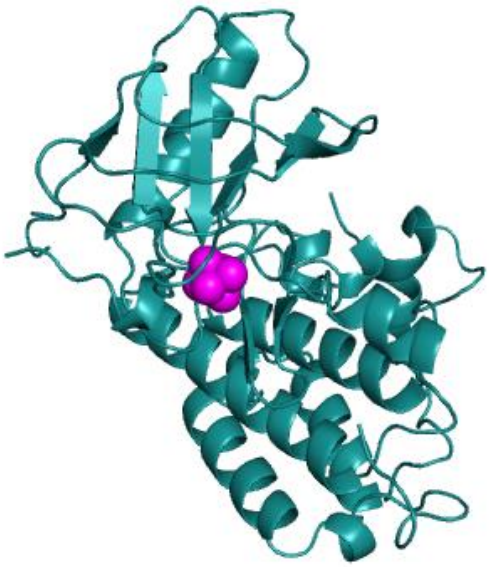

(d) 2ITY PDB docked with Ni cluster

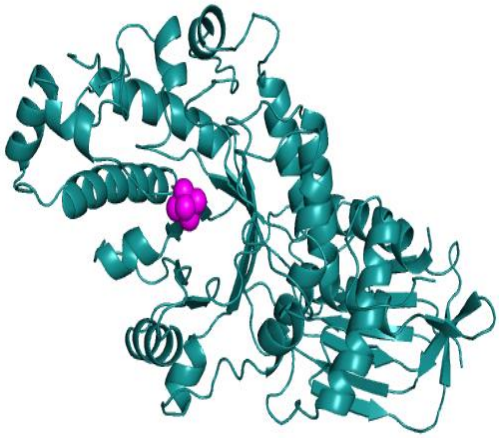

(e) INOW PDB docked with Ni cluster

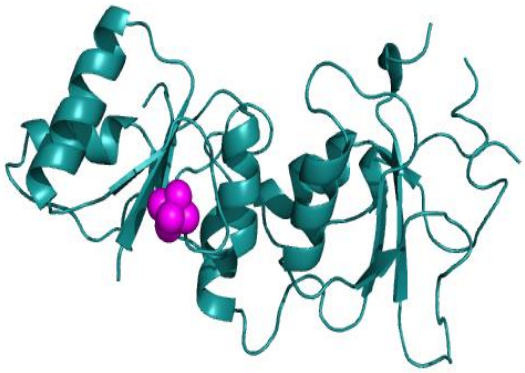

(f) 2ING PDB docked with Ni cluster

Fig. 6.10 a-f. PDB docking with Ni Cluster

6.3.4. Result and Discussion

The molecular docked binding energies of all protein-drug complexes are given in Table 1. The tabulated data is indicating that the binding energies of all proteins with the Nickel cluster are in different ranges. The binding energy of all the complexes is negative, showing that the complex system is most stable. The binding modes and geometrical orientation of all compounds are almost identical; which is suggesting that all the inhibitors occupied a common cavity in the receptor. The ligand binds in the same active pocket for all the proteins. The Nickel nanocluster is making non-bonded interactions for all the protein. The HEK-293 cell lines protein 6D96 represents the highest binding energy as a comparison with 4C6C complex, as shown in Figure 6.10 (a) and (b) also given in Table 1. The Lung Cancer Protein 2ITX complex expresses more interaction as a comparison with the 2ITY complex, as shown in Figure 6.10 (c) and (d). The Breast Cancer protein id 1NOW exhibits more non bonded interaction as a comparison with 2ING complex, as shown in Figure 6.10 (e) and (f). The molecular docking is giving the stable conformations of the ligand with proteins in the receptor active pocket. For each category of protein, an active pocket has shown with the one with better binding energy with the Nickel cluster.

Table 1: Binding energies of all protein-drug complexes

Proteins	PDB Id	Binding Energy(kcal/mol)
HEK-293 cell	4C6C	-4.3
lines	6D96	**-4.7**
Lung Cancer	2ITX	**-3.7**
	2ITY	-3.6
Breast Cancer	1NOW	**-3.8**
	2ING	-3.4

6.3.5. Cytotoxicity

Cell viability of synthesized Ni NPs was investigated against breast carcinomas MCF-7 cell lines. In this study the different concentration of Ni NPs was treated with known amount of cells and % cytotoxicity in dose level was measured by MTT assay (Fig. 6.11 a-c). The diluted ranges of extract were added and final concentration of cell extracts were 15, 30, 45, 60, 75, 90 and 100 μg/mL. MTT assay (3,(4,5 dimetylthiazol-2-yl)-2, 5-diphenyltetrazolium bromide)was performed to assess the cytotoxicity and cell viability against Ni NPs prepared via sonochemical method. The insoluble crystal of formazan was mixed with dimethyl sulfoxide (DMSO) for complete solubility and absorbance of purple solution was quantified by recording the spectra at a certain wavelength (540 nm) using a spectrophotometer.[50] The cytotoxicity was recorded as the drug concentration causes 50% (IC_{50}) growth inhibition of breast cancer cell lines using the formula given below

% Cell viability = (OD sample mean/OD control mean)*100

Ni NPs has a huge record for their cytotoxic effects over various cell lines like human airway epithelial (Hep-2) and HT-29 (colon cancer cell lines) and many more. The effective cytotoxicity of as-synthesized Ni NPs against MCF-7 (Breast cancer cell lines) may be attributed due their small particles size and large surface area which enhances the absorption of biomolecules and chemicals on Ni NPs and supports cellular influences.[51] The effective cytotoxic effect of Ni NPs in the present study reveals that the level of metal ion release is high thereby inducing directly or indirectly through mitochondrial dysfunction and subsequent cell death in an exposed cell. The results agree with the previous studies where Ni NPs have induced viability in human lung epithelial cell lines.[52] The cell viability increased slightly as the

concentration decreases from 75-45 µg/mL. The Figure 6.11.a-c shows a pictograph which describes the % cell viability against concentration and cell death at dose dependent manner (Fig.6.12.a-d). The result confirms that synthesized Ni NPs possess the anticancer activity and cytotoxic activity. Hence it can be used in different cancer therapy and used in colorectal cancer human breast cancer etc. Before its clinical usage, through toxicological profile has to be determined to confirm the safety of drug.[53]

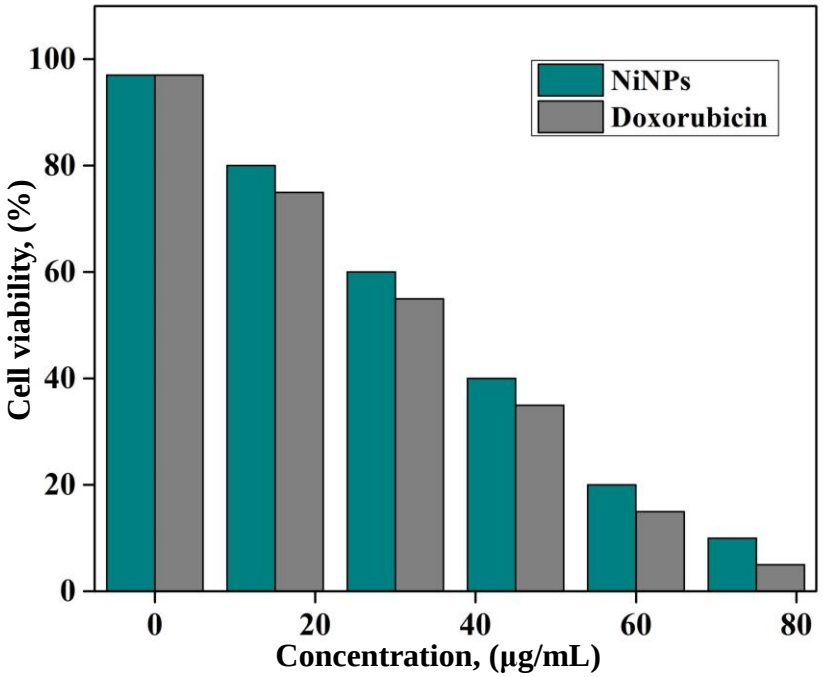

Fig.6.11 a. Cell viability of Ni NPs

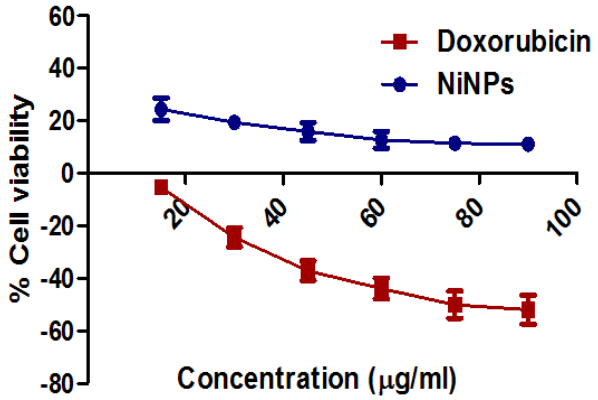

Fig.6.11.b. Cytotoxicity of Ni NPs

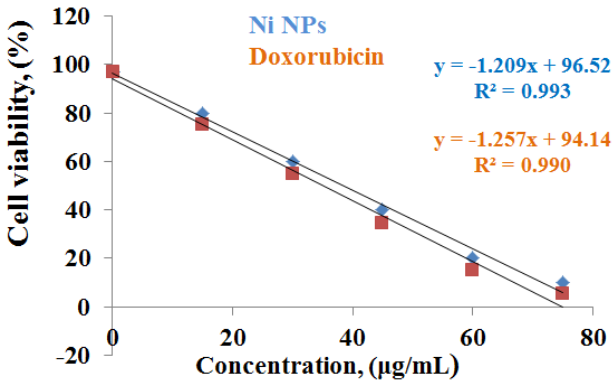

Fig.6.11c. IC_{50} analysis of Ni NPs

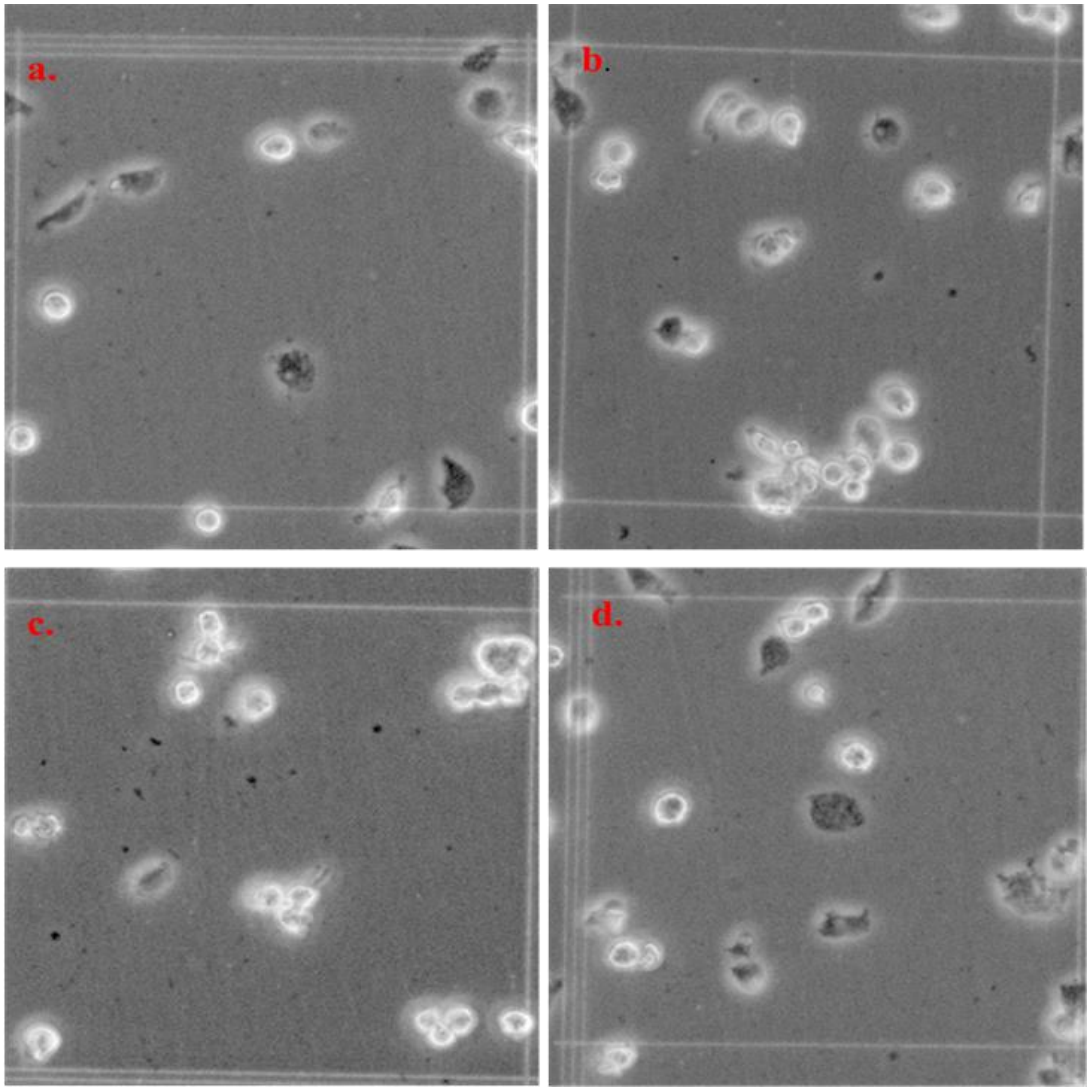

Fig.6.12.a-d.Microscopic images of Ni NPs at dosage concentration,(µg/mL)

Conclusion

To conclude, we have reported the sonochemical method of synthesis of nickel nanoparticles. UV-visible absorption spectroscopy shows λ_{max} value due to the quantum confinement of Ni NPs. The XRD analysis shows that the Ni NPs are highly crystalline with face centred cubic (fcc) structure. EDAX data confirms the presence of prepared Ni NPs. The FTIR and Raman spectra confirm the formation of PEG grafted and L-ascorbic acid coated Ni NPs and presence of fundamental phonon peaks. Morphological studies using the SEM, FESEM and TEM analysis shows cube shaped nickel nanoparticles. BET results show formation high surface area mesoporous Ni NPs. The prepared Ni NPs are shown effective cytotoxicity against MCF-7 breast cancer cell lines. The results were supported by morphological analysis of treated and controlled cells. The normal and regular morphological pattern is observed in untreated cells and irregular cell morphology is seen in cells treated with Ni NPs. This study has proposed the best and simple protocol to synthesize Ni NPs with an effective anticarcinomas activity against MCF-7 breast cancer cell lines.

References

1. Wunderbaldinger, P.; Josephson, L.; Weissleder, R., Tat peptide directs enhanced clearance and hepatic permeability of magnetic nanoparticles. *Bioconjugate chemistry* 2002, 13, (2), 264-268.
2. Larson, D. R.; Zipfel, W. R.; Williams, R. M.; Clark, S. W.; Bruchez, M. P.; Wise, F. W.; Webb, W. W., Water-soluble quantum dots for multiphoton fluorescence imaging in vivo. *Science* 2003, 300, (5624), 1434-1436.
3. Nah, J.-W.; Paek, Y.-W.; Jeong, Y.-I.; Kim, D.-W.; Cho, C.-S.; Kim, S.-H.; Kim, M.-Y., Clonazepam release from poly (DL-lactide-co-glycolide) nanoparticles prepared by dialysis method. *Archives of pharmacal research* 1998, 21, (4), 418-422.
4. Williams, J.; Lansdown, R.; Sweitzer, R.; Romanowski, M.; LaBell, R.; Ramaswami, R.; Unger, E., Nanoparticle drug delivery system for intravenous delivery of topoisomerase inhibitors. *Journal of Controlled Release* 2003, 91, (1-2), 167-172.
5. Brannon-Peppas, L.; Blanchette, J. O., Nanoparticle and targeted systems for cancer therapy. *Advanced drug delivery reviews* 2004, 56, (11), 1649-1659.
6. Bellocq, N. C.; Pun, S. H.; Jensen, G. S.; Davis, M. E., Transferrin-containing, cyclodextrin polymer-based particles for tumor-targeted gene delivery. *Bioconjugate chemistry* 2003, 14, (6), 1122-1132.
7. Benns, J.; Kim, S., Tailoring new gene delivery designs for specific targets. *Journal of drug targeting* 2000, 8, (1), 1-12.
8. Kong, G.; Braun, R. D.; Dewhirst, M. W., Hyperthermia enables tumor-specific nanoparticle delivery: effect of particle size. *Cancer research* 2000, 60, (16), 4440-4445.

9. Riboh, J. C.; Haes, A. J.; McFarland, A. D.; Ranjit Yonzon, C.; Van Duyne, R. P., A nanoscale optical biosensor: real-time immunoassay in physiological buffer enabled by improved nanoparticle adhesion. *The Journal of Physical Chemistry B* 2003, 107, (8), 1772-1780.
10. Hoet, P. H.; Nemmar, A.; Nemery, B., Health impact of nanomaterials? *Nature Biotechnology* 2004, 22, (1), 19-19.
11. Giles, J., Size matters when it comes to safety, report warns. *Nature* 2004, 430, (7000), 599-600.
12. Colvin, V. L., The potential environmental impact of engineered nanomaterials. *Nature Biotechnology* 2003, 21, (10), 1166-1170.
13. Vestal, C. R.; Zhang, Z. J., Effects of surface coordination chemistry on the magnetic properties of MnFe2O4 spinel ferrite nanoparticles. *Journal of the American Chemical Society* 2003, 125, (32), 9828-9833.
14. Mangeney, C.; Ferrage, F.; Aujard, I.; Marchi-Artzner, V.; Jullien, L.; Ouari, O.; Rékaï, E. D.; Laschewsky, A.; Vikholm, I.; Sadowski, J. W., Synthesis and properties of water-soluble gold colloids covalently derivatized with neutral polymer monolayers. *Journal of the American Chemical Society* 2002, 124, (20), 5811-5821.
15. Mayya, K. S.; Schoeler, B.; Caruso, F., Preparation and organization of nanoscale polyelectrolyte-coated gold nanoparticles. *Advanced Functional Materials* 2003, 13, (3), 183-188.
16. Derfus, A. M.; Chan, W. C.; Bhatia, S. N., Probing the cytotoxicity of semiconductor quantum dots. *Nano letters* 2004, 4, (1), 11-18.
17. Sayes, C. M.; Fortner, J. D.; Guo, W.; Lyon, D.; Boyd, A. M.; Ausman, K. D.; Tao, Y. J.; Sitharaman, B.; Wilson, L. J.; Hughes, J. B., The differential cytotoxicity of water-soluble fullerenes. *Nano letters* 2004, 4, (10), 1881-1887.

18. Hilger, I.; Frühauf, S.; Linß, W.; Hiergeist, R.; Andrä, W.; Hergt, R.; Kaiser, W. A., Cytotoxicity of selected magnetic fluids on human adenocarcinoma cells. *Journal of magnetism and magnetic materials* 2003, 261, (1-2), 7-12.
19. Ferrando, R.; Jellinek, J.; Johnston, R. L., Nanoalloys: from theory to applications of alloy clusters and nanoparticles. *Chemical reviews* 2008, 108, (3), 845-910.
20. Lee, H. J.; Song, J. Y.; Kim, B. S., Biological synthesis of copper nanoparticles using Magnolia kobus leaf extract and their antibacterial activity. *Journal of Chemical Technology & Biotechnology* 2013, 88, (11), 1971-1977.
21. Argueta-Figueroa, L.; Morales-Luckie, R. A.; Scougall-Vilchis, R. J.; Olea-Mejía, O. F., Synthesis, characterization and antibacterial activity of copper, nickel and bimetallic Cu–Ni nanoparticles for potential use in dental materials. *Progress in Natural Science: Materials International* 2014, 24, (4), 321-328.
22. Mohammadkhani, F.; Montazer, M.; Latifi, M., Microwave absorption and photocatalytic properties of magnetic nickel nanoparticles/recycled PET nanofibers web. *The Journal of The Textile Institute* 2019, 110, (11), 1606-1614.
23. Kango, S.; Kalia, S.; Celli, A.; Njuguna, J.; Habibi, Y.; Kumar, R., Surface modification of inorganic nanoparticles for development of organic–inorganic nanocomposites—A review. *Progress in Polymer Science* 2013, 38, (8), 1232-1261.
24. Zou, J.; Huang, X.; Li, W.; Lin, T.; Li, T.; Zhang, K.; Deng, Z.; Cao, G. In *SNiPER: an offline software framework for non-collider physics experiments*, Journal of Physics: Conference Series, 2015; IOP Publishing: 2015; p 072053.
25. Mittal, S.; El-Serag, H. B.; Sada, Y. H.; Kanwal, F.; Duan, Z.; Temple, S.; May, S. B.; Kramer, J. R.; Richardson, P. A.; Davila, J. A., Hepatocellular

carcinoma in the absence of cirrhosis in United States veterans is associated with nonalcoholic fatty liver disease. *Clinical gastroenterology and hepatology* 2016, 14, (1), 124-131. e1.

26. Piskorz, W.; Zasada, F., Catalytic Properties of Selected Transition Metal Oxides—Computational Studies. In *Transition Metals in Coordination Environments*, Springer: 2019; pp 345-408.
27. Mohammadkhani, F.; Montazer, M.; Latifi, M., Microwave absorption characterization and wettability of magnetic nano iron oxide/recycled PET nanofibers web. *The Journal of The Textile Institute* 2019, 110, (7), 989-999.
28. Yin, H.; Too, H.; Chow, G., The effects of particle size and surface coating on the cytotoxicity of nickel ferrite. *Biomaterials* 2005, 26, (29), 5818-5826.
29. Ispas, C.; Andreescu, D.; Patel, A.; Goia, D. V.; Andreescu, S.; Wallace, K. N., Toxicity and developmental defects of different sizes and shape nickel nanoparticles in zebrafish. *Environmental science & technology* 2009, 43, (16), 6349-6356.
30. Abbas, G.; Kumar, N.; Kumar, D.; Pandey, G., Effect of Reaction Temperature on Shape Evolution of Palladium Nanoparticles and Their Cytotoxicity against A-549 Lung Cancer Cells. *ACS omega* 2019.
31. Ezhilarasi, A. A.; Vijaya, J. J.; Kaviyarasu, K.; Maaza, M.; Ayeshamariam, A.; Kennedy, L. J., Green synthesis of NiO nanoparticles using Moringa oleifera extract and their biomedical applications: Cytotoxicity effect of nanoparticles against HT-29 cancer cells. *Journal of Photochemistry and Photobiology B: Biology* 2016, 164, 352-360.
32. Aazam, E. S.; El-Said, W. A., Synthesis of copper/nickel nanoparticles using newly synthesized Schiff-base metals complexes and their cytotoxicity/catalytic activities. *Bioorganic chemistry* 2014, 57, 5-12.

33. Mani, M. P.; Jaganathan, S. K.; Md Khudzari, A. Z.; Ismail, A. F., Green synthesis of nickel oxide particles and its integration into polyurethane scaffold matrix ornamented with groundnut oil for bone tissue engineering. *International Journal of Polymer Analysis and Characterization* 2019, 24, (7), 571-583.
34. Moazzenchi, B.; Montazer, M., Click electroless plating of nickel nanoparticles on polyester fabric: Electrical conductivity, magnetic and EMI shielding properties. *Colloids and Surfaces A: Physicochemical and Engineering Aspects* 2019, 571, 110-124.
35. Bashir, B.; Rahman, A.; Sabeeh, H.; Khan, M. A.; Aboud, M. F. A.; Warsi, M. F.; Shakir, I.; Agboola, P. O.; Shahid, M., Copper substituted nickel ferrite nanoparticles anchored onto the graphene sheets as electrode materials for supercapacitors fabrication. *Ceramics International* 2019, 45, (6), 6759-6766.
36. Chaudhary, J.; Tailor, G.; Yadav, B.; Michael, O., Synthesis and biological function of Nickel and Copper nanoparticles. *Heliyon* 2019, 5, (6), e01878.
37. Rudge, S.; Kurtz, T.; Vessely, C. R.; Catterall, L.; Williamson, D., Preparation, characterization, and performance of magnetic iron–carbon composite microparticles for chemotherapy. *Biomaterials* 2000, 21, (14), 1411-1420.
38. Xu, J.; Yeung, C. M.; Ni, J.; Meunier, F.; Acerbi, N.; Fowles, M.; Tsang, S. C., Methane steam reforming for hydrogen production using low water-ratios without carbon formation over ceria coated Ni catalysts. *Applied Catalysis A: General* 2008, 345, (2), 119-127.
39. El-Kemary, M.; Nagy, N.; El-Mehasseb, I., Nickel oxide nanoparticles: synthesis and spectral studies of interactions with glucose. *Materials Science in Semiconductor Processing* 2013, 16, (6), 1747-1752.

40. Elango, G.; Roopan, S. M.; Dhamodaran, K. I.; Elumalai, K.; Al-Dhabi, N. A.; Arasu, M. V., Spectroscopic investigation of biosynthesized nickel nanoparticles and its larvicidal, pesticidal activities. *Journal of Photochemistry and Photobiology B: Biology* 2016, 162, 162-167.
41. Coates, J., Interpretation of infrared spectra, a practical approach. *Encyclopedia of analytical chemistry: applications, theory and instrumentation* 2006.
42. Pandian, C. J.; Palanivel, R.; Dhananasekaran, S., Green synthesis of nickel nanoparticles using Ocimum sanctum and their application in dye and pollutant adsorption. *Chinese journal of Chemical engineering* 2015, 23, (8), 1307-1315.
43. Dave, H.; Ledwani, L.; Chandwani, N.; Kikani, P.; Desai, B.; Nema, S., Surface modification of polyester fabric by non-thermal plasma treatment and its effect on coloration using natural dye. *Journal of Polymer Materials* 2013, 30, (3), 291-304.
44. Hoghoghifard, S.; Mokhtari, H.; Dehghani, S., Improving the conductivity of polyaniline-coated polyester textile by optimizing the synthesis conditions. *Journal of Industrial Textiles* 2016, 46, (2), 611-623.
45. Shviro, M.; Zitoun, D., Nickel nanocrystals: fast synthesis of cubes, pyramids and tetrapods. *Rsc Advances* 2013, 3, (5), 1380-1387.
46. Kalaiselvi, A.; Roopan, S. M.; Madhumitha, G.; Ramalingam, C.; Elango, G., Synthesis and characterization of palladium nanoparticles using Catharanthus roseus leaf extract and its application in the photo-catalytic degradation. *Spectrochimica Acta Part A: Molecular and Biomolecular Spectroscopy* 2015, 135, 116-119.
47. Wang, H.; Imura, M.; Malgras, V.; Li, C.; Wang, L.; Yamauchi, Y., A Solution Phase Synthesis of Dendritic Platinum Nanoelectrocatalysts with the

Assistance of Polyoxyethylene Nonylphenyl Ether. *Journal of Inorganic and Organometallic Polymers and Materials* 2015, 25, (2), 245-250.

48. Ganguli, A. K.; Ganguly, A.; Vaidya, S., Microemulsion-based synthesis of nanocrystalline materials. *Chemical Society Reviews* 2010, 39, (2), 474-485.
49. Iwahori, K.; Yamashita, I., Bio-template synthesis of nanoparticle by cage-shaped protein supramolecule, apoferritin. *Journal of Cluster Science* 2007, 18, (2), 358-370.
50. Sheena, P.; Priyanka, K.; Sabu, B.; Varghese, T., Effect of calcination temperature on the structural and optical properties of nickel oxide nanoparticles. *Наносистемы: физика, химия, математика* 2014, 5, (3).
51. Varunkumar, K.; Hussain, R.; Hegde, G.; Ethiraj, A. S., Effect of calcination temperature on Cu doped NiO nanoparticles prepared via wet-chemical method: structural, optical and morphological studies. *Materials Science in Semiconductor Processing* 2017, 66, 149-156.
52. Freitas, M., Nickel hydroxide powder for NiO· OH/Ni (OH) 2 electrodes of the alkaline batteries. *Journal of Power Sources* 2001, 93, (1-2), 163-173.
53. Torresi, R.; Vázquez, M.; Gorenstein, A.; de Torresi, S. C., Infrared characterization of electrochromic nickel hydroxide prepared by homogeneous chemical precipitation. *Thin Solid Films* 1993, 229, (2), 180-186.

Chapter 7

Synthesis of 3D sponge shape LAA-PEG@Ag-Au nanocomposite and its cytotoxicity against bronchial carcinomas Lung cancer cell lines: in vitro and computational analysis

Synthesis of 3D sponge shape LAA-PEG@Ag-Au nanocomposite and its cytotoxicity against bronchial carcinomas Lung cancer cell lines: *in vitro* and computational analysis

Abstract

In the present study Ag-Au nanocomposite has been prepared by reduction of silver and gold complexes ($K_3[AgCl_4]$),($K_3[AuCl_6]$) using L-Ascorbic acid (LAA) and polyethylene glycol (PEG) as reducing and capping agents respectively via sonochemical approach. The Ag-Au nanocomposite has been characterized by UV-visible absorption spectroscopy, FTIR, Dynamic Light Scattering (DLS), particle size distribution analysis, X-ray diffraction analysis, TEM, FESEM, EDX and BET. The data obtained exhibited formation of variable shape (like needles, rods, spirillum structures), mesoporous, LAA-PEG-coated Ag-Au nanocomposite (LAA-PEG@Ag-Au). Cytotoxicity of synthesized LAA-PEG@Ag-Au nanocomposite was analyzed against bronchial carcinomas A-549 lung cancer cell lines by MTT and SRB assays. Nanocomposites also induces the reactive oxygen species, (ROS) and suppression of reduced Glutathione, (GSH) resulting in damage to various cell components, DNA breaks, lipid membrane peroxidation and protein carbonylation which causes cytotoxicity by oxidative stress induced apoptosis and damage to cellular components The study suggests that LAA-PEG@Ag-Au nanocomposite is a promising material against bronchial carcinomas A-549 lung cancer cell lines. The docking study has confirmed anti-proliferative action of NPs through binding affinity with bronchial carcinoma molecular targets. The synthesized nanocomposite has shown the synergistic effect with *cis*-platin as an anti-cancer drug effective against bronchial carcinoma cell lines. ROS and 1,1-diphenyl-2-picrylhydrazine (DPPH) free radical scavenging assay have shown the good antioxidant capability of synthesized LAA-

PEG@Ag-Au nanocomposite. The sulphorhodamine-B (SRB) assay is used for the cell density determination, based on the measurement of cellular protein content. The study demonstrated that the lung cancer stem like cells obtained from A-549, which were cultured in serum free conditioned medium, had strong proliferation and self-renewal abilities and expressed higher level of stem cell markers, (CD24, CD44, CD90, CD133, CD147, CD166, CD326 etc.) as compared with A-549 adherent cells. The efficient biocatalytic activity of LAA-PEG@Ag-Au nanocomposite emphasizes its use as one of the best suited drugs for the future perspectives against fatal bronchial carcinoma and thus it is reckoned that synthesized LAA-PEG@Ag-Au nanocomposite will have broad utilization in different field of medical applications.

Keywords: LAA-PEG@Ag-Au nanocomposite; A-549 bronchial carcinoma; docking; targeted drug delivery

7.1. Introduction

Since the origin of nanoscience and nanotechnology, nanocomposites in polymer matrices have been emerged as a prominent discipline of research.[1] Recent years are witnessing an increasing demand and popularity of polymer grafted silver and gold composites as unique functional materials. Beyond their organometallic catalytic activity, unique properties have emerged from their nano-scaled structure which opens a pathway to open up a wide range of applications. For instance, aurum nanoparticles, (Au NPs) shows high performance and unique flexibility in bio-sensing due to their plasmonic optoelectronic properties.[2] Argentum nanoparticles, (Ag NPs) exhibited an anti-immunological and antimicrobial behavior and therefore they have widely been utilized in the biomedical industry as well as in food packaging industry.[3] The usage of silver or gold nanoparticles has been greatly enhanced with the introduction of polymer chemistry to synthesized composite structure and hybrid nanostructures.[4] In the nanocomposite complements, the characteristics of functional polymers provide improved electrical, optical and mechanical properties.[5] Additionally, a simple but important advantage of polymer capped nanocomposites is their high stability as well as adjustable dispersibility into a different environment, like solvents and polymer matrices.[6] One of the most convenient techniques to modify surface is polymer grafting approach, which involves conjugation of pre-synthesized polymers having defined structure and functional anchoring group onto the surface of nanoparticles in a self-assembled manner.[7] The advantage of this route is the access to full predetermination and characterization of polymer to ensure that the polymer shell fits the required applications. To achieve appropriate grafting densities and sufficient stabilization effects on metal-nanocomposites surfaces, strong interactions between the polymer and the metal surface are required.

Silver and gold nanoparticles are well known noble metals having interesting properties and they are widely applied in various biological treatments. Silver nanoparticles have shown tremendous antimicrobial properties, [10,11] because of ability of colloidal silver to damage cell membrane and intracellular metabolic activity.[12] Colloidal silver is therefore an interesting "inorganic" alternative to classical antibiotics, especially for the use on medical surfaces and implants.[13–21] Gold nanoparticles have been used as promising materials in diagnosis and therapy of cancer.[2,3] Au-NPs have ability to absorb visible light wavelength-specific energies within picoseconds which can be delivered with targeted precision and efficiency. Therefore, they can be applied in light-mediated clinical treatments, for which bimetallic alloy NPs could be seen to exhibit better functionalities. The visible region spectra of Au NPs have ability to bind with biological molecules or ligands which aids in bioimaging and other biomedical applications.

The contributing factor for nanocomposite toxicity are their size chemical composition, shape, particle aging and surface charge[8]. As they are smaller than cell organelle, they can penetrate basic biological structure, which may in turn disrupt the normal functioning of these structures.[9] Further the unique physicochemical properties of nanocomposites can't be simply predicted from the properties of fine particles or bulk material with same chemical composition which is supported by fact that nanocomposites are more toxic than fine particles or bulk materials with same chemical composition.[10] Recent studies indicated the great potential of silver and gold nanocomposites in biomedical applications including cancer diagnosis and therapy. Hossain et al. shown that silver and gold nanowire induces ROS mediated apoptotic cell death in human pancreatic adenocarcinomas cancer cells whereas Guo et al.[11] suggested that a combination of nanocomposites and anticancer drugs cis-platin may

have synergistic effects on the efficient toxicity in leukemia cancer cell lines. Recently Chan et al. found that the synergistic effect of silver and gold nanocomposites with an anticancer drug verbascoside with an induction of apoptosis with K562 cells. Pietruska et al.[12] found that nanocomposites found a rapid and prolonged activation of hypoxia inducible factor 1-alpha pathway, which is responsible for tumor growth, bronchial carcinomas A-549 Lung cancer cell lines. Although the potential benefits of nanocomposites are considerable and there is distinct need to identify any potential hazard associated with these nanocomposites. Our knowledge about the interaction between nanocomposites and cancer cell lines and effect of these on human health is still infancy. This study was design to examine the cytogenotoxic effect of silver and gold nanocomposites against bronchial carcinomas A-549 Lung cancer cell lines. The goal has been achieved by the analyzing the SRB analysis to obtain IC_{50} value, cell membrane damage, ROS generation, glutathione, (GSH), mitochondrial membrane potential, (MMP), DNA damage, caspase-3 enzyme in A-549 Lung cancer cell lines exposed to different concentration of 15-75μgml^{-1} for the 72 hours of time interval. A-549 Lung cancer cell lines which are obtained from Lung cancer cell lines have been widely used in toxicological/pharmaceutical studies.[13]

Polyethylene glycol) with a hydroxyl group and L-Ascorbic acid with carboxylic end group moieties provide strong interactions with silver and gold nanocomposite sufaces.[14] Till date, little has been known regarding interaction of nanocomposites with living cells. Nanocomposites have small sizes compared to cellular components or proteins and thus may bypass the natural barriers, such as cell membranes, possibly returning in harm to living cells. Therefore, further understanding is necessary considering that these nanocomposites may cause adverse

effects to living cells. Silver and gold nanoparticles are two versatile constituents in biomedical and immunological applications. Au NPs can easily bind with amine and thiol group that has enabled the surface modification with amino acids[15] and DNA.[16] In this approach, Au NPs widely used for cell tracers,[17] biodiagnostics,[18] transfection vectors,[19] drug delivery,[20] and biosensing.[21] In the clinical application, biocompatibility of Au NPs is crucial. Au NPs with size range from 14-100 nm were taken up into mammalian cells and did not indicates any cytotoxicity.[22] The kinetics of cellular uptake has been demonstrated to depend on the physical dimension of Au NPs. Connor *et al.* reported that Au NPs in a diameter range of 18 nm containing a variety of surface modifiers were taken up by cells without causing cytotoxicity.[23] Au NPs in range of 3.5 nm capped by lysine or poly(L-lysine) were found to be bio-compatible and not-immunogenic.[24] Pernod *et al.* reported that the presence of intracellular Au NPs in a size range of 13 nm reduced actin stress fibres and induced major adverse effects on cell viability. Goodman *et al.* demonstrated that cationic Au NPs were moderately toxic whereas anionic Au NPs were nontoxic.[25] Huang and coworkers reported that aggregated Au NPs are more toxic than well-dispersed nanoparticles against HeLa cells.[26] The cytotoxicity is associated with the increase of ROS level and aggregated gold nanoparticles enter into cells *via* macro pinocytosis more easily than well-dispersed ones. Ag NPs may inhibit the segregation of chromosomes. Researchers have observed genotoxicity including DNA damages and chromosomal aberrations in human glioblas-toma cells treated with Ag NPs.[27] Koji Kawata investigated toxic effects of Ag NPs to human hepatoma derived cell line HepG2 that were exposed to Ag NPs at low doses. It was concluded that both "nano-sized particle of Ag" as well as "ionic Ag+" contributed to the toxic effects of Ag NPs.[28] Effects of poly (methacrylic acid)-coated Au NPs on C17.2 neural progenitor

cells, human umbilical vein endothelial cells, and PC12 rat pheochromocytoma cells have shown that higher NP concentrations (200 nM) reduce cell viability mostly through induction of reactive oxygen species, which was significantly induced at concentrations of 50 nM Au NPs or higher. At these concentrations, both actin and tubulin cytoskeletons were deformed and resulted in reduced cell proliferation and cellular differentiation. In terms of cell functionality, the NPs significantly impeded neurite outgrowth of PC12 cells up to 20 nM concentrations.[29]

The cytotoxicity of Au NPs has been described as toxic and nontoxic depending on size, concentration, surface modification and surface charge. The remarkable anti-immunological activity of Ag NPs is a major advantage for the development of products. For medical treatment, Ag NPs were coated on or embedded in the wound dressings, contraceptive devices, surgical instrument and bone-prosthesis.[30] Since the applications of Ag NPs have become more widespread in medicines, the exposure of Ag NPs in the body increases and the consequent toxicological issues becomes important. Hyperthermia from the photothermal effect and the Ag ions released from the LAA-PEG@Ag-Au NCs were both utilized for anti-carcinomatous therapy. Several studies reported that Ag NPs significantly decreased the functions of mitochondria and induced cell-necrosis and apoptosis for several cell types,[31] however researches on interaction of Ag NPs with cells are limited.

Grafting of conducting or block copolymers are some of the effective ways to improve properties and process ability of conducting polymers.[32] In the light of recent researches, attention has been made to prepare Ag-Au nanohybrid composite grafted by polyethylene glycol and coated by L-Ascorbic acid having inherent structural features which yielding distinctive 3D structure with extended conjugated linear

conducting polymer chains resulting in unique electrical as well as optical properties.[33] Furthermore, L-Ascorbic acid coating was applied on the surface of LAA-PEG@Ag-Au NCs to improve the biocompatibility and realize the sustained release of Ag ions which could affect the anti-carcinomatous properties of LAA-PEG@Ag-Au NCs.

Lung cancer, among them 80-85 % cases are non-small cell lung cancer (NSCLC) is at present the leading cause of cancer related mortality in both men and women globally.[34] The adequate therapeutic regimens are largely dependent on an early diagnosis and surgery remains the preferred treatment administered to an early stage patients.[35] cis-platin based doublet chemotherapy has been has commonly been recommended as standard regiment for these advanced patients.[36] Hence understanding the mechanism underlying radiotherapy and chemotherapy failure is of great importance. Tumor stem cell has provided a new insight into the developing strategies for the treatment of malignancies. The emerging evidence indicates that cancer stem cells, (CSCs) contribute to tumor initiation[37], maintenance[38], metastasis,[39] and drug resistance.[37, 40] Till date, CSCs has been identified in several types of malignancies viz. leukemia[41], brain tumor[42], breast[43] and prostate cancer.[44] CSCs has been characterized in lung cancer by using a variety of cell markers including CD133.[45] Although a recent study demonstrated that $CD133^+$ and $CD133^-$ cells contain CSCs in A-549 Lung cancer cell lines[46], indicating the new markers with higher specificity and accuracy in identifying Lung CSCs should be further explored. CD90, (Thy-1) is a 25-37 kDa glycosylphosphatydilnositol (GPI)-anchored glycoprotein expressed mainly in leukocytes and is involved in cell-cell and cell-matrix interaction[47]. CD90 expression was identified in murine breast CSCs[48], primary high grade glioma[49], and in liver malignancy[50]. To survey from literature analysis demonstrated that A-549 Lung cancer cell lines had a stronger capacity for

proliferation and self-renewal and expressed higher level of stem cell markers Sox2 and Oct4 than A-549 adherent cell. So, present study demonstrated the flow cytometry analysis and other analysis to explore whether CD90 would be a marker for an identification of Lung CSCs.

In this context, we reported the synthesis of polyethylene glycol grafted, L-Ascorbic acid-coated silver and gold, (LAA-PEG@Ag-Au NCs) nanocomposites via chemical oxidative technique under high shearing effect homogenizer. The cytogenotoxic effect has been investigated against bronchial carcinomas A-549 lung cancer cell lines. The goal has been achieved by the analyzing the MTT and SRB analysis to obtain IC_{50} value, cell membrane damage, ROS generation, glutathione, (GSH), mitochondrial membrane potential, (MMP), DNA damage, caspase-3 enzyme in A-549 Lung cancer cell lines exposed to different concentration of 10 to 60 μgml^{-1} for the 72 hours of time interval.

7.2. Materials and method

7.2.1. Materials

DMEM (Gibco Invitrogen), FBS US Origin (Gibco Invitrogen), Trypsin (0.25%, Gibco Invitrogen), Trypan Blue (Gibco Invitrogen), DPBS (Gibco Invitrogen), FBS, Silver chloride, (AgCl), gold chloride, ($AuCl_3$), potassium chloride, (KCl), L-Ascorbic acid and (LAA), polyethylene glycol (PEG) were purchased from Sigma Aldrich chemical supplier and used without further purification.

7.2.2. Synthesis of PEG@AgAu-LAA NCs

For synthesis of silver coordinate complex, ($K_3[AgCl_4]$) and gold coordinate complexes, ($K_3[AuCl_6]$), aqueous solution mixtures AgCl and KCl as well as $AuCl_3$

and KCl were in 1:3 molar ratio were continuously stirred for 8 hours at room temperature. Resulting precipitates were filtered, washed with double distilled water and dried at 80 °C in oven. For the formation of LAA-PEG@Ag-Au nanocomposite, 5 mL of 20 mM each of ($K_3[AgCl_4]$) and ($K_3[AuCl_6]$) were mixed with 5 mL 1 mg/mL of polyethylene glycol in a vessel at room temperature for 10 hours with continuous stirring and thereafter 0.1M L-Ascorbic acid solution was added for complete reduction of metal complexes to nanocomposite. The resulting compound was sonicated for homogenization and centrifuged at 10000 rpm for 30 minutes. The extract was washed several times with deionized water and ethanol to remove excess polymer and reducing agent. Thus formed nanocomposite kept in an oven before analysis to remove the moisture and any other gaseous impurities and filled in a sterile micro centrifuge tube for the further characterization.

7.2.3. Characterization

The X-ray diffraction pattern of the product was recorded on Pananalytical's X'Pert Pro X-ray diffractometer in the 2θ range 10 to 80° with a step size of 0.025°. Scanning electron microscope (SEM) images of the material were observed on JEOL 6490 LB equipment at operating electrical energy of 3 kV. Particles shapes and sizes of the materials were examined on JEOL-2100 transmission electron microscope (TEM). The zeta potential of LAA-PEG@Ag-Au NCs was measured using a Zetasizer ZS90 (Nano series Malvern Instrument) at room temperature. Dispersion of nanoparticles was sonicated for 20 minutes and diluted to make a solution with concentration 80 µg/mL in phosphate buffer saline (pH = 7.4). The particle size and size distribution were carried out on a Zetasizer ZS90 (Nano series Malvern Instrument). SERS spectrum of LAA-PEG@Ag-Au NCs, formed at room temperature, was recorded on NSCOM/Raman/Confocal/AFM used for UV/lithography (200 nm) and near field imaging of features as small as 100 nm

Raman spectra and imaging for an excitation wavelength of 532 nm with an extinction coefficient of 8000 $M^{-1}cm^{-1}$. UV-visible absorption spectral analysis was carried out on a Shimadzu UV-3600 spectrophotometer. Brunauer-Emmett-Teller (BET) analysis of the materials was recorded on Belsorp-mini II instrument.

7.2.4. Cytotoxicity Test

7.2.4.1. MTT Assay

To analyze cytotoxicity of synthesized LAA-PEG@Ag-Au, MTT [3-(4,5-Dimethylthiazol-2-yl)-2,5-diphenyl tetrazolium bromide] viability assay was performed as per previously reported protocols. The bronchial carcinoma lung cancer (A-549) cells were seeded in 96-wells plate (5.0×10^3cells/well) and kept undisturbed for 24 h. The cells were treated with 200 µL of varying concentrations of LAA-PEG@Ag-Au NCs (15 to 60 µg/mL) and the sample was incubated in a humid atmosphere of CO_2 at 37°C. After 24 h, 50 µL of MTT solution (1 mg/mL) was added separately to each well and incubated again for 4 h. Then, the media and excess MTT were removed, after which 150 µL of dimethyl sulfoxide (DMSO) was also added. The absorbance of analytes was recorded at 570 nm using the Infinite M200 microplate reader (Tecan Group Ltd., Mannedorf, Switzerland). Samples containing media with and without cells were also analyzed and labeled as 'control' and 'blank', respectively. All the experiments were performed in triplicates. The final organic solvent concentration was 0.3% (v/v). Cell survival (% of control) was calculated relative to untreated control cells.

7.2.4.2. SRB Assay

The sulforhodamine B (SRB) assay is the highly efficient method used to quantify cell density, based on the measurement of protein content of cells (Skehan et al., 1990). The protein bound dye is dissolved in 10 mM Tris base solution for OD

determination at 510 nm using a microplate reader. The study comprising the cellular effects of silver and gold nanocomposites on mesenchymal stem cells, (MSCs) and associated molecular mechanism, which described that the nanocomposites prompted the differentiation of bronchial carcinomas A-549 Lung cancer cell lines by inducing stem cell markers (CD24, CD44, CD90, CD133, CD147, CD166, CD326 etc.). The culture of A-549 human lung cancer cells (~ 100000 cellmL^{-1}) were taken in 10% fetal bovine serum, (FBS)-supplemented Dulbecco's Modified Eagle's Medium (DMEM) in a 24-well microtitre plate. Different amounts of LAA-PEG@Ag-Au NCs (formed at room temperature) were suspended in deionized water to make solutions with concentration from 10 to 60 µg mL^{-1}. Homogenization of each solution was carried out with an ultrasonic processor (LABSONIC® M, Sartorius StedimBiotech GmbH) for 15 minutes and added separately to cultures, keeping one blank as reference. The cultures were incubated for 24 hours in an incubator with 5% CO_2 in a humid atmosphere at 37 °C. After incubation, the cells were removed from the culture by trypsinisation and washed a coupled by Dulbecco's phosphate-buffered saline (PBS; pH: 7.4) to remove the residual presence of serum. The cells were again suspended in PBS, and aliquots of 20µL were prepared from all the cultures. Equal amounts (v/v) of pre-filtered 0.4% trypan blue stain added to the aliquots and were put aside to settle for 1 minute. To determine the cell viability, the samples were observed on an inverted microscope in a Fuchs-Rosenthal Haemocytometer. The results of cytotoxicity were expressed by plotting cell viability histogram and curve and analyzed by IC_{50} value.

7.2.4.3. Dose dependent induction cell membrane damage due to silver and gold nanocomposites

LDH is an enzyme extensively present in cytosol that converts lactate to pyruvate. When plasma membrane integrity is disrupted LDH leaks into culture

medium and its extracellular levels are elevated depending on the toxicity of nanocomposites. Consequently, higher LDH value in culture media in a dose dependent manner. A significant negative correlation was also observed between LDH leakage and MTT cell viability.

7.2.4.4. Dose dependent induction of ROS generation due to silver and gold nanocomposite exposure

Reactive oxygen species, (ROS) is continually generated and eliminated in biological systems, that play an important role in a variety of normal biochemical functions and abnormality in their functions results in pathological processes. Excessive production of ROS in the cell is known to induce apoptosis.[51] ROS generation has been shown to play an important role in apoptosis induced by treatment with nanomposites.[52] The c-Jun N terminal kinase (JNP) is a member of mitogen activated protein (MAP) kinase family and plays a pro-apoptotic functions in response to various cellular stresses.[53] JNK is strongly activated by ROS or a mild oxidative shift of intracellular thiol/disulphide redox state leading to apaotosis.[54] A number of research groups from the global era, have investigated the toxicity of nanocomposites in respect to cell death via ROS generation[55] little is known about the mechanism of nanocomposites mediated toxicity. Our results suggested that the composites risen the production of intracellular ROS and decreased glutathione levels, leading to an apoptosis.

The higher production of ROS in cells due to pollutants has been suggested as signaling molecules involved in initiation and execution of DNA damage[56] and apoptosis.[57] Both fluorescence microscopy and quantitative data revealed that silver and gold nanocomposites in a range of 15 to 60 μgml^{-1} induced intracellular ROS generation in a dose dependent manner.

7.2.4.5. Dose dependent depletion of GSH levels due to silver and gold nanocomposites

The depletion of GSH which is indicative of ROS generation has also been implicated in the oxidative damage of cellular macromolecules such as protein[58] and DNA[59]. The evaluation of GSH levels bronchial carcinomas A-549 Lung cancer cell lines has been analyzed in a concentration range of 15-60 $\mu g ml^{-1}$ for the time tenure of 48 hours and results showed that the GSH levels were depleted with all concentration range of nanocomposites. We also observed the inverse correlation of ROS with GSH (R^2=0.92) and MTT (R^2=0.93) cell viability.

7.2.4.6. Dose dependent depletion of MMP due to silver and gold nanocomposites exposure

It is well known that during apoptosis, the MMP of cells decreases. Nanocomposites induces differences in MMP in bronchial carcinomas A-549 Lung cancer cell lines were recorded in terms of fluorescent intensity of mitochondria specific dye Rh-123.[60] Both fluorescent microscopy and quantitative data revealed that nanocomposites decreased the MMP of A-549 Lung cancer cell lines in a dose dependent manner.

7.2.4.7. Dose dependent induction of DNA damage due to silver and gold nanocomposite exposure

The sign of genotoxicity is the induction of DNA damage by using the FACS analysis, a widely used method for the detection as well as measurement of DNA strand breaks.[61] The analysis was carried out using A-549 Lung cancer cell lines

against silver and gold nanoomposites at a concentration range of 15-60 μgml^{-1} for 72 hours. A dose dependent increase in DNA damage was observed in silver and gold nanocomposite treated cell lines as evident by an increase in 1% tail DNA and Olive oil treatment (Fig.17). We also found a significant positive correlation between ROS and % tail DNA (R^2=0.98).

7.2.4.8. Dose dependent induction of apoptosis due to silver and gold nanopcomposite

RT-PCR was used to analyze the messenger RNA (mRNA) levels of apoptotic gene caspase-3 in bronchial carcinomas A-549 Lung cancer cell lines exposed to silver and gold nanocomposites at a concentration of 15-60 μgml^{-1} for 72 hours. It is observed from the histogram that expression of gene in a dose dependent manner. In agreement with the mRNA result, it is also seemed out that nanocomposites induced the activity of caspase-3 enzyme in accordance with dose dependent manner.[62] A significant positive correlation was also confirmed between the ROS and caspse-3 enzyme (R^2=0.95).

7.3. Computational Details

7.3.1. Optimization

The structure of the LAA-PEG@Ag-Au NCs was optimized by NWChem[63] software using the Def2QZVP [&] basis set.

7.3.2. Molecular Docking

Docking operation was estimated by using version 4.2 of AutoDock program package and Lamarckian genetic algorithm (LGA) in an Autodock 4.2, proven to be a

most reliable, effective and advantageous.[64] LAA-PEG@Ag-Au NCs was docked with both DNA and protein. The docking was performed by treating the DNA and the proteins as rigid receptor molecules and LAA-PEG@Ag-Au NCs was treated as a flexible ligand. Composites have gained attention for their binding energies with the targeted DNA and proteins. PDB (Protein data bank) format of the DNA with PDB ID 1BNA and proteins with PDB ID 21TW, 21TX, 21TY, 2J6M, and 4LQM were collected from RSCB protein data bank.[65] 1BNA consisting the structure of B-DNA found in the human body and protein PDB IDs are crystal structure of EGFR kinase domain. Mutation in EGFR kinase is a cause of non-small-cell-lung cancer cell lines.[66]

7.3.3. DNA Docking

LGA was used in the docking study of composites with double-stranded DNA with base pairs 5'-CGCGAATTCGCG-3'. The DNA duplex receptor from Protein Data Bank, (PDB) contained 12 base pairs. The water of crystallization and hydrogen atoms were removed and hydrogen atoms assimilated via Chimera USCF software.[40] The grid box size was set at 50, 50 and 100 Å for x, y and z respectively and grid centre were set to14.748, 20.984 and 8.809 for x, y and z respectively. The Gasteiger charges were added to the complex by Auto Dock tools (ADT) before performing docking calculations. In metals, modifications were completed in the parameter file to include silver (Ag) and Gold (Au) LAA-PEG@Ag-Au NCs. The lowest dock confirmation, by Auto Dock scanning functions, was preferred as the binding mode.

7.3.4. Protein Docking

Grid boxes of various dimensions were used to prepare grid maps using Auto-Grid for each protein. The Gasteiger charges were added to the complex by Auto Dock Tools (ADT) before performing docking calculations. Lamarckian genetic

algorithms, as implemented in Auto Dock, were employed to perform blind docking calculations. All other parameters were default settings. For metals, modifications were done in the parameter file to include silver (Ag) and Gold (Au). According to the Auto Dock scoring function, the lowest energy docked conformation was selected as the binding mode.

7.4. Results and discussion

UV-visible spectrum of LAA-PEG@Ag-Au shows a characteristics peaks of 390 nm which attributed to the conjugated composite formation (Fig.7.1.a).[67] Optical band gap energy of formed nanocomposite has been elucidated using Tauc's relation[67]:

$$\alpha h\nu = A(h\nu - E_g)^n$$

Where, α is absorption coefficient, A is energy independent constant and $h\nu$ is photon energy. E_g is the optical band gap energy and the exponent n depends on the nature of the electronic transition. The coefficient, α can also be calculated by using Beer-Lambert relation.[68]

$$\alpha = 2.303 \times \frac{A}{L}$$

Where, L is the path length and A is absorbance. The band gap energy, E_g value of composite has been elucidated from the plot of $(\alpha h\nu)^2$ versus $h\nu$ as shown from Fig. 7.1.b. The band gap was estimated by extrapolating of a straight line to $(\alpha h\nu)^2 = 0$. The optical band gap energy of LAA-PEG@Ag-Au NCs is calculated to be 2.6 eV, which is much lesser than pure individual metal nanoparticles.[69]

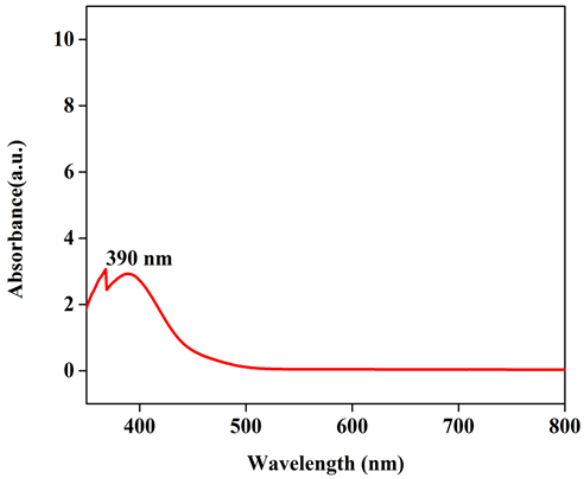

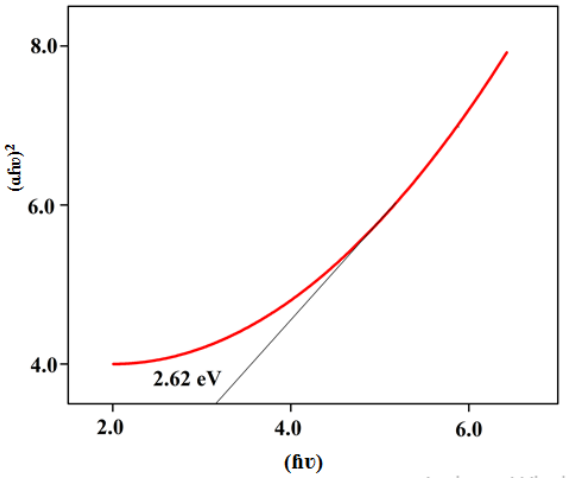

Fig.7.1.a. UV/Visible spectra of Ag-Au NCs. **Fig.7.1.b. Band gap analysis of Ag-Au NCs.**

The FTIR spectral analysis of the LAA-PEG@Ag-Au NCs was carried out in a range of 500-3500 cm^{-1} at room temperature to analyze the interaction of nanocomposite with functional groups of L-Ascorbic acid and polyethelene glycol. The graph shows an absorption peak at 3428 cm^{-1} due to –OH stretching of carboxyl group (Fig. 7.2).[70] The broadness of this peak indicated the presence of hydrogen bonding between LAA-PEG@AgAu NCs. The peaks at 1740 and 1628 cm^{-1} is due to C=O of five membered lactone ring and C=C stretching of L-Ascorbic acid respectively. These peaks are red shifted compared to those of pure L-Ascorbic acid due to its adsorption on the nanoparticle's surface. The peaks at 680 cm^{-1} are due to the out of plane bending vibration of –CH of PEG. The FTIR analysis of LAA-PEG@Ag-Au NCs shows a characteristics peak at 1094 cm^{-1} due to the fingerprint region of the nanocomposite. The characteristics band at 1528 cm^{-1} is due CH_2 scissoring and band at 1740 $cm^{-1}$is due to C=C stretching vibration of L-Ascorbic acid ring residue.[71]

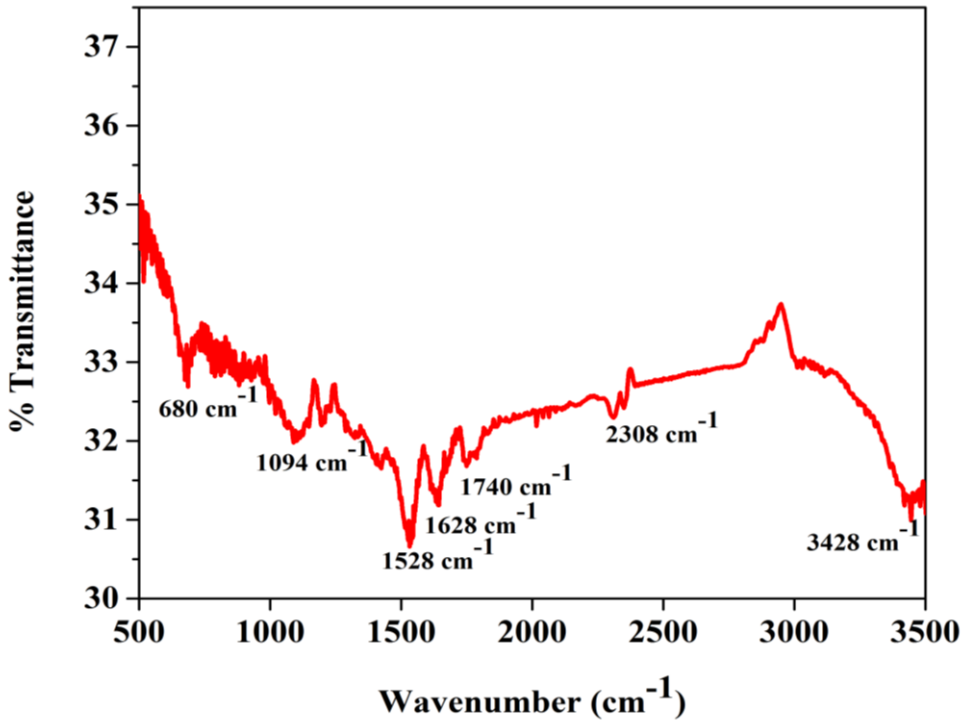

Fig.7.2. FTIR spectrum of LAA-PEG@Ag-Au nanocomposite.

Vibrational analysis of LAA-PEG@Ag-Au NCs has further been examined using Raman spectral measurement excited at a wavelength of 532 nm with an extinction coefficient of 8000 $M^{-1}cm^{-1}$. The SERS spectrum of the LAA-PEG@Ag-Au NCs has been obtained by plotting the graph between intensity versus Raman shift. In the Raman spectrum (Fig. 7.3) a peak observed at 480 nm is due to Ag-Au NC banding with oxygen from hydroxyl groups of PEG chains.

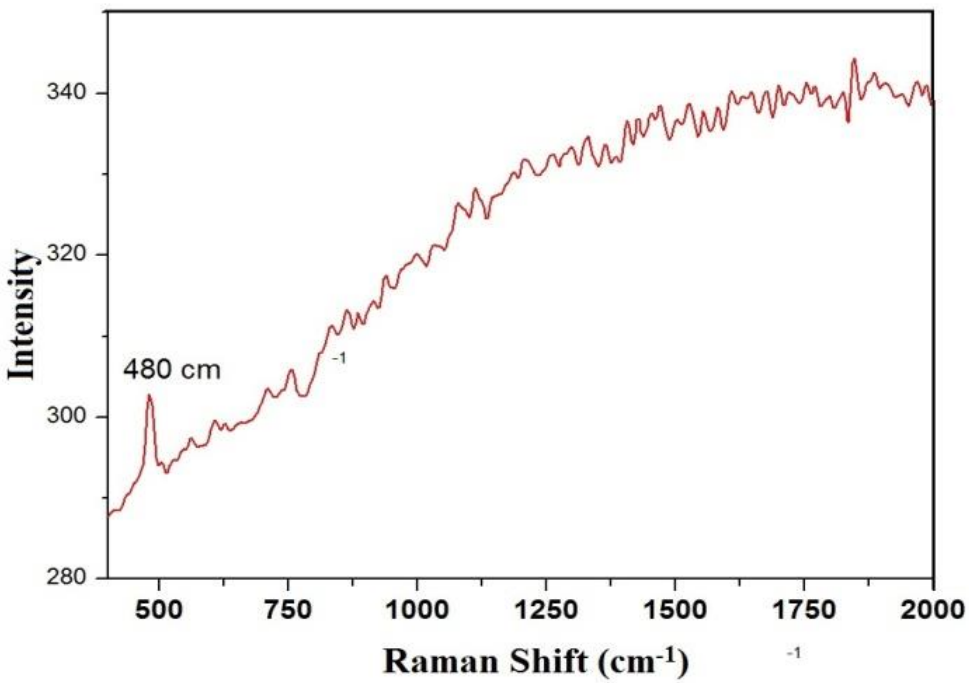

Fig. 7.3. Raman spectrum of LAA-PEG@Ag-Au nanocomposite

The crystal phase and purity of LAA-PEG@Ag-Au NCs were analyzed using X-ray diffraction analysis shown in Fig. 7.4. The diffraction peaks for LAA-PEG@Ag-Au NCs at a 2θ range of 38.03, 44.17, 65.07, and 78.02 correspond to (111), (200), (220), (311) lattice planes respectively (JCPDS file no: 04-0784). The diffraction pattern obtained agreed with earlier report.[72] The Bragg's equation reveals face centered cubic (fcc) crystalline lattice nature of formed nanocomposites (Fig. 7.4). Lattice planes at (111) and (200) clearly indicate LAA-PEG@Ag-Au NCs as typical monoclinic cuprite phase.[73] Furthermore, the obtained XRD peaks are intense and broadened indicating the formation of good crystalline and small-sized LAA-PEG@Ag-Au NCs. From the graph it has been found that crystalline size corresponding to (111), (200) planes are larger than rest of the peaks, indicating the orientation of nanocomposites preferentially towards (111) facet and particles growth is anisotropic.

The mean crystallite size can be determined by Scherrer's formula, considering that the XRD line broadening caused due to decreasing crystallite size. The average particle size of nanocomposites has been determined to be 10.1 nm using above formula which is in agreement to the particles diameter observed in the TEM images.

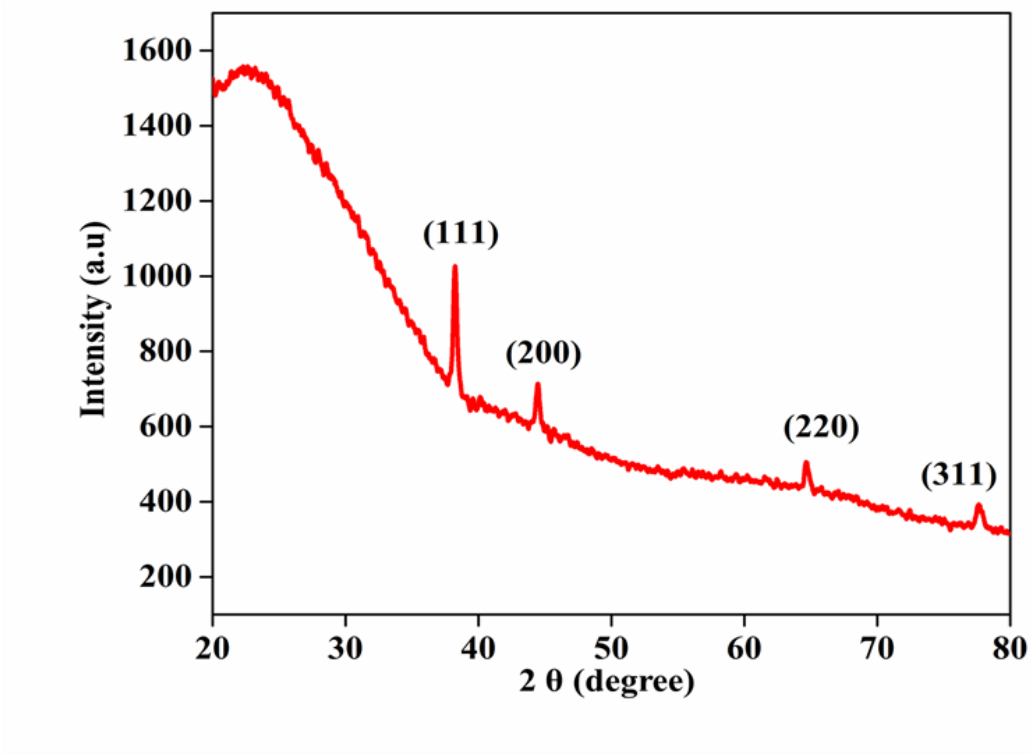

Fig.7.4. XRD pattern of LAA-PEG@Ag-Au NCs.

Morphological and compositional study of as synthesized material was performed by SEM and EDX analyses. In the SEM micrographs 3D sponge shape LAA-PEG@Ag-Au structures are observed (Fig. 7.5 a). The micrographs show that surface of sponge is composed of rods and spheres like cluster groups. In the corresponding EDX pattern, the peaks due to Ag and Au observed indicating the formation of phase pure LAA-PEG@Ag-Au NCs (Fig.7.5 b). The morphology of the product has further been analyzed by high resolution FE-SEM analysis as shown in Fig. 7.6 a-d. FE-SEM images revealed that sponge shape structure is composed of variable shaped like rod (80-100 nm long and 10-20 nm diameters), polyhedral

structures and 10-15 nm diameter spherical particles (Fig. 7.6 a-d). FE-SEM images further revealed that most of the LAA-PEG@Ag-Au NCs have similar shapes and sizes, indicating uniformity throughout the sample. The representative TEM images, shown in Fig. 7.7 a-b, further clarify shape, size and structure of LAA-PEG@Ag-Au NPs. The TEM images indicate that Ag-Au nanocomposites have initially grown in varieties of shapes, like spheres, rods and polyhedral structured nanoparticles. The dimension of these initially grown NPs is in the similar range i.e. 10-20 nm in diameter however some particles have grown anisotropically, probably due to presence of capping agents PEG/LAA. These initially grown different shapes NPs agglomerated to evolve ultimately sponge shape LAA-PEG@Ag-Au NCs as reported in earlier studies.[72a, 74]

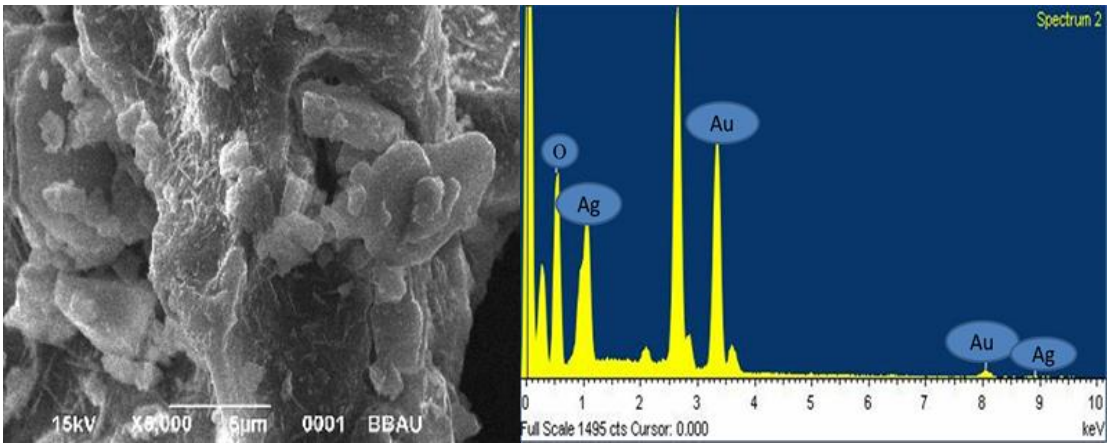

Fig.7.5 a-b. SEM micrograph and EDX pattern of LAA-PEG@Ag-Au nanocomposite.

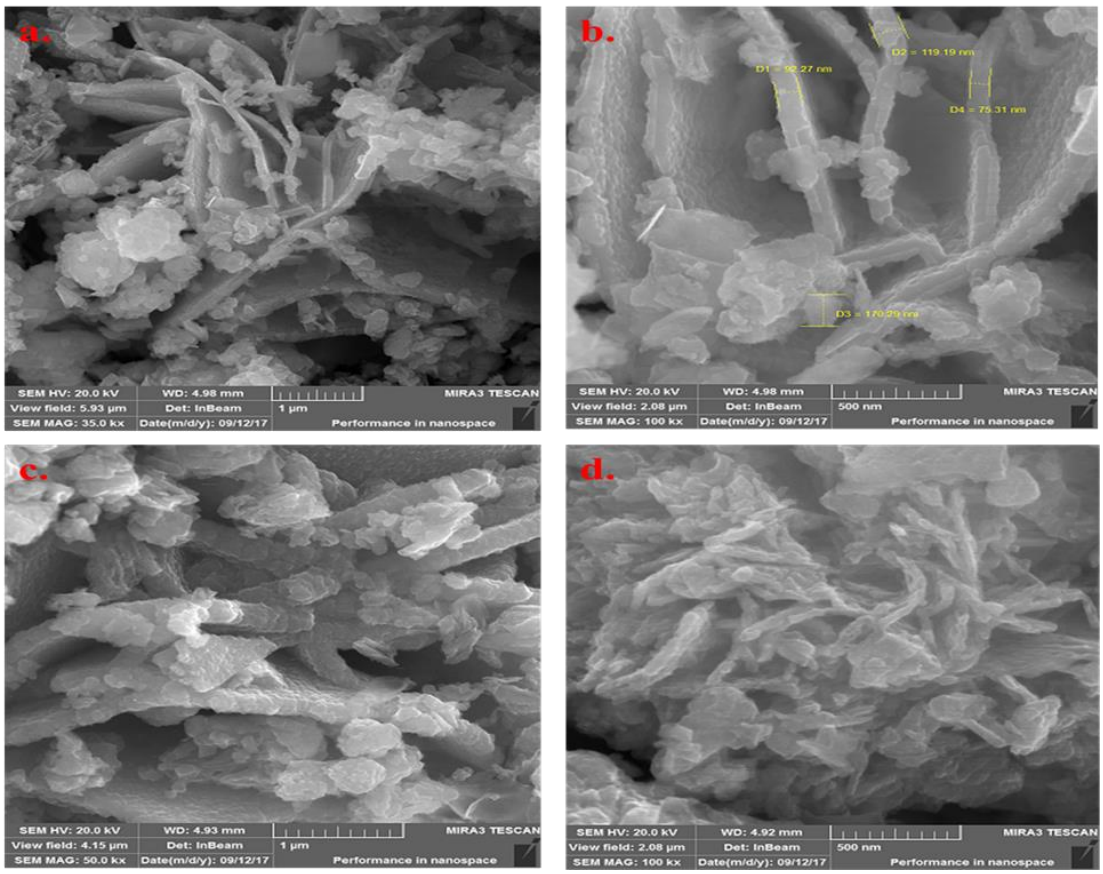

Fig. 7.6. a-d. FESEM images of LAA-PEG@Ag-Au nanocomposite.

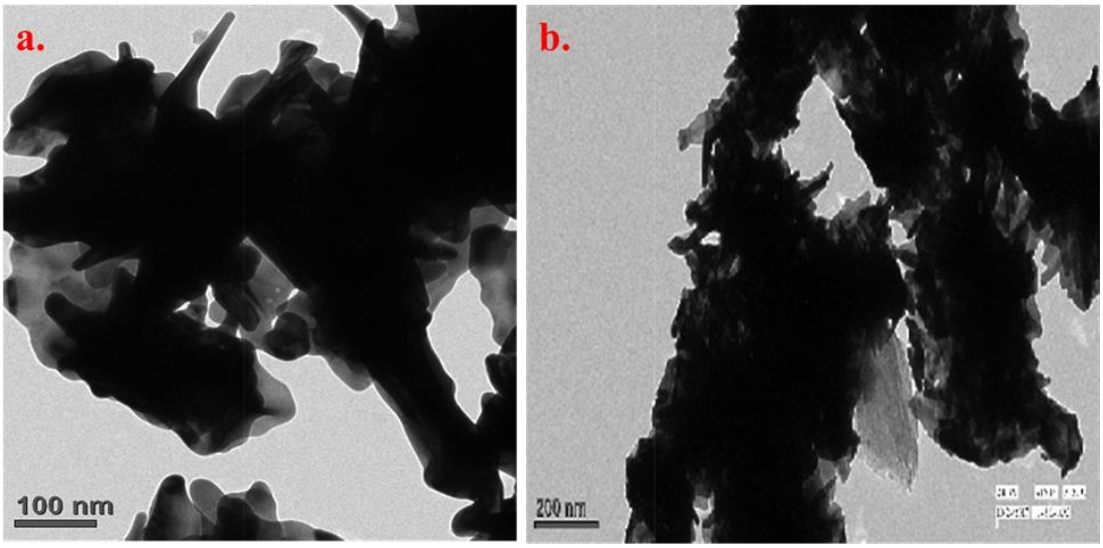

Fig.7.7 a-b. TEM images of LAA-PEG@Ag-Au nanocomposite.

The Zeta potential curve of LAA-PEG@Ag-Au NCs was determined in the range of -100 to +100 mV. Zeta potential analysis described stable nature of formed

nanocomposites at -28 ± 15mV which indicated that the surface is negatively charged and thus maintained their good stability (Fig. 7.8). The particle size analysis of formed LAA@IONP-PEG was analyzed by particle size distribution curve shown in Fig. 7.9. The curve shows that the size of particles is distributed in a range of 70-100 nm while the maximum population falls at 80 nm.

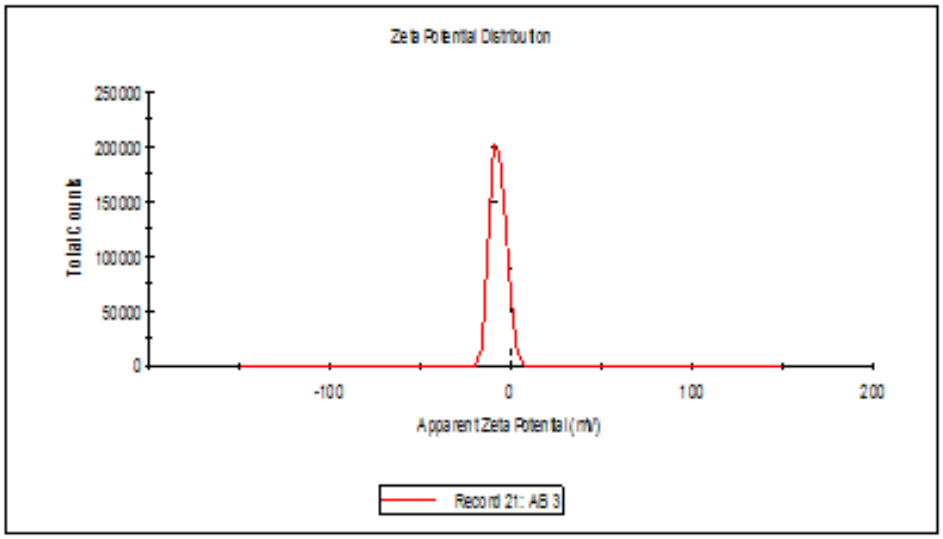

Fig. 7.8. Zeta potential analysis of LAA-PEG@Ag-Au NCs.

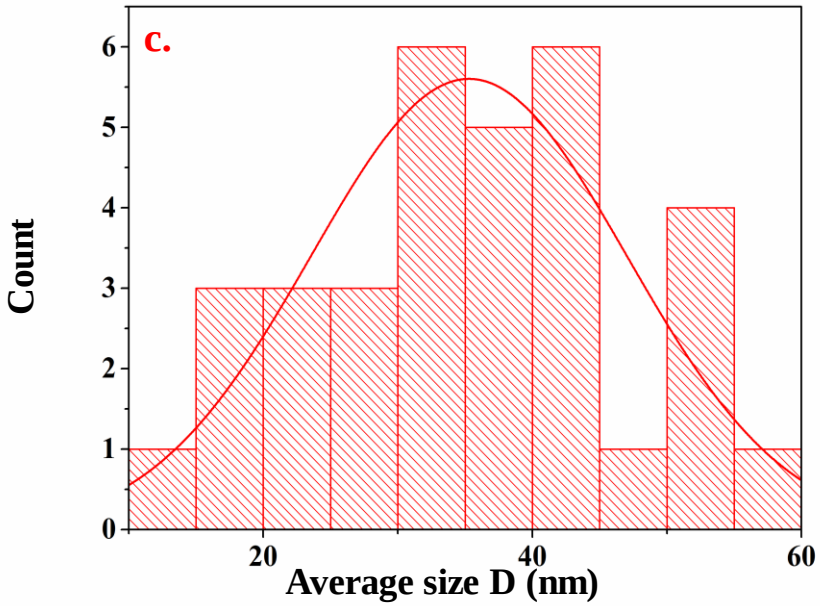

Fig. 7.9. Particle distribution of LAA-PEG@Ag-Au NCs

The specific surface area and pore-size distribution of was analyzed via N_2 adsorption-desorption isotherm plots (Fig. 7.10 a-b). A type-IV isotherm and H1-type hysteresis loop were confirmed for LAA-PEG@Ag-Au NCs (Fig. 7.10 a), suggesting mesoporosity.[75] The specific surface area obtained via Brunauer-Emmett-Taylor, (BET) was approximately, 55 m^2g^{-1}. Barrett-Joyner-Halenda (BJH) method was applied to estimate the average pore diameter and was found to be 8 nm (Fig. 7.10 b). The high surface area of LAA-PEG@Ag-Au NC indicates a large number of catalytic sites and is thus expected to show high catalytic properties.[76]

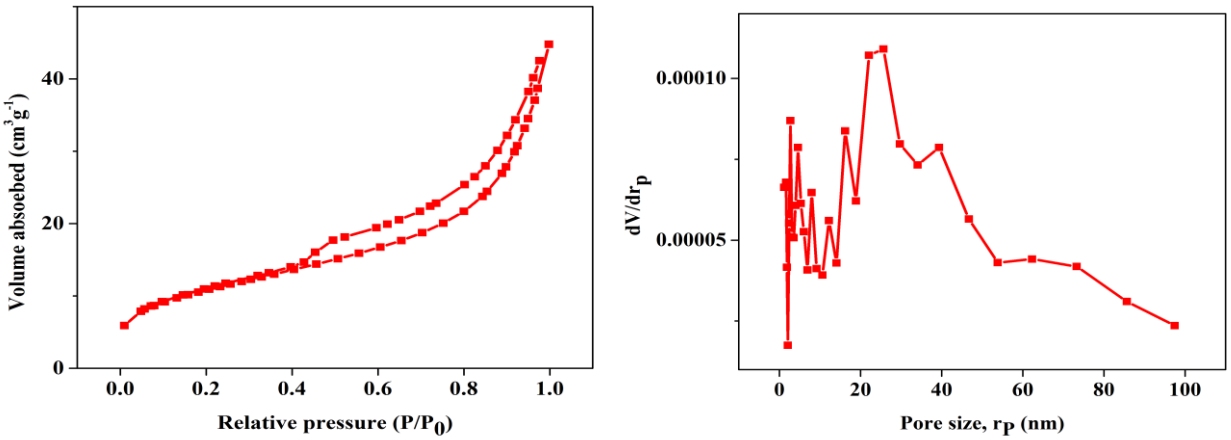

Fig. 7.10 a-b. BET surface analysis and BJH plot of LAA-PEG@Ag-Au NCs.

7.4.3. Molecular Docking Studies of PEG@Ag-Au-LAA NCs with DNA

7.4.3.1. Computational details

7.4.3.2. Dataset

7.4.2.1. DNA

The PDB format file of DNA sequences with PDB ID 1BNA was downloaded from RCSB Protein Data Bank.[77] Ligands and water molecules were removed from DNA sequence using CHIMERA.[65]

7.4.2.2. Drugs

The structure of LAA-PEG@Ag-Au NCs cluster was taken after optimization. Fig.7.11 shows the chemical structure of the cluster.

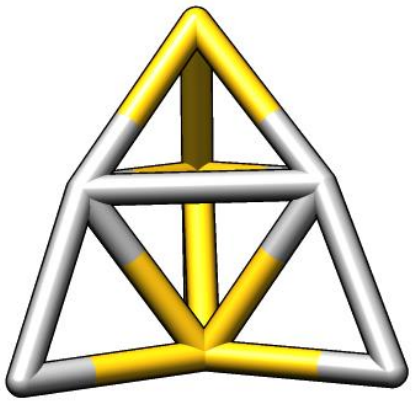

Fig.7.11. Three dimensional structure of Ag-Au NCs

7.4.3.3. Molecular Docking

AutoDock4.2 was used for molecular docking simulations using Lamarckian Genetic Algorithm (LGA).[78] Docking were performed using DNA sequences as a rigid receptor molecule, whereas LAA-PEG@Ag-Au NCs cluster was treated as a flexible ligand. The receptor and ligand files were prepared for docking using Auto Dock Tools (ADT).[65,79] The grid box size was set at 50-50 and 100 A˚ for x, y and z respectively, and the grid centre was set to 14.748, 20.984 and 8.809 for x, y and z respectively. The Gasteiger charges were added to the complex by AutoDock Tools (ADT) before performing docking calculations. Lamarckian genetic algorithms, (LGA) as implemented in Auto Dock, were employed to perform blind docking calculations. For metal, modifications were done in the parameter file to include LAA-PEG@Ag-Au NCs. The lowest energy docked confirmation, according to the AutoDock scoring function, was selected as the binding mode (Figure 7.12).

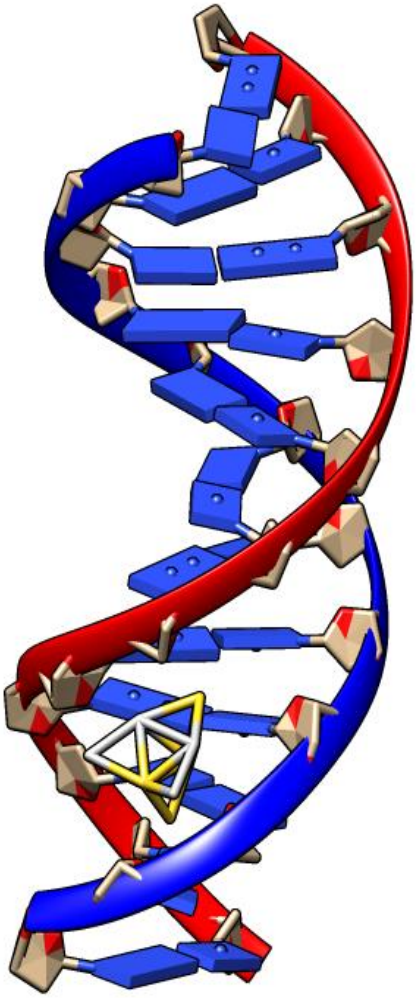

Fig.7.12. Minor groove binding of Ag-Au cluster with 1BNAs

7.4.3.4. Result

The figure shows the Minor groove binding of LAA-PEG@Ag-Au NCs-cluster with 1BNA present in lung cancer A549 cell lines. Ag-Au cluster binds in the minor groove of the DNA sequences concluding that cluster is minor groove binder. The computationally calculated binding energy is -0.14 kcal/mol, which indicates this it is an effective drug against cancer cells (Figure 7.13).

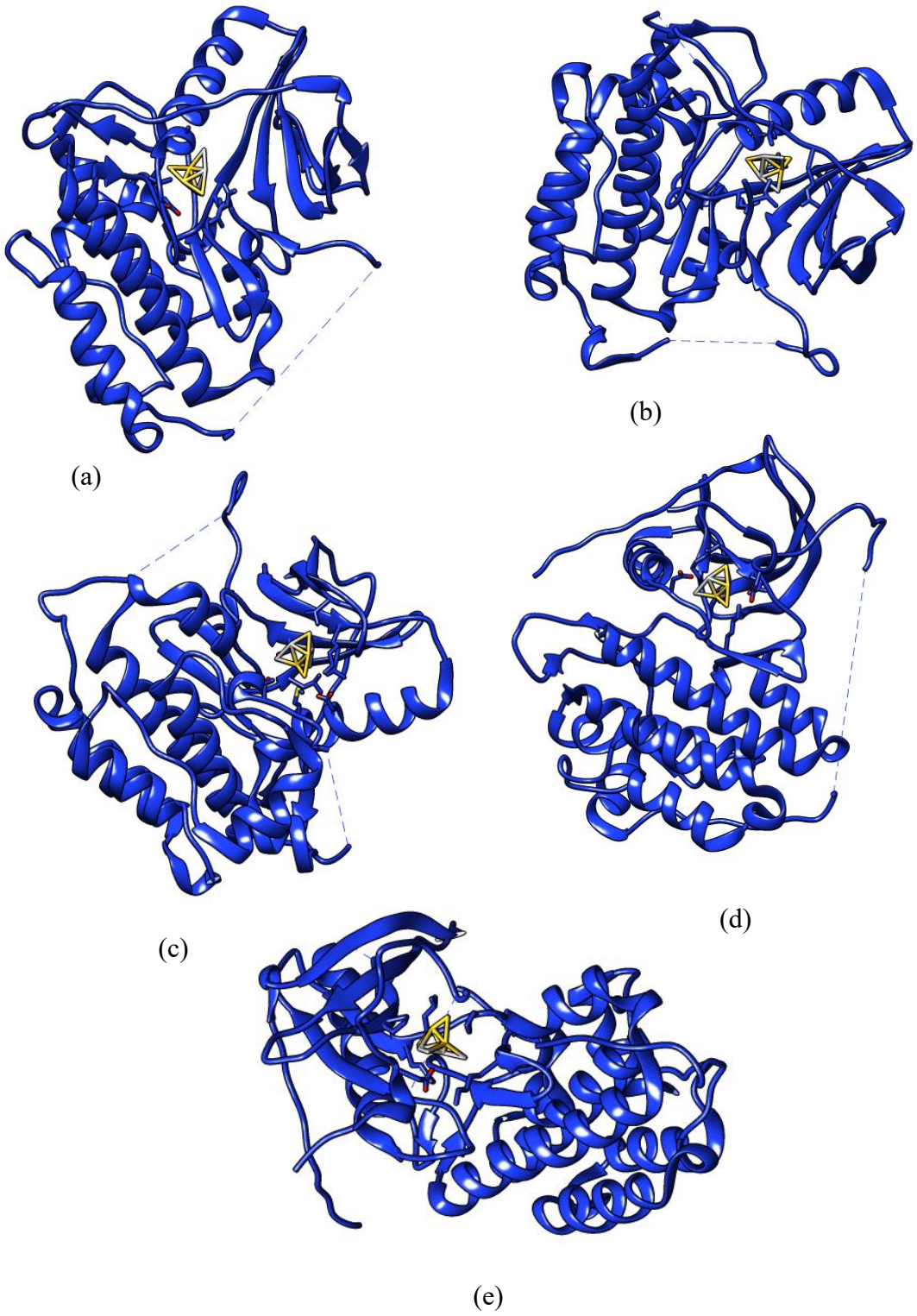

Fig.7.13. Interaction of Ag-Au cluster with (a) 2ITW (b) 2ITX (c) 2ITY (d) 2J6M (e) 4LQM

7.4.3.5 Molecular Docking Studies of LAA-PEG@Ag-Au NCs with Lung Cancer proteins

7.4.3.5.1. Computational Details

7.4.3.5.2. Dataset

DNA

The PDB format file of proteins with PDB ID 2ITW, 2ITX, 2ITY, 2J6M and 4LQM were downloaded from RCSB Protein Data Bank.[80] These are crystal structures of the EGFR kinase domain. Mutations in the EGFR kinase are a cause of non-small-cell lung cancer.[65, 80-81] Ligands and water molecules were removed from each protein using CHIMERA.[82]

Drugs

The structure of LAA-PEG@Ag-AuNCs cluster was taken after optimization. Figure 7.11 shows the chemical structure of the cluster.

7.4.3.5.3. Molecular Docking

AutoDock4.2 was used for molecular docking simulations using Lamarckian Genetic Algorithm (LGA).[83] The docking was performed using Protein as a rigid receptor molecule, whereas LAA-PEG@Ag-AuNCs cluster was treated as a flexible ligand. The receptor and ligand files were prepared for docking using Auto Dock Tools (ADT).[84] Grid boxes of various dimensions were used to prepare grid maps using Auto-Grid for each protein. The Gasteiger charges were added to the complex by Auto Dock Tools, (ADT) before performing docking calculations. Lamarckian genetic algorithms, as implemented in Auto Dock, were employed to perform blind docking calculations. All other parameters were default settings. For metals,

modifications were done in the parameter file to include LAA-PEG@Ag-Au NCs. According to the Auto Dock scoring function, the lowest energy docked conformation was selected as the binding mode.

7.6.3.5.4. Result

The computationally calculated binding energies of all protein-drug complexes are given in Table 1. From the tabulated data it is very much clear that binding energies of all EGFR proteins with LAA-PEG@Ag-Au NCs cluster are of the same range. The binding modes and geometrical orientation of all compounds were almost identical; suggesting that all the inhibitors occupied a common cavity in the receptor. The lowest binding energy is with 2ITY complex. Molecular Docking gives the best and stable conformations of the ligand with proteins in the receptor active pocket. Figure.7.13 shows the interaction of the ligand with proteins.

In silico studies revealed the entire synthesized molecule showed good binding energy toward the target protein. LAA-PEG@Ag-Au NCs cluster binds in the pocket of the proteins (Table1).

7.4.3.5.5. Molecular Docking Results

LAA-PEG@Ag-Au NCs binds in the minor groove of the DNA sequences concluding that cluster is minor groove binders. The computationally calculated binding energy[85] is -1.09 kcal/mol. So it can prove to be an effective drug against carcinomas therapy and other pathogenic disorders. Fig. 7.12 shows the Minor groove binding of Ag-Au cluster with 1BNA.

The computationally calculated binding energies of all protein-drug complexes are summarized in Table1, which shows a very much clearance with

all EGFR proteins with LAA-PEG@Ag-Au NCs of all ranges. The binding modes and geometrical orientation of all compounds are almost identical suggesting that all inhibitors have occupied a common cavity in the receptor. The lowest energy is estimated with 2J6M complex. Molecular Docking gives best and stable conformation of the ligand with protein in receptor active pocket (Fig. 7.13).

In silico studies revealed the entire synthesized molecule showed good binding energy toward the target proteins where LAA-PEG@Ag-Au NCs binds in the pocket of the proteins.

Table 1: Binding energies of protein-drug complexes

S.No.	Protein	Binding Energy, (kcal/mol)
1	21TW	-1.28
2	21TX	-1.23
3	21TY	-1.26
4	2J6M	-1.39
5	4LQM	-1.28

7.5. In Vitro cytotoxicity assay

The MTT assay was performed to investigate the cytotoxicity of synthesized LAA-PEG@Ag-Au NCs against bronchial carcinoma A-549 lung cancer cell lines. The results were analyzed by plotting percentage cell viability *verses* concentration graph and IC_{50} value (Fig. 7.14-7.15). 15-60 µg/mL concentrations LAA-PEG@Ag-Au NCs were added to cell lines for 24 hrs incubation period at 37 °C temperature. A significant abatement in cell viability has been observed in the treated cells lines showing LAA-PEG@Ag-Au NCs as a potential anticancer agent for bronchial

carcinomas A-549 Lung cancer cell lines. The standard graph has been plotted between percentage cell viability versus concentration of nanocomposite and IC_{50} calculation was done (Fig.7.14.a-b). The microscopic observation of cells at an increasing concentration of L-Ascorbic acid-coated LAA-PEG@Ag-Au NCs was done along with appropriate control (Fig. 7.15 a-e). The A-549 Lung cancer cell morphology was gradually altered with an increased concentration of LAA-PEG@Ag-Au NCs. A-549 cell lines, when treated with nanocomposites inhibited the proliferation of cell lines within dose-dependent and time-dependent manner. The morphology altered slightly with treatment of 15µg/mL LAA-PEG@Ag-Au NC. Alteration of morphology intensified with addition of 60µg/mL of nanocomposite. Cell debris was found in the cell with 60 µg/mL treated nanocomposite with complete destruction of cells, indicating significant anticancer activity of LAA-PEG@Ag-Au NCs. However, there is a significant statistical difference in every condition when compared to the negative control. The number of live cells that were quantified from microscopic images is listed in Fig.7.15 a-e.

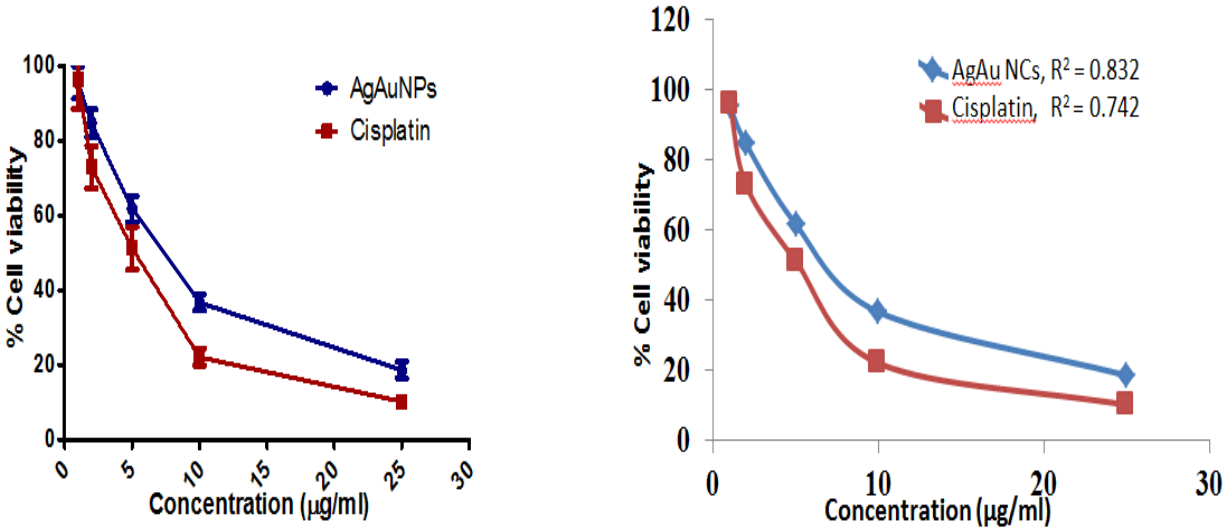

Fig. 7.14 a-b. IC_{50} value of Ag-AuNCs against A-549 Lung cancer cells.

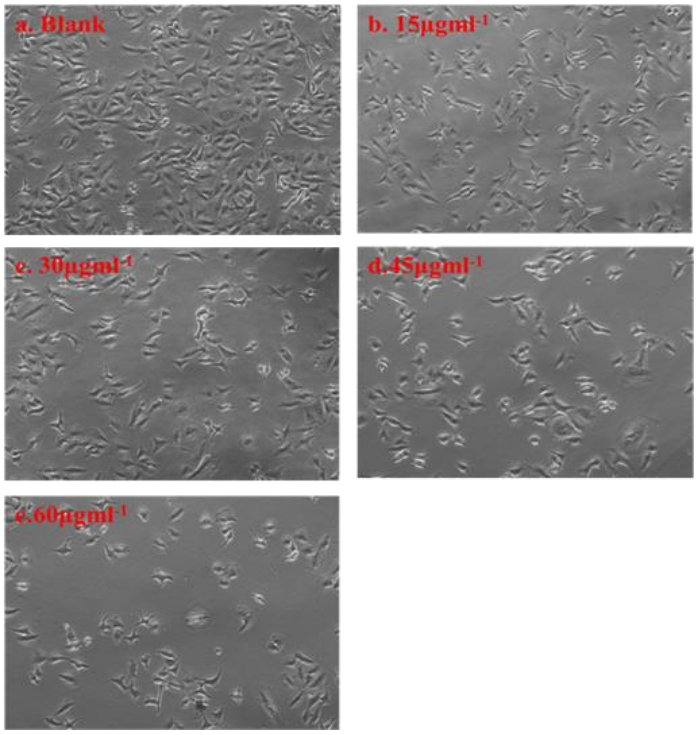

Fig.7.15 a-e. Microscopic images of A-549 Lung cancer cell lines.

In our study we found that treatment of bronchial carcinomas A-549 Lung cancer cell lines with LAA-PEG@Ag-Au NCs has induced cytotoxicity, genotoxicity and oxidative stress in A-549 Lung cancer cell lines. Our results suggested that bronchial carcinomas A-549 Lung cancer cell lines are more susceptible to A-549 Lung cancer cell lines. The SRB assay represent the damage in mitochondrial and lysosomal membranes,[86] that eventually triggers cell death,[87] These assays serve as sensitive and integrated measures of cell integrity and of the inhibition of cell proliferation. SRB assay results are consistent with the observed low MMP in cells exposed to nanocomposites. Damage to lysosomal membrane is known to release lysosome protease into intracellular spaces which affects the neighboring cells and triggers cell death due to apoptosis.[88] LDH leakage from cell is further evidence for both penetration of nanocomposites into cell[89] and cell membrane damage.[90] A significant reverse correlation between MTT and LDH was also observed (Fig. 7.16).

ROS generation is likely to be most effective mechanism for the nanocomposite toxicity as these increase ROS production[91] and thereby cause interference in biological antioxidant defense system.[92] ROS induce DNA damage including a multitude of oxidized base lesions, a basic sites and single and double strand breaks, all of which can be cytotoxic[93] and mutagenic.[94] In this study we examine the toxicity of nanocomposites of bronchial carcinomas A-549 Lung cancer cell lines using a number of stem cell markers (CD24, CD44, CD90, CD133, CD147, CD166, CD 326) and concluded that nanocomposites induced the cytotoxicity in A-549 Lung cancer cell lines via oxidant generation and antioxidant depletion. Indeed nanoconposites shown to generate ROS (oxidant) and GSH (antioxidant) depletion in A-549 cell lines in a dose dependent manner. Furthermore the negative correlation between the ROS and GSH indicated that free oxygen radical species were generated by exposure to nanocomposites, which reduced intracellular antioxidant GSH levels. However a strong correlation between the cell viability and increased ROS level shows that higher production of ROS and concomitant decrease in antioxidant such as GSH scavenge free oxygen radical appear to be underlying mechanism of nanocomposites in A-549 Lung cancer cell lines.

FACS analysis assay was used to analyze the DNA damage caused by nanocomposites in A-549 Lung cancer cell lines. The assay is able to detect the single strand breakage or other lesions such as alkali-labile salts, DNA cross-links[95] and incomplete excision repair events.[96] The technique offers considerable advantage over other cytogenetic method like chromosome aberration, sister chromatid exchanges and micronuclear test used to detect DNA damage as cells do not need to mitotically active for the FACS analysis assays.[97] Therefore this assay has been widely used in the field of genetic toxicology.[98] We also found a strong positive correlation between

the DNA damage (% tail DNA) and ROS suggesting that oxidative stress may be one of the cause to damage DNA in nanocomposite toxicity. Studies have shown that ROS work as signaling molecules for initiation[99] and execution of the apoptotic pathway.[100]

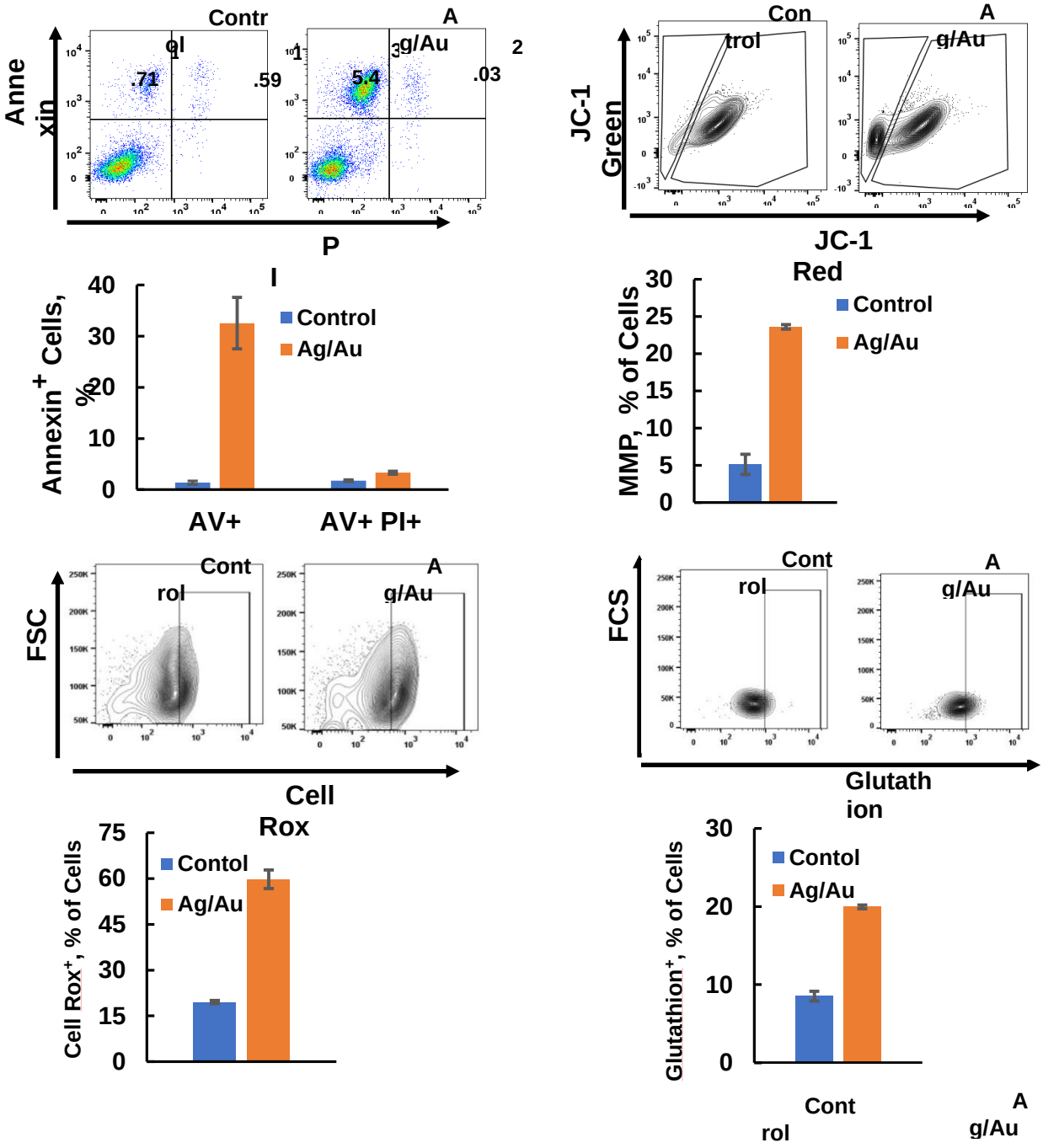

Fig.7.16. SRB, MMP, ROS analysis of A-549 Lung cancer cell lines.

Conclusion

Synthesis of LAA-PEG@Ag-Au NC has been successfully synthesized by using the simple sonochemical method. A comparative study of their characterization and pharmacognostic properties has been estimated. Our finding makes another proof that the stability of AA-PEG@Ag-AuNCs increased coating of L-Ascorbic acid. Further, it also seems that the L-Ascorbic acid-coated LAA-PEG@Ag-Au NCs are effective against lung carcinomas A-549 Lung cancer cell lines as the MTT cytotoxicity analysis has shown a decrease in cell viability with an increase in drug concentration. The increased cell ROS, glutathione and MMP shows that the nanocomposites are to be effective for the A-549 Lung cancer cell lines and be best drugs for the future perspectives. Thus our present study proved that L-Ascorbic acid loaded LAA-PEG@Ag-Au NCs may lead to a greater impact in the carcinomas clinical area as targeted drug delivery besides recommending it for lung cancer in particular. Therefore it is concluded that LAA-PEG@Ag-Au NCs possess the versatility to overcome some of the challenging impediments in the treatment of carcinomas.

References

1. (a) Bell, A. T., The impact of nanoscience on heterogeneous catalysis. *Science* **2003,** *299* (5613), 1688-1691; (b) Compañó, R.; Hullmann, A., Forecasting the development of nanotechnology with the help of science and technology indicators. *Nanotechnology* **2002,** *13* (3), 243.
2. (a) Zeng, S.; Yong, K.-T.; Roy, I.; Dinh, X.-Q.; Yu, X.; Luan, F., A review on functionalized gold nanoparticles for biosensing applications. *Plasmonics* **2011,** *6* (3), 491; (b) Stratakis, M.; Garcia, H., Catalysis by supported gold nanoparticles: beyond aerobic oxidative processes. *Chemical reviews* **2012,** *112* (8), 4469-4506.
3. (a) Li, W.-R.; Xie, X.-B.; Shi, Q.-S.; Zeng, H.-Y.; You-Sheng, O.-Y.; Chen, Y.-B., Antibacterial activity and mechanism of silver nanoparticles on Escherichia coli. *Applied microbiology and biotechnology* **2010,** *85* (4), 1115-1122; (b) Wagner, J.; Peng, W.; Vana, P., Polyethylene-Grafted Gold and Silver Nanoparticles Using Catalyzed Chain Growth (CCG). *Polymers* **2018,** *10* (4), 407.
4. Palza, H., Antimicrobial polymers with metal nanoparticles. *International journal of molecular sciences* **2015,** *16* (1), 2099-2116.
5. Kumar, S. K.; Jouault, N.; Benicewicz, B.; Neely, T., Nanocomposites with polymer grafted nanoparticles. *Macromolecules* **2013,** *46* (9), 3199-3214.
6. Balazs, A. C.; Emrick, T.; Russell, T. P., Nanoparticle polymer composites: where two small worlds meet. *Science* **2006,** *314* (5802), 1107-1110.
7. Zdyrko, B.; Luzinov, I., Polymer brushes by the "grafting to" method. *Macromolecular rapid communications* **2011,** *32* (12), 859-869.
8. Reidy, B.; Haase, A.; Luch, A.; Dawson, K. A.; Lynch, I., Mechanisms of silver nanoparticle release, transformation and toxicity: a critical review of

current knowledge and recommendations for future studies and applications. *Materials* **2013,** *6* (6), 2295-2350.

9. Panariti, A.; Miserocchi, G.; Rivolta, I., The effect of nanoparticle uptake on cellular behavior: disrupting or enabling functions? *Nanotechnology, science and applications* **2012,** *5*, 87.
10. (a) Chen, W.; Wang, S.; Westcott, S.; Zhang, J., Energy-transfer nanocomposite materials and methods of making and using same. Google Patents: 2009; (b) Lesniak, W.; Bielinska, A. U.; Sun, K.; Janczak, K. W.; Shi, X.; Baker, J. R.; Balogh, L. P., Silver/dendrimer nanocomposites as biomarkers: fabrication, characterization, in vitro toxicity, and intracellular detection. *Nano letters* **2005,** *5* (11), 2123-2130.
11. Panzarini, E.; Mariano, S.; Carata, E.; Mura, F.; Rossi, M.; Dini, L., Intracellular transport of silver and gold nanoparticles and biological responses: an update. *International journal of molecular sciences* **2018,** *19* (5), 1305.
12. Bourfaa, F.; Boutelala, A.; Aida, M. S.; Attaf, N.; Ocak, Y. S., Influence of Seed Layer Surface Position on Morphology and Photocatalysis Efficiency of ZnO Nanorods and Nanoflowers. *Journal of Nanomaterials* **2020,** *2020*.
13. (a) Piazza, G. A.; Chen, X.; Keeton, A. B., Ras-inhibiting indenyl acetamide compounds, compositions, and uses. Google Patents: 2017; (b) Boyd, M. R.; Gustafson, K. R., Chondropsin-class antitumor V-ATPase inhibitor compounds, compositions and methods of use thereof. Google Patents: 2009.
14. (a) Peng, W.; Rossner, C.; Roddatis, V.; Vana, P., Gold-Planet–Silver-Satellite Nanostructures Using RAFT Star Polymer. *ACS Macro Letters* **2016,** *5* (11), 1227-1231; (b) Hotchkiss, J. W.; Lowe, A. B.; Boyes, S. G., Surface modification of gold nanorods with polymers synthesized by reversible addition− fragmentation chain transfer polymerization. *Chemistry of Materials*

2007, *19* (1), 6-13; (c) Lowe, A. B.; Sumerlin, B. S.; Donovan, M. S.; McCormick, C. L., Facile preparation of transition metal nanoparticles stabilized by well-defined (co) polymers synthesized via aqueous reversible addition-fragmentation chain transfer polymerization. *Journal of the American Chemical Society* **2002,** *124* (39), 11562-11563.

15. Selvakannan, P.; Mandal, S.; Phadtare, S.; Gole, A.; Pasricha, R.; Adyanthaya, S.; Sastry, M., Water-dispersible tryptophan-protected gold nanoparticles prepared by the spontaneous reduction of aqueous chloroaurate ions by the amino acid. *Journal of Colloid and Interface Science* **2004,** *269* (1), 97-102.
16. Gearheart, L. A.; Ploehn, H. J.; Murphy, C. J., Oligonucleotide adsorption to gold nanoparticles: a surface-enhanced Raman spectroscopy study of intrinsically bent DNA. *The Journal of Physical Chemistry B* **2001,** *105* (50), 12609-12615.
17. Yi, H.; Leunissen, J. L.; Shi, G.-M.; Gutekunst, C.-A.; Hersch, S. M., A novel procedure for pre-embedding double immunogold–silver labeling at the ultrastructural level. *Journal of Histochemistry & Cytochemistry* **2001,** *49* (3), 279-283.
18. Storhoff, J. J.; Lazarides, A. A.; Mucic, R. C.; Mirkin, C. A.; Letsinger, R. L.; Schatz, G. C., What controls the optical properties of DNA-linked gold nanoparticle assemblies? *Journal of the American Chemical Society* **2000,** *122* (19), 4640-4650.
19. (a) Sandhu, K. K.; McIntosh, C. M.; Simard, J. M.; Smith, S. W.; Rotello, V. M., Gold nanoparticle-mediated transfection of mammalian cells. *Bioconjugate chemistry* **2002,** *13* (1), 3-6; (b) O'Brien, J.; Lummis, S. C., An improved method of preparing microcarriers for biolistic transfection. *Brain research protocols* **2002,** *10* (1), 12-15.

20. Voskerician, G.; Shive, M. S.; Shawgo, R. S.; Von Recum, H.; Anderson, J. M.; Cima, M. J.; Langer, R., Biocompatibility and biofouling of MEMS drug delivery devices. *biomaterials* **2003,** *24* (11), 1959-1967.

21. Olofsson, L.; Rindzevicius, T.; Pfeiffer, I.; Käll, M.; Höök, F., Surface-based gold-nanoparticle sensor for specific and quantitative DNA hybridization detection. *Langmuir* **2003,** *19* (24), 10414-10419.

22. Chithrani, B. D.; Ghazani, A. A.; Chan, W. C., Determining the size and shape dependence of gold nanoparticle uptake into mammalian cells. *Nano letters* **2006,** *6* (4), 662-668.

23. Connor, E. E.; Mwamuka, J.; Gole, A.; Murphy, C. J.; Wyatt, M. D., Gold nanoparticles are taken up by human cells but do not cause acute cytotoxicity. *small* **2005,** *1* (3), 325-327.

24. Pernodet, N.; Fang, X.; Sun, Y.; Bakhtina, A.; Ramakrishnan, A.; Sokolov, J.; Ulman, A.; Rafailovich, M., Adverse effects of citrate/gold nanoparticles on human dermal fibroblasts. *small* **2006,** *2* (6), 766-773.

25. Shukla, R.; Bansal, V.; Chaudhary, M.; Basu, A.; Bhonde, R. R.; Sastry, M., Biocompatibility of gold nanoparticles and their endocytotic fate inside the cellular compartment: a microscopic overview. *Langmuir* **2005,** *21* (23), 10644-10654.

26. Qin, L.; Zeng, G.; Lai, C.; Huang, D.; Xu, P.; Zhang, C.; Cheng, M.; Liu, X.; Liu, S.; Li, B., "Gold rush" in modern science: fabrication strategies and typical advanced applications of gold nanoparticles in sensing. *Coordination Chemistry Reviews* **2018,** *359*, 1-31.

27. Aum, D. J.; Kim, D. H.; Beaumont, T. L.; Leuthardt, E. C.; Dunn, G. P.; Kim, A. H., Molecular and cellular heterogeneity: the hallmark of glioblastoma. *Neurosurgical focus* **2014,** *37* (6), E11.

28. Kawata, K.; Osawa, M.; Okabe, S., In vitro toxicity of silver nanoparticles at noncytotoxic doses to HepG2 human hepatoma cells. *Environmental science & technology* **2009,** *43* (15), 6046-6051.

29. Soenen, S. J.; Manshian, B.; Montenegro, J. M.; Amin, F.; Meermann, B.; Thiron, T.; Cornelissen, M.; Vanhaecke, F.; Doak, S.; Parak, W. J., Cytotoxic effects of gold nanoparticles: a multiparametric study. *Acs Nano* **2012,** *6* (7), 5767-5783.

30. (a) Moaddab, S.; Ahari, H.; Shahbazzadeh, D.; Motallebi, A. A.; Anvar, A. A.; Rahman-Nya, J.; Shokrgozar, M. R., Toxicity study of nanosilver (nanocid?) on osteoblast cancer cell line. *International Nano Letters* **2011,** *1* (1), 11; (b) Cheng, D.; Yang, J.; Zhao, Y., Antibacterial materials of silver nanoparticles application in medical appliances and appliances for daily use. *Chin Med Equip J* **2004,** *4*, 26-32; (c) Cohen, M. S.; Stern, J. M.; Vanni, A. J.; Kelley, R. S.; Baumgart, E.; Field, D.; Libertino, J. A.; Summerhayes, I. C., In vitro analysis of a nanocrystalline silver-coated surgical mesh. *Surgical infections* **2007,** *8* (3), 397-404.

31. (a) Alt, V.; Bechert, T.; Steinrücke, P.; Wagener, M.; Seidel, P.; Dingeldein, E.; Domann, E.; Schnettler, R., An in vitro assessment of the antibacterial properties and cytotoxicity of nanoparticulate silver bone cement. *biomaterials* **2004,** *25* (18), 4383-4391; (b) Hussain, S.; Hess, K.; Gearhart, J.; Geiss, K.; Schlager, J., In vitro toxicity of nanoparticles in BRL 3A rat liver cells. *Toxicology in vitro* **2005,** *19* (7), 975-983; (c) Hussain, S. M.; Javorina, A. K.; Schrand, A. M.; Duhart, H. M.; Ali, S. F.; Schlager, J. J., The interaction of manganese nanoparticles with PC-12 cells induces dopamine depletion. *Toxicological sciences* **2006,** *92* (2), 456-463.

32. (a) Ak, M.; Toppare, L., Synthesis of star-shaped pyrrole and thiophene functionalized monomers and optoelectrochemical properties of corresponding

copolymers. *Materials Chemistry and physics* **2009,** *114* (2-3), 789-794; (b) Chronakis, I. S.; Grapenson, S.; Jakob, A., Conductive polypyrrole nanofibers via electrospinning: electrical and morphological properties. *Polymer* **2006,** *47* (5), 1597-1603.

33. Elhalawany, N.; Awad, M. A.; Zahran, M. K., Synthesis, characterization, optical and electrical properties of novel highly dendritic polythiophene nanocomposites with silver and/or gold. *Journal of Materials Science: Materials in Electronics* **2018,** *29* (11), 8970-8977.
34. Siegel, R.; Naishadham, D.; Jemal, A., Cancer statistics, 2012. *CA: a cancer journal for clinicians* **2012,** *62* (1), 10-29.
35. Jemal, A.; Siegel, R.; Xu, J.; Ward, E., Cancer statistics, 2010. *CA: a cancer journal for clinicians* **2010,** *60* (5), 277-300.
36. Davidoff, A. J.; Tang, M.; Seal, B.; Edelman, M. J., Chemotherapy and survival benefit in elderly patients with advanced non–small-cell lung cancer. *Journal of Clinical Oncology* **2010,** *28* (13), 2191-2197.
37. Wicha, M. S.; Liu, S.; Dontu, G., Cancer stem cells: an old idea—a paradigm shift. *Cancer research* **2006,** *66* (4), 1883-1890.
38. Dean, M.; Fojo, T.; Bates, S., Tumour stem cells and drug resistance. *Nature Reviews Cancer* **2005,** *5* (4), 275-284.
39. Reya, T.; Morrison, S. J.; Clarke, M. F.; Weissman, I. L., Stem cells, cancer, and cancer stem cells. *Nature* **2001,** *414* (6859), 105-111.
40. Bautch, V. L., Tumour stem cells switch sides. *Nature* **2010,** *468* (7325), 770-771.
41. Bonnet, D.; Dick, J. E., Human acute myeloid leukemia is organized as a hierarchy that originates from a primitive hematopoietic cell. *Nature Medicine* **1997,** *3* (7), 730-737.

42. Singh, S. K.; Clarke, I. D.; Terasaki, M.; Bonn, V. E.; Hawkins, C.; Squire, J.; Dirks, P. B., Identification of a cancer stem cell in human brain tumors. *Cancer research* **2003,** *63* (18), 5821-5828.

43. Al-Hajj, M.; Wicha, M. S.; Benito-Hernandez, A.; Morrison, S. J.; Clarke, M. F., Prospective identification of tumorigenic breast cancer cells. *Proceedings of the National Academy of Sciences* **2003,** *100* (7), 3983-3988.

44. (a) Collins, A. T.; Berry, P. A.; Hyde, C.; Stower, M. J.; Maitland, N. J., Prospective identification of tumorigenic prostate cancer stem cells. *Cancer research* **2005,** *65* (23), 10946-10951; (b) Eramo, A.; Lotti, F.; Sette, G.; Pilozzi, E.; Biffoni, M.; Di Virgilio, A.; Conticello, C.; Ruco, L.; Peschle, C.; De Maria, R., Identification and expansion of the tumorigenic lung cancer stem cell population. *Cell Death & Differentiation* **2008,** *15* (3), 504-514.

45. Jiang, F.; Qiu, Q.; Khanna, A.; Todd, N. W.; Deepak, J.; Xing, L.; Wang, H.; Liu, Z.; Su, Y.; Stass, S. A., Aldehyde dehydrogenase 1 is a tumor stem cell-associated marker in lung cancer. *Molecular cancer research* **2009,** *7* (3), 330-338.

46. Meng, X.; Li, M.; Wang, X.; Wang, Y.; Ma, D., Both CD133+ and CD133− subpopulations of A549 and H446 cells contain cancer-initiating cells. *Cancer science* **2009,** *100* (6), 1040-1046.

47. Rege, T. A.; Hagood, J. S., Thy-1 as a regulator of cell-cell and cell-matrix interactions in axon regeneration, apoptosis, adhesion, migration, cancer, and fibrosis. *The FASEB journal* **2006,** *20* (8), 1045-1054.

48. Cho, R. W.; Wang, X.; Diehn, M.; Shedden, K.; Chen, G. Y.; Sherlock, G.; Gurney, A.; Lewicki, J.; Clarke, M. F., Isolation and molecular characterization of cancer stem cells in MMTV-Wnt-1 murine breast tumors. *Stem cells* **2008,** *26* (2), 364-371.

49. He, J.; Liu, Y.; Zhu, T.; Zhu, J.; DiMeco, F.; Vescovi, A. L.; Heth, J. A.; Muraszko, K. M.; Fan, X.; Lubman, D. M., CD90 is identified as a candidate marker for cancer stem cells in primary high-grade gliomas using tissue microarrays. *Molecular & Cellular Proteomics* **2012,** *11* (6).

50. Yang, Z. F.; Ho, D. W.; Ng, M. N.; Lau, C. K.; Yu, W. C.; Ngai, P.; Chu, P. W.; Lam, C. T.; Poon, R. T.; Fan, S. T., Significance of CD90+ cancer stem cells in human liver cancer. *Cancer cell* **2008,** *13* (2), 153-166.

51. Piao, M. J.; Kang, K. A.; Lee, I. K.; Kim, H. S.; Kim, S.; Choi, J. Y.; Choi, J.; Hyun, J. W., Silver nanoparticles induce oxidative cell damage in human liver cells through inhibition of reduced glutathione and induction of mitochondria-involved apoptosis. *Toxicology letters* **2011,** *201* (1), 92-100.

52. Foldbjerg, R.; Dang, D. A.; Autrup, H., Cytotoxicity and genotoxicity of silver nanoparticles in the human lung cancer cell line, A549. *Archives of toxicology* **2011,** *85* (7), 743-750.

53. Xu, P.; Shen, Y.; Fukuda, Y.; Liu, Y., Variance component estimation in linear inverse ill-posed models. *Journal of Geodesy* **2006,** *80* (2), 69-81.

54. Zhang, C.; Su, M.; He, Y.; Zhao, X.; Fang, P.-a.; Ribbe, A. E.; Jiang, W.; Mao, C., Conformational flexibility facilitates self-assembly of complex DNA nanostructures. *Proceedings of the National Academy of Sciences* **2008,** *105* (31), 10665-10669.

55. Arora, S.; Jain, J.; Rajwade, J.; Paknikar, K., Cellular responses induced by silver nanoparticles: in vitro studies. *Toxicology letters* **2008,** *179* (2), 93-100.

56. Matés, J. M.; Segura, J. A.; Alonso, F. J.; Márquez, J., Intracellular redox status and oxidative stress: implications for cell proliferation, apoptosis, and carcinogenesis. *Archives of toxicology* **2008,** *82* (5), 273-299.

57. Redza-Dutordoir, M.; Averill-Bates, D. A., Activation of apoptosis signalling pathways by reactive oxygen species. *Biochimica et Biophysica Acta (BBA)-Molecular Cell Research* **2016,** *1863* (12), 2977-2992.

58. Waris, G.; Ahsan, H., Reactive oxygen species: role in the development of cancer and various chronic conditions. *Journal of carcinogenesis* **2006,** *5*, 14.

59. Muthuswamy, A. D.; Vedagiri, K.; Ganesan, M.; Chinnakannu, P., Oxidative stress-mediated macromolecular damage and dwindle in antioxidant status in aged rat brain regions: Role of L-carnitine and DL-α-lipoic acid. *Clinica chimica acta* **2006,** *368* (1-2), 84-92.

60. Caballero-Díaz, E., Analytical Nanotoxicology. *Encyclopedia of analytical chemistry: applications, theory and instrumentation* **2006**, 1-28.

61. Lee, R. F.; Steinert, S., Use of the single cell gel electrophoresis/comet assay for detecting DNA damage in aquatic (marine and freshwater) animals. *Mutation Research/Reviews in Mutation Research* **2003,** *544* (1), 43-64.

62. Zhang, X.-F.; Huang, F.-H.; Zhang, G.-L.; Bai, D.-P.; Massimo, D. F.; Huang, Y.-F.; Gurunathan, S., Novel biomolecule lycopene-reduced graphene oxide-silver nanoparticle enhances apoptotic potential of trichostatin A in human ovarian cancer cells (SKOV3). *International journal of nanomedicine* **2017,** *12*, 7551.

63. Valiev, M.; Bylaska, E. J.; Govind, N.; Kowalski, K.; Straatsma, T. P.; Van Dam, H. J.; Wang, D.; Nieplocha, J.; Apra, E.; Windus, T. L., NWChem: A comprehensive and scalable open-source solution for large scale molecular simulations. *Computer Physics Communications* **2010,** *181* (9), 1477-1489.

64. (a) Ensafi, A. A.; Hajian, R.; Ebrahimi, S., Study on the interaction between morin-Bi (III) complex and DNA with the use of methylene blue dye as a fluorophor probe. *Journal of the Brazilian Chemical Society* **2009,** *20* (2), 266-276; (b) Pillai, S. I.; Vijayaraghavan, K.; Subramanian, S., Evaluation of DNA-binding, cleavage, BSA interaction of Zn-hydroxy flavone complex. *Der. Pharma. Chemica* **2014,** *6*, 379-389.

65. Berman, H. M.; Bourne, P. E.; Westbrook, J.; Zardecki, C., The protein data bank. In *Protein Structure*, CRC Press: 2003; pp 394-410.

66. (a) Yun, C.-H.; Boggon, T. J.; Li, Y.; Woo, M. S.; Greulich, H.; Meyerson, M.; Eck, M. J., Structures of lung cancer-derived EGFR mutants and inhibitor complexes: mechanism of activation and insights into differential inhibitor sensitivity. *Cancer cell* **2007,** *11* (3), 217-227; (b) Yasuda, H.; Park, E.; Yun, C.-H.; Sng, N. J.; Lucena-Araujo, A. R.; Yeo, W.-L.; Huberman, M. S.; Cohen, D. W.; Nakayama, S.; Ishioka, K., Structural, biochemical, and clinical characterization of epidermal growth factor receptor (EGFR) exon 20 insertion mutations in lung cancer. *Science translational medicine* **2013,** *5* (216), 216ra177-216ra177.

67. Kamat, S.; Tamboli, S.; Puri, V.; Puri, R.; Yadav, J.; Joo, O. S., Optical and electrical properties of polythiophene thin films: effect of post deposition heating. *Journal of optoelectronics and advanced materials* **2010,** *12* (11), 2301-2305.

68. Shanmugapriya, C.; Velraj, G., Investigation on structural and electrical properties of FeCl3 doped polythiophene (PT) blended with micro and nano copper particles by mechanical mixing. *Optik* **2016,** *127* (20), 8940-8950.

69. Chandra, S.; Chowdhury, J.; Ghosh, M.; Talapatra, G., Adsorption of 3-thiophene carboxylic acid on silver nanocolloids: FTIR, Raman, and SERS study aided by density functional theory. *The Journal of Physical Chemistry C* **2011,** *115* (29), 14309-14324.

70. Kumar, A.; Ahuja, M., Carboxymethyl gum kondagogu–chitosan polyelectrolyte complex nanoparticles: Preparation and characterization. *International journal of biological macromolecules* **2013,** *62*, 80-84.

71. Yagci, Y.; Yilmaz, F.; Kiralp, S.; Toppare, L., Photoinduced polymerization of thiophene using iodonium salt. *Macromolecular Chemistry and Physics* **2005,** *206* (12), 1178-1182.

72. (a) Nagaonkar, D.; Rai, M., Sequentially reduced biogenic silver-gold nanoparticles with enhanced antimicrobial potential over silver and gold monometallic nanoparticles. *Adv. Mater. Lett* **2015,** *6* (4), 334-341; (b) Wang, H.; Imura, M.; Malgras, V.; Li, C.; Wang, L.; Yamauchi, Y., A Solution Phase Synthesis of Dendritic Platinum Nanoelectrocatalysts with the Assistance of Polyoxyethylene Nonylphenyl Ether. *Journal of Inorganic and Organometallic Polymers and Materials* **2015,** *25* (2), 245-250.

73. Li, B.; Liu, T.; Hu, L.; Wang, Y., A facile one-pot synthesis of Cu2O/RGO nanocomposite for removal of organic pollutant. *Journal of Physics and Chemistry of Solids* **2013,** *74* (4), 635-640.

74. Shankar, S. S.; Rai, A.; Ahmad, A.; Sastry, M., Rapid synthesis of Au, Ag, and bimetallic Au core–Ag shell nanoparticles using Neem (Azadirachta indica) leaf broth. *Journal of Colloid and Interface Science* **2004,** *275* (2), 496-502.

75. Al Bataineh, M. T.; Dash, N. R.; Lassen, P. B.; Banimfreg, B. H.; Nada, A. M.; Belda, E.; Clément, K., Revealing links between gut microbiome and its fungal community in Type 2 Diabetes Mellitus among Emirati subjects: A pilot study. *Scientific reports* **2020,** *10* (1), 1-11.

76. Abbas, G.; Kumar, N.; Kumar, D.; Pandey, G., Effect of Reaction Temperature on Shape Evolution of Palladium Nanoparticles and Their Cytotoxicity against A-549 Lung Cancer Cells. *ACS omega* **2019,** *4* (26), 21839-21847.

77. Marcon, V.; Raos, G., Free energies of molecular crystal surfaces by computer simulation: Application to tetrathiophene. *Journal of the American Chemical Society* **2006,** *128* (5), 1408-1409.

78. Krug, J., Four lectures on the physics of crystal growth. *Physica A: Statistical Mechanics and its Applications* **2002,** *313* (1-2), 47-82.

79. Pettersen, E. F.; Goddard, T. D.; Huang, C. C.; Couch, G. S.; Greenblatt, D. M.; Meng, E. C.; Ferrin, T. E., UCSF Chimera—a visualization system for exploratory research and analysis. *Journal of computational chemistry* **2004,** *25* (13), 1605-1612.

80. Morris, G. M.; Goodsell, D. S.; Halliday, R. S.; Huey, R.; Hart, W. E.; Belew, R. K.; Olson, A. J., Automated docking using a Lamarckian genetic algorithm and an empirical binding free energy function. *Journal of computational chemistry* **1998,** *19* (14), 1639-1662.

81. Marenich, A. V.; Cramer, C. J.; Truhlar, D. G.; Guido, C. A.; Mennucci, B.; Scalmani, G.; Frisch, M. J., Practical computation of electronic excitation in solution: vertical excitation model. *Chemical science* **2011,** *2* (11), 2143-2161.

82. Morris, G. M.; Olson, A. J.; Goodsell, D. S., Protein-ligand docking. *Evolutionary algorithms in molecular design* **2000**, 31-48.

83. Morris, G. M.; Huey, R.; Lindstrom, W.; Sanner, M. F.; Belew, R. K.; Goodsell, D. S.; Olson, A. J., AutoDock4 and AutoDockTools4: Automated docking with selective receptor flexibility. *Journal of computational chemistry* **2009,** *30* (16), 2785-2791.

84. Chen, B. Y.; Bandyopadhyay, S. In *A statistical model of overlapping volume in ligand binding cavities*, 2011 IEEE International Conference on Bioinformatics and Biomedicine Workshops (BIBMW), IEEE: 2011; pp 424-431.

85. Weigend, F.; Ahlrichs, R., Balanced basis sets of split valence, triple zeta valence and quadruple zeta valence quality for H to Rn: Design and assessment of accuracy. *Physical Chemistry Chemical Physics* **2005,** *7* (18), 3297-3305.

86. Jaeschke, H.; McGill, M. R.; Ramachandran, A., Oxidant stress, mitochondria, and cell death mechanisms in drug-induced liver injury: lessons learned from acetaminophen hepatotoxicity. *Drug metabolism reviews* **2012,** *44* (1), 88-106.

87. Heid, M. E.; Keyel, P. A.; Kamga, C.; Shiva, S.; Watkins, S. C.; Salter, R. D., Mitochondrial reactive oxygen species induces NLRP3-dependent lysosomal damage and inflammasome activation. *The Journal of Immunology* **2013,** *191* (10), 5230-5238.

88. Kroemer, G.; Jäättelä, M., Lysosomes and autophagy in cell death control. *Nature Reviews Cancer* **2005,** *5* (11), 886-897.

89. Reddy, A. R. N.; Reddy, Y. N.; Krishna, D. R.; Himabindu, V., Multi wall carbon nanotubes induce oxidative stress and cytotoxicity in human embryonic kidney (HEK293) cells. *Toxicology* **2010,** *272* (1-3), 11-16.

90. Gurunathan, S.; Han, J. W.; Park, J. H.; Kim, E.; Choi, Y.-J.; Kwon, D.-N.; Kim, J.-H., Reduced graphene oxide–silver nanoparticle nanocomposite: a potential anticancer nanotherapy. *International journal of nanomedicine* **2015,** *10*, 6257.

91. Savitha, S.; Tamilselvan, J.; Anusuyadevi, M.; Panneerselvam, C., Oxidative stress on mitochondrial antioxidant defense system in the aging process: Role of DL-α-lipoic acid and L-carnitine. *Clinica chimica acta* **2005,** *355* (1-2), 173-180.

92. Jaleel, C. A.; Lakshmanan, G.; Gomathinayagam, M.; Panneerselvam, R., Triadimefon induced salt stress tolerance in Withania somnifera and its relationship to antioxidant defense system. *South African Journal of Botany* **2008,** *74* (1), 126-132.

93. Hegde, M. L.; Hazra, T. K.; Mitra, S., Early steps in the DNA base excision/single-strand interruption repair pathway in mammalian cells. *Cell research* **2008,** *18* (1), 27-47.

94. Lomax, M.; Folkes, L.; O'neill, P., Biological consequences of radiation-induced DNA damage: relevance to radiotherapy. *Clinical oncology* **2013,** *25* (10), 578-585.

95. Saffran, W. A.; Ahmed, S.; Bellevue, S.; Pereira, G.; Patrick, T.; Sanchez, W.; Thomas, S.; Alberti, M.; Hearst, J. E., DNA repair defects channel interstrand DNA cross-links into alternate recombinational and error-prone repair pathways. *Journal of Biological Chemistry* **2004,** *279* (35), 36462-36469.

96. Minko, I. G.; Kurtz, A. J.; Croteau, D. L.; Van Houten, B.; Harris, T. M.; Lloyd, R. S., Initiation of repair of DNA− polypeptide cross-links by the UvrABC nuclease. *Biochemistry* **2005,** *44* (8), 3000-3009.

97. Clements, C.; Ralph, S.; Petras, M., Genotoxicity of select herbicides in Rana catesbeiana tadpoles using the alkaline single-cell gel DNA electrophoresis (comet) assay. *Environmental and molecular mutagenesis* **1997,** *29* (3), 277-288.

98. Boehler, C.; Gauthier, L. R.; Mortusewicz, O.; Biard, D. S.; Saliou, J.-M.; Bresson, A.; Sanglier-Cianferani, S.; Smith, S.; Schreiber, V.; Boussin, F., Poly (ADP-ribose) polymerase 3 (PARP3), a newcomer in cellular response to DNA damage and mitotic progression. *Proceedings of the National Academy of Sciences* **2011,** *108* (7), 2783-2788.

99. Galadari, S.; Rahman, A.; Pallichankandy, S.; Thayyullathil, F., Reactive oxygen species and cancer paradox: to promote or to suppress? *Free Radical Biology and Medicine* **2017,** *104*, 144-164.

100. Circu, M. L.; Aw, T. Y., Reactive oxygen species, cellular redox systems, and apoptosis. *Free Radical Biology and Medicine* **2010,** *48* (6), 749-762.

Chapter 8

Conclusion and Scope of Future Research

8.1 Conclusion

In summary, different shapes and sizes Pd nanoparticles, like 8-10 nm edge length truncated octahedron/fivefold twinned pentagonal rods and 17-20 nm edge length hexagonal/trigonal plates have been prepared in aqueous solution phase by reducing K_2PdCl_4 with ascorbic acid in the presence of surfactant PEG via sonochemical method at room temperature. XRD study revealed particles growth took place anisotropically at both temperatures. FTIR and SERS studies revealed adsorption of AA and PEG at NP's surface. The particle's size distribution graph indicates formation of particles having wide size distribution while the zeta potential value -13 mV indicated that the particle's surface is negatively charged and hence stable. The truncated octahedron/fivefold twinned pentagonal rods shaped Pd NPs, formed at room temperature while thermally stable and kinetically controlled hexagonal/trigonal plate-like Pd NPs have been evolved at a higher temperature 65 °C. The obtained Pd NPs has a high surface area and narrow pore size distribution. The computationally calculated binding energy indicates this Pd cluster is an effective drug against cancer cells. The lowest binding energy is with 2ITY complex. Molecular Docking gives the best and stable conformations of the ligand with proteins in the receptor active pocket. Biochemically, the effect of PD NPs on A-549 human lung cancer cells exhibited that cytotoxicity is dependent on the dose of NPs. The results described here indicate much potential for use of these NPs in biomedical applications as described in third chapter.

Synthesis of PEG-coated and L-ascorbic acid stabilized mesoporous α-Fe_2O_3 NPs (LAA@IONP-PEG) has been achieved in the sonochemical assisted method using aqueous solution mixture of complex $K_3[FeCl_6]$, PEG and L-ascorbic acid.

LAA@IONP-PEG have been evolved in varieties of shapes and size as revealed in TEM, FESEM, EDX, UV-visible, FTIR, XRD and BET studies. Initially formed metastable β-FeOOH transformed into a stable α-Fe_2O_3 phase during the reaction at 37 °C. The anti-cancer study of LAA@IONP-PEG against renal carcinoma HEK-293 human embryonic kidney cell lines study suggests that high surface area with a large number of active sites mesoporous α-Fe_2O_3 nanoparticles are well suited anti-cancer agent and serve as promising candidate for treatment of renal carcinoma HEK-293 human embryonic kidney cell lines. Docking study has confirmed the anti-proliferative action of NPs through binding affinity with renal carcinoma molecular targets. The synthesized NPs show a synergistic effect with Axitinib as an anti-cancer drug effective against renal carcinoma cell lines. Cytotoxicity and IC_{50} analysis led to detailed changes in the enzyme structure. The nanoparticles sample may be a good antioxidant agent during the cancerous condition of a cell. The results from the experimental and theoretic studies served as a valuable anti-cancer tool against renal carcinoma drug therapy in future as described in fourth chapter.

LAA@Cu_2O-PEG nanopolyhedra has been via sonochemical assisted method using aqueous solution mixture of complex $K_3[FeCl_6]$, PEG and L-ascorbic acid at a temperature 37°C. LAA@Cu_2O-PEG has been evolved polyhedral. The anti-cancer study of LAA@Cu_2O-PEG against renal carcinoma HEK-293 human embryonic kidney cell lines study suggests that high surface area with a large number of active sites nanopolydera are well suited anti-cancer agent and serve as promising candidate for treatment of renal carcinoma HEK-293 human embryonic kidney cell lines. Docking study has confirmed the anti-proliferative action of NPs through binding affinity with renal carcinoma molecular targets. The synthesized NPs show a synergistic effect with Axitinib as an anti-cancer drug effective against renal

carcinoma cell lines. Cytotoxicity and IC_{50} analysis led to detailed changes in the enzyme structure. The nanoparticles sample may be a good antioxidant agent during the cancerous condition of a cell. The results from the experimental and theoretic studies served as a valuable anti-cancer tool against renal carcinoma drug therapy in future as described in fifth chapter.

Sonochemical method for synthesis of nickel nanoparticles was analysed via UV-visible absorption spectroscopy shows λ_{max} value due to the quantum confinement of Ni NPs. The XRD analysis shows that the Ni NPs are highly crystalline with face centred cubic (fcc) structure. EDAX data confirms the presence of prepared Ni NPs. The FTIR and Raman spectra confirm the formation of PEG grafted and L-ascorbic acid coated Ni NPs and presence of fundamental phonon peaks. Morphological studies using the SEM, FESEM and TEM analysis shows cube shaped nickel nanoparticles. BET results show formation high surface area mesoporous Ni NPs. The prepared Ni NPs are shown effective cytotoxicity against MCF-7 breast cancer cell lines. The results were supported by morphological analysis of treated and controlled cells. The normal and regular morphological pattern is observed in untreated cells and irregular cell morphology is seen in cells treated with Ni NPs. This study has proposed the best and simple protocol to synthesize Ni NPs with an effective anticarcinomas activity against MCF-7 breast cancer cell lines as shown in sixth chapter.

LAA-PEG@Ag-Au NCs have been successfully synthesized by using the simple sonochemical method. A comparative study of their characterization and pharmacognostic properties has been estimated. Our finding makes another proof that the stability of AA-PEG@Ag-AuNCs increased coating of L-Ascorbic acid. Further, it also seems that the L-Ascorbic acid-coated LAA-PEG@Ag-Au NCs are effective

against lung carcinomas A-549 Lung cancer cell lines as the MTT cytotoxicity analysis has shown a decrease in cell viability with an increase in drug concentration. The increased cell ROS, glutathione and MMP shows that the nanocomposites are to be effective for the A-549 Lung cancer cell lines and the best drugs for the future perspectives. Thus our present study proved that L-Ascorbic acid loaded LAA-PEG@Ag-Au NCs, may lead to a greater impact in the carcinomas clinical area as targeted drug delivery besides recommending it for lung cancer in particular. Therefore it is concluded that LAA-PEG@Ag-Au NCs possess the versatility to overcome some of the challenging impediments in the treatment of carcinomas as shown in seventh chapter.

8.2 Scope and Further Research

In the present work an inorganic nanoparticle/nanocomposite of various metal salts has been synthesized, however shape and size distribution of the materials may also modify to alter the responsiveness of the prepared nanoparticles. Hence an effort may be used to different type of growth of materials to made optimisation of various nanostructure.

To risen the value of effectiveness of nanoparticles against diagnosis, number of suraface modifications has been performed via capping with organic polymers like polyaniline, polydodecylether (Brij-58) etc.

To explore surface modifications of nanostructures with different morphology against analysis like anticarcinomas, pathogenic and virological responses.

List of Publications

List of Publications

1. **Gulam Abbas,** Gajanan Pandey, "Effect of Reaction Temperature on Shape Evolution of Palladium Nanoparticles and Their Cytotoxicity against A-549 Lung Cancer Cell" **ACS Omega**, 2019, 4, 21839-21847.

2. **Gulam Abbas**, Gajanan Pandey, "Efficient anticarcinogenic activity of α-Fe_2O_3 nanoparticles: In-vitro and Computational study on human renal carcinoma cells HEK-293" Material Today Communications **(Elsevier)** 2020, 26, 102175.

Conferences

1. **Gulam Abbas,** Gajanan Pandey, "Application of materials and their application in cancerous treatment by sonochemical method" International Conference on Updates in Cancer Prevention and Research, ICUCPR-2017 organized by **Babasaheb Bhimrao Ambedkar University, Lucknow. (Oral Presentation)** 14-20 February 2017.

2. **Gulam Abbas,** Gajanan Pandey, "Synthesis of nanoparticles and their cytotoxicity against cancerous cell lines by sonochemical method" Recent Advances and Innovations in Chemical and Materials Science, RAICMS-2017 organized by **Sri Jai Narayan PG College, Lucknow. (Poster presentation)** 23-24 February 2017.

3. **Gulam Abbas,** Gajanan Pandey, " Synthesis of silver and gold nanocomposite and their cytotoxicity against HEK-293 cell lines" organized by Department of Chemistry, (GCGHGSPCT-2k19), **Babasaheb Bhimrao Ambedkar University, Lucknow. (Oral Presentation)** 22-24 April 2019.

Workshop

1. QIP short term course on, "Computational Chemistry and its Applications" March 05-09, 2020, organized by Center for Continuing Education, **Indian Institute of Technology (IIT), Kanpur. (Participated)** 05-09 March 2020.